Electrochemical Society

Indianapolis Meeting Program Issue

GLC Anodes Are CUSTOM MADE
for
Stauffer Chemical Company

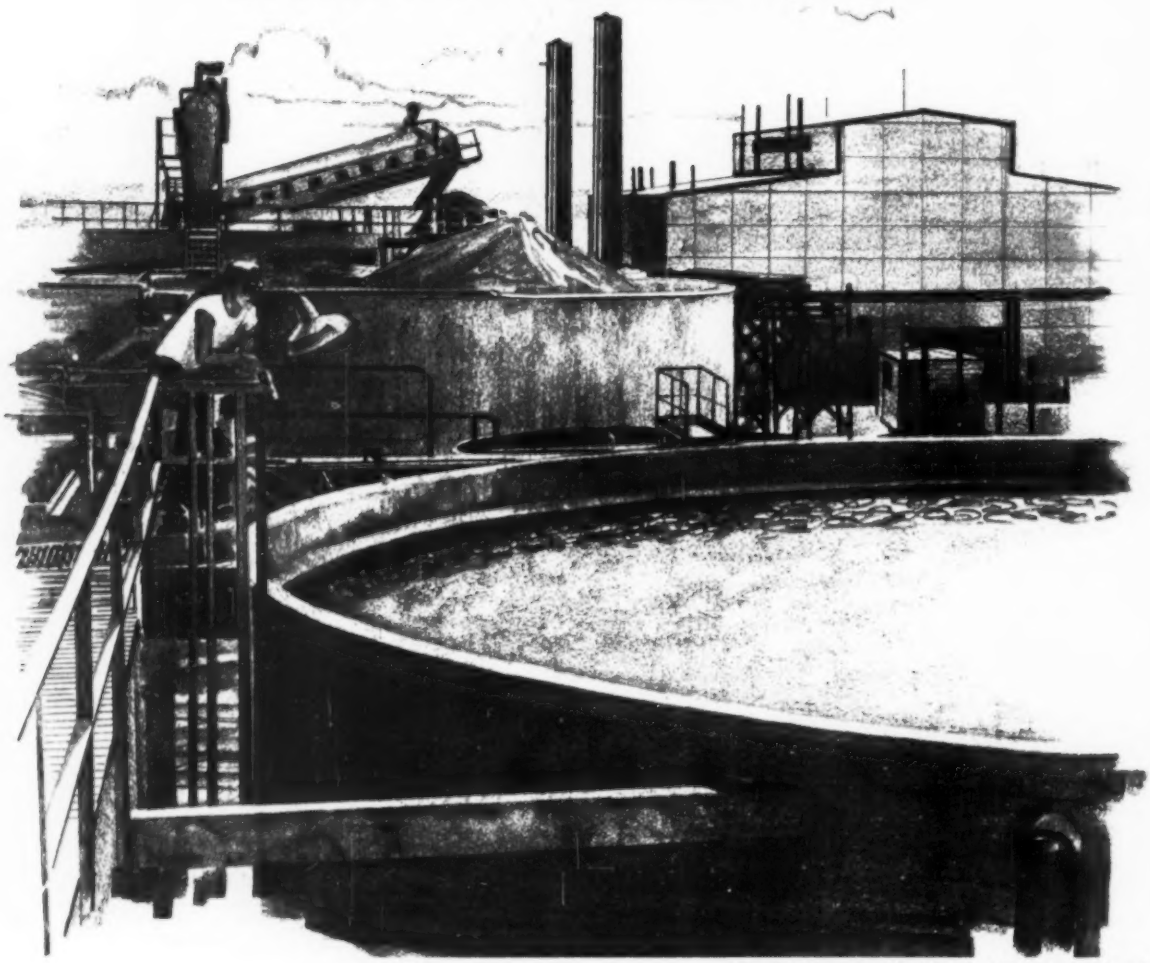

The Stauffer Chlor-Alkali Plant at Henderson, Nevada

Most chlor-alkali producers have lowered their operating costs by using GLC anodes.

Unless you have some GLC anodes in your cells now, you are missing an opportunity to prove their outstanding performance to your satisfaction.

The difference lies in custom making GLC anodes to individual cell requirements. May we demonstrate that difference for you?

PRODUCTS YOU CAN TRUST — GLC ELECTRODE DIVISION

GREAT LAKES CARBON CORPORATION

18 EAST 48TH STREET, NEW YORK 17, N.Y. OFFICES IN PRINCIPAL CITIES

EDITORIAL STAFF

C. L. Faust, Chairman, Publication Committee

Cecil V. King, Editor

Norman Hackerman, Technical Editor

Ruth G. Sterns, Managing Editor

U. B. Thomas, News Editor

H. W. Salzberg, Book Review Editor

Natalie Michalski, Assistant Editor

DIVISIONAL EDITORS

W. C. Vosburgh, Battery

Milton Stern, Corrosion, I

R. T. Foley, Corrosion, II

T. D. Callinan, Electric Insulation

Seymour Senderoff, Electrodeposition

H. C. Froelich, Electronics, I

Ephraim Banks, Electronics, II

Ernest Paskell, Electronics—Semiconductors

Sherlock Swann, Jr., Electro-Organic, I

Stanley Wawzonek, Electro-Organic, II

John M. Blocher, Jr., Electrothermics and Metallurgy, I

J. H. Westbrook, Electrothermics and Metallurgy, II

N. J. Johnson, Industrial Electrolytic

C. W. Tobias, Theoretical Electrochemistry, I

A. J. deBethune, Theoretical Electrochemistry, II

ADVERTISING OFFICE

ECS

1860 Broadway, New York 23, N. Y.

ECS OFFICERS

R. A. Schaefer, President
Electric Storage Battery Co., Yardley, Pa.

Henry B. Linford, Vice-President
Columbia University, New York, N. Y.

F. L. LaQue, Vice-President
International Nickel Co., Inc., New York, N. Y.

W. J. Hamer, Vice-President
National Bureau of Standards, Washington, D. C.

Lyle I. Gilbertson, Treasurer
Air Reduction Co., Murray Hill, N. J.

I. E. Campbell, Secretary
National Steel Corp., Weirton, W. Va.

Robert K. Shannon, Executive Secretary
National Headquarters, The ECS, 1860 Broadway, New York 23, N. Y.

Manuscripts submitted to the Journal should be sent, in triplicate, to the Editorial Office at 1860 Broadway, New York 23, N. Y. They should conform to the revised Instructions to Authors, published on pp. 46C-47C of this issue. Manuscripts so submitted become the property of The Electrochemical Society and may not be published elsewhere, in whole or in part, unless permission is requested of and granted by the Editor.

Inquiries re positive microfilm copies for volumes should be addressed to University Microfilms, Inc., 313 N. First St., Ann Arbor, Mich.

The Electrochemical Society does not maintain a supply of reprints of papers appearing in its Journal. A photoprint copy of any particular paper, however, may be obtained by corresponding directly with the Engineering Societies Library, 29 W. 39 St., New York 18, N. Y.

Journal of the

Electrochemical Society

MARCH 1961 **VOL. 108 • NO. 3**

CONTENTS

Editorial

Television in the Classroom 41C

Technical Papers

Investigation on the Silver-Zinc Storage Battery with Radioactive Zn^{65} Isotope. *T. Z Palágyi* 201

The Effect of Metallic Cations on the Corrosion of Iron and Tin in Boiling Acids. *W. R. Buck, III, and H. Leidheiser, Jr.* 203

Effects of Anions on the Dissolution Kinetics of Metals. *J. M. Kolotyrkin* 209

Oxidation of Iron-Nickel Alloys, IV. Further Electron Diffraction Studies at Elevated Temperatures. *R. T. Foley* 216

Anodic Behavior of Austenitic Stainless Steels and Susceptibility to Stress Corrosion Cracking. *S. Barnartt and D. van Rooyen* 222

Capacitor Grade Tantalum. *L. H. Belz* 229

Lead- and Manganese-Activated Calcium Cadmium Silicate Phosphors. *Y. Uehara, Y. Kobuke, I. Masuda, and T. Kushida* 235

A Study of Growth Processes in Germanium Dendrites Using Pulse Electroplating Techniques. *R. C. Smith* 238

Capillary Alloying: An Improved Alloying Method. *K. Lehovec, K. Busen, J. Casey, C. Pochop, and A. Webb* 241

Photovoltages in Silicon and Germanium Layers. *H. Kallmann, B. Kramer, W. J. McAleer, H. Barkemeyer, and P. I. Pollack* 247

The Preparation and Floating Zone Processing of Gallium Phosphide. *C. J. Frosch and L. Derick* 251

Anisotropic Segregation in Insb. *W. P. Allred and R. T. Bate* 258

The Formation of Chromium or Molybdenum Stabilized Tungsten Silicon Carbide. *V. I. Matkovich and H. H. Rogers* 261

Electrolytic Micromachining of Iron Whisker Surfaces. *B. C. Banerjee and P. L. Walker, Jr.* 262

Anodic Behavior of Copper in Phosphoric Acid. *F. H. Giles and J. H. Bartlett* 266

A Precision Conductance Bridge of New Design. *G. J. Janz and J. D. E. McIntyre* 272

Characteristic Functions and Parameters in the Theory of Hydrogen Overpotential, I. Theoretical. *G. W. Castellan* 277

Characteristic Functions and Parameters in the Theory of Hydrogen Overvoltage, II. Interpretation of Some Measurements of Hydrogen Overpotential on Palladium. *G. W. Castellan* 282

Conductivities in Emulsions. *R. E. Meredith and C. W. Tobias* 286

Exchange between Single-Crystal Cadmium and Its Ions. *C. V. King, D. S. Newman, and E. Suriani* 291

Technical Notes

Effect of Dissolved Gases on Oxide Film Formation. *J. J. Polling* 294

Recombination Radiation from an N-Type Germanium Cathode in Heavy Water. *P. F. Schmidt and C. H. Church* 296

Dissolution Rate of Germanium in Aqueous Hydrogen Peroxide and Saturated Ozone Solutions. *K. J. Miller* 296

Is the Lead-Acid Storage Battery Obsolete? *P. Rüetschi* 297

Brief Communication

Brookite Film on Titanium. *S. Yamaguchi* 302

Indianapolis Meeting Program 49C-74C

Current Affairs 75C-80C

Published monthly by The Electrochemical Society, Inc., from Manchester, N. H., **Executive Offices, Editorial Office** and **Circulation Dept.,** and **Advertising Office** at 1860 Broadway, New York 23, N. Y., combining the JOURNAL and TRANSACTIONS OF THE ELECTROCHEMICAL SOCIETY. Statements and opinions given in articles and papers in the JOURNAL OF THE ELECTROCHEMICAL SOCIETY are those of the contributors, and The Electrochemical Society assumes no responsibility for them. Subscription to members as part of membership service; subscription to nonmembers $24.00. Single copies $1.70 to members, $2.25 to nonmembers.

Copyright 1961 by The Electrochemical Society, Inc.

Entered as second-class matter at the Post Office at Manchester, N. H., under the act of August 24, 1912.

FUTURE MEETINGS OF
The Electrochemical Society

Indianapolis, Ind., April 30, May 1, 2, and 3, 1961
Headquarters at the Claypool Hotel
Sessions will be scheduled on
Electric Insulation, Electronics (including Luminescence and Semiconductors), Electrothermics and Metallurgy, Industrial Electrolytics (including a Symposium on Fuel Cells), and Theoretical Electrochemistry (including a Symposium on Instrumentation)

★ ★ ★

Detroit, Mich., October 1, 2, 3, 4, and 5, 1961
Headquarters at the Statler Hotel
Sessions probably will be scheduled on
Batteries, Corrosion (including a Symposium on Surface Structure vs. Corrosion Behavior), Electrodeposition (including symposia on Addition Agents and on Electrodeposited Magnetic Films), Electronics (Semiconductors), Electro-Organics, and Electrothermics and Metallurgy

★ ★ ★

Los Angeles, Calif., May 6, 7, 8, 9, and 10, 1962
Headquarters at the Statler Hilton Hotel

★ ★ ★

Boston, Mass., September 16, 17, 18, 19, and 20, 1962
Headquarters at the Statler Hilton Hotel

Papers are now being solicited for the meeting to be held in Detroit, Mich., October 1-5, 1961. Triplicate copies of each abstract (*not exceeding 75 words in length*) are due at Society Headquarters, 1860 Broadway, New York 23, N. Y., *not later than May 15, 1961* in order to be included in the program. *Please indicate on abstract for which Division's symposium the paper is to be scheduled, and underline the name of the author who will present the paper.* No paper will be placed on the program unless one of the authors, or a qualified person designated by the authors, has agreed to present it in person. An author who wishes his paper considered for publication in the JOURNAL should send triplicate copies of the manuscript to the Managing Editor of the JOURNAL, 1860 Broadway, New York 23, N.Y.

Presentation of a paper at a technical meeting of the Society does not guarantee publication in the JOURNAL. However, all papers so presented become the property of The Electrochemical Society, and may not be published elsewhere, either in whole or in part, unless permission for release is requested of and granted by the Editor. Papers already published elsewhere, or submitted for publication elsewhere, are not acceptable for oral presentation except on invitation by a Divisional program Chairman.

Editorial

Television in the Classroom

A great many people are familiar with the names "Sunrise Semester" and "Continental Classroom." Probably not so many realize that televised material is part of the daily classroom instruction of a half million students in the United States. Starting with KUHT in Houston in 1953, at least 50 stations for purely educational TV broadcasting have sprung up, and 200 or more closed-circuit systems are in use in schools and colleges. Those who are responsible for the introduction of TV into teaching are highly enthusiastic; but sober examination of the published reports and surveys does not bear out their statements.

First, it has become obvious that students exposed to TV instruction do no better on achievement tests. But, as one enthusiast says, if fifth-graders in Pittsburgh can actually see and hear Robert Frost reading his own poems, it must leave *some* impression they could gain in no other way.

Second, the use of TV does not result in better teaching at lower cost; the cost is much higher. Television can seldom be used for the full classroom period, and fully qualified follow-up teachers, not merely proctors, must be in constant attendance. The "star" who lectures and demonstrates should have no more than one broadcast per day, since several hours must be spent with the camera and lighting technicians, the purveyor of "props," and other helpers, for each broadcast.

Some of the experiments seem designed purely to help distribute Ford Foundation funds. New York University tried closed-circuit TV with several freshman classes in English Composition (could any course be more inappropriate?). The difference in marks was "statistically nonsignificant," and the follow-up instructors were far from enthusiastic. Better results were obtained, not in marks but in student and faculty acceptance, in such courses as "Man's Cultural Heritage" and "History of Civilization."

In the winter of 1958, the NYU group conducted a questionnaire survey, the results of which were summarized in the *Journal of Educational Sociology*, May 1959. In all, 256 returns were received from individual instructors in 89 colleges. "However, 71 did not answer the open-ended question here discussed or gave responses which were irrelevant, unclear, or obviously wholly idiosyncratic." Of 145 returns from 30 public school systems, "again omission, lack of clarity, and irrelevance" spoiled 26 of the replies. Among the "usable" returns, a commonly expressed concern "dealt with the assessment or amelioration of faculty attitudes toward television . . . such phrases as 'the need of combatting negative attitudes' . . . may reflect a feeling that the effectiveness of televised instruction is hampered by factors external to the technique itself, i.e., by such faculty attitudes." We translate in simple words: Many teachers detest the intrusion of TV in their classrooms and resent the fact that it is foisted on them.

Washington County, Md., has been the site of a five-year experiment bringing closed-circuit TV instruction to some 18,000 primary school students, and financed to the extent of $2,000,000 by the Electronics Industry Association and the Ford Foundation. A report of a personal study of its operation, hair-raising in some details, comic-humorous but mainly serious, has been published by Richard Franko Goldman (yes, the conductor-composer and music teacher) in the Columbia University Forum (Winter 1961). We can only quote part of his main conclusions here. "I saw no evidence that the TV instruction was in any way superior to the general run of non-TV elementary school teaching one can find every day in any part of the U. S. . . . . I saw nothing worse than usual. But the important thing is that I saw nothing *better*, for improvement in quality is the claim made for the whole business. My feeling is very strong that the teaching on TV *will not get better* . . . ."

—CVK

Wiley BOOKS

SEMICONDUCTOR ABSTRACTS

VOLUME VI, 1958 ISSUE

Compiled by Battelle Memorial Institute, under auspices of The Electrochemical Society, Inc. Edited by J. J. BULLOFF *and* C. S. PEET. Sponsored by the Air Force Office of Scientific Research and Battelle Memorial Institute, this is the most recent addition to a well-known series. It provides scientists and technologists with the latest developments in the field of semi-conducting and luminescent materials. Also, it is a unified source of references to important and useful articles on application and utilization of electronic processes in solids. **1961. 528 pages. $14.00**

THE FERMI SURFACE

Proceedings of an International Conference

Edited by W. A. HARRISON *and* M. B. WEBB, *General Electric Research Laboratory.* Summarizes the remarkable recent progress in understanding electronic properties of metals, clarifies the current status of the science, and defines problems yet to be solved. The contributions of ninety scientists afford both general discussion and detailed data on the size and shape of Fermi surfaces. Featured are the importance of many-body effects in theory and experiment, experimental and theoretical information on the noble metals, progress in the understanding of polyvalent metals, and the electronic structure of alloys. **1961. 356 pages. $10.00**

ORGANIC COATING TECHNOLOGY

VOLUME II: PIGMENTS AND PIGMENTED COATINGS

By HENRY F. PAYNE, *University of Florida.* Stresses chemistry, manufacture, and use and covers both theoretical and practical aspects. Has sufficient theory to give a working knowledge of the necessary physics and chemistry. Consistency and flow properties are treated thoroughly. Surface-active agents, because of their importance both in oil and water emulsion paints, are given basic coverage. Supporting the theory, specific formulations are included. **1961. 1363 pages. $17.50**

INTRODUCTION TO CERAMICS

By W. D. KINGERY, *M.I.T.* Embodies a fresh concept in the treatment of ceramics. Rather than focussing on various divisions of the industry, it concentrates on phenomena (densification during firing, etc.), properties, and strength. This approach leads to a rational understanding of traditional ceramic compositions and the novel space-age developments. NOTE: Includes an extensive collection of micrographs, showing compositions, processing techniques, and properties. **1960. 781 pages. $15.00**

PROGRESS IN SEMICONDUCTORS

VOLUME V

Edited by A. F. GIBSON, R. E. BURGESS, *and* F. A. KROGER. This latest in the series covers electrical properties of semiconductor surfaces; absorption edge spectrum of semiconductors; the chemical bond; thermal conductivity; indium antimonide; magneto-optical phenomena; band structure and electronic properties of graphite crystals. **1961. In Press**

AN INTRODUCTION TO TRANSITION-METAL CHEMISTRY

By LESLIE ORGEL, *Cambridge University.* "Just occasionally there comes a book which says just the right thing, in the right way, at the right time. This is such a book . . . shows how characteristic properties of these molecules—and the exceedingly interesting group of compounds now referred to as "molecular sandwiches", where a transition metal atom lies between two aromatic molecules such as C_5H_5—are due to the number and geometrical disposition of their d-electrons. Nearly all of the account is illustrated in terms of pictures. This is the first book really to expound this field."—C. A. Coulson. in The New Scientist. **1960. 180 pages. $4.50**

ORGANOMETALLIC COMPOUNDS

By G. E. COATES, *University of Durham.* A complete rewriting and great expansion of material which appeared some years earlier in a Methuen Monograph. "(Prof. Coates) has a knack for picking out the truly important points for emphasis and he presents them well."—pre-publication reviewer. Contents: The Alkali Metals; Group II; Group III; Group IV; Antimony and Bismuth; The Transition Elements. **1961. In Press**

Send now for your on-approval copies **JOHN WILEY & SONS, INC.** 440 PARK AVENUE SOUTH, NEW YORK 16, N. Y.

"IMAGINATION IS MORE IMPORTANT THAN KNOWLEDGE"

Albert Einstein

There are some who might argue this point with Einstein. But this much is certain: Wherever new knowledge is sought, imagination lights the way. And surely, only imagination of rare quality could have led Einstein to formulate his principle of relativity.

Einstein applied the insight of imagination to basic science. But imagination can be just as powerful in the creation and application of technology. And nowhere, perhaps, is imagination challenged over so wide a range in both science and technology as in the problems of electrical communications.

At Bell Telephone Laboratories, scientists and engineers range far and deep in search of the answers. They probed deep into solid-state physics to discover the transistor principle, and they speculated and synthesized in an entirely different area of knowledge to create the giant microwave system that carries your TV programs across the country. They study ways to protect the giant molecules in plastic cable sheath, and they explore the basic information content of speech to devise better ways to transmit it. They devise ultrasensitive amplifiers to capture radio signals from distant places, while they conceive and develop new switching systems of unprecedented capabilities. Side by side with the development of transoceanic cable systems they are exploring the possibilities of world-wide communications via man-made satellites.

By exploring every pathway to improved electrical communications, they have helped make your Bell System communications the world's best and they will work to keep it so.

BELL TELEPHONE LABORATORIES

WORLD CENTER OF COMMUNICATIONS
RESEARCH AND DEVELOPMENT

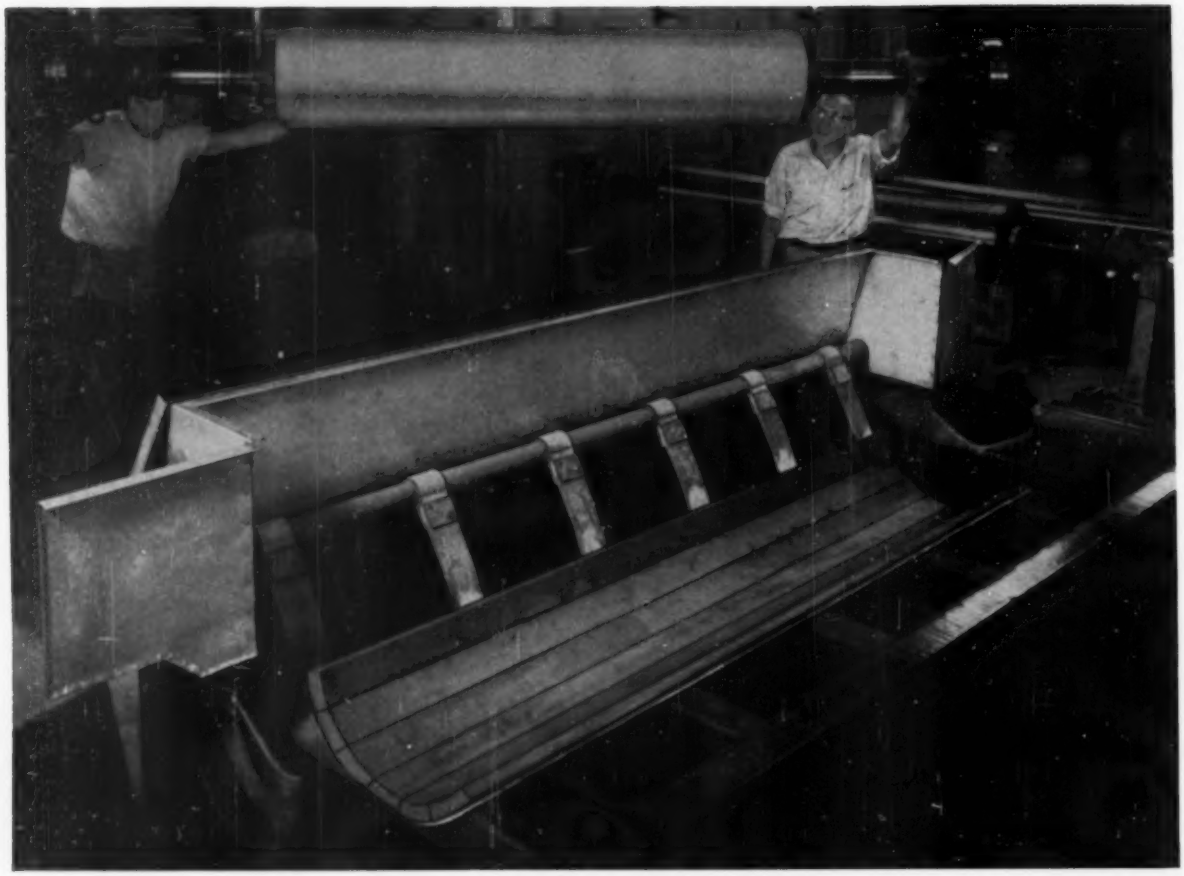

Curved anodes fit the curve of the current-carrying saddle, parallel the surface of the cylinder being plated.

CURVED TO FIT THE SADDLE, ANACONDA "PLUS-4" COPPER ANODES PLATE SMOOTHER – CUT COSTS

Anaconda "Plus-4" Curved Anodes are 1" thick, 3" across inside surface. You simply specify the inside radius of the anode, to fit your tank. There is no extra die cost.

At Pulitzer Publishing Co., St. Louis, Mo., Anaconda "Plus-4" (phosphorized copper) Curved Anodes have been doing a superior job of plating cylinders. Mr. Jack Snyder of the Rotogravure Section says:

"Curved design lets anodes at top of saddle holder slide together by gravity, eliminating submerged arcing.

"Curved design gives better contact–saves electric power.

"Phosphorized anodes corrode very uniformly. There's less scrap.

"Copper build-up in solution has been greatly reduced by phosphorized anodes. Sludging is minimum.

"'Plus-4' plated cylinders have a smoother finish."

Similar reports are coming in from users all over the country. You can start profiting from these advantages in your own plant by calling your Anaconda representative – or write: Anaconda American Brass Company, Waterbury 20, Conn. In Canada: Anaconda American Brass Ltd., New Toronto, Ont. 60103

"PLUS-4"® PHOSPHORIZED COPPER ANODES

ANACONDA®

products of

Anaconda American Brass Company

Investigation on the Silver-Zinc Storage Battery with Radioactive Zn^{65} Isotope

Tivadar Z. Palágyi

Central Research Institute for Chemistry, Hungarian Academy of Sciences, Budapest, Hungary

ABSTRACT

Zn^{65} isotope was deposited electrolytically on the middle negative electrode of silver-zinc storage batteries assembled in three different ways. The path of the dissolved zinc ions could be followed by measuring the radioactivity of the nonlabelled electrodes. In the deteriorated cells all the negative and nearly all the positive plates became contaminated with the isotope. The cycle life was longest with cells assembled tightly and with little electrolyte.

In a previous paper (1) the general results of investigations on the silver-zinc storage batteries with radioactive isotopes were discussed. In the present paper the experiments performed with Zn^{65} isotope and their results are presented.

Experimental

The experiments were carried out with cells of 10 amp-hr nominal capacity. Each cell had 4 positive and 5 negative electrodes wrapped in cellophane separators and mounted parallel to the longer base-edge of the casing. The cells were manufactured in the Institute for Chemical Technology of the Technical University at Budapest. The positive plates were pressed of silver powder and the negative ones of zinc oxide powder, each plate having dimensions of 83 x 35 x 1 mm and silver wire terminals

The electrodes were mounted in a casing made of Lucite plates. Thus, it was possible to open the cells while cycling by removing one of the side plates of the casing and, after measuring the plate activities, to replace the measured plates in the cell casing and to reseal the casing.

The Zn^{65} isotope was deposited electrolytically on the electrodes. The electrolyses were performed in 50 ml of solution having a specific activity of 0.5 μC/ml and containing 13.5 g $ZnCl_2$, 26 g NH_4Cl, and 10 g H_3BO_3 per liter. A Pt anode and a plastic electrolyzing vessel were employed with a current density of 0.167 amp/dm^2 and an electrode distance of 2 cm. The surface of the cathode amounted to 60 cm^2. The zinc electrode was immersed and taken out of the electrolyzing solution under current. The electrolyses were continued until the activity of the deposited Zn^{65} isotope was 10μC. This corresponded to deposition of 0.13 g Zn, requiring 64 min. After electrolysis the electrodes were rinsed with distilled water. The quantity of the deposited isotope as well as the activity of the electrodes was measured by the methods described before (1).

The investigations were performed with three methods of assembling the cells. The electrodes of six cells were assembled in casings of normal dimensions. In addition, six cells were assembled in casings with dimensions larger than the usual; in these cells the quantity of electrolyte was larger than in the normal cells and the electrodes were not fitted as tightly. Third, before putting the electrodes in, plastic plates of dimensions identical with an electrode were put into the casing of eight other test cells. In these cells the quantity of electrolyte was smaller than in the normal cells, and the electrodes were packed in very tightly. When possible, the measurements were carried out simultaneously on cells assembled according to the three different methods.

After putting the electrodes in, covers were put on and sealed with beeswax. Then the cells were filled with 35% KOH electrolyte and connected in series. The first charge was performed with 250 ma for 20 hr. The times of the additional charges were the same, but the current was increased 10% each time. Thus, the nominal capacity was reached after the sixth charging. The cells were discharged individually, with a resistance of 1.5 ohm to an end voltage of 1.0 v.

After formation, the cells were subjected to cyclical charges and discharges. They were connected in series and charged with 0.65 amp for 18 hr, or 12 amp-hr. The discharges were carried out individually through 0.5 ohm, to an end voltage of 1.0 v. Thus, the period of 1 cycle was 1 day. After each tenth cycle, a measuring discharge was performed through 1.5 ohm to an end voltage of 1.5 v.

The cells were considered deteriorated when they could no longer be charged or when the current given during the measuring discharge decreased below 80% of the nominal capacity.

Experimental Results

After the initial 20 cycles three cells were opened from the loosely and three from the normally assembled cells by dismantling the cell cover, pouring out the electrolyte, and removing one of the side plates of the plastic casing. After measuring the plate activities and replacing the electrodes, fresh 35% KOH electrolyte was filled in and the cycling continued. After each additional 20 cycles the opening and examination of the cells was repeated. A different method, described below, was employed for the tightly assembled cells.

The electrodes of cells opened while cycling were dried with filter paper and wrapped in an additional cellophane envelope. The activities were measured by putting a cylindrical GM-tube on both sides of the electrode in such a position that the longitudinal

Table I. Zn^{65} contamination of nonlabelled electrodes as a function of cycle life in loosely assembled cells with one negative electrode labelled with Zn^{65}*

Cell No.	Time of measurement	Activity of electrodes mr/hr corrected for background on the electrode No.							
		negative				positive			
		1	3	7	9	2	4	6	8
1	After 20 cycles	0.06	0.10	0.12	0.05	—	0.04	0.05	—
	After 40 cycles	0.10	0.15	0.18	0.08	0.02	0.07	0.06	0.04
	After 52 cycles	0.12	0.30	0.25	0.10	0.04	0.12	0.15	0.05
2	After 20 cycles	0.02	0.08	0.05	0.02	—	—	—	—
	After 40 cycles	0.05	0.12	0.08	0.04	—	0.04	0.03	—
	After 60 cycles	0.08	0.18	0.12	0.08	0.02	0.08	0.05	0.01
	After 70 cycles	0.12	0.25	0.18	0.15	0.06	0.15	0.08	0.02
3	After 20 cycles	0.01	0.06	0.04	0.02	—	—	—	—
	After 40 cycles	0.04	0.12	0.06	0.03	—	0.03	0.02	—
	After 60 cycles	0.08	0.18	0.12	0.08	0.01	0.04	0.02	—
	After 76 cycles	0.15	0.25	0.20	0.12	0.02	0.10	0.06	0.02
4	After 74 cycles	0.15	0.20	0.25	0.15	0.04	0.08	0.12	0.04
5	After 87 cycles	0.10	0.15	0.20	0.12	0.06	0.12	0.08	0.04
6	After 93 cycles	0.20	0.30	0.35	0.25	0.04	0.06	0.15	0.06

* In each cell electrode No. 5 is labelled with Zn^{65} isotope.

axis of the tube was parallel to the longitudinal center line of the plate. After measurements, the additional cellophane envelopes were removed and the electrodes were replaced in the casing in the same arrangement as before.

The results obtained with the loosely assembled cells are shown in Table I. The failure of cells 1 and 2 was due to the formation of acicular zinc crystals resulting in short circuit, while that of cells 3, 4, 5, and 6 was caused by loss of reversibility of the negative electrode and shedding of the electrolytically active material of the plates. In these cells, all the electrodes were contaminated with radioactive isotope.

The results obtained with the normally assembled cells are shown in Table II. The degree of contamination with isotope of the nonlabelled negative electrodes of the deteriorated cells was about the same as that of the loosely assembled cells, but the positive electrodes were contaminated with isotope to a lesser degree. All the nonlabelled plates except one showed some radioactivity, but the cycle lives of these cells were longer. The cause of failure of cells 8, 9, and 10 was short circuit, while that of cells 7 and 12 was shedding and sludging of the zinc electrodes. In cell 11 the separators of the positive electrodes disintegrated.

On the basis of preliminary experiments, it could be predicted that after opening the tightly assembled cells the electrodes would not be replaceable without the danger of bursting the cell casings. Therefore, one cell only was opened and tested after the 40th cycle and after each further twenty cycles another cell was tested. All the nonlabelled electrodes of these cells were contaminated with isotope. The failure of the tightly assembled cells was caused by the separator, which not only became black as in many of the other cells, but in several places also disintegrated and lost its insulating properties. In cells 18 and 19 the formation of silver

Table II. Zn^{65} contamination of nonlabelled electrodes as a function of cycle life in normally assembled cells with one negative electrode labelled with Zn^{65}*

Cell No.	Time of measurement	Activity of electrodes mr/hr corrected for background on the electrode No.							
		negative				positive			
		1	3	7	9	2	4	6	8
7	After 20 cycles	—	—	—	—	—	—	—	—
	After 40 cycles	0.02	0.08	0.06	0.03	—	—	—	—
	After 60 cycles	0.04	0.12	0.08	0.04	—	0.03	0.02	—
	After 80 cycles	0.05	0.20	0.12	0.05	0.02	0.04	0.04	0.01
	After 86 cycles	0.06	0.25	0.12	0.05	0.03	0.08	0.04	0.01
8	After 20 cycles	—	—	—	—	—	—	—	—
	After 40 cycles	0.01	0.04	0.06	0.03	—	—	—	—
	After 60 cycles	0.06	0.08	0.14	0.08	—	0.01	0.02	—
	After 80 cycles	0.15	0.15	0.25	0.15	—	0.02	0.04	0.01
	After 94 cycles	0.20	0.25	0.35	0.22	0.02	0.08	0.10	0.02
9	After 20 cycles	—	—	—	—	—	—	—	—
	After 40 cycles	—	—	—	—	—	—	—	—
	After 60 cycles	0.03	0.06	0.05	0.02	—	—	—	—
	After 80 cycles	0.08	0.15	0.15	0.10	—	0.02	0.02	—
	After 100 cycles	0.18	0.25	0.25	0.15	—	0.04	0.02	—
	After 102 cycles	0.20	0.25	0.30	0.15	—	0.05	0.10	0.04
10	After 104 cycles	0.15	0.25	0.35	0.30	0.05	0.08	0.12	0.04
11	After 118 cycles	0.15	0.20	0.30	0.30	0.02	0.04	0.06	0.02
12	After 138 cycles	0.20	0.25	0.30	0.15	0.02	0.05	0.08	0.04

* In each cell electrode No. 5 is labelled with Zn^{65} isotope.

Table III. Zn^{65} contamination of nonlabelled electrodes as a function of cycle life in tightly assembled cells with one negative electrode labelled with Zn^{65}*

Cell No.	Time of measurement	Activity of electrodes mr/hr corrected for background on the electrode No.							
		negative				positive			
		1	3	7	9	2	4	6	8
13	After 40 cycles	—	0.05	0.08	—	—	—	—	—
14	After 60 cycles	0.08	0.15	0.20	0.15	—	—	—	—
15	After 80 cycles	0.20	0.25	0.15	0.10	—	0.02	0.06	—
16	After 100 cycles	0.25	0.35	0.25	0.20	0.01	0.06	0.04	0.02
17	After 120 cycles	0.10	0.20	0.15	0.10	0.02	0.08	0.04	0.02
18	After 114 cycles	0.20	0.30	0.30	0.20	0.04	0.08	0.04	0.02
19	After 126 cycles	0.25	0.30	0.25	0.15	0.06	0.10	0.06	0.04
20	After 143 cycles	0.20	0.25	0.15	0.10	0.04	0.06	0.04	0.01

* In each cell electrode No. 5 is labelled with Zn^{65} isotope.

"trees" could be observed. The results obtained with the tightly assembled cells are shown in Table III.

Conclusions

From these experiments it can be seen that it is possible to follow the path of dissolved zinc ions while cycling the cells. The Zn^{65} ions reached all the nonlabelled negative plates in every cell. The two positive plates next to the labelled negative were contaminated with isotope in each deteriorated cell, and the radioactive ions reached also the external silver electrodes in all cells but one. In the tightly and normally assembled cells, in spite of the longer cycle life, the positive plates were contaminated with the isotope to a lesser degree than in the loosely assembled cells. This proves that from the point of view of reversibility of the negative electrode, it is advisable to build in the electrodes tightly and with little electrolyte, thus reducing migration of the zinc ions and formation of acicular zinc crystals. Furthermore, the failure of the cells can be followed on the basis of the degree of contamination of the nonlabelled plates with the isotope. The breakdown of the loosely assembled cells was generally caused by shedding and sludging of the zinc electrode as well as by the formation of acicular zinc crystals. The failure of the tightly assembled cells was induced largely by failure of the separator, dissolution of the silver oxide from the positive electrode plus migration to the negative electrode, and formation of zinc trees causing direct short circuit.

Manuscript received April 21, 1960; revised manuscript received Sept. 19, 1960.

Any discussion of this paper will appear in a Discussion Section to be published in the December 1961 JOURNAL.

REFERENCE

1. T. Z. Palágyi, *This Journal*, **106**, 846 (1959).

The Effect of Metallic Cations on the Corrosion of Iron and Tin in Boiling Acids

W. Roger Buck, III, and Henry Leidheiser, Jr.

Virginia Institute for Scientific Research, Richmond, Virginia

ABSTRACT

In the presence of metallic cations in both boiling 0.2M citric acid and 2M HCl the rate of corrosion of tin was apparently determined solely by the cathodic hydrogen evolution reaction. The corrosion potential *vs.* log corrosion rate curves obtained for iron in 0.2M citric acid in the presence of various cations were complex, and 5 types of behavior were observed: (*a*) activation of the cathodic reaction, such as obtained with nickel, rhodium, ruthenium, iridium, and platinum; (*b*) activation of the anodic reaction such as observed with antimony and by bubbling oxygen through the solution; (*c*) inhibition of the anodic reaction such as observed with tin, lead, and indium; (*d*) inhibition of the cathodic reaction such as observed with mercury and cadmium; and (*e*) inhibition of both the anodic and cathodic reactions such as observed with arsenic. Effective inhibition of corrosion of iron in contact with tin in 0.2M citric acid was only obtained under conditions where the Sn(II) ions came in contact with the iron surface.

The ultimate purpose of this investigation is an understanding of the galvanic couple between iron and tin in acid solution. Previous phases of the continuing study have been concerned with the corrosion of Fe single crystals in the presence of tin ions (1), and a general survey of the effect of metallic cations on the corrosion of 15 metals (2, 3). The present report represents an extension of these studies.

It is well known that small amounts of dissolved Sn have an inhibiting effect on the corrosion of Fe in fruit acids (4-6). Koehler's (7) potential meas-

urements suggest that this inhibition is effective because of interference with the anodic reaction. The present study was carried out with the objective of getting a better understanding of how foreign metallic cations in general influence the corrosion of Fe and Sn. The topics covered include: effect of metallic cations on the corrosion of Sn in boiling 0.2M citric acid and 2M HCl; effect of metallic cations on the corrosion of Fe in boiling 0.2M citric acid; and potential studies on the Fe-Sn system.

Experimental Method

The corrosion samples were machined in the form of ¼ or ⅜ in. cylinders with a threaded hole in one end. After etching and weighing, the sample was screwed onto a threaded metal rod which passed through a Teflon holder, 5 in. in length. The end of the specimen was sealed against the end of the Teflon holder by tightening a locking nut at the top of the Teflon assembly. Since the Teflon had a higher coefficient of expansion than the threaded rod, a liquid-tight seal formed at the sample-Teflon boundary when the assembly was inserted in the boiling solution. Potential measurements of individual specimens, or of two metals coupled together externally, were made against a saturated calomel electrode (S.C.E.) in a second vessel kept at room temperature and bridged to the boiling flask by a capillary tube. Three different types of reaction vessels were used. In one vessel the metallic cations which were formed during the corrosion process freely bathed both electrodes. In a second-type vessel the electrodes were protected from the cations of the other metal by means of an inner compartment which made electrical contact with the body of the solution through a fritted glass disk. In a third-type vessel both electrodes were protected from the cations of the other metal by means of two inner compartments.

The corrosion specimens were degreased and heavily etched to remove the strain introduced by machining to shape. A final light etch was given in the solution of the same composition as that used in the test, followed by thorough washing in distilled water and storage in a desiccator. Corrosion rates were determined by weight loss over the period of the experiment. Iron was obtained from the Vacuum Metals Corporation as ½ in. rods under the trade name Ferrovac-E, purity 99.92%, and tin was obtained from the Vulcan Detinning Company as 1-lb sticks, purity 99.998%.

Results

Corrosion of tin in boiling 2M HCl in the presence of foreign metallic cations.—Tin cylinders exposing surface areas of approximately 2.5 cm^2 were corroded for periods of time ranging from ½ to 2 hr. In the majority of the experiments the foreign cations were added to a concentration of 0.001M, but in a few experiments, such as with iridium, the concentration of the cation was varied. In all cases the foreign metal was added to the acid as the chloride. The curve drawn in Fig. 1 represents the best line through all data points, although many

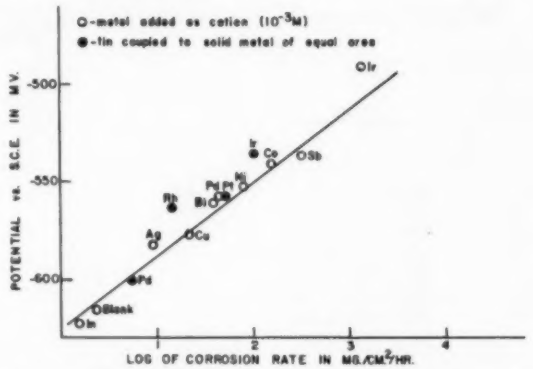

Fig. 1. Plot of the potential of a Sn cylinder in boiling 2M HCl vs. the logarithm of the corrosion rate.

points are omitted from the drawing because they occur very close to the plotted points. The solid circles plotted in Fig. 1 represent results from a recent investigation (8) in which cylinders of Sn were coupled externally to cylinders of the platinum metals of equal surface area in boiling 2M HCl. It will be noted that the best straight line drawn through these four points would be approximately parallel to the line drawn in the figure. Two experiments were run with the nitrate ion when present in concentrations of 0.1 and 0.01M. These values fell on the curve.

Corrosion of tin in boiling 0.2M citric acid in the presence of foreign metallic cations.—The results of a series of experiments run for 24 hr are summarized in Fig. 2. For reasons unknown, the results obtained with added Ni and Co were not reproducible. Part of the difficulties of reproducibility may be attributed to the fact that the corrosion of Sn in citric acid is low. Differences in stress in the metal and in the surface at the start of the experiment may have an important influence under such conditions.

Corrosion of iron in boiling 0.2M citric acid in the presence of added cations.—The experiments with the cations were carried out at an added cation concentration of 0.001M with the exception of Sn, in which case concentrations as low as 10^{-6}M were used.

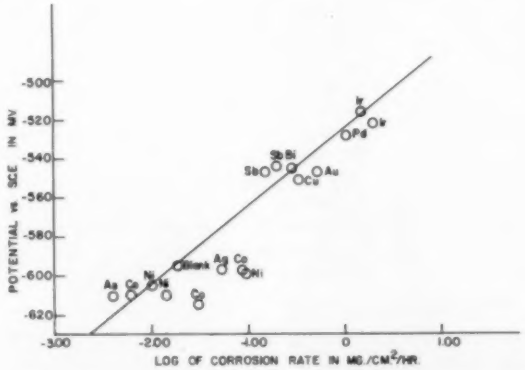

Fig. 2. Plot of the potential of a Sn cylinder in boiling 0.2M citric acid vs. the logarithm of the corrosion rate for experiments in which metallic cations were added to the acid.

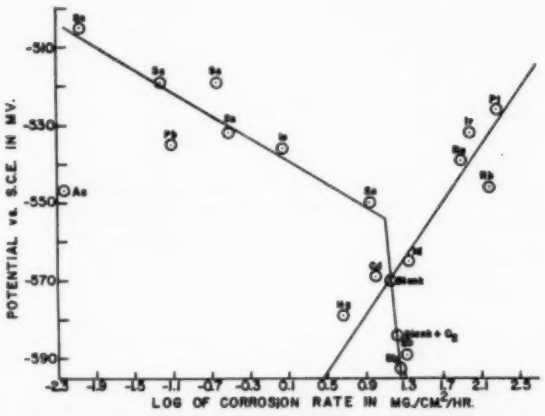

Fig. 3. Plot of the potential of an Fe cylinder in boiling 0.2M citric acid vs. the logarithm of the corrosion rate for experiments in which metallic cations were added to the acid.

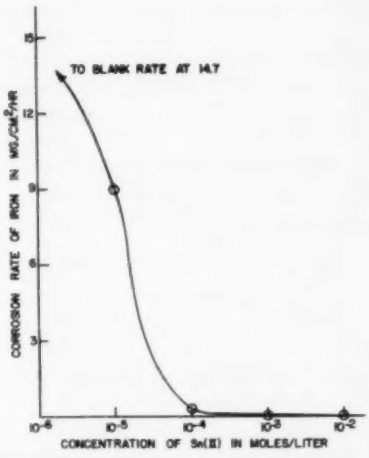

Fig. 4. Rate of corrosion of Ferrovac-E Fe in boiling 0.2M citric acid in the presence of various concentrations of Sn(II).

During the 24-hr corrosion test with As as an additive the Fe sample lost only 0.0005 g, and the potential behaved very erratically. The electrode was polarized very readily during the process of making potential measurements so meaningful numbers were difficult to obtain. Plots of the potential *vs.* corrosion rate are given in Fig. 3. Since the potential was essentially constant during the experiment, the curves drawn represent a best estimate of: (*a*) anodic polarization curve of Fe, (*b*) cathodic polarization curve of Fe in the presence of dissolved Sn (upper left segment), and (*c*) cathodic polarization curve of Fe in the absence, or presence in very low concentration, of anodic inhibitors. Ample evidence exists from experiments in progress that the curves are reasonable as drawn.

Rates of corrosion in the absence of foreign metallic cations.—Although potential and corrosion experiments have been carried out on the Sn-Fe system by workers in the past, no one appears to have segregated effects due to coupling of the two dissimilar metals and effects due to the exposure of the corroding metals to the cations of the second metal. A series of experiments is described here which shows very clearly that good corrosion inhibition of uncoated Fe by contact with Sn only occurs when the Fe is bathed by Sn ions. The experiments leading to this conclusion are described separately, and the essential facts are summarized in Table I.

Table I. Summary of experiments carried out to test the importance of external coupling of Fe and Sn and of exposure of the metals to cations of the second metal in boiling 0.2M citric acid

	Rate of corrosion, mg/cm²/hr	
	Fe	Sn
In absence of foreign metallic cations	14.7	0.018
In presence of 0.001M cations of other metal	0.062	0.018
Coupled externally, both metals freely bathed by cations of other metal. No metallic cations present initially	0.83	0.30
Coupled externally, metals protected from exposure to cations of other metal	10.0	0.27

Iron corroded vigorously in boiling 0.2M citric acid at a rate of 14.7 mg/cm²/hr. Under the same conditions Sn corroded comparatively slowly at a rate of 0.018 mg/cm²/hr.

Rates of corrosion in the presence of cations of the second metal.—As described in a previous publication (3), the corrosion of Fe in citric acid is greatly inhibited when Sn ions are present in solution, and the rate becomes very low when the concentration of Sn(II) exceeds 10^{-4}M. The experiments reported in Fig. 4 agree in essentials with those (3) for an Armco iron with a slightly lower blank rate. In the present series of experiments the rate of corrosion of Fe in the presence of 10^{-3}M Sn(II) was 0.062 mg/cm²/hr. Although no extensive quantitative study was made, it was observed that Sn(IV) ions also were effective in reducing the corrosion of Fe. Under the reducing and anaerobic conditions existing in these experiments it would be expected that Sn(IV) would be converted to Sn(II), however.

The potential of an Fe sample in boiling 0.2M citric acid became more noble as increasing amounts of Sn(II) were added. A summary of the experiments showing the rate of corrosion as a function of the potential of the Fe in the presence of different concentrations of Sn(II) is included in the data given in Fig. 3.

So far as could be determined, Fe(II) ions had no influence on the rate of corrosion of Sn in the boiling acid.

Rate of corrosion of externally coupled specimens when cations of each metal freely bathe the second metal.—The potential of the Fe, the Sn, and the couple were measured often during the experiment. The two metals were coupled externally except during the measurements, when uncoupling was essential. As shown in Fig. 5 the potential of Fe

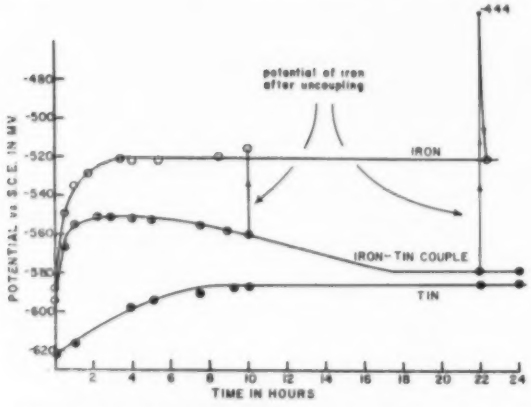

Fig. 5. Potential measurements on Fe, Sn and the Fe-Sn couple in boiling 0.2M citric acid under conditions where the ions formed during corrosion freely bathe each electrode.

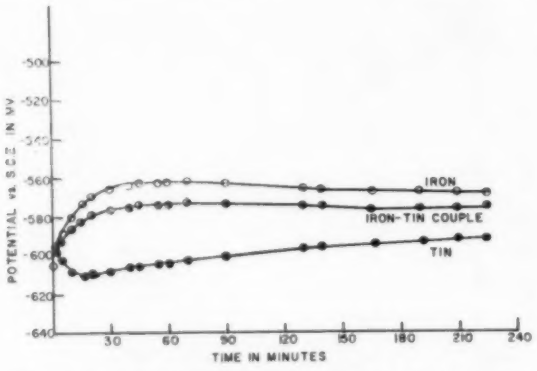

Fig. 6. Potential measurements on Fe, Sn and the Fe-Sn couple in boiling 0.2M citric acid under conditions where the ions formed during corrosion are prevented from contacting the other electrode.

achieved an approximately constant value of −520 mv at the end of 3 hr at which time apparently the Fe(II) ion concentration became significant and the Sn ion concentration had become sufficient to control the potential. The potential of the couple reached a maximum after approximately 3 hr and then became more negative with time as the couple became more and more polarized to the potential of that of Sn. The Sn potential became more noble during the first 10 hr as the Sn(II) concentration increased. Apparently after approximately 10 hr, the Fe electrode was sufficiently polarized so that no appreciable sacrificial corrosion of Sn occurred and the Sn(II) concentration remained approximately constant. For comparison purposes the potentials of Sn and Fe corroding singly under the same experimental conditions were −616 and −573 mv, respectively, after 10 hr of exposure to the acid. The Fe potential remained approximately constant at −575 to −570 mv during the majority of the experiment, and the Sn potential increased from a low of −625 mv to a high of −605 mv during the 24 hr period.

Perhaps the most interesting feature of these experiments was the big change in potential of the Fe sample observed near the end of the experiment (Fig. 5) when the two metals were uncoupled. In the representative experiment plotted, the potential changed from that of the couple at −577 mv to a more noble value of −444 mv during a period of 2 min and then returned to that characteristic of Fe in the presence of 10^{-3}M Sn(II) at −520 mv over a period of 30 min. Koehler (7) observed this same phenomenon previously under experimental conditions similar to those used in this study, except at a lower temperature. In Koehler's experiments the time taken to drift back to a constant potential was much longer than observed in these studies, but perhaps the difference in temperature accounts for this difference.

Rate of corrosion of externally coupled specimens when cations of the one metal are prevented from coming in contact with the second metal.—The Sn and Fe samples were exposed to the acid within individual chambers which made electrical contact with the body of the solution through fritted glass disks. Since ions of one metal had to diffuse through one or two fritted glass disks to reach the second metal, the two metals were essentially protected from the ions of the other metal. In order to make these experiments comparable to those shown in Fig. 5, the time of experiment was reduced appreciably. The volume of solution within each of the chambers was so much less that the metallic ion concentration built up much more rapidly.

Potential measurements made during these experiments are summarized in Fig. 6. The results were different in three ways from those described in the previous section: (*A*) the potential of the Fe was −570 mv in the absence of Sn (II) *vs.* −520 mv in the presence of 10^{-3}M Sn(II). (*B*) The potential of the couple during the entire experiment was closer to that of Fe than that of Sn. (*C*) There was no shift in the potential of the Fe on uncoupling.

The corrosion of Fe in these experiments was reduced slightly to 10.0 mg/cm²/hr and the rate of corrosion of tin was increased to 0.27 mg/cm²/hr over the uncoupled values of 14.7 and 0.018 mg/cm²/hr, respectively. Part of the reduction in Fe corrosion may have resulted from the decrease in hydrogen ion concentration during the experiment because of the small solution volume within the fritted disk chamber.

Discussion

In the case of Sn, the shape of the log corrosion rate *vs.* corrosion potential curve was the same in both 2M HCl and 0.2M citric acid as shown in Fig. 1 and 2. In HCl the slope of the curve was 37 mv and in citric acid 38 mv. In both cases the cations of metals exhibiting low hydrogen overvoltages were most active in increasing the corrosion rate, and metals of high or moderate hydrogen overvoltage had an inhibiting or an inappreciable effect. It appears that the best straight line drawn through the experimental points describes the anodic polarization curve of Sn in these two media. It is not possible to say this with certainty, however, since it is

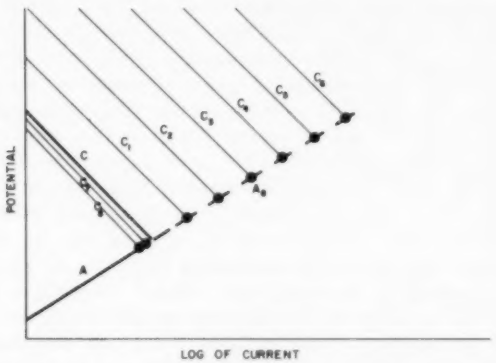

Fig. 7. Schematic diagram showing the probable manner in which the data of Fig. 1 and 2 represent an extension of the anodic polarization curve of Sn. C is the cathodic polarization curve, A is the anodic polarization curve, A_e is the experimentally determined curve, and C_1, C_2, C_3, etc., represent the cathodic polarization curve as the cathodic current is changed by experimental conditions.

not known whether the anodic surface area of exposed Sn remains constant as cations are added which deposit on the Sn surface and presumably occupy some of the available surface sites. Evidence given below, however, supports the assumption that the anodic surface area of the tin remains constant within rather broad limits.

A schematic diagram is given in Fig. 7 describing the probable manner in which the data of Fig. 1 and 2 represent the anodic polarization curves of tin. The bold lines *C* and *A* represent the assumed cathodic and anodic polarization curves of Sn and A_e represents the experimental curve shown in Fig. 1 and 2. As the foreign metals plate out on the Sn surface, they participate in the cathodic reaction. If the hydrogen overvoltage of the foreign metal is less than that of Sn, the hydrogen evolution reaction can proceed at a higher rate and the cathodic polarization curve (plotted as a function of the logarithm of current and not current density) moves in the direction of C_1, C_2, C_3, etc. If the surface area of the Sn can indeed be assumed to remain approximately constant, the intersection of the various cathodic polarization curves with the extension of the anodic polarization curve yields the experimental curve.

In a previous study (8, 9) the corrosion rates and potentials were determined for a number of metals when coupled singly to Ir, Pt, Rh, and Pd cylinders of equal surface area in boiling 2M HCl. The results obtained for tin are the solid circles of Fig. 1. It will be noted that a line could be drawn through these four points approximately parallel to the straight line shown. Experiments in progress on other systems confirm that, in cases in which the metals are coupled to inert solid metals, results are obtained which fall on approximately the same experimental curve obtained from experiments in which cations are added to the acid. Since the apparent surface area of the Sn was constant in these experiments, the parallelness of the two lines is evidence that the apparent anodic surface area of the Sn was approximately constant in the experiments carried out with cations.

Stern's analysis (10) shows that big changes in the corrosion potential and the corrosion current with small change in the anode area only occur when the anode area fraction is very large or very small. His analysis indicates, for a hypothetical case, that the corrosion potential changes from −0.14 to −0.11 v as the fraction of anodic area changes from 0.7 to 0.3.

It is interesting to point out here, that the slope (Tafel slope) of the curve of potential *vs.* logarithm of corrosion rate for Pb, when coupled to Ir, Pt, Rh, and Pd cylinders of equal surface area, is 36 mv, approximately the same as that for Sn in citric and hydrochloric acids and for Fe in citric acid. A slope of 37 mv corresponds to 2.303 $RT/2F$ in these experiments at the boiling point. Studies are now underway to determine how general this slope is in different acids and with different metals.

Under the conditions used in the experiments summarized in Fig. 1 and 2 it appears clear that the dissolution of Sn is under purely cathodic control. If a low rate of Sn corrosion is desired, contaminants which catalyze the hydrogen evolution reaction or compounds which can assimilate hydrogen, such as oxidizing agents, should be avoided. The relative effects of the metallic cations in accelerating the corrosion of tin in 0.2M citric acid and 2M HCl are shown in Table II. The only serious difference in the two acids was the ineffectiveness of Ni and Co in accelerating the corrosion rate in citric acid and their great effectiveness in HCl. The explanation for this may possibly be found in the manner in which these metals are bound in citrate complexes and their consequent low tendency to exist in the free metallic state in this medium.

As shown in Fig. 3 the log corrosion rate *vs.* the corrosion potential curve for Fe in citric acid is rather complex. Five different types of behavior can be recognized: (*a*) acceleration of the cathodic reaction, such as obtained with Ni, Rh, Ru, Ir, and Pt; (*b*) acceleration of the anodic reaction such as observed with Sb and by bubbling oxygen through the solution; (*c*) inhibition of the cathodic reaction such as observed with Hg and Cd; (*d*) inhibition of the anodic reaction such as observed with Sn, Pb, and In; and (*e*) inhibition of both the anodic and cathodic reactions such as observed with As.

Table II. Relative effects of cations in accelerating the corrosion rate of Sn in boiling 0.2M citric acid and 2M HCl when present at an original concentration of 0.001M

Avg rate relative to blank in 0.2M citric acid	Avg rate relative to blank in 2M HCl
As(III)—0.22	Ag(I)—3
Ni(II)—2(?)	Cu(II)—8
Co(II)—2(?)	Au(III)—9
Ag(I)—3	Bi(III)—13
Sb(III)—10	Pd(II)—16
Bi(III)—16	Ni(II)—29
Cu(II)—18	Co(II)—56
Au(III)—29	Sb(III)—115
Pd(II)—61	Ir(III)—480
Ir(III)—100	

The diagram shown in Fig. 3 for the effect of the various cations on the potential and corrosion rate of Fe is not capable of adequate interpretation without considerable additional data. Chief among the missing pieces of information are the anodic and cathodic polarization curves for Fe under the conditions used in these experiments. From studies in other acids it appears that the anodic curve with numerical slope of 36 mv is the anodic polarization curve of Fe. The left segment of the cathodic curve with numerical slope of 18 mv does not appear to correspond to the cathodic polarization curve of Fe in acid solution. This low value of the slope may mean that the cathodic reaction is other than hydrogen evolution and may correspond to a more complex cathodic reaction.

Corrosion inhibition has been studied in four systems: the inhibition of iron corrosion by Sn and Pb as reported herein and the inhibition of Ni and Co corrosion by Cu (11). The five key features which these systems had in common were the following: (*A*) The metal acting as the inhibitor exhibited a low corrosion rate in the acid; (*B*) The metal acting as the inhibitor had a higher hydrogen overvoltage than the corroding metal; (*C*) The corroding metal and the inhibiting metal, when immersed singly in the acids, exhibited corrosion potentials at low metal ion concentrations which differed by 10-30 mv; (*D*) In the presence of cations of the inhibiting metal, the inhibiting metal was anodic to the corroding metal; (*E*) As judged by the naked eye and by microscopic examination, little or no deposit of the inhibiting metal was observed on the surface in intervals of several hours or more.

The following explanation for the observed inhibition is proposed. Since the inhibiting metal is present at the start of the experiment as a dissolved species, it is freely available to the entire surface and the region where reaction occurs is determined by local conditions. The potential relationships are such that the inhibiting metal has a higher preference relative to the corroding metal for the aqueous phase. It will thus assume a position as a free atom on the surface at those regions where electron exchange takes place most readily. Such positions would be expected to be those in which the surface atoms have the fewest number of neighbors; kink sites are an example in point. Clumps of atoms might be expected to form in the vicinity of such active sites in much the same way as the beautiful experiments of Bassett (12) have demonstrated for Au on NaCl. It would be expected that if the active sites were immobilized, the dissolution of Fe, for example, would be greatly inhibited. On the other hand, since the inhibiting metal in all cases has a higher hydrogen overvoltage than the corroding metal, it can also be inferred that the activity of the surface for the cathodic hydrogen evolution reaction would not be increased. Inhibition of the anodic reaction would not, therefore, be counteracted by activation of the cathodic reaction.

Acknowledgment

Grateful acknowledgment is given for the support of this research by the United States Steel Corporation.

Manuscript received Feb. 23, 1960; revised manuscript received Oct. 8, 1960. This paper was presented at the Southeastern Regional Meeting of the American Chemical Society, Richmond, Va., Nov. 6, 1959.

Any discussion of this paper will appear in a Discussion Section to be published in the December 1961 JOURNAL.

REFERENCES

1. W. Roger Buck, III, and Henry Leidheiser, Jr., *This Journal*, **104**, 474 (1957).
2. W. Roger Buck, III, and Henry Leidheiser, Jr., *Corrosion*, **14**, 308 (1958).
3. W. Roger Buck, III, and Henry Leidheiser, Jr., *Z. Elektrochem.*, **62**, 690 (1958).
4. R. M. Lueck and H. T. Blair, *Trans. Electrochem. Soc.*, **54**, 257 (1928).
5. E. F. Kohman and N. H. Sanborn, *Ind. Eng. Chem.*, **20**, 1373 (1928).
6. T. P. Hoar, *Trans. Faraday Soc.*, **30**, 472 (1934).
7. E. L. Koehler, *This Journal*, **103**, 486 (1956).
8. W. Roger Buck, III, and Henry Leidheiser, Jr., Paper (Abstract No. 68) presented at the Ottawa Meeting, Electrochemical Society, Oct. 2, 1958.
9. W. Roger Buck, III, and Henry Leidheiser, Jr., *Nature*, **181**, 1681 (1958).
10. M. Stern, *Corrosion*, **4**, 329 (1958).
11. Unpublished experiments.
12. G. A. Bassett, *Phil. Mag.*, **3**, 1042 (1958).

Effects of Anions on the Dissolution Kinetics of Metals

Ja. M. Kolotyrkin

Karpov Institute of Physical Chemistry, Moscow, U.S.S.R.

ABSTRACT

In acidic solutions Cl^-, Br^-, and I^- ions increase the true anodic dissolution rate of cadmium and of indium amalgam considerably. This is accounted for by the direct participation of these ions in elementary processes of ionizing metal atoms. The chemoadsorptive interaction of halide ions with surface atoms of a metal takes place at potentials much more negative than the dissolution potential of the metal. The extent of "filling" the surface with adsorbed anions increases considerably with shift of potential to more positive values. Some concepts are developed about the mechanism of dissolution of metal with direct participation of the solution components. These concepts explain both the dissolution rate acceleration by ions that specifically adsorb and the passivation of a metal surface by adsorbed oxygen from water.

The mechanism of formation and development of pits on the surface of a corroded metal has been considered, zirconium dissolution in chloride, bromide, and iodide solutions being an example. It is postulated that a necessary condition for formation of pits is a greater affinity of the corroded metal for oxygen than for the attacking anion and that formation of pits is a result of the substituted adsorption of halide ions for passivating oxygen at certain sites on the metal surface.

The dissolution of metals in electrolytic solutions is, by its nature, an electrochemical process, and its rate depends not only on the usual variables of chemical kinetics, concentration and temperature, but also on these electrochemical parameters of the system and, first and foremost, on the electrode potential and the structure of the electric double layer at the metal-solution boundary.

According to the laws of electrochemical kinetics, the dependence of the dissolution rate on the potential, in the simplest case, can be expressed by

$$i_1 = K_1 \cdot \exp(\beta F/RT\,\phi) \qquad [1]$$

where i_1 is the dissolution rate in terms of electric current, ϕ is the electrode potential, β is the transfer coefficient, and K_1 is a constant depending on the metal and its surface condition.

Equation [1] holds for a process which can be expressed generally by

$$Me \rightarrow Me^{+n} + ne \qquad [2]$$

In the case of the spontaneous dissolution of metal in acid, reaction [2] is accompanied by simultaneous cathodic hydrogen evolution

$$2H^+ + 2e \rightarrow H_2 \qquad [3]$$

the kinetics of which can be expressed by

$$i_2 = K_2 [H^+] \cdot \exp(-\alpha F/RT\,\phi) \qquad [4]$$

Combining [1] and [4], the dependence of the spontaneous dissolution rate of the metal on the acid concentration is given by the equation

$$V = K_3 [H^+]^{\beta/\alpha+\beta} \qquad [5]$$

which, in a number of cases, is borne out by experiments (1-3).

Anjon concentration and dissolution rates.— There are, however, many cases when the dissolution rate of metals in acid solutions depends not only on the concentration of hydrogen ions directly participating in the process, but also on the nature and concentration of anions which, at first sight, do not seem to take part.

Recent research in this laboratory has shown that changes in the anion composition can influence both the cathodic (hydrogen evolution) (4-7) and the anodic processes (8, 9).

The influence of anions on the anodic process is connected frequently with their action on the state of the passivating phase film, *i.e.*, on the diffusion barrier. In recent years, however, evidence has accumulated which indicates that the anions contribute directly to the discharge reactions and to the formation of metallic ions (8-14).

In an investigation (8) of the effect of halide salts on the electrochemical behavior of Cd in acid solutions, it was established that the dependence of the rate of anodic dissolution of the metal on the potential is characterized by a Tafel line with a slope of 0.035 v, which makes the constant β equal to 1.66 (if $\alpha + \beta = 2$). The position of the curve depends largely on the type and concentration of the halide salt. Figure 1 shows the dependence of the dissolution rate on KI concentration at a given potential. This shows that at some critical salt concentration ($0.1N$) a tenfold increase is accompanied by a 10^3-fold increase in the rate of the anodic process. Similar dependences have also been obtained with bromide and chloride solutions, the difference being that the transition from I^- to Br^- and to Cl^- was accompanied by an increase in the critical concentration of the added salt.

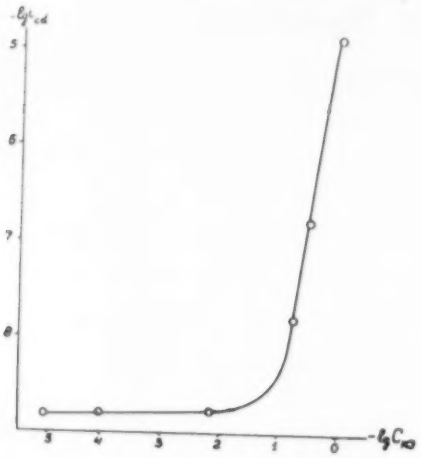

Fig. 1. Dependence of the cadmium dissolution rate at a constant potential on concentration of KI in a 1.0N H_2SO_4 solution.

Similar results were reported recently by Losev and Molodov (9) who investigated the influence of the anion type and its concentration on the process of anodic dissolution of indium amalgam. In this case, radioactive indicators were used to determine both the value of the exchange current between the amalgam and the solution of the indium salt at corresponding equilibrium potentials, and the rate of the true anodic process of the dissolution of indium at different potentials close to equilibrium. This method combined with the conventional polarization measurements made it possible for them to study the kinetics of the anodic reaction as well.

The results of the measurements showed that the dependence of the rate of the anodic process on the potential was again characterized by a Tafel line with a slope of 0.025 v. The slope and, consequently, the transfer coefficient β equal to 2.3 $RT/\beta_a F = 2.32$ (if $\alpha + \beta = 3$) remained unchanged even though the halide salt and its concentration were changed. Changes in anion composition, however, led to changes in the overvoltage. Figure 2 shows the dependence of the rate of the anodic reaction on the halide salt concentration at a given potential (−0.330 v for Cl^- and 0.276 v for Br^- and I^-).

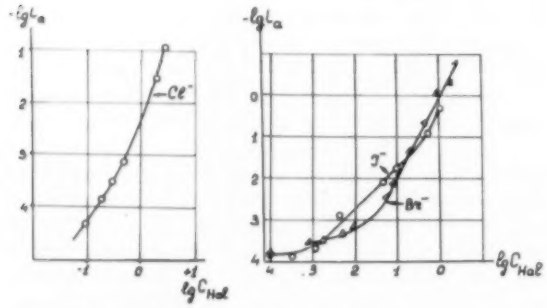

Fig. 2. Dependence of the dissolution rate at indium amalgam at constant potential on concentration of NaCl, NaBr, and NaI in solution of 0.01N $In(ClO_4)_3$ + 0.01N $HClO_4$.

The critical concentration becomes noticeably greater in the order I^- to Br^-, Cl^-, and equals 2×10^{-3}, 5×10^{-2}, and $5 \times 10^{-1}N$, respectively. A further tenfold increase in salt concentration causes the dissolution rate of the amalgam to increase almost 10 times in the case of iodide, 100 times in the case of bromide, and 1000 times in the case of chloride.

From these results it can be concluded that in the cases under consideration the dissolution of metals occurs with the direct participation of halide ions and, consequently, the kinetics of these reactions at constant pH may be expressed as follows

$$i_a = K \cdot C^{\delta} \cdot \exp(\beta F/RT\,\phi) \qquad [6]$$

where C is the halide salt concentration, δ is a constant equal to 3 for cadmium dissolution reaction in the presence of I^- ions, and 1, 2, and 3, respectively, for the dissolution of the indium amalgam in iodide, bromide, and chloride solutions.

Ion adsorption.—To understand the mechanism of the stimulating action of halide ions on the anodic dissolution of some metals, the results obtained recently with a silver electrode are of interest (3). A noticeable decrease was observed in the anodic process overvoltage when going from sulfuric acid alone to a solution containing KI. Using tracer methods (I^{131}), the adsorption of iodine ions on the electrode surface was investigated at different potentials. In preliminary experiments it was established that iodine ions are very strongly adsorbed on the silver surface. This fact enables us to make adsorption measurements on smooth electrodes using low initial concentrations of KI in the solutions (10^{-6} — 10^{-3} g eq./l).

The measurements showed that the chemico-adsorptional interaction between iodine ions and the surface atoms of silver takes place at more negative potentials than those of the metal dissolution. Both the degree of coverage by the adsorbed ions and the strength of the bonds of these ions with the surface metallic atoms becomes greater as the potential increases. Figure 3 shows a linear relationship between the quantity of adsorbed ions and the potential. Assuming that this dependence is true for extremely small coverages, the results lead to the

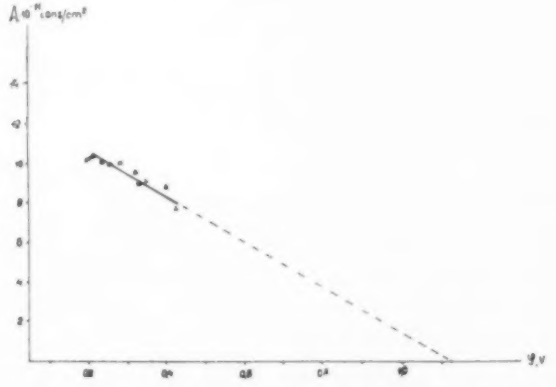

Fig. 3. Dependence of the amount of iodide ion (A x 10^{14}) adsorption on 1 cm^2 of silver electrode surface on potential in 1N H_2SO_4 + 2.6 x 10^{-6}N KI solution.

conclusion that at 2.6 x 10^{-6} g eq./l this interaction begins at a potential of 1.15 v, which is almost 1.5 v more negative than the corresponding dissolution potential of silver.

It is important to note that in this case the adsorption is reversible in the sense that at a certain KI concentration the number of adsorbed I^- ions has only one meaning for a given potential: the transition toward a more negative potential always leads to a desorption of a certain number of ions.

The existence of the effect of strengthening the adsorption bond with the potential is borne out by the results obtained when investigating the dependence of the I^- desorption rate on the potential of the preliminary polarization of the electrode. Our experiments being conducted in solutions having extremely low KI concentration, it was easy to reach the potential at which the iodine ions from solution were adsorbed completely. At different potentials having a greater value, the degree of surface coverage remained the same.

The results of one of these experiments are given in Fig. 4. Curves 1 and 2 characterize the desorption rate of iodine ions at a potential of −0.355 v after the preliminary polarization of silver at potentials of −0.174 v and −0.124 v, respectively. Both of these corresponded to the same surface coverage amounting to 16.9 x 10^{11} ions/cm^2. As is seen from Fig. 4, shift of the preliminary polarization potential toward positive values led to considerable slowing down of desorption. Thus, for example, the desorption of 3 x 10^{10} I^-/cm^2 took 27 min in the first case and as much as 110 min in the second.

From these results it can be concluded that the specific adsorption of anions beginning at far more negative values of the potential than that of electrode dissolution should be regarded as the beginning of the formation of the corresponding salt (as a result of covalent bonds). But at the early stage of adsorption there is a noticeable difference in the strength of the bond and that of the corresponding salt. As the potential shifts toward positive values, the difference becomes smaller and eventually disappears altogether. Starting from this potential, the metal ions begin passing into solution as complexes with adsorbed anions.

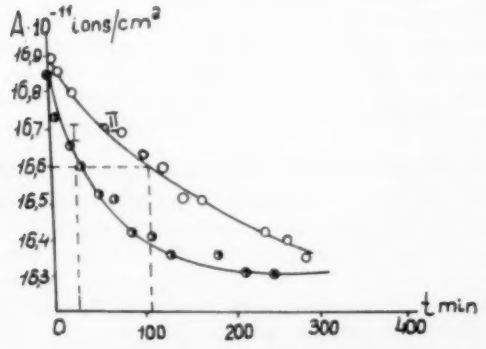

Fig. 4. Dependence of the desorption rate of iodide ions at potential —0.335 v on the preliminary polarization potential (—0.174, curve 1; —0.124, curve 2).

Evidently the dissolution mechanism can be expressed in the form of two consecutive reactions

$$Me + \delta\Gamma^- \rightarrow Me\,\Gamma_\delta^{-\delta} \qquad [7']$$

$$Me\,\Gamma_\delta^{-\delta} \rightarrow Me\,\Gamma_\delta^{+(n-\delta)} + ne \qquad [7]$$

The first corresponds to the specific adsorption of the anion on the metal surface with the formation of a complex, and the second represents the ionization of a metallic atom forming part of this complex.

The ψ potential.—In explaining the mechanism of the influence of anions on the kinetics of electrode processes, one should bear in mind the change in the structure of the electric double layer as a result of the adsorption of anions and the appearance of the negative ψ_1 potential at the metal-solution boundary. An analysis shows that, if these factors alone are taken into consideration, there is no satisfactory explanation for much of the experimental data available at present. It is obvious, in particular, that a change in the ψ_1 potential should result in the same changes in the rates of the direct (anodic) and reverse (cathodic) reactions and, consequently, to a change in the exchange current (i_0). However, as was shown in the work cited above (9), such a parallelism is not observed. Thus, for instance, it was shown that an increase in chloride concentration up to 0.5*N*, which is accompanied by a noticeable increase in the dissolution rate of indium amalgam, does not result in an increase of the exchange current, which remains the same as in the initial solution of $NaClO_4$ (without additions of NaCl).

From the data available at present the conclusion can be drawn that the direct participation of the solution components in the elementary act of ionization of metallic atoms appears to be an inevitable stage in these processes. It is natural that the components possessing the greatest chemical affinity for the electrode metal are the ones which take part predominantly in the process. Losev showed, for instance, that such a part could be played not only by specifically adsorbed anions, but also by molecules of water. It was established by these experiments that the rate of anodic dissolution of indium amalgam in the acidified concentrated solution of perchlorates, which are not known to display any trend to specific adsorption, decreases as the concentration of free water in the solution becomes less. These results seem to show that the hydration of the metallic ions, at least in part, takes place before its transition from the metallic lattice into the solution.

Postulate of anion effect.—It follows from the above that the stimulating influence of a certain anion on the anodic dissolution process is manifested only after a certain critical potential has been reached at which the strength of the covalent bond between the surface atom of the metal and adsorbed ion equals the covalent bond strength in the corresponding individual compound. Evidently the different anions must have different values of critical potentials. Consequently, it could be expected that, when the electrode potential of the metal is maintained in a range at which the activating influence

on the anodic process can be affected by only one of the components in the solution, the adsorption on the surface of other components, active at more positive potentials, should bring about a slowing down of the dissolution process. In other words, if at a given potential several components of the solution are adsorbed, then not all the surface complexes can pass into the solution, but only those the strength of whose chemical bond has attained the required value. This probably explains the passivating effect of iodine and chlorine ions on the spontaneous dissolution of iron in sulfuric acid (15-20), even though at potentials of a more positive value these anions are extremely aggressive agents.

Passivation of Metals

Developing these ideas, it is presumably possible to account not only for the stimulation of anodic dissolution of the electrode metal by the adsorbed components of the solution, but also for passivation of the metallic surface.

The results of recent investigations have convinced us that many of the peculiarities of the electrochemical behavior of passivated metals cannot be explained on the basis of the phase theory of passivity, without recourse to additional and frequently highly improbable assumptions. One of the basic conclusions of this theory is known to be the irreversibility of the anode passivation process, in the sense that, on reaching a certain potential at which the formation of the phase film takes place, the metal becomes inert and the inertness persists at all potentials having a more positive value. Any change of the passivating film resulting in an increased rate of metal dissolution should also lead to an electrode potential shifting toward negative values.

In recent years, however, it has been firmly established that this concept of passivation is incorrect. Detailed studies of chromium, nickel, stainless steels, and other metals and alloys have shown that the passive state is firmly preserved only in a comparatively narrow potential range, which depends on the nature of the metal and on the *p*H of the solution, and that in regions more positive than this the metal again begins to dissolve well. The most remarkable fact is that in this case the dissolution rate changes with the potential in accordance with the ordinary Tafel line, *i.e.*, according to the laws of electrochemical kinetics (21-32). Obviously this dependence, which shows the absence of the diffusion limitation of the process, is incompatible with the existence of a continuous oxide film on the metal surface.

This contradiction can be avoided if the adsorption theory of passivity is adopted. In addition, however, it should be assumed that, along with the common adsorption of water which accelerates the anodic dissolution of the metal as ions of the lowest degree of oxidation, there also takes place an adsorptive chemical interaction between the surface atoms of the metal and the oxygen of the water, which leads to passivation; and the bond between the passivating oxygen and the surface atoms corresponds to the bond in the oxygen complexes of metal ions of the highest degree of oxidation, such as $Cr_2O_7^{-2}$. This means that this kind of adsorption should be regarded as the beginning of the formation of a metallic salt of the highest degree of oxidation.

This suggestion is justifiable if what was said above is taken into consideration, namely, that the halide ions also begin to interact with the metallic surface at appreciably more negative potentials than those of metal dissolution in the presence of these ions.

Bearing this in mind, the adsorptive-chemical interaction of water molecules (or of OH^-) with the surface atoms of the metal can be represented as follows

$$\left[Me\right] + mH_2O \longrightarrow \left[Me(H_2O)_m\right] \begin{cases} \xrightarrow{a} \left[Me(H_2O)\right]^{+n} + n\bar{e} & [8a] \\ \xrightarrow{b} \left[Me(O^{=}\cdots H^{+})_m\right] & [8b] \end{cases}$$

This model resembles in form one suggested before for the passivation of iron in alkalis (33). It should be noted, however, that in the earlier work no suggestions were made about the nature of the bond between passivating oxygen and the surface of the metal.

It is natural to suppose that the probability of the reaction proceeding along the second route [8b] (*i.e.*, the adsorptive chemical bond between oxygen of water and the metal atom becoming stronger and changing in time) increases the longer the adsorbed H_2O (or OH') stay on the metal surface. This seems to be favored by an increase in the *p*H of the solution and the shift toward more positive values of the electrode potential. It is well known at present that the passivating reactions begin to take place at an appreciable rate only on reaching a certain potential (the potential of passivation), which increases for each metal as the *p*H of the solution decreases. It is quite probable that the passivating adsorption starts on the most active parts of the surface, and only as the potential shifts to more positive values does it extend to other parts as well.

In accordance with what has been said above, the passivating oxide of the type under consideration can remain on the surface and slow down the anodic reaction until a certain potential has been reached, after which the oxide can pass into solution in the form of a complex with the metallic ion in the highest degree of oxidation. Evidently at these positive potentials the surface complex will be easy to reproduce, which in turn will cause a continuous dissolution of the metal, according to this mechanism.

Electrochemical Basis of Pitting Corrosion of Metals

It is known at present that the passive state of a metal or an alloy can be destroyed (in part or entirely) by introducing into the solution certain anions, such as Cl^-, Br^-, or I^-. These ions in many cases cause nonuniform corrosion which gives rise to pits on the metallic surface.

Many investigators have studied pitting corrosion, but the mechanism of the process is still uncertain. Some investigators (34) are inclined to believe that

pitting corrosion is not an electrochemical process, but a purely chemical one. We believe this view to be totally unfounded. An analysis of the available data shows that, if some very probable assumptions are made, the formation and development of pits can be explained by the electrochemical mechanism for dissolution of metals.

The available data indicate that the presence of Cl^-, Br^-, and I^- in a solution is an essential but not sufficient condition for the acceleration of the corrosion process with the formation of pits. In a number of cases the aggressive action of these ions is observed only at potentials which are more positive than a certain critical value which depends on the type and the concentration of the halide ion in solution. This can be seen from the results obtained recently in our laboratory by V. A. Gilman who studied the electrochemical and corrosive behavior of zirconium in acid electrolytic solutions.

This invesigation showed convincingly that, under conditions suitable for spontaneous dissolution in 1.0*N* H_2SO_4, zirconium retained its passive state, and its corrosion rate (with hydrogen depolarization) did not exceed 5×10^{-7} amp/cm^2. It is very important that the rate did not change appreciably when the potential moved toward positive values up to 2.5 v (see curve 1, Fig. 5). When chloride, bromide, or iodide is added to the acid solution it does not cause any noticeable change in the corrosion rate of the zirconium or in the mixed potential of the metal. The aggressive action of these ions, however, manifests itself when anodic polarization is applied and the electrode potential is shifted toward a certain value, which increases in the transition Cl^-, Br^-, I^-. As can be seen from Fig. 5 (curves 2-4) under stationary conditions the value of this critical potential practically does not depend on the polarizing anodic current and, therefore, on the dissolution rate of the zirconium, although at the very first instant after the current has been increased (or decreased) it is possible to observe a temporary shift of the potential to the positive (or negative) direction, followed by a rather quick return to the initial potential (Fig. 6). Visual observations showed that in these conditions

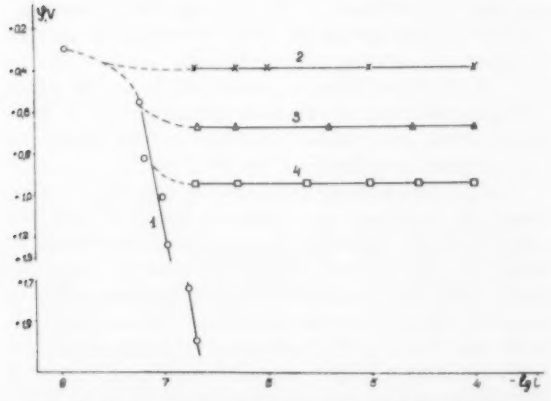

Fig. 5. Dependence of the zirconium dissolution rate on the potential in solution of 1.0N H_2SO_4 (curve 1); 1.0N HCl (curve 2); 1.0N H_2SO_4 + 1.0N KBr (curve 3), and 1.0N H_2SO_4 + 1.0N KI (curve 4).

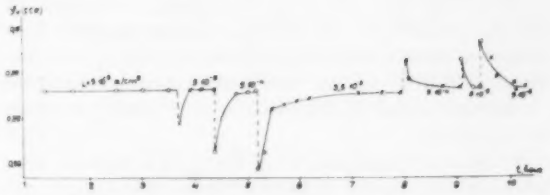

Fig. 6. Change of potential in time when the current density decreased or increased during anodic dissolution of zirconium in 1.0N HCl solution.

zirconium dissolution does not take place uniformly throughout the surface, but was of clearly expressed local character and leads to the formation of pits.

The critical values of the potential can be obtained not only by superimposing polarization, but also by introducing an oxidizing agent into the solution. In Gilman's work ferric sulfate was used. When introduced in sufficiently high concentrations into the chloride solution it led to a shift of the zirconium potential toward its critical value and the appearance of pits on the surface.

The behavior of zirconium in solutions containing chlorides, bromides, and iodides does not differ essentially from that of a whole series of other metals (iron, magnesium, aluminum, chromium, etc.) and alloys.

Taking into consideration the fact that zirconium dissolution in acid solutions of chlorides is a distinctly irreversible process, the lack of dependence of the critical potential on the current can be explained satisfactorily if it is assumed that in this case the value of the effective working surface (S) increases in a direct ratio to the increase of the current (I). Under these conditions we can write

$$\phi = K - \beta \cdot \lg I/S \qquad [9]$$

From Eq. [9] it follows that the constancy of ϕ is the result of the constancy of the value I/S.

This assumption is in agreement with the results obtained for aluminum, whose critical potentials of dissolution in acid solutions of chlorides, bromides, and iodides lie in more negative ranges than the corresponding values of the reversible hydrogen electrode potential. It has been shown (35) that the shift of potential to the critical value is accompanied in this case by an increase not only of the over-all dissolution rate, but also of the spontaneous dissolution, which is manifested by an increased amount of escaping hydrogen gas (the negative difference effect). It was also definitely established that the hydrogen evolution rate increased linearly with the increase of polarizing current. Taking into account the fact that corrosion in this case is clearly of a local character and that hydrogen evolution on passive parts of the aluminum surface is slowed down seriously, the existence of this dependence seems to indicate that the effective surface of the active parts grows linearly with increase in polarizing current. This conclusion conforms to the visual observations of the author, which show that an increase in the current leads to a greater number of pits.

Obviously the observed temporary deviation of the potential from the critical value at the very first moment after the current has been increased or decreased is due to the fact that, when polarization is changed quickly, the increase of S cannot keep up with that of I.

From the coincidence of the direct and reverse polarization curves observed experimentally, one can conclude that the depassivation of the metallic surface by halide ions is a reversible process, in the sense that the elimination of the causes leading to surface activation lead to the surface becoming passivated again. From this it can be concluded that under these conditions two concurrent processes take place: the passivating adsorption of the oxygen of the water (8b) and the activating adsorption of chloride ions. This can be expressed by the following reaction

$$\left[Me\begin{pmatrix} O^{=} & H^{+} \\ H^{+} & \end{pmatrix}_m\right] + pCl^{-} \rightleftharpoons \left[Me\,(Cl)_p^{-p}\right] + m\,H_2O \qquad [10]$$

It is obvious that the possibility of this equilibrium shifting toward the right should depend not only on the electrode potential, but also on the concentration of halide ion in the vicinity of the metal surface. Engell and Stolica (34) showed in a recent work that the stimulating influence of chloride ions on corrosion of a passive iron electrode (when pits are formed) is observed only on reaching a certain critical concentration of these ions in the solution.

The question naturally arises as to why the metal dissolution under these conditions is clearly of a local character. We believe that the experimentally observed dependence of the area of the active sites on the polarizing current is very important for understanding this phenomenon. The dependence can be understood and accounted for if it is assumed that the chloride ions are carried to the metal surface by the current. This assumption agrees well with experimental results, according to which the aggressive action of Cl^- or other halide ions may be lessened or avoided by increasing the concentration of "supporting" electrolyte in solution. Thus, for instance, Gilman showed recently that the influence of Cl^- on the anodic dissolution of zirconium disappears completely in sulfate solutions when the ratio of sulfate to chloride concentration comes close to 5. If, however, perchlorate is used as the principal electrolyte, the critical ratio of concentrations comes close to 9 or 10.

This assumption is also borne out by the results obtained in the investigations of Engell and Stolica (34) cited above, who showed that, at a given value of the potential of passive iron, the activating action of Cl^- on the anodic dissolution of this metal was not observed immediately after it had been added to the solution. Instead it was seen after a certain time which was longer the greater the Cl^- concentration. When the volume concentration of the chloride remained below the critical value, the appearance of the induction period could be ascribed to the increase of Cl^- concentration in the vicinity of the electrode surface to the critical value.

Taking into consideration the fact that the dissolution of solid metals (even though they are in a passive condition) always takes place nonuniformly, and therefore the current is distributed unevenly on the surface, it would be natural to conclude that the critical concentration of Cl^- is achieved first near those sections of the metallic surface which dissolve at the highest rate. If the current is kept constant, the activation which has begun on these sections inevitably will lead to a far greater localization of the current, and consequently to a much more rapid migration of activating anions to the active centers, which in turn will result in the acceleration of the dissolution process. It is highly probable that the dissolution of the metal on the active sections takes place with diffusion restriction, as a result of which a further increase of the anodic current inevitably will increase the area of these sections.

On the basis of these assumptions it is easy to explain the formation and development of pits in the absence of external anodic polarization, that is, when corrosion takes place at the expense of the reduction of the oxidizing agent, particularly oxygen. Taking into consideration the data now available concerning the electrochemical properties of passive metals, it could be supposed that in this case the cathodic reaction takes place mainly on the passivating section of the surface. A local current inevitably arises, which can play the same role as does an external current.

It follows from what has been said above that the formation and development of pits on the metallic surface in the presence of Cl^-, Br^-, or I^- ions can take place only when the critical potentials ($\phi_K{}^\Gamma$) for metal dissolution in the presence of these ions are more positive than the passivation potential of the metal (ϕ_P). This seems to mean that the affinity of the metal for oxygen must greatly surpass its affinity for the corresponding halide. Obviously in the case of a reverse relationship ($\phi_P > \phi_H{}^\Gamma$) the halide ion adsorption will interfere with the passivating adsorption of the oxygen of the water and will stimulate the dissolution of the metal in the active state. This is the case for zirconium when the F^- which possesses greater affinity for zirconium than does oxygen is introduced in the solution (36). The complete activation of the surface of zirconium in an acid solution, as well as a considerable increase in the rate of its dissolution, is observed. It follows that similar conditions arise when dissolving silver, cadmium, lead, and indium amalgam in acid solutions of chlorides, bromides, and iodides.

The condition formulated above ($\phi_P < \phi_H{}^\Gamma$) is an essential, although not sufficient condition for the development of pitting corrosion in the absence of external polarization. Evidently, even if this condition remains, the addition of an aggressive ion to the solution can lead to the formation and development of pits only if the stationary potential of the corroding metal is more positive than ϕ_K, i.e., only if the following relationship exists $\phi_{st} \geq \phi_H{}^\Gamma > \phi_P$. Since ϕ_{st} depends on the factors determining the kinetics not only of the anodic, but also of the cathodic reaction, its fulfillment can depend on the concentration

of the oxidizing agents in the solution, on the migration rate of these agents to the metallic surface and, finally, on the true rate of its reduction. This conclusion agrees with numerous experimental results which show that, if aggressive anions are present, the development of pitting corrosion is promoted by the presence of an oxidizing agent, especially O_2 or Fe^{3+}. Evidently the maximum allowable concentration of oxidizing agent is dependent on a number of factors, including the nature of the corroding metal, pH of solution, nature and concentration of the aggressive anion, temperature, and rate of stirring of the solution.

It should be noted that the relationship between ϕ_P and ϕ_H can be altered by changing the composition of the solution. According to a large amount of data now available from recent studies conducted by various investigators, for every metal or alloy the value ϕ_P depends on the pH of solution and becomes increasingly positive as the acidity of the solution increases (22, 37-39). At the same time, ϕ_H changes noticeably as the concentration of the aggressive anion changes and for all practical purposes does not depend on the pH of the solution. Thus, according to Gilman's results, obtained when investigating zirconium, a tenfold increase in the Cl^- concentration leads to a shift of ϕ_K toward negative values by an amount nearly equal to 58 mv (see Fig. 7).

If these assumptions hold and it is assumed as above (see Eq. [10]) that the stimulating influence of the halide ion on the anodic dissolution of metals with the formation of pits is connected with the participation of these ions not only in the depassivation of certain sections of the surface, but also in the elementary act of ionization of the metallic ion, then there is every reason to expect that in this case the process will begin to slow down as a result of the slow rate of migration of aggressive ions to the metallic surface. However, this is not confirmed by existing experimental evidence. The experiments with zirconium have shown that even at relatively low Cl^- concentrations, an increase in anodic current density to 10^{-1} amp/cm^2 does not lead to a noticeable deviation of the electrode potential from the critical value. We believe that this result can be understood and explained if one takes into consideration what has been said before, namely, that pitting corrosion is capable of developing only if the metal affinity for oxygen is greater than its affinity for the corresponding halide. This condition being fulfilled, the stable form of the existence of the metallic ion in the solution will be its oxygen complex of the type ZrO^{+2}.

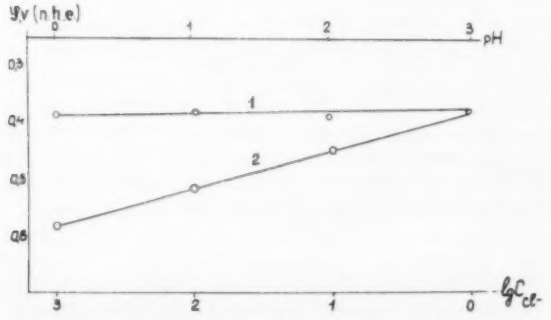

Fig. 7. Dependence of the critical potential zirconium dissolution on the concentration of Cl^- (at constant pH) and on the pH (at constant Cl^- concentration).

It is quite possible that under ordinary conditions the dissolution of the metal takes place with the direct formation of these ions, whereas when a critical potential is reached new conditions are formed which favor the formation, as a primary product, of the complex ions of the metal with an aggressive anion. It is natural, however, that, as the diffusion from the metallic surface into the solution proceeds, these will be wholly hydrolyzed to form oxygen complexes and free halide ions which can again take part in the process. In this case, the concentration of halide ions at the metallic surface, as well as in the solution, will remain unchanged, and they will play the part of catalysts of corrosion. Evidently, the mechanism of metallic dissolution can be represented as follows

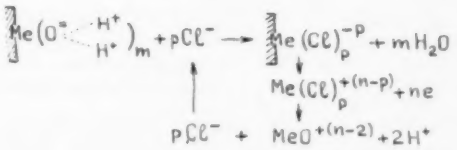

[11]

The fact that the aggressive action of the halide ions is manifested in each case only when a certain value of the electrode potential has been reached testifies to an increase in their chemical activity with an increase in the positive charge of the metallic surface which evidently polarizes such ions. It can be concluded that the value of the potential at which the halide ions can eject the passivating oxygen from the metallic surface must change as the zero point of the metal and its affinity for oxygen change. Therefore, it should depend not only on the nature and concentration of the halide ion, but also on the nature of the metal. This conclusion agrees with existing experimental data.

As can be seen from Table I, zirconium, which has the greatest affinity for oxygen, has the greatest positive value of the dissolution potential in the presence of Cl^- and Br^-.

In conclusion it should be noted that halide ions are not the only ones that cause pitting corrosion. This was observed for iron (41), and in this laboratory for zirconium by Gilman, who showed that perchlorate ions have a similar ability. However, in this case the dissolution potential is of a much greater positive value.

Table I. Dissolution potentials of some metals in the presence of halide ions, 1 g eq. l

Metal	Potential in volts to n.h.e.	
	Cl^-	Br^-
Magnesium	—1.419	—1.269 (40)
Aluminum	—0.509	—0.369 (35)
Zirconium	0.380	0.660

Manuscript received Oct. 18, 1960.

Any discussion of this paper will appear in a Discussion Section to be published in the December 1961 JOURNAL.

REFERENCES

1. J. M. Kolotyrkin and A. N. Frumkin, *Doklady Acad. Nauk USSR*, **33**, 446 (1941).
2. J. M. Kolotyrkin, *Zhur. Fiz. Khim.*, **25**, 1248 (1951).
3. J. M. Kolotyrkin and L. A. Medvedeva, *ibid.*, **27**, 1344 (1953).
4. L. A. Medvedeva and J. M. Kolotyrkin, *ibid.*, **31**, 2668 (1957).
5. N. J. Bune and J. M. Kolotyrkin, *Doklady Acad. Nauk USSR*, **100**, 295 (1955).
6. J. M. Kolotyrkin and N. J. Bune, *Zhur. Fiz. Khim.*, **29**, 435 (1955).
7. J. M. Kolotyrkin, *Trans. Faraday Soc.*, **55**, 455 (1959); Proc. Ninth Meeting of CITCE, p. 406.
8. J. M. Kolotyrkin and L. A. Medvedeva, *Zhur. Fiz. Khim.*, **29**, 1477 (1955).
9. V. V. Losev and A. I. Molodov, *Doklady Acad. Nauk USSR*, **130**, 111 (1960).
10. J. Heyrovsky, *Discussions Faraday Soc.*, **1**, 212 (1947); *Z. Elektrochem.*, **59**, 812 (1955).
11. J. Randles and K. Somerton, *Trans. Faraday Soc.*, **48**, 937, 951 (1952).
12. H. Gerischer, *Z. Phys. Chem.*, **202**, 292, 302 (1953); *Z. Elektrochem.*, **57**, 604 (1953).
13. A. G. Stromberg, *Zhur. Fiz. Khim.*, **31**, 1704 (1957).
14. K. Piontelli, *Chem. & Ind.*, **1957**, N40, 1304.
15. G. Wolpert, *Z. Phys. Chem.*, **A-151**, 219 (1931).
16. Z. A. Iofa and L. A. Medvedeva, *Doklady Akad. Nauk USSR*, **69**, 213 (1949).
17. S. M. Babizky and H. L. Zeitlin, *Issledovaniya po nerzhaveyushim stalyam, izd A.N. USSR*, **1956**, p. 69.
18. Z. A. Iofa, E. I. Lyakhovezkaya, and K. Sharifov, *Doklady Akad. Nauk USSR*, **84**, 543 (1952); Z. A. Iofa and G. B. Rozhdestvenskaja, *ibid.*, **91**, 1159 (1953); Z. A. Iofa, *Vestnik Mosk. Gos. Univ.*, N2, 139 (1956); E. A. Avazyan, *Doklady Akad. Nauk USSR*, **100**, 473 (1950).
19. Hua Bao-Din, Shen Sin-Su, Z. A. Iofa, and E. I. Michailova, *Doklady Akad. Nauk USSR*, **130**, 129 (1960).
20. A. N. Frumkin, *This Journal*, **107**, 461 (1960).
21. J. M. Kolotyrkin and V. M. Knjazheva, *Zhur. Fiz. Khim.*, **30**, 1990 (1956).
22. V. M. Knjazheva and J. M. Kolotyrkin, *Doklady Akad. Nauk USSR*, **114**, 1265 (1957).
23. J. M. Kolotyrkin, *Z. Elektrochem.*, **62**, 664 (1958).
24. N. J. Bune and J. M. Kolotyrkin, *Doklady Akad. Nauk USSR*, **111**, 1050 (1956).
25. G. M. Florianovitch, J. M. Kolotyrkin, and N. K. Smirnova, *ibid.*, **120**, 845 (1958).
26. J. M. Kolotyrkin and G. M. Florianovitch, *Khim. nauka i Prom.*, **3**, 483 (1958).
27. J. M. Kolotyrkin, *Problemy Fiz. Khimi, Gos. khim. izd.*, **1958**, N1, 81.
28. N. J. Bune, J. M. Kolotyrkin, and G. S. Tjurikov, *Zhur. Fiz. Khim.*, **32**, 2679 (1958).
29. G. M. Florianovitch and J. M. Kolotyrkin, *Doklady Akad. Nauk USSR*, **130**, 585 (1960).
30. J. M. Kolotyrkin and N. J. Bune, *Z. Phys. Chem.*, in print.
31. Th. Heumann and W. Rösener, *Z. Elektrochem.*, **59**, 722 (1955).
32. G. Okamoto, H. Kobayshi, M. Nagayama, and N. Sato, *ibid.*, **62**, 775 (1958).
33. B. N. Kabanov, R. H. Burstein, and A. N. Frumkin, *Discussions Faraday Soc.*, **1**, 259 (1947).
34. H. I. Engell and N. D. Stolica, *Z. Phys. Chem.*, **20**, 113 (1959).
35. N. D. Tomashov and V. N. Modestova, "Jssledovaniya po korrosiimetallov," izd. A. N. USSR, **1951**, p. 75.
36. W. J. James, W. G. Custead, and M. E. Straumanis, *J. Phys. Chem.*, **64**, 286 (1960).
37. U. F. Franck, *Z. Naturforsch.*, **4a**, 378 (1949).
38. P. F. King and H. H. Uhlig, *J. Phys. Chem.*, **63**, 2026 (1959).
39. M. Maraghini, G. B. Adams, and P. van Ryssel-berghe, *This Journal*, **101**, 400 (1954).
40. D. V. Kokoulina and B. N. Kabanov, *Doklady Akad. Nauk USSR*, **112**, 682 (1957); **120** (1958).
41. L. Vanjukova and B. Kabanov, *ibid.*, **59**, 917 (1948).

Oxidation of Iron-Nickel Alloys

IV. Further Electron Diffraction Studies at Elevated Temperatures

R. T. Foley

General Engineering Laboratory, General Electric Company, Schenectady, New York

ABSTRACT

The oxide films formed on Fe-Ni alloys containing 30%, 41%, 78% (3.8% Mo) and 80% Ni have been studied at their temperature of formation, up to 1000°C, with reflection electron diffraction. The influence of the alloy substrate is very conspicuous in the structure of the first formed films. The existence of MoO_3 at 900° on the surface of the 78% Ni (3.8% Mo) alloy is documented. It is concluded that MoO_3 forms in the first instance of oxidation and is seen in only a few cases because it remains at the metal-oxide interface as the film grows. When H_2O vapor is present in the oxidizing gas (dew points up to + 80°F were used) a spinel of unit cell dimension $a_o = 8.50 - 8.60$ is observed on the 30% and 41% alloys. This lattice is expanded in comparison with the spinel $NiFe_2O_4$ ($a_o = 8.33$) observed on these alloys previously and agrees with $MnO \cdot Fe_2O_3$ or Mn_3O_4.

Previous reports from this laboratory (1-3) have dealt with the oxidation behavior of iron-nickel alloys nominally 30, 41, and 78% Ni. Electron diffraction examinations of the oxide films by the reflection technique were made at 600°, 700°, 800°, and 900°C during the oxidation process. The kinetics of oxidation was also studied. The over-all extended investigation has as its primary objective the clarification of the mechanism and kinetics of oxidation of the Fe-Ni system.

In the earlier electron diffraction investigation there were certain points that were not established as conclusively as desired, and because these points bear in a critical way on the interpretation of the reaction mechanism it was desirable to study them in more detail.

The 78% Ni-Fe alloy contained 3.8% Mo and there was some evidence supporting the existence of MoO_3 at temperatures above its melting point where its vapor pressure is high. To draw an accurate picture of the mechanism of reaction it is necessary to know whether NiO, MoO_3, or $NiFe_2O_4$ is the predominant oxide grown on the alloy. If more than one compound is formed, it is important to know the relative position, with respect to the basis metal, of the several oxide layers.

Another point to be resolved had to do with the distortion of the electron diffraction patterns of the alloy or its oxide on heating to 1000°C. This distortion was observed in certain instances. Any change in the lattice dimensions not only would make the interpretation of the data difficult but also would be reflected in the kinetics of oxidation through influence on the ionic diffusion rate in the oxide.

In the extended study of the oxidation of Fe-Ni alloys the influence of H_2O in the oxidizing atmosphere is of significance, for example in explaining some unusual effects that occurred in laboratory air. A parallel investigation is being made of the influence of H_2O on the kinetics of oxidation of the three alloys. To support this investigation a study was made wherein electron diffraction patterns were obtained from the three alloys during oxidation in O_2-N_2 mixtures containing H_2O vapor equivalent to dew points of +38°F and +80°F.

This paper describes the work done to resolve these various points with the more general objective of contributing to our knowledge of oxidation theory.

Experimental

Electron diffraction equipment.—The electron diffraction apparatus is equipped with a special furnace capable of maintaining sample temperatures of up to about 1000°C. The construction of the furnace has been described in a previous publication (2).

Alloys.—The composition of the alloys, the heat treatment prior to oxidation, and the technique of surface preparation has also been described before (2). In this work a technique involving chemical etching has been preferred on the basis that following this treatment electron diffraction patterns of the alloy itself were usually obtained whereas abrasion and polishing techniques sometimes gave doubtful patterns.

As mentioned above one of the points to be resolved had to do with the fate of the Mo in the 78% Ni-Fe alloy. The particular weight percentage, 3.8, lies at a figure below that at which Mo is responsible for accelerated oxidation and above that in which Mo is present only as an impurity without a role in the oxidation process. In order to have a basis for comparison of patterns developed on this Mo-containing alloy, to learn the influence of Mo in the development of the oxide film, an 80% Ni-20% Fe alloy with only trace quantities of impurities was studied. This alloy was prepared by melting electrolytic Fe and high-purity Ni shot in vacuum (10^{-5}mm Hg). The ingot was remelted twice in vacuum and reduced in thickness through several stages to 0.010 in. with intermediate vacuum anneals at 950°C. Chemical analysis gave an Fe content of 20.42 and Ni 79.58, with all other elements present only in trace quantities according to spectroscopic determination.

Electron diffraction studies.—Patterns were first taken at room temperature and a pressure of 0.01-0.1 μ Hg. The sample was then brought to the designated temperature and a pattern obtained before oxidation. Oxidation was achieved by admitting air to the diffraction chamber until atmospheric pressure was reached and then oxidizing for 2 min. The system was evacuated and another pattern obtained. This procedure was repeated to obtain total oxidation times of 32 min. Where it was desired to control the moisture content of the gas the oxidizing atmosphere was a controlled mixture of 21.7% oxygen and 78.3% nitrogen by volume. The dew point was increased by bubbling the gas mixture through water held at about 0°C for the +38°F dew point or room temperature for the +80°F dew point. The actual dew point was measured with a General Electric Dew Point potentiometer with a precision of ± 3°F.

The electron diffraction patterns were obtained by the reflection technique wherein the electron beam strikes the sample at an angle of less than 1°. With the etched, polycrystalline specimens used in this investigation the areas illuminated are facets of small crystallites that protrude from the surface. What is viewed is an "average" structure over an area quite large in comparison to atomic dimensions. In reality, this would also be the case if a single crystal were used, as in such cases the electron beam would be diffracted by steps that must exist in the face unless extraordinary care is taken to prepare the crystal for study.

Results

Oxides formed on 80% Ni 20% Fe.—The patterns formed on the 80% Ni-20% Fe alloy (Mo free) are given in Table I. At both 700° and 900° the pattern for the alloy is observed when the sample is brought to temperature and before the oxidizing gas is admitted. Alloy spacings are carried through to the thicker films. This preservation of the alloy atomic distances in the oxide layer is caused by an alinement effect rather than simply the penetration of a superficial layer by the electrons as films of many thousand angstroms in thickness are formed during these oxidation times. At 900°C in the vacuum of the instrument evidently the Fe is oxidized selectively to give some FeO spacings. However this species is absorbed, or covered, by the nickel ferrite structure. In the interpretation of the patterns obtained from the oxides formed on Ni-Fe alloys a difficult question to answer relates to the existence

Table I. Patterns formed on 80% Ni—20% Fe alloy

Temp, °C	At temperature & before oxidation	First formed film 2 min	Film formed after 12 min	Film formed after 32 min
700°	Alloy	$NiFe_2O_4$	$NiFe_2O_4$	$NiFe_2O_4$
900°	Alloy (FeO)	$NiFe_2O_4$ (Alloy)	$NiFe_2O_4$ (Alloy)	$NiFe_2O_4$

of NiO or the Ni containing spinel which is denoted here as $NiFe_2O_4$. [That the oxide is a Ni containing spinel rather than Fe_2O_4 as interpreted by Bénard, *et al.* (4) seems quite evident in view of actual chemical analyses performed by Brabers and Birchenall (5) and previously in this investigation (1). Further, measurements of lattice parameters by Yearian and co-workers (6) as well as recent studies by Kennedy, Calvert, and Cohen (7) support this thesis.] The difficulty is based on the fact that the "d" spacings for the Ni ferrite include all of those for NiO as well as additional spacings. Thus the decision must be made on the basis of these additional spacings. The oxides developed upon this 80% alloy at 700° and 900° conform well to the nickel ferrite structure. Thus, the production of other structures on the 78% Ni alloy must be due to the other constituents present in sensible amounts; Mo, 3.8% and Mn, 0.73%.

Influence of Mo *on patterns obtained from* Ni-Fe *alloy.*—The diffraction patterns obtained on oxidation of the 80% Ni-20% Fe alloy (Mo not present) are extremely useful in the interpretation of patterns obtained from the Mo containing alloy. For example, the d spacings (Å) obtained after oxidizing both of these alloys for 2 min at 700°C are compared with those of the $NiFe_2O_4$ spinel in Table II. It is concluded that the agreement among these patterns is quite good. Obviously, the pattern obtained from the 80% Ni-20% Fe alloy must be furnished by oxides of iron and nickel. In the actual experimental d values obtained from the 78% Ni Mo-containing alloy there were certain deviations from the accepted values for the spinel. Often deviations of the same magnitude were seen in the Mo-free alloy, as seen in Table II, and in such cases no attempt was made to associate these deviations with other structures. However, even bearing in mind the possibility of the existence of such deviations it is still concluded that a MoO_2 type structure exists in certain of the thin films. The data presented in Table III are illustrative. Comparison of the pattern obtained after oxidizing the 78% Ni alloy (Mo containing) at 900°C for 2 min with known patterns for MoO_2 results in good agreement. MoO_2 is an orthorhombic unit cell with lattice constants of a = 13.848Å, b = 3.697Å, and c = 3.966Å (8) and gives a large number of reflections many of which are weak. The d spacings taken from the ASTM file are shown in the fourth column. The letter i appearing beside the line denotes a reflection obtained in the electron diffraction examination of oxide film formed on molybdenum during other investigations in our

Table II. Spacings obtained from electron diffraction examination of 78% Ni-Fe (Mo) alloy and 80% Ni-Fe alloy

Pattern obtained after 2 min at 700°C

78% Alloy (Mo)	"Pure" 80% 20% alloy	Spinel* ($NiFe_2O_4$)
2.92 vs	3.00 vs	2.95 (30)
2.50 vs	2.54 vs	2.51 (100)
2.38 w	2.38 vw	2.41 (7)
2.07 m	2.10 m	2.08 (25)
1.89 m	1.90 w	1.92 (3)
1.71 s	1.73 m	1.70 (7)
1.62 s	1.61 s	1.60 (30)
1.49 vs	1.48 vs	1.48 (40)
1.42 w	1.40 w	1.42 (1)
1.33 vw	1.32 w	1.32 (5)
1.28 m	1.27 m	1.27 (9)
1.22 w	1.21 w	1.21 (5)
1.18 w		
1.11 vs	1.11 w	1.11 (5)
	1.09 s	1.09 (15)
		1.04 (5)
0.98 s	0.97 s	0.98 (1)
0.94 w	0.93 w	0.96 (9)

Legend to intensities: vs = very strong; s = strong; m = medium; w = weak; vw = very weak.
* Nat. Bur. Standards (U.S.) Rep. 6415, p. 23, March-April (1959). Figure in parenthesis is relative intensity.

Table III. Spacings obtained from electron diffraction examination of 78% Ni-Fe (Mo) alloy and 80% Ni-Fe alloy

Alloy (X-ray data)	Patterns obtained after 2 min at 900°C 80% Ni-20% Fe alloy	78% Ni (Mo) alloy	MoO_2
		3.14 m	3.26 i j
	2.90 w		3.01, 2.70
			2.66 j
			2.61
	2.52 s	2.54 m	2.55 i
		2.34 vs	2.33
			2.31 j
			2.23 i
2.05	2.07 vs	2.11 m	2.13 i
			2.03 j
		1.98 s	1.98 j
			1.96
		1.89 s	1.85
			1.82
1.78	1.78 s	1.78 w	1.77 i j
			1.76 i
			1.73
		1.69 s	1.69
			1.66, 1.63
	1.61 m		1.61 j
			1.59
		1.58 m	1.57 i
		1.51 m	1.51 i j
	1.49 vs		1.48
		1.44 m	1.44 j
			1.40 i
		1.35 w	1.35, 1.33 i
1.26	1.27 m	1.24 w	1.23 i j
		1.11 w	1.11 i
1.07	1.09 w		1.06 i j
			1.01 j
			0.98 i
		0.93 s	0.93 i

laboratory. Spacings with a j are those reported by Iitaka and co-workers (9) in an investigation discussed below. The conclusion is that the lines marked with an i and j should represent the stronger reflections insofar as the diffraction of electrons is the measurement. On the basis of this comparison it is concluded that a MoO_2 type structure is present in the first formed film on this particular alloy. Why such a pattern was not always obtained in the first formed films or why in the cases cited here good patterns for MoO_2 were not obtained in the 700°C experiments cannot be explained. Considerable effort was made to establish the existence of this structure at these elevated temperatures because of the difficulty of reconciling these observations with some of the physical properties of the bulk oxide, its melting point, and vapor pressure. In interpreting the patterns the possible existence of lower oxides of molybdenum was considered but rejected on the basis of the experimental data.

In Table III the pattern for the basis alloy is given. This pattern is that obtained both by x-rays and electron diffraction. These d spacings are significant in the interpretation of oxide film patterns developed on the alloy because the corresponding reflections are carried through many of the thinner films. Thus in the particular pattern for the 80% Ni-20% Fe alloy given in the second column it is quite apparent that the alloy pattern itself is predominant either by virtue of the thinness of the oxide film or by virtue of an ionic alinement effect.

The influence of Mo in the alloy is evidenced also in the rate of oxidation. This was observed in a qualitative way. An electron diffraction pattern was obtained from the 80% Ni-20% Fe alloy at room temperature. Only spacings for the alloy were obtained. The sample was heated to 400°, a pattern obtained, then to 700°C and another pattern obtained. The sample was cooled to room temperature and a final pattern obtained. In each case only the d spacings of the basis alloy were seen indicating that in the vacuum of the apparatus, approximately 0.01 μ Hg, over the 4-5 hr period, an oxide layer of less than about 100Å was developed.

Temperature and preservation of ionic distances.—In the interpretation of these electron diffraction patterns, wherein the experiment involved heating the sample from room temperature to 1000°C quite rapidly, it was important to know what changes would occur in lattice parameter spacings and what was responsible for them. Several experiments were performed wherein the sample was heated in the vacuum of the electron diffraction apparatus and patterns taken at various temperatures up to 1000°C. These experiments lead to the conclusion that there is a shift in lattice spacings but it is caused by the tendency of the oxide during growth to preserve substrate interatomic distances (alinement effect) rather than any direct thermal effect. Representative experiments may be cited.

Where an alloy does not oxidize readily the alloy spacing may be retained upon heating and cooling in the vacuum of the apparatus as described above.

Where an alloy has a higher rate of oxidation a superficial film will be produced in the vacuum of the instrument, but what may be observed will probably not be the pattern of the basis metal or the normal structure of the oxide but a structure which represents an attempt to fit an oxide structure onto the basis alloy. Certain pertinent d spacings produced during such an experiment with the 30% Ni alloy are given in Table IV. Other spacings associated with the α-Fe_2O_3 pattern were also observed but are not included because they are not involved in the particular effect to be illustrated. The corresponding (hkl) values are given in parenthesis. A strong d spacing corresponding to the (200) plane in FeO occurs at 2.15Å. FeO is a possible reaction product when the oxygen pressure is quite low at elevated temperature. A similar situation was observed for the 78% alloy, again the oxidation occurring in the vacuum of the instrument. The spacings are listed in Table V.

Table IV. D spacings observed on heating 30% Ni-Fe alloy

Alloy spacings	Observed spacings: Room temp	400°	800°	1000°	Strong Fe_2O_3 spacings
2.03(111)	2.03	2.04	2.11	2.15	2.20(113)
1.80(200)	1.83	—	—	1.87	1.84(204)
1.27(220)	—	1.28	—	1.34	1.35(208), 1.31(119)
1.08(311)	—	1.08	1.12	1.15	1.19(312) 1.16(2,0,10), 1.14(314)

The interpretation placed on the results obtained in experiments of this type is that what is observed is a thin film of a reaction product the lattice spacings of which are distorted to accommodate to the basis metal but which will eventually assume the characteristic lattice parameter of the oxide.

Influence of moisture on oxides formed on Ni-Fe *alloys.*—In this series of experiments the oxidations were carried out with O_2-N_2 mixtures of dew points +38° and +80°F. The results are summarized in Table VI and can be compared with previous experiments (2) as well as other determinations of lattice parameters reported in the literature (7). Referring to the spinel formed on the 30% and 41% alloys the general effect observed in oxidizing atmospheres of controlled high dew point was one of increased lattice parameter. This enlarged unit cell is designated as spinel* in Table VI. Average a_o values for this cubic unit cell are 8.60Å for the oxide grown on the 30% alloy and 8.58Å for the structure on the 41% alloy. This may be contrasted with 8.33Å for $NiFe_2O_4$ and suggests either $Fe_2O_3 \cdot MnO$ or Mn_3O_4. The actual presence of Mn in the spinel lattice cannot be established with the present data, and the

Table V. D spacings observed on heating 78% Ni-Fe alloy

Alloy	410°C	800°C	Strong lines for MoO_2	Strong lines for $NiFe_2O_4$
		2.89	3.26	2.95
2.05	2.11	2.22	2.23	
1.78	1.88	1.84	1.85	1.90
1.26	1.31	1.33	1.33	1.32
1.07	1.10		1.11	1.11

Table VI. Electron diffraction patterns observed with high dew point gas

Alloy, %	Temp, °C	Dew point of O_2-N_2 oxidizing atm, °F	Patterns observed			
			Before oxidation	After 2 min	After 12 min	After 32 min
30	800	+38	—	Alloy, spinel*	Spinel*	Spinel*
30	800	+80	(Spinel)	Spinel*	Spinel*	Spinel*
41	800	+38	Fe_2O_3	Spinel*	Spinel*	Spinel*
41	800	+80	Spinel	Spinel*	Spinel*	Spinel*
78	800	+38	Alloy (distorted)	NiO (Spinel)	NiO (Spinel)	NiO (Spinel)
78	700	+80	?	$NiFe_2O_4$	$NiFe_2O_4$	$NiFe_2O_4$
78	900	+80	Alloy	NiO (+ alined growth on alloy)		

agreement of the lattice spacings may be fortuitous. This will be discussed below, but the apparent effect of moisture in the oxidizing gas stream is to yield an expanded lattice in the oxidation product.

In the case of the 78% alloy the results are much the same as reported previously (2) for experiments in laboratory air. At 700°C and a dew point of +80°F the oxide formed agrees with $NiFe_2O_4$, at 900°C the film is mainly NiO. At 900° the patterns obtained may be interpreted as consisting almost entirely of NiO and a few spacings characteristic of the basis alloy structure. These latter we attribute to the alined growth of NiO on the alloy rather than the alloy itself. In the runs at 800° and 900° with the 78% alloy the "before oxidation" results, wherein the samples were oxidized only by the low pressure of oxygen existing in the vacuum of the instrument, the patterns may be best interpreted by the alloy spacings distorted by the existence of MoO_3. Certain strong MoO_3 lines are in evidence, but the result seems to be one of a thin film being distorted in an effort to preserve the interatomic spacing of the basis metal.

Discussion

The interpretation of the electron diffraction patterns even after this detailed investigation remains somewhat speculative, but it represents in our opinion the best explanation of the experimental results.

The presence of and the important role played by the alinement effect is observed repeatedly throughout this experimental work, and certainly this is the outstanding factor influencing the structure of the first formed films on these alloys. The necessity for the existence of an easy transition from the basis metal to the oxide was recognized some time ago by Mehl, McCandless, and Rhines (10, 11), by Goldschmidt (12), and perhaps in an intuitive manner by Kistyakovskii (13). The first authors demonstrated experimentally that when FeO is grown on α-Fe the Fe-Fe atomic distance is retained. Goldschmidt also showed from crystallographic considerations that the transition from the cubic α-Fe to the cubic FeO, and/or to the cubic Fe_3O_4 involved relatively small changes in spacings of Fe atoms. Benard and Bardolle (14) pointed out that the oxide formed as nuclei on iron oxidized in low pressure of oxygen is dependent on the crystallographic orientation of the surface and that the constitution of the film formed in the first instant influences the whole of the reaction. Recently Collins and Heavens (15) rather thoroughly investigated the epitaxial growth of Ni, Co, and Fe on rocksalt and the growth of oxide films on these metals. They emphasize the general rule that the oxide will tend to form in such a way that the positions occupied by the metal atoms in the oxide correspond as nearly as possible to those in the metal themselves. If there is a small misfit, it would be expected that this influence would be carried through to fairly thick films, and our data may be interpreted from this standpoint. The oxide layer formed by a small misfit would be strained and certainly contain dislocations as the film thickness increases. This might well account for some of the physical properties which do not agree with those of the bulk, for example, the existence of MoO_3 at the metal-oxide interface at a temperature when it should be volatile liquid. The fact that there is a misfit and thus a strained lattice also accounts for the difficulty in interpreting the patterns of some of the very thin films.

As pointed out in the "experimental" section above, the strained lattice observed is an average measurement on several crystallites on the etched polycrystalline surface and the results presented here do not constitute support of the "pseudomorphic layer theory." Pashley (16) has criticized the "basal plan pseudomorphism" theory on the basis that in most of the cases that have been studied the structure of the oriented overgrowth was identical to that of the bulk material. Most of the evidence cited by Pashley and indeed most of the experimental evidence available at present refers to metals vapor-deposited on metallic or nonmetallic substrates. There has been very little work reported on the oriented overgrowth of films by chemical action and even less on such films produced by oxidation at high temperature.

While the strained (alined) layer that is observed, for example, in Table IV and V constitutes an early phase of oxidation process it probably does not constitute the earliest phase. It has been shown that the first oxide grown consists of nuclei developed in many sites on the surface (17).

Certain of the patterns obtained with the 78% Ni-Fe alloy containing 3.8% Mo lead to the conclusion that a MoO_3-type structure exists in the first formed film. Some experimental work reported in the literature would tend to agree with this observation while other work would argue against it. Iitaka, Nakayama, and Sekiguchi (9) oxidized an Fe alloy of approximate composition 7% Mo, 18% Ni, and 9% Cr for 2-5 min at 900°C, stripped the oxide so formed, and examined it at room temperature with reflection electron diffraction. A good pattern for

MoO_3 was observed, and the spacings so reported have been used above for comparison with our data. While the fact that MoO_3 in bulk form has a melting point of 795°C would lead one to expect ready evaporation at 900° evidently the MoO_3 formed was stable enough to be observed at the metal-oxide interface upon cooling. Radavich (17) studied the oxidation products formed on a number of heat resistant steels, among them an austenitic alloy of composition 3.5 Mo, 21.89 Cr, and 20.48 Ni and others. Various techniques were used in examining the oxide layers at room temperature. The presence of MoO_3 was not observed by reflection electron diffraction, but x-ray spectroscopic data showed that Mo was present in the oxide film after the alloy was oxidized for 5 min at 815°C. Obviously the exact form of the Mo-containing compound cannot be deduced from these data.

On the other hand Hickman and Gulbransen (18) obtained electron diffraction patterns from oxide films developed during the oxidation of two commercial alloys containing approximately the same amount of Mo as our alloy. Commercial alloys, Worthite (3.0 Mo, 20 Cr, 23 Ni, 3.25 Si, balance Fe and small percentages of other elements) and S-588, grade 1072 (4.2 Mo, 17.4 Cr, 19.85 Ni, 3.89 W, 4.19 Cb, balance Fe and other trace elements) were oxidized in O_2 of 1 mm pressure for times up to 60 min and temperatures up to 900°C without reporting the observance of a pattern for MoO_3. In another study (19) this oxide was reported but the alloy contained 25-30% Mo and MoO_3 was observed at 600°C, not at higher temperatures.

It appears quite reasonable that the MoO_3 existing as a thin film would behave quite differently from the bulk material insofar as melting and evaporation are concerned. Analogous cases may be cited. Gulbransen and Wysong (20) observed that the oxides of tungsten evaporate at a measurable rate at 800°C when present as thick films but require 900°C for thinner films. The thickness of the film influences what at first glance would appear to be a totally independent property. From the many observations that have been made it is concluded that Mo in the 78% Ni alloy is oxidized in the first instant at these elevated temperatures. The MoO_3 so formed may in time volatilize or may remain at the alloy-oxide interface. Thus in some instances MoO_3 is actually observed, but normally the influence of this compound is in the strained first formed film.

The correct assignment of the enlarged spinel structure found after oxidation in the O_2-N_2 mixtures of high dew point is difficult without supporting chemical analysis. The lattice spacings show good agreement with Mn_3O_4 and $MnO \cdot Fe_2O_3$. The cubic modification of MnO_2O_4 has an a_o value of 8.7 and MnO-Fe_2O_3, according to Purdue work (17), may be assigned 8.50 or 8.44. The data reported above give average a_o values of 8.58 and 8.60, but within experimental error it can only be stated that the parameter falls in the range of 8.50-8.60. There is literature to support the idea that the Mn content of the alloy even when less than 1% will have a significant effect on the structure of the film. Yearian, Randell, and Longo (21) in their investigation of oxide scales on chromium steels observed the $MnCr_2O_4$ species in steels containing only 0.40% Mn. The extensive studies by Gulbransen, *et al.* (22, 23) on heater alloys indicate that Mn contents in the 0-2% range will affect the heat resistance of steels, and it is reasonable to conclude that Mn enters into the structure of the film in some manner. Working with alloys containing 80% Ni and 20% Cr, in one case 2.30% Mn and in the other 0.05% Mn, it was observed that the oxidation rate of the alloy with the higher Mn content was greater than the lower.

The influence of H_2O on the reaction between Fe_2O_3 and metallic monoxides has been studied (24) at low temperatures (150°C). It was concluded that the presence of moisture favors spinel formation. Why moisture should favor the formation of a spinel which contains Mn or has a larger lattice parameter than nickel ferrite is not obvious.

Manuscript received March 4, 1960; revised manuscript received Oct. 26, 1960.

Any discussion of this paper will appear in a Discussion Section to be published in the December 1961 JOURNAL.

REFERENCES

1. R. T. Foley, J. U. Druck, and R. E. Fryxell, *This Journal*, **102**, 440 (1955).
2. R. T. Foley, C. J. Guare, and H. R. Schmidt, *ibid.*, **104**, 413 (1957).
3. R. T. Foley and C. J. Guare, *ibid.*, **106**, 936 (1959).
4. J. Benard and J. Moreau, *Rev. Met.*, **47**, 317 (1950); *Compt rend.*, **232**, 1842 (1951).
5. M. J. Brabers and C. E. Birchenall, *Corrosion*, **14**, 179t (1958).
6. H. J. Yearian, H. E. Boren, Jr., and R. E. Warr, *ibid.*, **12**, 561t (1956).
7. S. W. Kennedy, L. D. Calvert, and M. Cohen, *Trans. Am. Inst. Mining Met. Engrs.*, **215**, 64 ((1959).
8. G. Hägg and A. Magneli, *Arkiv Kemi, Mineral., Geol.*, **19A**, No. 2, 14 pp. (1944).
9. I. Iitaka, T. Nakayama, and K. Sekiguchi, *J. Sci. Research Inst. (Japan)*, **45**, 57 (1951).
10. R. F. Mehl, E. L. McCandless, and F. N. Rhines, *Nature*, **134**, 1009 (1934).
11. R. F. Mehl and E. L. McCandless, *ibid.*, **137**, 702 (1936).
12. H. J. Goldschmidt, *J. Iron Steel Inst.*, **146**, 157 (1942).
13. "Electron Diffraction" p. 359 Z. G. Pinsker, Butterworths Scientific Publications, London, (1953).
14. J. Benard and J. Bardolle, *Compt. rend.*, **232**, 231 (1951); **232**, 2217 (1951).
15. L. E. Collins and O. S. Heavens, *Proc. Phys. Soc.*, **70(B)**, 265 (1957).
16. D. W. Pashley, *Advances in Physics*, **5**, 173 (1956).
17. J. F. Radavich, ASTM Special Publication #171 (1955).
18. J. W. Hickman and E. A. Gulbransen, *Trans. Electrochem. Soc.*, **91**, 605 (1947).
19. J. W. Hickman, *The Iron Age*, Aug. 12, 1948 p. 90, Aug. 19, 1948 pp. 90.
20. E. A. Gulbransen and W. S. Wysong, *Am. Inst. Mining & Met. Engrs. Inst. of Met. Div.*, **175**, 611 (1948).
21. H. J. Yearian, E. C. Randall, and T. A. Longo, *Corrosion*, **12**, 515t (1956).
22. E. A. Gulbransen and W. R. McMillan, *Ind. Eng. Chem.*, **45**, 1734 (1953).
23. E. A. Gulbransen and K. F. Andrew, *This Journal*, **106**, 941 (1959).
24. J. Longuet, *Compt. rend.*, **213**, 577 (1941).

Anodic Behavior of Austenitic Stainless Steels and Susceptibility to Stress Corrosion Cracking

S. Barnartt and D. van Rooyen

Research Laboratories, Westinghouse Electric Corporation, Pittsburgh, Pennsylvania

ABSTRACT

The anodic behavior of a purified 16 Cr-20 Ni stainless steel, which was unsusceptible to stress corrosion cracking, was compared with that of a susceptible 18 Cr-8 Ni alloy in 42% $MgCl_2$ at 146°C. Potential-time curves, potential-current curves, and potentiostatic current-time curves were compared. The potential-time behavior of pure iron, chromium, and nickel was also determined and indicated that dissolution from a nickel-rich surface controlled the anodic behavior of the stainless steels. Potentiostatic corrosion at potentials 50-100 mv more noble than the initial immersion potential eliminated the crack-initiation period and increased the density of cracks by two orders of magnitude in the susceptible alloy. In the 16-20 alloy these potentials caused rapid corrosion and/or deep pitting but no cracking. Potentiostatic corrosion in this potential range provides a highly accelerated test for susceptibility to cracking. From potential-current curves it was shown that propagation is accompanied by enhanced metal dissolution, in agreement with the general electrochemical mechanism of cracking.

Commercial austenitic stainless steels all exhibit susceptibility to stress corrosion cracking (1-3). The susceptibility is not an inherent one fixed by the proportions of iron, chromium and nickel, for in some alloys it may be completely overcome by purification or by a change in concentration of minor elements (4-6). In susceptible alloys cracking is primarily transgranular, and stress, either applied or internal, is essential for crack propagation at a finite rate. The greater the stress the shorter the time for complete fracture through a given specimen, and there appears to be no threshold stress level below which failure will not occur (8).

Crack propagation in stainless steels is slow relative to brittle fracture; this and the observation that a growing crack can be stopped by cathodic protection have led to the concept of a purely electrochemical mechanism of stress corrosion cracking (8-11). According to this mechanism, a definite period of corrosion is required before a crack can initiate, after which the crack grows at a rate controlled by the anodic metal dissolution reaction at the advancing edge of the crack, where the anodic current within the crack is concentrated. It is not yet established whether an initiated crack will propagate only when it occurs at the site of a preexisting susceptible path, as was first suggested by Dix (10), or whether any initiation site will permit propagation under stress as long as the anodic current to the advancing edge is not impeded by corrosion products within the crack, as was suggested by Hoar and Hines (8).

A cyclic mechanism in which slow electrochemical propagation alternates with a short but rapid mechanical fracture was proposed by Keating (12). The strongest support for this mechanism was provided by motion picture studies of crack propagation along the surface of a susceptible metal, which revealed short and rapid steps of surface propagation, both for austenitic stainless steels (13) and for brass (14). This is not sufficient evidence, however, because it is possible for a crack growing smoothly in three dimensions to break through the surface in bursts, particularly if surface parting is impeded by an oxide film (15). The mechanical fracture step, according to Keating (12), is initiated when the corrosion process produces a stress-concentrating notch which is located at an appropriate lattice site or boundary. A different cause was assumed by Nielsen (16) who, from electron microscope studies of corrosion products deposited within cracks, concluded that solid corrosion products can exert a wedging action and produce periodic mechanical fracture.

Attempts to reveal mechanical fracture steps by discontinuities in the elongation of a cracking wire and by sudden potential drops (7, 8), or by acoustical detectors (7) have been negative in the case of austenitic stainless steels. There is a need for more detailed investigations of these alloys to determine the extent of mechanical or anodic-dissolution contributions to crack propagation. This paper is concerned with the latter contribution.

The aim of the present study was to investigate local anodic reactions by direct electrochemical measurements during stress corrosion cracking. In particular, a comparison was made of a commercial 18 Cr-8 Ni (AISI type 304) stainless steel, highly susceptible to cracking, with an unsusceptible 16 Cr-20 Ni steel. The corroding liquid selected was boiling 42% $MgCl_2$ solution, since this has been shown to be generally effective in cracking susceptible austenitic stainless steels (5, 8, 17).

Experimental

Materials.—The purified 16-20 alloy was prepared by vacuum casting a mixture of electrolytic iron, electrolytic chromium, and electrolytic nickel. It

Table I. Composition and mechanical properties of the stainless steels

	18-8	16-20
Composition (%)		
Cr	18.6	16.2
Ni	9.45	19.9
C	0.057	0.013
N	0.068	0.010
O	0.013	0.016
Mn	0.71	
Si	0.55	
Al	0.058	
S	0.03	0.011
P	0.035	<0.003
Yield stress (0.2% strain):		
kg cm^{-2}	2400	910
lb in^{-2}	34,000	13,000
Ultimate tensile strength:		
kg cm^{-2}	6500	4400
lb in^{-2}	93,000	63,000

was hot forged and then drawn to wire, 0.7 mm (0.028 in.) diameter, in successive steps of 50% reduction and vacuum annealing at 1065°C. The commercial 18-8 alloy was received as wire 0.6 mm (0.024 in.) in diameter. The wires of each alloy were straightened, electropolished anodically at 0.5 amp cm^{-2} in the solution 10M H_3PO_4, 4.5M glycerol at 100°C, to reduce the diameter by 25 μ (1 mil), and activated cathodically in 3M HCl at 50 ma cm^{-2} for 1 min to remove any film from the electropolishing process. They were then annealed in vacuum ($<4 \times 10^{-4}$ mm Hg) at 1065 (±5)°C for 15 min, and quenched by rapidly moving them to a cold section of the vacuum chamber. The chemical composition and mechanical properties of the two alloys are listed in Table I. Just before use the wires were cleaned, with pure acetone, water, and alcohol. When it was desired to reactivate the surface, the above electropolishing-activation treatment was repeated just before insertion of the wire into the cell.

Nickel wire of 99.4% purity was used after vacuum annealing at 875°C for 15 min. The iron was 99.9+% strip, vacuum annealed at 915°C for 15 min. Chromium, 99.95% arc-melted "ductile" strip, was used as received.[1] Just before use each metal was activated by anodic treatment for 1 min in 3M HCl at 50 ma cm^{-2}.

A single batch of reagent-grade $MgCl_2 \cdot 6H_2O$ was used for all of the experiments reported here. This batch gave a pH of 5.6 for a 1M solution at 25°C. It was found in previous experiments that some batches of salt showed higher pH and this affected measurements of time to fracture.

Cell.—The Pyrex reaction cell is shown schematically in Fig. 1. The wire being tested passed through capillary ends of the horizontal section, which was heated to maintain 42.5% $MgCl_2$ solution at its boiling point. The boiling point was measured in a Cottrell-type apparatus and was found to be 146°C at 730 mm Hg, a value consistent with the older data (18) and in disagreement with the value of 154°C

[1] Supplied by U. S. Bureau of Mines, Albany, Oregon.

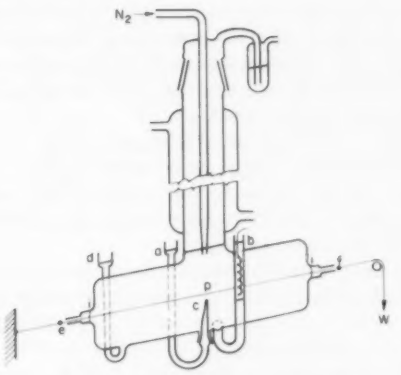

Fig. 1. Stress corrosion cracking cell

reported in more recent papers (8, 17, 19, 20) for 42% $MgCl_2$.

When adding solution to the cell, the reference electrode tube ac was first filled, cooled, and inserted into the cell, then the hot solution was poured through tube d. The solution solidified in tubes a, b, and d, as well as in the capillary ends, thus sealing off these points while the bulk of the liquid was maintained at the boiling point. The upper portion of the cell, which carried a condenser, was sealed by means of a water trap. Nitrogen, purified by passage through a tube filled with copper wire at 430°C and through a distilled-water humidifier, was passed through the cell during each experiment, except where otherwise noted. The above cell arrangement was varied for potential measurements on unstressed chromium or iron strip; the strip was suspended vertically from inside the nitrogen-inlet tube.

The potential of the corroding metal was measured with reference to a saturated calomel electrode (SCE) at 25°C. The latter was connected to the cell through a saturated KCl bridge which contacted the solidified $MgCl_2$ solution at a. The potentials reported herein included the liquid junction potential plus the thermal gradient potential in tube ac, resulting in a constant small shift in the potential of the reference electrode. All potential measurements were corrected for any *IR* drop in the wire and in the solution as described below. Potential-time curves were recorded on a high-impedance potentiometer-type recorder (input impedance = 10^8 ohms, maximum out-of-balance voltage = 0.05 v).

By means of the stainless steel auxiliary electrode in tube b, current was passed to the test specimen when it was desired to maintain the latter at constant potential. The potentiostat used for this purpose controlled to ±1 mv. Since electrical connection to the test wire was made at both ends, points e and f, the current distribution was assumed to be uniform over the wire. This assumption would be expected to produce no serious error considering the high conductivity of the solution (K = 0.27 ohm^{-1} cm^{-1} at 146°C) and the dimensions involved: wire diameter = 0.06 — 0.07 cm, cell diameter = 5.0 cm, effective wire length between liquid-solid boundaries (i in Fig. 1) = 10 cm.

This cell represents an improvement over that of Hoar and Hines (8) in eliminating their gas-wire-solution contact and in permitting accurate correction for the *IR* drops included in the potential measurements as described below.

IR voltage corrections.—It was necessary to apply two corrections to the observed potential values: (*a*) *IR* voltage drop in the solution between the capillary tip c and the wire surface; (*b*) *IR* drop in the wire from p to e (Fig. 1).

A capillary tip of external diameter $d = 0.07$ cm was used, and this was positioned at a distance $3d$ from the wire, far enough away to avoid shielding errors (21, 22). To calculate the *IR* drop in the solution, Ohm's law in the form $i = -\kappa\, dV/dn$ was integrated for coaxial cylinders from $n = r'$ to $n = r' + 3d - d/3$ to yield

$$IR_{(soln)} = \frac{i' r'}{\kappa} \ln \frac{r' + 3d - d/3}{r'} \qquad [1]$$

where r' is the radius of the wire electrode and i' the current density at the surface of the wire. Equation [1] is based on the observation previously made with parallel plane electrodes (21, 22) that the potential inside the capillary is equal to that at a distance $d/3$ closer to the electrode in the undistorted field. The $d/3$ correction applied to the coaxial cylinder case should be sufficiently accurate for the present purpose (23).

The correction for the *IR* drop within the wire, for total current I and wire resistance R_l ohm cm^{-1}, was calculated from

$$IR_{(wire)} = L_{ei} R_l I/2 + 5R_l I/4 \qquad [2]$$

The first term is the voltage drop over the wire length L_{ei} (from e to i, Fig. 1). The second term is the drop over the 5 cm length (i to p) exposed to the liquid, based on the assumption of uniform current distribution over this length. The total *IR* drop correction was considered to be accurate to ±10%. The maximum total correction encountered in the data to be presented was 25 mv.

Microscopic examination.—At the end of the reaction period the test wire was removed quickly from the cell and soaked in distilled water and acetone. For metallographic examination the wire was coiled loosely and mounted so that the corroded length could be scanned for cracks at magnifications up to 500. The coiling operation opened up some cracks but produced no new ones. The density of surface cracks was determined as the average number of cracks per cm length of wire along one edge.

Results and Discussion

Corrosion potentials in absence of applied current.—Pure iron and chromium, unstressed, corrode rapidly in boiling $MgCl_2$ with copious hydrogen evolution. Their corrosion potentials remain relatively active as shown in Fig. 2; the reactions were stopped after 30 min because of rapid metal dissolution. Pure nickel and the two stainless steels react much more slowly, and their corrosion potentials are considerably more noble. These data support the assumption of Hoar and Hines (24), that

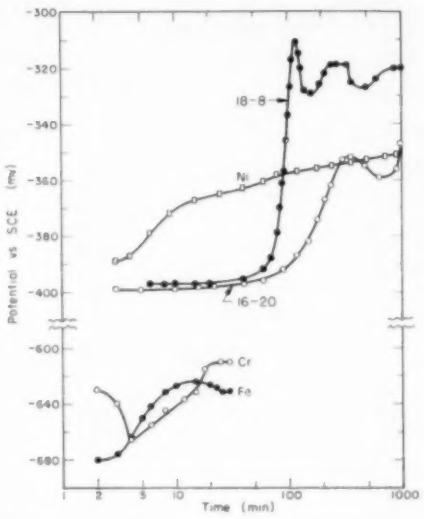

Fig. 2. Corrosion potential vs. time for unstressed metals in aqueous 42% $MgCl_2$, 146°C, nitrogen atmosphere.

iron and chromium dissolve preferentially at the local anodes on the stainless steel, leaving a nickel-rich surface which controls the anodic reaction.

The two stainless steels, unstressed, showed the same general shape of potential-time curve, although the 18-8 exhibited a quicker rise to final potential (2 hr, compared with 6 hr for the 16-20) and its potential tended to level off at a somewhat higher value. At the initial potential of about −400 mv, hydrogen was evolved from each alloy, presumably because of relatively rapid dissolution of iron and chromium; the rate of gas evolution decreased towards zero as the potential increased, indicating a large decrease in corrosion rate during the potential rise. This was confirmed by corrosion current measurements to be presented below.

Applied stress had no appreciable effect on the potential-time curve of the 16-20 steel; the curves were followed for about 72 hr at stresses up to 2800 kg cm^{-2} (40,000 psi). No cracking of this alloy was produced in any of the experiments to be described, even after 250 hr at 2800 kg cm^{-2}, the maximum time studied.

The potential-time curve of the crack-susceptible 18-8 steel also exhibited little effect of stress up to a few minutes before the wire broke, as shown in Fig. 3. Up to point G the general shape of the curves with stress was similar to that without stress; after

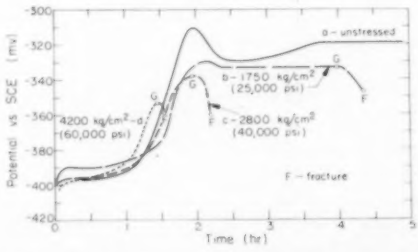

Fig. 3. Effect of stress and time on corrosion potential of 18-8 stainless steel, N_2 atm.

this point the potential fell abruptly until fracture occurred at point F. When corrosion was interrupted just before G, no cracking was found metallographically. Just after G very small cracks appeared and these elongated gradually from G to F. The cracks all tended to lie in planes perpendicular to the stress (and wire) axis. Thus the corrosion time to point G is the induction or crack-initiation period, and GF the propagation period. As seen in Fig. 3, increased stress shortened the induction period and lowered the maximum potential reached. Similar behavior has been reported by Hoar and Hines (8) for several susceptible 18-8 steels. Increased stress tended to shorten the propagation period as well for the 18-8 metal studied here, whereas Hoar and Hines discerned little effect of stress on propagation time. Certainly as the applied stress closely approaches the ultimate tensile strength one would expect greatly reduced propagation periods, since cracks could not penetrate appreciably before fracture.

Substitution of oxygen for the purified nitrogen atmosphere did not accelerate cracking and had no effect on the potential-time curve of either alloy under applied stress (curve a, Fig. 4 and 5). It was concluded that hydrogen-evolution was the primary cathodic reaction. It should be noted that Uhlig and Lincoln (19) found that the presence of oxygen reduced the time to failure of 18-8 U-bend specimens by 40%. Hoar and Hines (24), however, reported that substitution of an air atmosphere for argon did not affect the potential or the stress-corrosion process, but these workers suspected oxygen leakage into the cell and assumed that oxygen dissolution was the only cathodic reaction.

Reactivation of the wire surface just prior to testing in a nitrogen atmosphere was carried out by the electropolishing and cathodic HCl treatments, which removed any oxide film left by the "vacuum" annealing step, and this produced specific effects on the two metals. The effect on the 16-20 alloy (curve b, Fig. 5) was a higher initial potential, but the potential fell quickly and thereafter followed the usual course. Reactivation of the 18-8 alloy led to a considerable reduction in the crack-initiation period with no significant change in the crack-propagation time, the same result found by Hoar and Hines (8) for an acid-pickled surface, and also caused an increase in crack density from 2 to 10 cracks/cm.

Addition of 0.10% HCl to the solution (curve c, Fig. 4 and 5) raised the initial potential of each alloy up to or slightly above the steady-state potential and produced highly accelerated corrosion as evidenced by copious hydrogen evolution. In the case of the 18-8 wire, the crack-initiation period was eliminated by the HCl addition; the acid did not change the crack propagation time, but it increased crack density by two orders of magnitude (150 cracks/cm, Fig. 7a). The 16-20 alloy exhibited accelerated corrosion and general pitting, but no cracking (Fig. 7b). The corrosion rate decreased gradually over a period of several hours as the acid was used up by the corrosion reaction, after which hydrogen evolution virtually ceased.

Potentiostatic current-time curves.—When the crack-susceptible 18-8 alloy under stress was maintained at its initial potential of −400 mv by means of applied cathodic current, the corrosion rate in boiling 42% $MgCl_2$ and nitrogen atmosphere remained negligible, and cracking was postponed indefinitely. Similar cathodic protection has been demonstrated previously (8, 9, 19, 25, 26). It represents an important confirmation of the electrochemical nature of crack propagation, although it does not preclude a periodic mechanical component.

Potentiostatic behavior at more positive potentials, where acceleration of the corrosion process by applied anodic current takes place, can reveal more directly the contribution of the anodic reaction to stress corrosion cracking. Potentiostatic current-time curves, obtained at 2800 kg/cm² in nitrogen

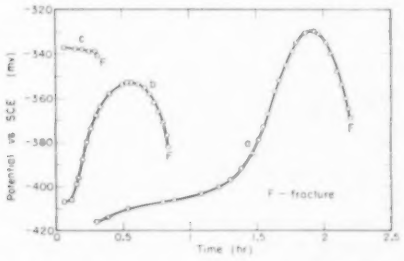

Fig. 4. Corrosion potential vs. time for 18-8 stainless steel, applied stress 2800 kg/cm²; a—O_2 atm; b—metal surface reactivated, N_2 atm; c—0.10% HCl added to solution, N_2 atm.

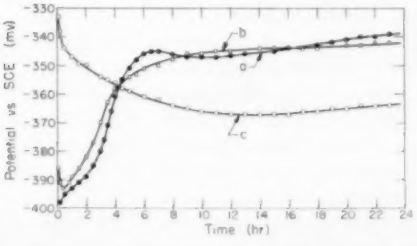

Fig. 5. Corrosion potential vs. time for 16-20 stainless steel, applied stress 2800 kg/cm²; a—O_2 atm; b—metal surface reactivated, N_2 atm; c—0.10% HCl added, N_2 atm.

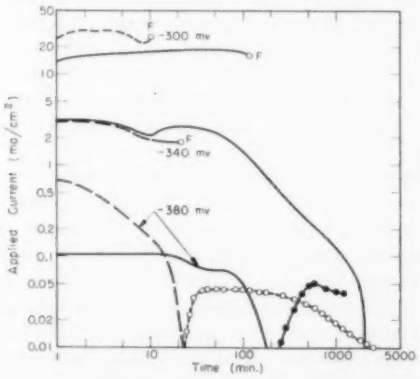

Fig. 6. Applied current vs. time for stainless steels at constant potential, 2800 kg/cm², N_2 atm. Solid lines 16-20; broken lines 18-8. Experimental points omitted where specimen made anode and shown where specimen cathode.

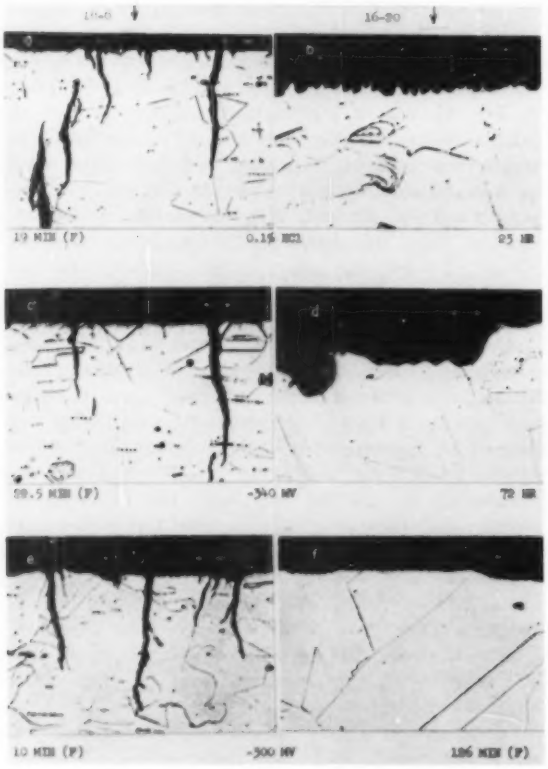

Fig. 7. Cross sections of stainless steel wires corroded in 42% $MgCl_2$, 146°C. N_2 atm, applied stress 2800 kg cm^{-2}: a,b—0.10% HCl added to solution, no applied current; c,d—potentiostatic corrosion at −340 mv vs. SCE; e,f—potentiostatic corrosion at −300 mv vs. SCE; F denotes fracture at time shown. Length of arrow = 20 μ.

atmosphere, are shown in Fig. 6. The selected potentials of −380, −340, and −300 mv, when referred to the normal potential-time curves (curve c in Fig. 3 and curve a in Fig. 5), correspond, respectively, to the beginning of the steep potential rise, the top of this rise, and a value appreciably higher than that attained during normal corrosion.

To maintain −380 mv the application of anodic current was required initially. With either metal the current decreased gradually towards zero, after which the metal remained cathodically protected. During the period of applied anodic current the total number of coulombs passed was relatively small, and little corrosion damage was found microscopically.

Considerably higher anodic currents were required to maintain −340 mv. In the case of the 16-20 alloy the resulting high corrosion rate was prolonged and caused severe general corrosion of the pitting type, but no cracks were produced (Fig. 7d). After 35 hr a small cathodic current (10 $\mu a/cm^2$) was required to maintain this potential, and the corrosion rate remained low. The 18-8 alloy suffered rapid and severe cracking at −340 mv. The cracking time and the crack density in this experiment (Fig. 7c), where the potential was maintained by applied anodic current, were approximately the same as found when a potential close to −340 mv was obtained by addition of HCl (Fig. 7a).

A rise in potential to −300 mv accentuated the corrosion rate of both alloys, and no passivity was induced. The 16-20 steel corroded very rapidly, although more uniformly than at −340 mv, until its cross section was decreased to the point where the ultimate tensile strength of the wire was exceeded and failure occurred (in 2 hr); no evidence of cracking was found (Fig. 7f). In the case of the 18-8 steel the increase in potential caused more general surface attack (Fig. 7e), as well as more rapid failure due to cracking and somewhat higher crack density. It is significant that unstressed 18-8 at −300 mv also exhibited rapid corrosion, resulting in deep pitting all over the surface, but no crack propagation was found. A distinct difference in the behavior of the two alloys at −300 mv was the presence of vigorous gas evolution on the stressed 18-8 wire and the absence of this effect on the 16-20. Since this potential is too low for anodic oxygen evolution, cathodic hydrogen evolution was suspected, and this was confirmed by mass spectrometer analysis of the nitrogen gas emerging from the cell. Normally hydrogen evolution is suppressed, rather than accelerated, at the higher potentials. An explanation of this effect is given later.

Both alloys became covered with a layer of corrosion product when made anodic at elevated potentials (−340 mv or higher). A green coating was produced on the 16-20 alloy, a black one on the 18-8.

These potentiostatic corrosion data indicate that forced corrosion at a fixed potential 50-100 mv more noble than the initial corrosion potential provides a cogent accelerated test for crack susceptibility. Both the rate of anodic dissolution and the density of pitting or cracking sites can be increased by two orders of magnitude at the higher potentials.

Accelerated corrosion, whether by this potentiostatic method or by HCl addition, proved ineffective in cracking the 16-20 alloy. This immunity to stress corrosion cracking is in agreement with data of Uhlig, White, and Lincoln (4, 5) for 20% Ni alloys having low nitrogen contents.

Anodic current as a function of potential.—The variation of corrosion potential with time (Fig. 2-5) signifies a time dependence of the corrosion reaction, but does not fix the magnitude of the corrosion rate. An evaluation of the latter can be made from curves of potential *vs.* applied anodic current (27) which, however, must be scanned relatively quickly when studying stainless steels in hot $MgCl_2$ solution in order to minimize time effects.

Figures 8, 10, and 11 present curves of potential *vs.* applied anodic current density,[2] obtained by taking points at 10 mv intervals every minute. The potentiostatic method was used, the potential being shifted abruptly from the previous value and maintained constant for 1 min before the current was recorded.

Data for the unstressed 16-20 alloy are given in Fig. 8, the initial curves a being taken after the

[2] Anodic current densities shown are averages based on total wire area exposed to the boiling solution, although local cathodes can be expected to remain partially active at low applied currents.

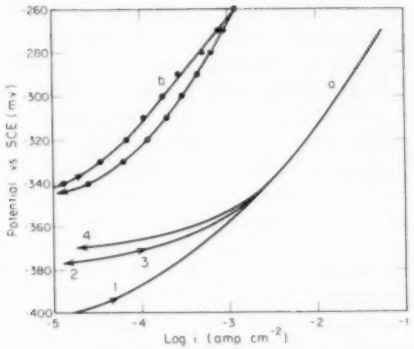

Fig. 8. Potentiostatic polarization curves for unstressed 16-20 stainless steel in 42% $MgCl_2$, 146°C, N_2 atm: a, initial (experimental points omitted for clarity); b, after corrosion to potential maximum.

wire was immersed for 5 min, curves b after normal corrosion to the maximum of the potential-time curve (refer Fig. 5, curve a). Essentially the same set of curves was obtained when the wire was stressed at 2800 kg cm^{-2}, in accord with the fact that stress did not affect the potential-time behavior. The initial curves represent consecutive measurements with increasing potentials followed by decreasing potentials (curves 1 and 2) and the cycle repeated (curves 3 and 4). The gradual shift of the corrosion potential toward more noble values was caused presumably by nickel dissolution; the portion of the curve at the high potentials remained reproducible. When the wire was first allowed to react until the maximum of the potential-time curve was reached, the subsequent polarization curves (b) were shifted toward much lower current densities. This shift represents a decrease in corrosion current. The return portion of curve b was displaced slightly in the direction of higher current and a less noble corrosion potential, *i.e.*, the wire surface became activated at the high potentials.

According to the theoretical treatment of Wagner and Traud (27), polarization curves of the type observed (Fig. 8) refer to a corroding metal, the anodic and cathodic reactions on which exhibit activation overpotential. These curves obey the equation:

$$I_{app} = I_{cor}\left(\exp\frac{E - E_{cor}}{\beta_a} - \exp\frac{E - E_{cor}}{\beta_c}\right) \quad [3]$$

where I_{app} is the applied anodic current; I_{cor} and E_{cor} are the corrosion current and corrosion potential existing before external current is applied; β_a and β_c are constants referring to the anodic and cathodic reactions, respectively. Equation [3] is equivalent to that derived by Wagner and Traud, and its relation to the kinetics of the anodic and cathodic processes is shown schematically in Fig. 9. Here CF represents the cathodic polarization curve for the process $H^+ + e \rightarrow \frac{1}{2} H_2$, BD the anodic polarization curve for $Ni \rightarrow Ni^{+2} + 2e$, and AB the observable curve for applied anodic current (Eq. [3]). In the Tafel region the latter curve becomes identical with the anodic curve BD, so that extrapolation of this region back to E_{cor} yields the corrosion current.

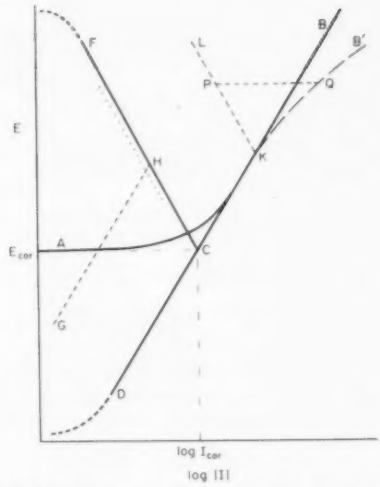

Fig. 9. Schematic diagram of local anodic and cathodic reaction rates.

The value of I_{cor} obtained by this extrapolation procedure for the 16-20 alloy (Fig. 8) was 3×10^{-4} amp cm^{-2} initially (curve a), decreasing by an order of magnitude at the potential maximum (curve b). The 18-8 alloy, either annealed or stressed, gave approximately the same value for the initial corrosion current (curve a, Fig. 10 and 11), again decreasing by an order of magnitude at the potential maximum (curve b). Thus in the absence of crack propagation the two alloys exhibited essentially the same corrosion rate at the same corrosion potential, the rate being a function of time but independent of applied stress. On each metal the active anode area must have diminished by an order of magnitude during corrosion to the potential maximum.

At potentials above −320 mv the unstressed 18-8 alloy exhibited marked activation (bending of the polarization curve toward higher currents), particularly after corrosion to the potential maximum (Fig. 10, b). This activation was accompanied by rapid localized pitting, but no cracks were produced. When the 18-8 metal was stressed, bending of the polarization curve was even more pronounced (Fig. 11,b). The latter curve covered only 8 min of corrosion time before fracture, at which time a very high crack density existed and

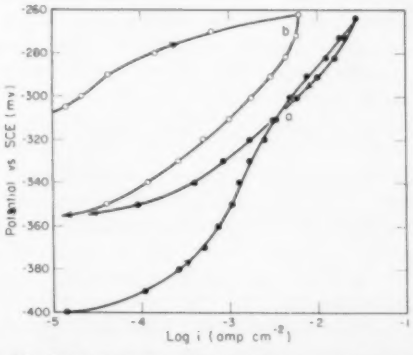

Fig. 10. Potentiostatic polarization curves for unstressed 18-8 stainless steel: a, initial; b, after corrosion to potential maximum.

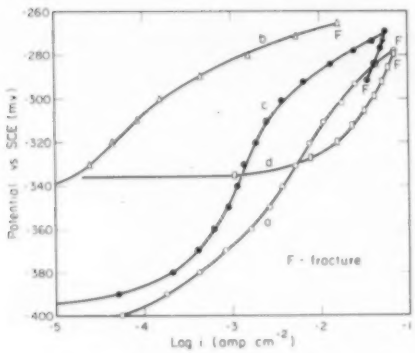

Fig. 11. Potentiostatic polarization curves for 18-8 stainless steel at 2800 kg/cm²: a, initial; b, after corrosion to potential maximum; c, initial but with reactivated surface; d, initial but with 0.10% HCl added.

a correspondingly high metal-dissolution rate (2×10^{-2} amp cm^{-2}) was achieved. These results demonstrate that crack propagation is accompanied by high rates of anodic metal dissolution, although they do not rule out the possibility of a short mechanical fracture alternating with the electrochemical step. Uhlig and Lincoln (19) have shown by weight loss measurements that 304 stainless steel U-bend specimens exhibit increased corrosion rates when stressed.

Another effect characteristic of the cracking metal at potentials above −320 mv was the presence of vigorous hydrogen evolution, which was observed during the constant-potential experiments described above and during the runs of Fig. 11. Little or no gas evolution was observed at high potentials with unstressed 18-8 (Fig. 10) or with the 16-20 alloy stressed or unstressed (Fig. 8).

The addition of HCl had a marked effect on corrosion rate of the stressed 18-8, as shown in Fig. 11. When the potential $E_{cor} \cong -340$ mv was reached after corrosion to the potential maximum (curve b), I_{cor} was relatively small; but when the same potential was produced by HCl addition (curve d), I_{cor} was roughly three orders of magnitude higher.

An explanation of these results in terms of local anodic and cathodic reactions is provided by the schematic curves of Fig. 9. The corroding metal, stressed or unstressed, has an initial potential represented by C, and metal dissolution occurs over an appreciable fraction of the surface until some of the anodic areas become covered with a coating. As the active anode surface becomes smaller, the anodic polarization curve CD shifts in the direction of GH. The cathodic polarization curve would shift slightly to the left (dotted line) for any pH rise resulting from corrosion in the absence of applied current but this effect should be small. Point H represents the corroding wire at the initial maximum of the potential-time curve (Fig. 3-5), up to which time the corrosion current gradually decreased while the potential increased.

The application of stress to the crack-sensitive alloy does not affect the anodic and cathodic reaction rates within the initiation period. During this period metal dissolution develops cracking sites, either by uncovering active metal or by creating stress-raising pits or both. If cracks propagate by an entirely electrochemical mechanism, the metal surface at cracking sites must, by stress-induced changes in composition or structure, have a reversible potential appreciably more active than the surrounding metal. At a given potential such sites will exhibit unusually high metal-dissolution rates. During crack propagation, therefore, the over-all anodic polarization curve would be shifted toward higher currents and the corrosion potential would decrease (from H toward C), as was observed. This shift of the anode polarization curve produces gradual bending of the E — log i curves (Fig. 8, 10, 11) as the potential is raised and new cracks generated.

If the potential is raised abruptly to a value close to H by addition of HCl, the hydrogen-overpotential curve is displaced to KL. The hydrogen-evolution and metal-dissolution rates, both given by K, are now high and a high density of cracks results. Similarly any other cathodic depolarizer (such as Fe^{+3}) would be expected to cause more rapid and severe cracking provided the addition did not impede the anodic reaction.

Stress-induced changes at the tip of a propagating crack tend to direct the anodic penetration into a path perpendicular to the stress axis. The resulting narrow crevice, and localization of the anodic reaction at the advancing edge, lower the pH within the crack. The following over-all anodic reaction is illustrative, although the precipitated oxide is actually more complex (16)

$$M + H_2O \rightarrow MO + 2H^+ + 2e \qquad [4]$$

The decrease in pH displaces the local cathodic polarization curve toward KL, thus creating cathodic areas of high current density within the crack. This displacement explains the observed gas evolution accompanying cracking at high potentials in the solution without added HCl. Thus at potential PQ, the cathodic polarization curve may be represented as having shifted to LK. The cathodic current, given by P, is relatively high and confined to the cracking site.

It may be concluded that stress corrosion cracks are initiated when localized dissolution uncovers sites having particularly active potentials. Propagation of the cracks along stress-oriented paths then occurs partly, if not entirely, by an electrochemical dissolution mechanism. Cracking paths are probably connected with impurities, which may simply concentrate or may induce structural changes. The pronounced effect of impurities on susceptibility of stainless steels has been described by Uhlig, White, and Lincoln (4-6). Enhanced metal dissolution at slip planes or stacking faults has been observed by Leu and Helle (20) for stainless steels, and by Edeleanu (14) and Swann and Nutting (28, 29) for copper alloys. It remains to be established which specific impurities give rise to electrochemical crack propagation, and whether or not a periodic mechanical component is necessary for sustained propagation.

Conclusions

1. During the crack-initiation period the susceptible 18-8 stainless steel corrodes in approximately the same potential range and with the same average current densities as does the unsusceptible 16-20.

2. Dissolution of a nickel-rich surface appears to be the controlling anodic process in the alloys.

3. The cathodic process is primarily hydrogen evolution, not oxygen reduction.

4. Crack propagation in the susceptible metal is accompanied by enhanced anodic dissolution.

5. Potentiostatic corrosion at a potential 50-100 mv more noble than the initial immersion potential provides a potent, accelerated test for susceptibility to stress corrosion cracking.

Acknowledgments

We are indebted to J. Heuschkel for the 16-20 stainless steel and to E. R. Kearns for assistance with preliminary measurements. One of us (van R.) wishes to thank the Office of Naval Research for partial support.

Manuscript received Aug. 15, 1960; revised manuscript received Oct. 31, 1960. This paper was prepared for delivery before the Houston Meeting, Oct. 9-13, 1960.

Any discussion of this paper will appear in a Discussion Section to be published in the December 1961 JOURNAL.

REFERENCES

1. "Physical Metallurgy of Stress Corrosion Fracture," T. N. Rhodin, Editor, Interscience Publishers, New York (1959).
2. "Stress Corrosion Cracking and Embrittlement," W. D. Robertson, Editor, John Wiley & Sons, Inc., New York (1956).
3. "Symposium on Stress Corrosion Cracking of Metals," ASTM-AIME, Philadelphia (1945).
4. H. H. Uhlig and R. A. White, *Trans. Am. Soc. Metals*, **52**, 830 (1960).
5. H. H. Uhlig, A. White, and J. Lincoln, *Acta Met.*, **5**, 473 (1957).
6. H. H. Uhlig, Ref. 1, p. 1.
7. D. van Rooyen, *Corrosion*, **16**, 421t (1960).
8. T. P. Hoar and J. G. Hines, *J. Iron Steel Inst.*, **182**, 124 (1956).
9. R. B. Mears, R. H. Brown, and E. H. Dix, Ref. 3, p. 323.
10. E. H. Dix, *Trans. AIME*, **137**, 11 (1940).
11. H. L. Logan, *J. Research Natl. Bur. Standards*, **48**, 99 (1952).
12. F. H. Keating, "Symposium on Internal Stresses in Metals and Alloys," p. 311, Institute of Metals, London (1948).
13. W. W. Kirk, F. H. Beck, and M. G. Fontana, Ref. 1, p. 227.
14. C. Edeleanu, Ref. 1, p. 79.
15. J. G. Hines, Ref. 1, p. 92.
16. N. A. Nielsen, Ref. 1, p. 121.
17. M. A. Scheil, Ref. 3, p. 395.
18. Gmelins Handbuch der Anorg. Chem., Magnesium B, p. 128, Verlag Chemie, Berlin (1937).
19. H. H. Uhlig and J. Lincoln, *This Journal*, **105**, 325 (1958).
20. K. W. Leu and J. N. Helle, *Corrosion*, **11**, 249t (1958).
21. S. Barnartt, *This Journal*, **99**, 549 (1952).
22. R. Piontelli, G. Bianchi, U. Bertocci, C. Guerci, and B. Rivolta, *Z. Elektrochem.*, **58**, 54 (1954).
23. S. Barnartt, *This Journal*, **108**, 102 (1961).
24. T. P. Hoar and J. G. Hines, International Committee for Electrochem. Thermod. and Kinetics (CITCE), **8**, p. 273, Butterworths Scientific Publications, London (1958).
25. J. G. Hines and T. P. Hoar, *J. Appl. Chem.*, **8**, 764 (1958).
26. V. V. Romanov and V. V. Dobrolyubov, *Metalloved. i Obrabotka Metal.*, No. 7, p. 19 (1958).
27. C. Wagner and W. Traud, *Z. Elektrochem.*, **44**, 391 (1938).
28. P. R. Swann and J. Nutting in "Structure and Properties of Thin Films," p. 196, C. A. Neugebauer, J. B. Newkirk, and D. A. Vermilyea, Editors, John Wiley & Sons, Inc., New York (1959).
29. P. R. Swann and J. Nutting, *J. Inst. Metals*, **88**, 478 (1960).

Capacitor Grade Tantalum

Kawecki Chemical Company, Boyertown, Pennsylvania

Lawrence H. Belz

ABSTRACT

The occurrence and cost of tantalum are reviewed. Requirements for electrolytic capacitor use are discussed along with methods of functional quality control. Different powder types are tabulated and their properties are related to porous anode design, production, and performance. The effects of anode density and sintering temperature are displayed, and recommendations are made in the interest of enhancing lifetime and d-c leakage stability. The production of sheet, wire, and foil are reviewed, and electrical characteristics are tabulated.

The tantalum content of the earth's crust has been estimated at 2 ppm, which indicates an abundancy comparable to scandium, beryllium, hafnium, and boron. Tantalum ore always contains columbium. Columbium is estimated to comprise 24 ppm of the earth's crust, which content compares with molybdenum and tungsten. The two metals occur as oxides, chemically bound to either iron or manganese, and are called either ferro- or mangano-tantalate or columbate.

At present, the major sources of ore are by-products of other mining operations. These include tin (cassiterite) mining in the Belgian Congo and the eastern hemisphere, the lithium pegmatite operations in Rhodesia and Nigeria, and certain beryl deposits in Brazil. In years past some tantalite ore,

as such, has been mined in South America, but these deposits have become difficult to use. The tantalite/columbite ore is separated from the major ore by a combination of electrostatic, electromagnetic, and hydraulic processes. In the case of the tin operation, some tantalite reports in the slag resulting from the smelting operation. This slag is an important but less desirable source of metal and is used in the production of ferrotantalum and ferrocolumbium. The ore is sold through brokers to the different tantalum metal producers who bid and buy in an open, competitive market where lots of ore are sold on a spot or contract basis. The prices vary from \$3.00/lb of Ta_2O_5 in 20% ore to \$7.00/lb of Ta_2O_5 in 70% ore.

Several methods for the production of salts and powder have been published (1). Most of these processes have common intermediate products, *i.e.*, K_2TaF_7 and metal powder. The powder is used directly as sintered porous anodes or is consolidated to wire, sheet, or foil.

Many attempts have been made to write a meaningful chemical specification for capacitor grade tantalum powder, recognizing that capacitor performance is related directly to powder purity. Obviously, good anodes are produced more readily from high-purity powder, but the purification achieved during sintering permits the use of powders with relatively high contents of some volatile materials. These impurities are mainly carbon and silicon, but apparently all impurities are volatilized to some degree. A typical analysis of capacitor grade powder is: Cb <0.01%; Ti <0.005; Fe 0.005; Mn <0.001; Sn 0.003; Ni 0.002; Cr <0.001; Ca 0.001; Na <0.005; Al <0.005; Si 0.02; C 0.005-0.08.

Porous Sintered Anodes

Tantalum, along with Al, Cb, and several other metals (2) can be oxidized anodically in an electrolyte such that the metal surface is covered by an insulating dielectric film. The different metal oxide films have varying properties as regards temperature and chemical stability, voltage breakdown, and dielectric constant. This dielectric film is the essence of an electrolytic capacitor and, in the case of tantalum, the good chemical and electrical stability of the oxide film allows the production of a capacitor with outstanding characteristics. The metal is relatively expensive so that every effort is made to use it in a form where the surface area is high per unit weight, such as thin metal foil, or a porous body of powder sintered at approximately 2000°C.

In some cases where impurities are abnormally high, due to the method of reduction, one can add substances that will react with the impurity to form volatile materials that are removed by sintering. Balke (3) has a patent on the addition of magnesium oxide to aid in carbon removal during sintering. Magnesium oxide has a low bulk density which is useful in obtaining a homogeneous distribution of the oxygen. The tantalum carbide reacts with the oxide to yield volatile carbon monoxide and magnesium. If the oxygen and carbon contents are in proper balance, no addition is required. O'Driscoll and Miller (4) have reported the reverse case where carbon is added to columbium to aid oxygen removal during sintering. The addition of such reactants is undesirable when preparing tantalum for an electrolytic capacitor.

Pressing

The porous slugs or pellets are produced by standard procedures for powder metallurgy. The physical characteristics of the powder and the sintered pellet contribute much to the electrical characteristics so special attention is given to the control of porosity (reciprocal of density), homogeneous porosity, constant weight, and uniform physical dimensions. In large-scale production the powder is fed automatically into a die cavity under circumstances that usually involve vibration. If the powder has a broad particle size distribution, vibration tends to classify the powder inventory in the feed device so that powders of different particle size are fed to the die over the course of a press run. This causes capacitance variation throughout the production.

The weight of each pellet must be controlled closely for the same reason of constant capacitance. This requires that the powder has flowing characteristics that will permit the same weight of powder to free-fall into the die cavity. Tantalum powder is somewhat abrasive to the tooling so that it is customary to add a pressing lubricant to the powder. The lubricant is selected, among other things, so that it will not interfere with the powder flow. Most lubricants are waxy, organic substances that possibly can leave carbonaceous residues in the sintered tantalum pellet. As a precaution, the lubricant usually is removed from the pellet prior to high-temperature sintering. One suitable means is to volatilize the lubricant under vacuum and mild temperature. This further defines the character of a good lubricant as having high vapor pressure. Some typical lubricants include paraffin wax, camphor, zinc stearate, and stearic acid.

The capacitor electrolyte fills the pores of the anode and as a general rule the ohmic resistance of the fill electrolyte varies with the pore size and density. Obviously, the porosity can be kept high by pressing to low densities. However, the powder must have good green strength to allow handling at very low densities. Several interests conflict at this point. Low green or pressed densities give low a-c losses in the finished capacitors but the lower weight of powder reduces the total capacitance in a given size. Also, low pressed densities tend toward high physical shrinkage which causes dimensional control problems. Some powders can be handled at pressed densities as low as 5 g/cm^3 which is 30% of the density of consolidated tantalum, i.e., 16.6 g/cm^3. In normal production the pressed density runs between 7.0-9.0 g/cm^3. Naturally, the sintered or finish densities are higher, due to shrinkage. Sometimes, a lubricant is selected that will add to green strength, in which case the lubricant may be called a binder.

The most popular pellet shape is a cylinder with the length to diameter ratio being less than 2.5 to 1. Some unique pellet shapes are produced where the characteristics or physical design of the capacitor are determinant. If the L/D ratio of the cylinder ex-

Table I. Properties of powder types

Type	Bulk density, g/in.³	Fisher sub sieve size, μ	% −325 Mesh	% Carbon	% Oxygen	Capacitance μf-v/g	% Dissipation factor	ESR, ohms	% Shrink.
C	51-66	6.0-8.5	50-65	0.005-0.012	0.09-0.15	2000-2600	15-28	10-17	8-10
D	60-70	7.0-9.0	50-65	0.005-0.012	0.09-0.15	2100-2500	16-24	10-14	6-8
T	60-80	7.0-8.5	50-65	0.005-0.012	0.05-0.12	2000-2400	14-24	9-12	6-8
Y	60-75	8.5-11	40-55	0.005-0.012	0.04-0.10	1800-2200	9-20	5-9	3-6
K	70-90	7-14	65-75	0.005-0.012	0.03-0.10	1700-2100	11-17	7-10	4-7
E	90-105	16-24	10-20	0.02-0.08	0.04-0.11	1000-1400	7-12	4-7	1-3
L	100+	30+	0-10	0.02-0.06	0.04-0.09	400-1000	—	—	1

ceeds 2.5/1, a tendency toward longitudinal warpage develops. Handling difficulties arise where the L/D ratio goes below 1/1. Between these limits the pellet dimensions are selected to give the proper capacitance values using the electrical constants of the selected powder. Normally, a tantalum wire is attached to the porous body by imbedding in the powder during the pressing.

Powder Types

The reduction processes mentioned above produce powder with different physical and, sometimes, chemical properties. When the powder is consolidated by vacuum casting, the powder properties cease to exist and the method of reduction does not have a direct effect on the performance characteristics of the tantalum. However, when used in the form of a sintered, porous pellet the powder properties are of prime importance. The surface area, and hence capacitance, is primarily a function of particle size and particle shape. New methods of reduction are evolving because of the need to produce powders that will impart requisite characteristics in the finished capacitor.

Table I lists several properties of some tantalum powders that are now available commercially. The powder types are identified by a letter that is arbitrarily chosen to describe a method of production. Powder types C, D, T, Y, and K are commonly called "Hicap" (high capacitance) because they give approximately 2000 μf-v/g of powder when sintered conventionally. Type E is "Locap" and gives about 1000 μf-v/g. Type L is a very low capacitance powder used in some special applications.

The apparent or bulk density is measured in a Scott volumeter device and is a quick and reliable indication of several powder characteristics. Directly, the apparent density (or Scott number) represents the weight of powder that will free-fall into a press die cavity, hence the press tooling and apparent density of the powder must be compatible in order to produce porous anodes of specific design. Indirectly, the same number gives an indication of the green strength, pressing difficulty, and physical shrinkage that will be realized during conventional processing. Low apparent densities indicate good green strength, easy pressing, high shrinkage, and high compression ratio. This relationship is not entirely rigorous but follows a trend. Table I presents apparent density in the conventional terms of grams per cubic inch.

The average particle size is measured by an air permeability method using a Fisher sub sieve sizer. The indicated value should be considered with knowledge of its limitations. This particle size measurement is quick, simple, and reproducible, which makes it suitable as a tool for production control. The limitations stem from the particle shape of the tantalum powder which, in different types, varies from flakes to chunks. Permeability methods are best suited to spherical or near-spherical particles, and the agreement with other methods disappears when the particle shape deviates from spherical. Note that a powder having 55% coarser than 325 mesh or 43 μ by sieve analysis reports as having an average particle size of 9 μ as measured by air permeability. Other methods of particle size measurement used in development work include the Roller gas elutriation method and the BET gas adsorption methods. Although these are more accurate, the cost and time involved make them less desirable for production control.

The functional quality is controlled by pressing and sintering sample anodes from each production powder lot. The characteristics of an anode vary widely with the conditions of pressing, sintering, and anodizing, as shown below. Accordingly, the conditions selected for this functional quality control were picked as representing normal pressing and sintering procedures while the anodizing and leakage test conditions were selected to provide a good test of performance stability. The functional values in Table I were determined on 3.5 g anodes measuring about 0.250 in. diameter x 0.500 in. long. The anodes are pressed to a density of 8.0 g/cm³ and sintered 1 hr at 2050°C, as read on an optical pyrometer. The finished density varies from 8.5 to 10.0 g/cm³ as determined by the physical shrinkage.

All the electrical parameters reported herein were measured in liquid electrolytes using the following procedure. The samples were anodized to 200 v in 0.01% phosphoric acid at 90°C, held at voltage for 2 hr, rinsed, and dried at 90°C. The d-c leakage was measured at 140 v in 10% phosphoric acid at 25°C using a 2-min voltage impression. The capacitance and dissipation factor were measured on a General Radio 1611-AS2 bridge using less than a 1 VAC signal and a 6 VDC bias. ESR values are calculated. The test cell cathode was 8 in.² of silver.

It is easy to make spurious comparisons of dissipation factor and a-c loss data. High ohmic resistance in any of the test circuit wiring will report as high dissipation factor. Also, the resistance of the test electrolyte is a constant value exclusive of the test anode. When comparing a-c loss data one must insure that the test conditions and reporting

method are constant. Capacitance is reported in terms of the product of capacitance times formation voltage, in this case 200 v. At a given formation temperature this value is constant over a wide voltage range.

The d-c leakage by this test is typically 1.0 μa/g. The d-c leakage on a finished capacitor may or may not correlate with this figure, depending on the methods of manufacture and the type of capacitor. The physical shrinkage is determined by measurements on the anode dimensions.

C- and D-type powders are quite similar. D-type has a higher bulk density and is used where existing press tooling has a limited fill depth. Both C and D are quite versatile regarding the many processing techniques currently in vogue. They are easily compacted, have excellent green strength, and provide a wide choice for capacitance performance. C and D have essentially flake shape particles.

T- and Y-type powders are intermediate between flake and chunk particle shape. They have lower green strength and provide slightly less capacitance. This particle shape gives less shrinkage and makes an anode with lower a-c losses. K-type has a chunk shaped particle and has still lower green strength. A lubricant/binder is used when pressing this type. Shrinkage and a-c losses are about equal to T and Y. The capacitance is slightly lower. K powder is used where the powder particle shape appears to have some effect on performance. The final choice of powder type is largely a function of capacitor type and size, voltage range, and production technique. Figures 1 and 2 are photomicrographs of loose and mounted powder samples, each type identified by the prefix letter.

Anode Characteristics

Once the powder type has been selected for a specific anode design, the producer must establish the conditions of pressing and sintering. These include, mainly, the pressed density, sintering temperature, and sintering time. Some functional characteristics of anodes made from powder lots T-1100 and Y-31 are presented here in order to exhibit the variation of anode characteristics with these process variables.

A series of 1.8-g anodes (0.170 in. diameter x 0.450 in. length) were prepared at four pressed densities, *i.e.*, 6.5, 7.0, 8.0, and 9.0 g/cm^3, and were sintered at 1975°C. Anodes below 6.0 g/cm^3 lacked green strength and could not be used. The capacitance per gram decreases as the finished density increases (Fig. 3). Apparently, at higher densities, more particles which would contribute area are sintered into the larger mass of the anode. This capacitance loss, however, is compensated by the presence of more powder at the higher densities. These two effects, *i.e.*, lower capacitance per gram and higher total capacitance in a specific anode, oppose each other as the anode density increases. The resulting capacitance can be followed by the product of unit weight capacitance and finished density which yields unit volume capacitance. This product value, in terms of microfarad volts per cubic centimeter, is included in Table II and is of prime importance when considering the function of a specific anode. With both powders, the total anode capacitance continues to increase at higher finished densities up to 10.5 g/cm^3. On the other powder types and using other sintering temperatures this may or

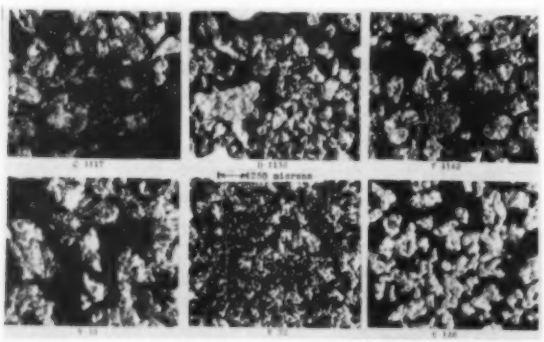

Fig. 1. Photomicrograph of loose, unmounted powder particles; left to right, top, C1117, D1132, T1142; bottom, Y31, K32, E128.

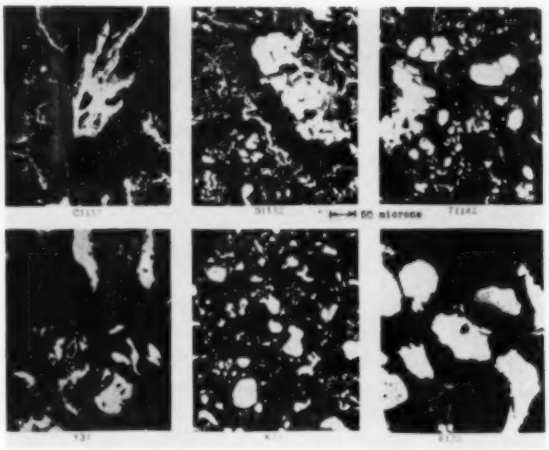

Fig. 2. Photomicrograph of mounted and polished powder particles; left to right, top, C1117, D1132, T1142; bottom, Y31, K32, E128.

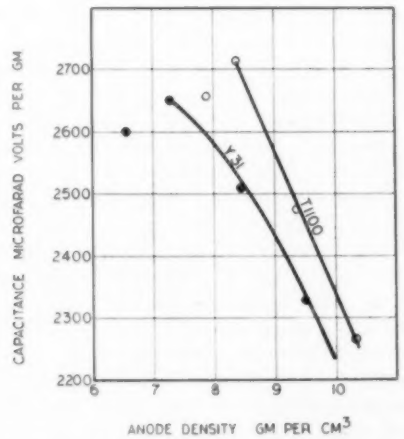

Fig. 3. Variation of unit weight capacitance with sintered anode density.

Table II. Variation of anode characteristics with pressed density
(Sintered 1 hr at 1975°C; anodized to 200 v)

Lot	Pressed density, g/cm³	Sintered density, g/cm³	μf-v/g	μf-v/cm³	μa/g	Equivalent series resistance, ohms	% Shrinkage
T 1100	6.5	7.9	2660	21,000	3.8	7.4	6.8
	7.0	8.3	2710	22,500	1.0	7.8	5.7
	8.0	9.3	2480	23,000	1.1	8.6	5.7
	9.0	10.3	2260	23,300	1.5	10.1	5.2
Y 31	6.3	6.7	2600	19,700	3.7	6.5	2.6
	7.0	7.3	2600	21,400	0.7	7.4	2.1
	8.0	8.5	2510	22,100	1.4	7.4	2.1
	9.0	9.4	2340	22,400	0.8	8.6	1.6

may not occur. Occasionally the volume capacitance reaches a maximum value depending on the slope of the weight capacitance *vs.* finished density curve. Obviously, the volume capacitance of lots T-1100 and Y-31 would decrease as we approached the true density of tantalum, but few porous anodes are used at densities higher than 10.5 g/cm³.

As predicted, the a-c losses vary directly with finished density. This is due to the pore size which establishes the ohmic resistance in the electrolyte path. The d-c leakage appears to rise at low density. The variation at the higher densities should be considered in view of the limitations and general reproducibility of this d-c leakage test.

A second series of anodes were pressed to a density of 8.0 g/cm³ and sintered at the four listed temperatures, all for a time of 1 hr. The results are presented in Table III and Fig. 4. The data show the capacitance varies inversely with sintering temperature. The capacitance also varies inversely with sintering time, as might be expected in view of the fact that sintering occasions a loss of area and consequently capacitance. The tantalum is the most expensive single item in the capacitor and every effort is made to achieve high capacitance and minimize the cost per microfarad. Extremely low sintering temperature gives very high capacitance but the d-c leakage stability is poor. The d-c leakage on the anodes sintered at 1600°C is not listed because it was quite erratic when checked at 140 v.

In some capacitor applications, however, where the working voltage is low, it becomes economically desirable to use the powder at these high unit capacitances. Where conditions are severe, due to high working voltages, it is advisable to recognize a maximum unit capacitance performance consistent with the working voltage, as in the case of the solid electrolyte capacitors built to operate at 35 v. This maximum can be expressed in terms of either unit weight or unit volume capacitance. The recommended ranges are 2200 to 2700 μf-v/g of powder and 20,000 to 24,000 μf-v/cm³ of anode volume. The ranges allow for variation in anode size and geometry. The use of unit volume capacitance has extra merit in that it combines the unit weight performance with operating density and thus compensates for the effect of density mentioned above. The recommended ranges for "Locap" powders are approximately one-half of these listed values.

Table III. Variation of anode characteristics with sintering temperature
(Sintered 1 hr; anodized to 200 v)

Lot	Sintering temp, °C	μf-v/g	μa/g	Equivalent series resistance, ohms	% Shrinkage
T 1100	1600	3620	—	6.5	1.0
	1750	2720	5.5	6.9	1.0
	1975	2480	1.1	8.6	5.6
	2100	2310	1.1	9.3	6.8
Y 31	1600	3080	—	6.7	0.5
	1750	3060	18	7.1	2.1
	1975	2480	1.4	7.4	2.6
	2100	2280	0.6	9.4	3.1

The a-c losses again increase as the pore size gets smaller, in this instance due to higher physical shrinkage at the higher sintering temperatures. The d-c leakage improves at the higher sintering temperatures.

Table IV lists the chemical analysis of the anodes from lot T-1100, sintered at the four temperatures. The analysis of the starting powder also is listed to give a more complete display of the chemical change that accompanies sintering. The metal impurities were done by emission spectrography, the carbon and oxygen with Leco conductometric equipment. The data for lot Y-31 are quite similar.

These remarks and data have been simplified to give a general picture of the variables involved in making porous anodes. The final choice of powder and anode type also depends on capacitor type,

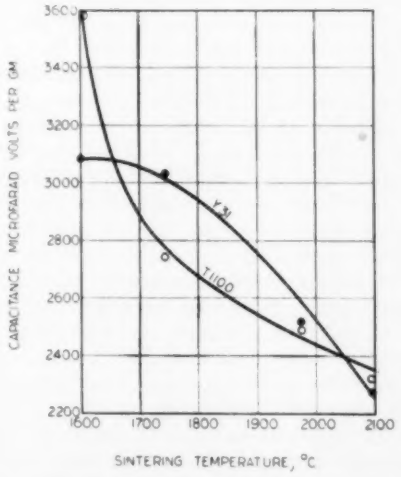

Fig. 4. Variation of unit weight capacitance with sintering temperature.

Table IV. Chemical changes in powder T-1100 sintered at different temperatures

	Powder %	1600°C %	1750°C %	1975°C %	2100°C %
Cb	<0.01	<0.01	<0.01	<0.01	<0.01
Ti	<0.005	<0.005	<0.005	<0.005	<0.005
Fe	0.005	0.003	<0.001	<0.001	<0.001
Mn	<0.001	<0.001	<0.001	<0.001	<0.001
Si	0.03	0.002	0.002	0.001	0.003
Sn	<0.001	<0.001	<0.001	<0.001	<0.001
Ni	0.002	0.002	<0.001	<0.001	<0.001
Cr	<0.001	<0.001	<0.001	<0.001	<0.001
Ca	0.002	<0.001	<0.001	<0.001	<0.001
Na	<0.005	<0.005	<0.005	<0.005	<0.005
Al	<0.005	<0.005	<0.005	<0.005	<0.005
C	0.008	0.0075	0.0051	0.0047	0.0045
O_2	0.094	0.076	0.063	0.047	0.028

< Indicates sensitivity limit of method.

manufacturing skill, production tolerances, and marketing philosophy. Some attempts are being made in behalf of standardization but these have met with numerous difficulties, one of which is the steady advancement of technology in this new field.

Consolidated Tantalum

Tantalum in the form of wire, sheet, and foil can be produced by either powder metallurgy techniques or vacuum casting. The powder is the starting point for both and in the first case is pressed into bars and sintered in vacuum at about 2400°C. This yields a high purity, ductile, porous bar which must be hammered to achieve adequate consolidation. The bar is further sintered after the hammering and the metal density slowly approaches the true tantalum density of 16.6 g/cm^3. In the case of vacuum casting, the metal goes to true density in a single operation. Presently, vacuum casting is done either by arc melting or electron beam melting.

Vacuum casting has the advantage over sintering of being able to produce larger weights of tantalum in a single piece which means larger weights of sheet, wire, etc. The vacuum sintered bar is resistance heated which imposes limitations as regards maximum bar size. Arc and electron beam melting are comparable in ingot quality with arc melting offering lower costs due to the cost of equipment and operation. Electron beam melting offers little technical advantage in the case of tantalum, where tantalum oxide is relatively volatile compared to tantalum metal.

Cast ingots in excess of 100 lb have been produced although average ingot weight is closer to 50 lb. The grain size of the cast ingot is very large due to the high purity, and special precautions must be exercised during the initial breakdown of the cast structure. Ingots intended for sheet and foil are forged to different geometry than those processed for wire and other round shapes. Large reduction can be made during breakdown due to the high ductility of the metal. Annealing is done in vacuum around 1200°C and again, care must be taken to insure the absence of impurity pick-up during processing and annealing. Surface impurities on the tantalum can become alloyed during the anneal at 1200°C. These impurities would then interfere with the film forming operation that is required if the metal will be used in a capacitor. The usual practice is to make in-process checks of the surface purity by actually anodizing samples.

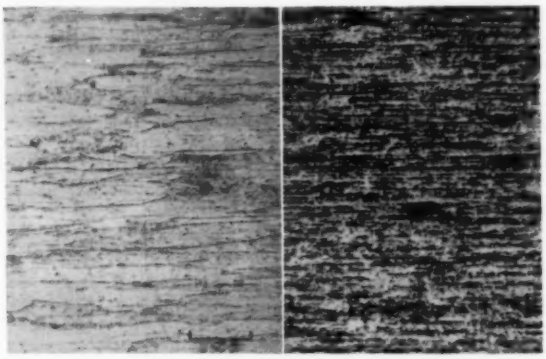

Fig. 5. Photomicrograph of tantalum foil (0.0005 in.) showing grain structure (left) and electrolytically "etched" for use in a capacitor (right).

The foils used in capacitors are less than 0.001 in. (1 mil) thick and are produced on a 20 high cluster mill, starting with high quality, capacitor grade sheet. The d-c leakage properties of foil are superior to heavier gauge sheet due to the surface condition of the finished foil. Typical feed to a cluster mill is annealed 0.010 in. sheet and foil down to 0.0002 in. thick is produced without intermediate annealing. Every extrinsic and intrinsic property of the foil is important when it is processed into a capacitor. The thickness must be held within ±0.00008 in.; the foil must be mechanically flat and show no tendency to warp, curl, or display bow or camber. The surface must be free of all defects. It must perform well on the metal slitting machine used to cut the large pieces into sizes for use in the capacitor. A relatively rigid test is made of d-c leakage, capacitance, and dissipation factor and ultimately it must be compatible with the various methods of etching that are used to increase the surface area and capacitance. Etching produces a relatively uniform pitting on the foil surface and can increase the area by a factor as high as 5 to 1. The technique, basically, is an electrolytic dissolution of the metal and involves many mechanisms not clearly understood. Most methods of foil etching are proprietory to individual companies. Figure 5 shows 0.0005 in. foil with a "metallographic" etch used to show the as-rolled grain structure and a "capacitor" etch used to increase the surface area. A relationship has been suggested be-

Table V. Properties of tantalum sheet, foil, and wire (anodized to 200 v, d-c leakage at 180 v)

	Capacitance, μf-v/in.^{2}	DC leakage, μa/in.^{2} (max.)
Sheet (over 0.005 in.)	75	9
Foil, plain	75	1.5
Foil, etched	to 400	—
Wire 0.020 in. diameter	75	25
Wire 0.010 in. diameter	75	50

tween grain size and the achievable surface area increase. Table V summarizes some of the electrical properties of capacitor grade sheet, wire, and foil.

Where wire and sheet are used as mechanical links in the capacitor, additional physical and mechanical requirements are imposed. These are beyond the scope of this present discussion. The chemical analysis of consolidated metal compares with the sintered anodes in Table IV above, except in interstitial content, which is lower in melted metal.

The average price of capacitor grade tantalum at different stages is presented here for purposes of general information. The prices are approximate because of the ranges involved in marketing commercial quantities, and are expressed as dollars per pound of metal: Ore \$6; K_2TaF_7 \$29; powder \$50; sheet \$65; foil \$80.

Manuscript received May 31, 1960. This paper was prepared for delivery before the Chicago Meeting, May 1-5, 1960.

Any discussion of this paper will appear in a Discussion Section to be published in the December 1961 JOURNAL.

REFERENCES

1. G. L. Miller, "Tantalum and Niobium," *Metallurgy of the Rarer Metals-6*, Academic Press, New York (1959).
2. H. A. Johansen, G. B. Adams, Jr., and P. Van Ryssselberghe, *This Journal*, **104**, 339 (1957).
3. C. W. Balke, U. S. Pat. 1,754,453 (1929).
4. W. G. O'Driscoll and G. L. Miller, *J. Inst. Metals*, **85**, 379 (1957).

Lead- and Manganese-Activated Calcium Cadmium Silicate Phosphors

Yasuo Uehara, Yoshimasa Kobuke, Isoo Masuda, and Takashi Kushida

Matsuda Research Laboratory, Tokyo Shibaura Electric Company, Ltd., Kawasaki, Japan

ABSTRACT

The preparation and properties of (Pb+Mn)-activated calcium cadmium silicate phosphors with various mole ratios of Cd to Ca are described. All phosphors produce a main, broad and variable emission band in the orange, and three minor, narrow and invariant bands at about 6880, 6950, and 7050A. The phosphors show a complicated shift of the main emission band with increasing Cd content, despite a linear relationship between Cd content and lattice spacings. The introduction of sulfate ions into the phosphor base changes the emission characteristics. With half of the Ca introduced as sulfate, the peak emission shifts from 6100 to 6200A. The results are discussed in the light of several assumptions.

Pb- and Mn-activated calcium cadmium silicate phosphors containing less than 30 mole % Cd have already been described by Schulman (1) who found that the peak of the emission spectrum shifts toward longer wave lengths with the introduction of Cd into the phosphor.

In the present investigation, it was found that (Pb + Mn)-activated calcium cadmium silicate phosphors with various mole ratios of Ca to Cd produced a complicated shift of the emission band and that the introduction of sulfate ions into the phosphors further changed its characteristics.

Preparation of Phosphors

Two series of phophors were prepared by firing mixtures of $(1-x)$ moles of purified calcium carbonate, x moles cadmium sulfate or carbonate, and 1.2 moles silica with 0.008 mole lead fluoride and 0.1 mole manganese chloride for two 2-hr periods at 1180°C with an intimate grinding between firings. The first and second groups of phosphors were prepared with cadmium sulfate and carbonate, respectively. All phosphors were fired in covered alumina crucibles in an electric furnace in air.

In order to investigate the effect of the introduction of sulfate ions on the emission spectrum, a part of the calcium carbonate was replaced by calcium sulfate in the preparation of the phosphors. In addition, cadmium silicates activated with Mn alone and with Pb and Mn were prepared by the same method in order to investigate the effect of Pb on the emission of Mn-activated cadmium silicate phosphors.

Methods of Measurements

The emission spectra of phosphors excited with 2537A were measured at room temperature with an automatic recording spectroradiometer which we constructed using a Zeiss Three Glass-Prism Monochromator. The details of this instrument will be reported elsewhere. The reflection spectra and the quantum efficiency of the phosphors were measured by the same method reported in a previous paper (2). The lattice spacings of the phosphors were measured by the x-ray powder photographic method.

Experimental Results

Emission characteristics.—Figure 1 shows typical examples of emission spectra of calcium and cadmium silicate phosphors activated with (Pb + Mn) or with Mn alone. The composition of these phosphors is also shown in Fig. 1. All these spectra show a main broad band with three minor narrow bands

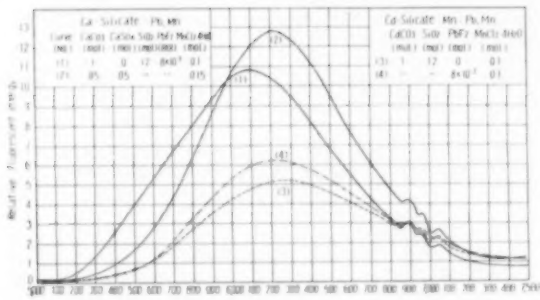

Fig. 1. Fluorescent spectra of calcium and cadmium silicate phosphors activated with Pb and Mn or with Mn. All phosphors were excited with 2537Å at room temperature. The phosphor labeled (1) was fired for three 2-hr periods at 1180°C and all other phosphors were fired for two 2-hr periods at the same temperature.

superimposed at the long wave-length tail. The peak positions of the narrow bands are independent of the composition of the phosphors and are at about 6880, 6950, and 7050Å. On the other hand, the peak position of the broad band is dependent upon the base matrices of the respective phosphors.

(Pb + Mn)-activated calcium silicate prepared with calcium carbonate has a peak emission at about 6100Å, as shown by curve 1, Fig. 1. The partial replacement of calcium carbonate by calcium sulfate in the phosphor shifts the emission peak toward longer wave lengths. When 0.5 mole calcium carbonate is replaced by calcium sulfate, the emission band has its peak at about 6200Å and its intensity is increased by about 20%, as shown by curve 2, Fig. 1. Further increase in sulfate content has little effect on the shift of the emission band, but it reduces its intensity. A concentration of 0.1 mole Mn produced optimum intensity without sulfate, and 0.15 mole was the concentration for optimum intensity with 0.5 mole sulfate; therefore the highest absolute intensity was obtained with phosphors prepared with some sulfate.

Comparing curve 4 with curve 3 for the corresponding singly activated phosphor in Fig. 1, it can be seen that the introduction of Pb into Mn-activated cadmium silicate increases the intensity of

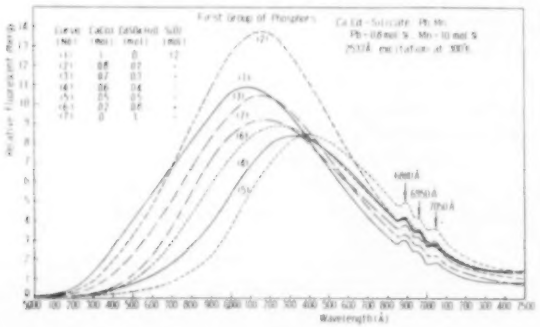

Fig. 2. Fluorescent spectra of Pb-and Mn-activated calcium cadmium silicate phosphors representing the first group of phosphors. (See text). All phosphors were excited with 2537Å at room temperature.

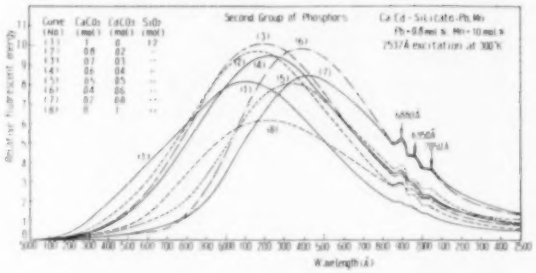

Fig. 3. Fluorescent spectra of Pb-and Mn-activated calcium cadmium silicate phosphors representing the second group of phosphors. All phosphors were excited with 2537Å at room temperature.

fluorescence by about 20% and has practically no effect on the peak position of the emission band.

Emission spectra of the first group of typical calcium cadmium silicate phosphors prepared with sulfate are shown in Fig. 2, together with their composition. All spectra again show a broad band with three minor narrow bands. The peak positions of the narrow bands are independent of the Cd content and identical with the ones of the phosphors shown in Fig. 1. On the other hand, the broad band shows a more complicated shift of peak emission with increasing Cd content, first toward longer wave lengths, then again back toward the blue. As shown in Fig. 3, the second group of calcium cadmium silicate made without sulfate shows similar fluorescent spectra and a slightly different progression of the peak positions.

For the first group of phosphors, the concentration dependence of the peak wave length is shown by curve 1 in Fig. 4a. As the Cd content increases up to 50 to 70 mole %, the peak of the emission band shifts from about 6100 to 6430Å. Further increase of the Cd content shifts it back toward shorter wave lengths, down to about 6200Å. For the second group of phosphors, a similar behavior of the emission band is observed as shown by curve 1 in Fig. 4b. In this case, however, the curve reaches a maximum at about 90 mole % Cd.

The relationship between fluorescent intensity and Cd content is shown by the curves labeled 2 in Fig. 4a and 4b. For the first group of phosphors, the curve attains a maximum at about 10-20 mole % Cd, while for the second group of phosphors, two maxima are observed at about 30 and 60 mole % Cd, together with one minimum at about 50 mole % Cd.

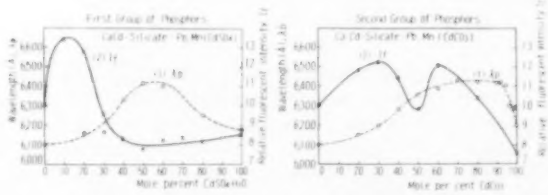

Fig. 4. Peak wave length of emission band (λ_p) and fluorescent intensity (If) as a function of Cd content for Pb- and Mn-activated calcium cadmium silicate phosphors excited with 2537Å at 300°K. (a) (left) The first group of phosphors; (b) (right) the second group of phosphors.

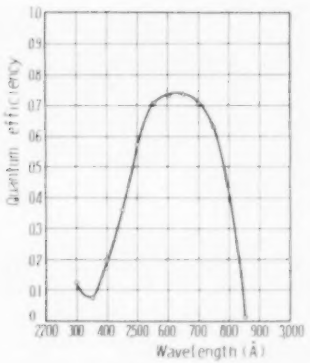

Fig. 5. Dependence of quantum efficiency on excitation wave length, for the phosphor in the second group containing 20 mole % Cd.

The output of 20-w fluorescent lamps made with the phosphors of the second group containing 20 and 60 mole % Cd were about 550 and 260 lumens at 100 hr, respectively.

The dependence of quantum efficiency on excitation wave length for the phosphor in the second group containing 20 mole % Cd is shown in Fig. 5. The quantum efficiency is 0.71 at 2537Å and its maximum value is 0.73 at 2650Å.

Crystal structure.—The measured lattice spacings of the calcium silicate phosphor represented by curve 1 in Fig. 1 were in reasonable agreement with the data reported for β-meta calcium silicate. The diffraction pattern of the phosphor represented by curve 2, Fig. 1, was quite similar except that the spacings of the former were about 1-2% larger than those of the latter. The diffraction pattern of cadmium silicate was also similar to that of β-meta calcium silicate. Furthermore, the diffraction patterns of calcium cadmium silicate phosphors representing the two groups of preparations and containing the same amount of Cd were similar to each other. As shown in Fig. 6, the relationship between the lattice spacings and the Cd concentration was linear.

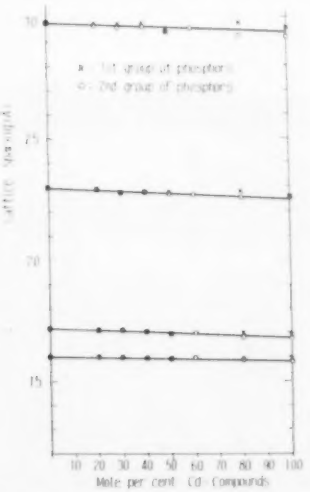

Fig. 6. Relationship between lattice spacings and Cd content of Pb- and Mn-activated calcium cadmium silicate phosphors.

Discussion

The broad band of the emission spectra can be ascribed to divalent Mn ions, while the narrow bands whose positions are independent of the composition of the phosphors may be attributed to tetravalent Mn ions, for the same reason given by several other investigators (3) for titanate, germanate, or arsenate phosphors. The shift in the position of the broad band may be caused by a variation in the lattice spacings, as determined by the interaction between divalent Mn and lattice ions. The behavior of the narrow bands may be explained by considering the shielding effect in tetravalent Mn ions. The positions of the three narrow bands, however, are somewhat different from those reported for titanate, germanate, or arsenate phosphors. In order to explain this difference, we assume that the different phosphor matrices have characteristic effects on the peak positions of the emission bands. In order to confirm this assumption, an investigation is needed to determine the valency of the Mn ions in these calcium silicate phosphors.

The observed linear relation between lattice spacings and concentration of Cd suggests the formation of a solid solution between Ca and Cd silicate. According to published reports (4), the crystal structures of β-calcium and of cadmium silicate are triclinic and orthorhombic, respectively. Their lattice constants, however, are fairly close, as are the ionic radii of the Ca and Cd ions. This may be the reason for the formation of the solid solution.

The complicated shifts of the peak positions in the emission spectra of both groups of phosphors may be explained by assuming the existence of triclinic and orthorhombic structures in the solid solutions. The triclinic structure probably exists below, and the orthorhombic structure above, the concentration at which the concentration dependence curve of the peak wave length showed its maximum value.

The difference between the characteristics of the two groups of phosphors may be explained by assuming the formation of sulfosilicate in the first group of phosphors. In fact, it could be verified by chemical analysis that all of the originally added sulfate was retained in the well-washed phosphors. In the case of the phosphor shown by curve 2, Fig. 1, the chemical analysis suggested the molecular formula of $CaO \cdot 2SiO_2 \cdot CaSO_4$: Pb, Mn.

Acknowledgments

The authors wish to express their thanks to Dr. Tsuneo Harada, Manager of Matsuda Research Laboratory of Tokyo Shibaura Electric Company, for his continuous support and encouragement. Thanks are also due to Dr. K. Tada and Mr. H. Endo for chemical analysis, and to Dr. Y. Fukao and Mr. S. Shikanai for x-ray analysis.

Manuscript received Aug. 12, 1960; revised manuscript received Oct. 12, 1960. Part of this paper was presented before the Tokyo Meeting of the Chemical Society of Japan, April 1 and Nov. 6, 1955, and part at the Chicago Meeting of The Electrochemical Society, May 1-5, 1960.

Any discussion of this paper will appear in a Discussion Section to be published in the December 1961 JOURNAL.

REFERENCES

1. J. H. Schulman, U. S. Pat., 2,471,082 (1949).
2. Y. Uehara, I. Masuda, and Y. Kobuke, *This Journal*, **107**, 1 (1960).
3. F. A. Kröger, "Some Aspects of the Luminescence of Solids," Elsevier Publishing Co., Inc., New York (1948); F. A. Kröger and J. van den Boomgard, *This Journal*, **97**, 377 (1950); L. Thorington, *J. Opt. Soc. Amer.*, **40**, 579 (1950); M. Travnicek, F. A. Kröger, TH. P. J. Botden, and P. Zalm, *Physica*, **18**, 33 (1952).
4. E. Voos, *Z. anorg. u. allgem. Chem.*, **222**, 201 (1953); J. D. Hanawalt, H. W. Rinn, and L. K. Frevel, *Ind. Eng. Chem.*, **14**, 425 (1931); G. R. Fonda and H. C. Froelich, *J. (and Trans.) Electrochem. Soc.*, **93**, 114 (1948); ASTM X-Ray Diffraction Data Cards (1955).

A Study of Growth Processes in Germanium Dendrites Using Pulse Electroplating Techniques

Robert C. Smith

Research Laboratories, Westinghouse Electric Corporation, Pittsburgh, Pennsylvania

ABSTRACT

Pulse electroplating is shown to reveal resistivity variations in germanium dendrites. The evolution of the edges of the dendrites is deduced from the configuration of the resistivity variations. The results suggest that dendritic growth involves at least two processes.

The work of Camp (1) showed that the technique best described as pulse electroplating could be used to reveal resistivity variations in semiconductor single crystals. Investigations along the same lines as those of Camp were done at this laboratory with similar results (2). The success of this method led to its application to germanium dendrites, and resistivity variations found on these dendrites have given us new insight into dendritic growth processes.

Pulse Electroplating Technique

Pulse electroplating is a technique in which pulses of current are applied to a piece of semiconductor alternately to periods without current, the piece to be plated being the cathode in a metallic salt solution such as that of copper sulfate. Variations in resistivity in the sample appear as corresponding variations in the plate, the lower the resistivity the thicker the plate. The thickness of the plate, however, is not necessarily proportional to the conductivity of the semiconductor base.

The mechanism which reveals the resistivity differences is not clear. It is possible that the nature of the electric double layer as discussed by Conway and Bockris (3) can help to explain the phenomenon. They compare the double layer to a leaky capacitor. Such a configuration might allow the buildup of a charge within the semiconductor when the pulse is applied which might then be dissipated to the solution preferentially through the areas of lower resistivity during the period without current. It is known that the presence of an oxide film on the semiconductor surface is necessary for good pulse electroplating, which suggests that this mechanism may be important.

During our work a new aspect of pulse electroplating was discovered. The special conditions which exist in the meniscus of the plating solution apparently are able to resolve the resistivity variations much better than they can be resolved in the main body of the solution. The cause of this effect is not clear. It may be that these conditions force the current carriers to cross the surface more nearly perpendicularly, causing them to cast more accurate shadows of the resistivity variations near the surface.

Experimental Procedure

The following procedure was used in plating the typical dendritic sample shown in Fig. 1 and 2. A piece of copper wire was soldered to one end of a sample of germanium dendrite, 9 x 2.2 x 0.2 mm, using tin-indium solder and an ultrasonic soldering gun. The sample had faces that are typical of dendrites, being virtually optically flat as previous investigators have reported (4, 5). It was degreased in electronic grade trichloroethylene, dried, and immersed to a depth of about 5.8 mm in a 5% by weight copper sulfate solution. Pulses of current were applied to the sample using a generator which delivered 104 pulses/min by discharging a 1 μfd capacitor charged to 500 v. Pulses were applied for

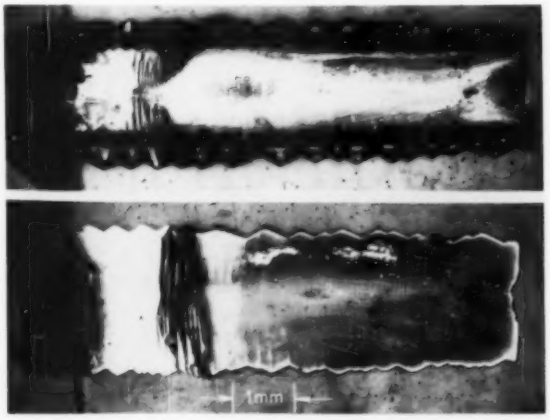

Fig. 1. Opposite sides of plated specimen showing whole plated region.

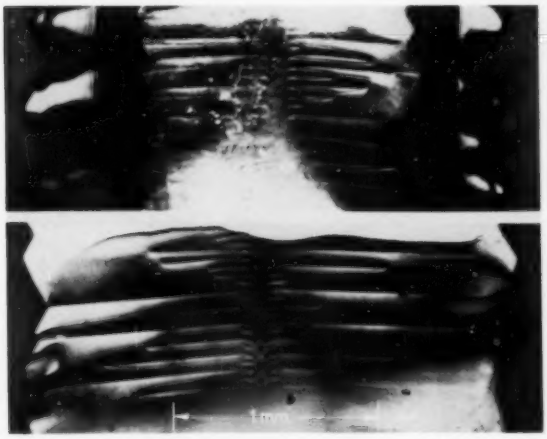

Fig. 2. Enlargements of meniscus regions of Fig. 1 specimen. Above, narrow side showing uniform growth on one edge; below, wide side showing good resolution of resistivity variations.

30 sec. The sample was removed from the plating solution, rinsed, dried, and examined under a microscope to see if the deposit was satisfactory. Samples on which plating was not satisfactory due to the lack of an adequate oxide film, were immersed 15-30 sec in concentrated nitric acid to strip the copper that had been deposited and to build up a thicker oxide film. When necessary, repeated immersions were used.

Experimental Results

The results which can be obtained in the meniscus area when germanium dendrites are pulse electroplated can be seen through the close inspection of the accompanying figures. Figures 1, 2, and 3 show that there are three types of resistivity boundary lines brought out by this technique. These are:

1. Lines which run parallel to the edges of the serrations, zigzagging along the length of the dendrite.

2. Lines which run to each indentation on the edge of the dendrite. These lines are sharply defined, essentially straight, and unbroken as far toward the center of the dendrite as they can be resolved. They are displaced toward the growing tip about 7° from a perpendicular to the longitudinal axis. The region above these lines is dark, indicating that more plating took place there. The region below these lines is light, indicating that less plating took place there.

3. Lines to each peak of the serrations of the dendrite edge. These lines tend to be curved and somewhat less well defined. As one traces them from the edge to the center of the dendrite, one sees that they branch to form multiple lines many times before they reach the center. Within each region that is formed by the branching of a peak line is a line similar to those that meet the edge at indentations. This line is complete with dark area above and light area below.

It is also noteworthy that the central portion of the dendrites in the figures have no clearly discernable resistivity variations of the types discussed above.

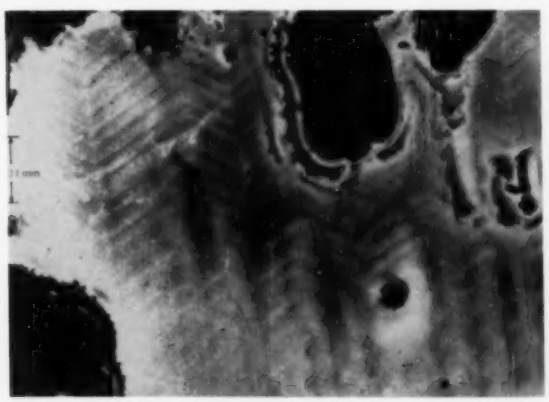

Fig. 3. Enlargement of a portion of a plated specimen showing zigzag resistivity variations.

Resistivity Differences in Relation to Growth

The significance of the differences in resistivity brought out by a pulse electroplating is that any such differences must have occurred as a result of the growth processes. An analysis of the results suggests that there are at least two growth processes at work in the development of a germanium dendrite. The first growth process is longitudinal, lengthening the dendrite. The growing tip is at an estimated depth of 10-15 mm below the melt surface (4, 5). During this portion of the growth the dendrite thickens essentially as rapidly as it widens, perhaps indicating its shape is thermally controlled as a result of its rapid growth rate. As the dendrite is withdrawn, a second growth process becomes dominant. This growth proceeds much better in the lateral directions, possibly because the broad, flat faces of dendrites are {111} planes and, crystallographically, it is more easy to extend {111} planes already present than it is to add on new ones.

A clearer view of what occurs during lateral growth can be gained from an analysis of Fig. 4 which is an idealized drawing that represents the growth of a segment of one side of a dendrite from an initial edge, represented by the solid, jagged line

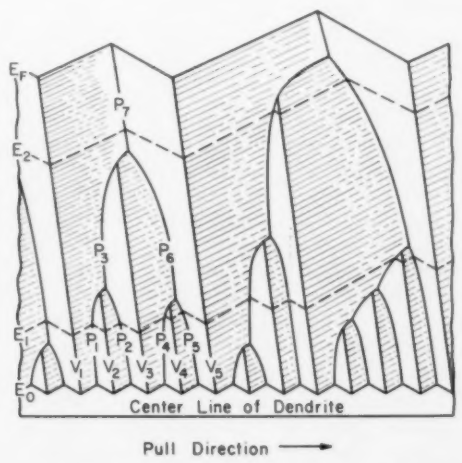

Fig. 4. Idealized drawing showing evolution of edge structure.

E_e, to a final edge, represented by the solid, jagged line E_f. Notice that the line E_e has many peaks in the region represented while the line E_f has only two. More specifically consider the regions between the lines V_1 and V_2. Here the line E_e has four peaks while the line E_f has one. It is apparent from the figure that, as lateral growth proceeds, the lines P_1, P_2, P_3, etc., trace the paths of growth of the peaks of the edge serrations and the lines V_1, V_2, V_3, etc., trace the paths of the indentations or valleys of the serrations. It should also be apparent that line P_3 is formed by the merging of lines P_1 and P_2, line P_6 is formed by the merging of P_4 and P_5, and P_7 by the merging of P_3 and P_6. The merging of peak lines in reality corresponds to the merging of the peaks themselves with the resultant termination of some of the valley lines.

The writer believes that the portion of an actual dendrite which is represented in Fig. 4 is that portion which appears as well-resolved lines in Fig. 2. The portion of the dendrite which is believed to be adjacent to the line E_e is the central portion wherein no clear lines are resolved, i.e., that part which is formed by the longitudinal growth process. The portion which is represented by the lines leading out to line E_f in Fig. 4 is that part which is added to the dendrite by the lateral growth process.

The dotted lines E_1 and E_2 in Fig. 4 show the assumed appearance of the edge of the dendrite at intermediate times in the growth. These lines have a general slope from one side of the figure to the other that is approximately normal to the valley lines. The slope results from the fact that the dendrite is growing from right to left. Consequently at any one instant prior to emergence from the melt, the edge at the right of the figure would represent a later stage of growth in relation to the center than the edge at the left of the figure.

General Discussion

Support for the contention that Ge dendrites are a product of at least two separate growth processes can be derived from a consideration of the two growth rates. If we assume steady-state operation and a pull rate of 150 mm/min with the growing tip at a depth of 10 mm (4, 5) below the surface of the melt, the tip would be growing at a rate of 2.5 mm/sec; thus it would take 4 sec for any point to be pulled from the position of the growing tip to the surface of the melt. The work of other investigators (5) suggests that it is reasonable to say that no more than one third of the distance from the growing tip to the surface of the melt would be thermally influenced. The major widening of the dendrite would occur in that region which has crystallographically influenced growth. This would correspond to approximately 8/3 sec. Since dendrites usually are not much wider than 2 mm and since lateral growth in general appears to proceed relatively evenly from both sides of the center, it would be reasonable to say that lateral growth during this period would be approximately 1 mm. The lateral growth is then taking place at a rate of about ⅜ mm/sec. In comparison it may be seen that the longitudinal growth rate is nearly seven times as rapid as the lateral growth rate. Furthermore, if we consider the possible sources of error in the assumptions made for these calculations, we see that the one most likely to decrease materially the ratio of longitudinal growth to lateral growth is that of a lesser depth for the growing tip. If we assume that this depth is 5 mm instead of 10 mm, the longitudinal growth rate would still be more than three times the lateral growth rate, a difference which remains significant.

Support for a two-step process of dendritic growth of germanium was also obtained visually while observing germanium dendrites being produced. When a melt of germanium is supercooled to the point that crystal growth can take place spontaneously, this growth usually takes place as dendritic growth proceeding from a point where nucleation occurs on the wall of the crucible. Since solid germanium is less dense than liquid germanium, these dendrites float on the surface of the melt. The growth of a number of these dendrites on the surface of a supercooled melt was observed. Typically growth began at a point on the edge of the melt. A rod was formed by very rapid growth from this point and proceeded across the melt. As the writer watched, this rod slowly began to widen and eventually assumed the shape which one usually sees in a dendrite. It was noted that in most cases growth took place in two clearly discernable steps, initially by the rapid formation of a thin rod, and second by lateral growth to final width.

A point of major importance in the growth of this and similar dendrites is that the dendrite reached a thickness very near to the final thickness during the longitudinal growth step and that the thickening which occurred during the lateral growth step was not a significant part of the whole. Any such thickening would probably be thin surface layers added according to a mechanism proposed by Longini, Bennett, and Smith (6). The point is supported when one notes that the lines to the peaks and indentations of the serrations can be resolved as well near the center as near the edge. If any significant thickening had occurred during lateral growth, the portion of the lines near the center would be blurred and diffuse. Moreover if thickening and widening had occurred simultaneously, it would be unreasonable to expect any resistivity variation lines thus formed to meet with the peaks and indentations of the serrations as accurately and suggestively as these do.

The lines to the indentations appear to have a rather simple origin. Since the dendrite is constantly being withdrawn from the melt, the upper edge of each serration is being swept with relatively fresh melt. The solid crystallized onto the upper edge consequently approaches the average impurity concentration one would expect to get from the melt. The lower edge of each serration is somewhat shielded from the flow of fresh melt and tends to carry a small amount of uncirculated melt along with it. Since the doping impurities tend to segregate in the liquid phase, this melt that is carried

along probably increases in impurity concentration. Solid crystallized from this melt of higher impurity concentration necessarily has a higher impurity concentration.

The mode of growth indicated by the explanation of Fig. 4 does not help in learning the origin of the serrations, but it does help to explain the wide variance of edge structure. It is apparent that the larger serrations one observes are the result of the merging of smaller ones. The reason why the peaks merge seems to be that minor differences in thermal geometry cause the growth of some to be more rapid than that of others. Consequently those peaks which grow faster tend to overtake and eliminate the slower ones, resulting in an edge with fewer peaks than originally. Close observation of Fig. 2 discloses that one side of the face of a dendrite may have peaks which tend to combine to form fewer peaks while the other side may have a tendency for uniform growth. The latter example is support for the belief that the larger serrations are evolved as a result of minor variations in thermal geometry. The face over which this difference in growth is exhibited is only about 1.4 mm, a distance small enough that major thermal effects appear to be ruled out. These conclusions concerning the evolution of the serrations differ from those of Billig and co-workers (5, 7-9) who suggested that the serrations were the result of a periodic reversal in growth brought about by the necessity of maintaining a constant mean growth rate and a constant heat loss.

It should be emphasized that pulse electroplating reveals resistivity variations only near the plated surfaces. The structure at some distance beneath the surface need not be similar. In fact there is reason to believe that other processes in addition to the ones discussed here operate in the growth of germanium dendrites (10).

Conclusions

1. At least two growth mechanisms are at work in the production of a germanium dendrite: First, longitudinal growth rapid enough that the shape of the growing face is probably thermally controlled resulting in as much thickening as widening and forming a sort of rod; second, lateral growth out from the rod that is slow enough to conform to preferred crystallographic growth patterns, resulting in much more widening than thickening.

2. The resistivity boundary lines which are brought out by pulse electroplating are a result of the lateral growth mechanism.

3. The resolution of these lines is best in that area of plate that is in the meniscus of the solution during plating.

Acknowledgment

The author wishes to thank R. G. Seidensticker for his helpful discussions and suggestions concerning the pulse electroplating technique.

Manuscript received June 3, 1960; revised manuscript received Nov. 14, 1960. This paper was prepared for delivery before the Chicago Meeting, May 1-5, 1960.

Any discussion of this paper will appear in a Discussion Section to be published in the December 1961 JOURNAL.

REFERENCES

1. P. R. Camp, *J. Appl. Phys.*, **25**, No. 4, 459 (1954).
2. R. G. Seidensticker, Unpublished data.
3. B. E. Conway and J. O'M. Bockris, *Plating*, **46**, No. 4, 371 (1959).
4. A. I. Bennett and R. L. Longini, *Phys. Rev.*, 1 (Oct. 1959).
5. E. Billig, *Proc. Roy. Soc.*, **A229**, 346 (1955).
6. R. L. Longini, A. I. Bennett and W. J. Smith, Paper prepared for submission to *J. Appl. Phys.*
7. E. Billig and P. J. Holmes, *Acta Cryst.*, **8**, 353 (1955).
8. E. Billig and P. J. Holmes, *Acta Met.*, **5**, 53 (1957).
9. E. Billig, *ibid.*, 54.
10. J. W. Faust and H. F. John, To be published.

Capillary Alloying: An Improved Alloying Method

Kurt Lehovec, Karl Busen, James Casey, Clifton Pochop, and Arthur Webb

Sprague Electric Company, North Adams, Massachusetts

ABSTRACT

Alloying of metals to semiconductors is studied by using a liquid alloy contained in a capillary and fed from a large reservoir of alloy. The diffusion constant of germanium in liquid indium is found to be $D = 4.9 \times 10^{-5}$ cm²/sec. The alloying method described permits the preparation of uniformly alloyed small contacts to semiconductors. It is demonstrated that extremely flat junctions can be prepared and that the distance of these junctions from the wafer surface can be controlled at as shallow a depth as 0.25 μ. Advantages of this new method include (*a*) very high degree of purity of the liquid alloy surface previous to alloying, (*b*) the possibility of investigating conveniently a large number of alloy compositions, and (*c*) avoiding the handling of extremely small pellets.

This paper describes studies on alloying of a metal to a semiconductor. Our alloying procedure differs from the conventional method of pellet alloying and permits a better control of alloying parameters. In addition to obtaining basic constants such as the diffusion constant of the dissolved semiconductor in the liquid metal, our method permits the preparation of alloy junctions of improved electrical properties for use in diodes and transistors.

Preparation of alloy junction contacts to germanium dates back to 1953 when Saby and Dunlap (1) investigated the capacitance of contacts prepared by

fusing metals such as indium or aluminum to germanium wafers. When selecting the proper alloying metal, an abrupt pn junction is formed as a result of the following process steps: (*A*) liquid metal dissolves part of the semiconducting wafer; (*B*) upon solidification of the alloy, part of the dissolved semiconducting material is recrystallized, containing doping impurities from the metal phase; (*C*) a pn junction arises between the undissolved and the recrystallized layers of the semiconducting material if the appropriate metal has been chosen.

In utilizing this method for the preparation of junctions for transistors, the following parameters need to be closely controlled: (*a*) depth of the junction from the wafer surface; (*b*) flatness of the junction (variation in depth across the junction area); (*c*) boundaries of the junction (periphery of the junction area); (*d*) uniformity of thickness of the recrystallized semiconducting material.

Difficulties in controlling the above parameters may result from surface contamination of the semiconducting wafer and of the alloy pellets, particularly oxide films, which prevents immediate and uniform wetting. These difficulties increase with shorter alloying time and in the past have limited the usefulness of the alloy junction method with respect to alloy contacts of small area and shallow depths. To remove the oxide layer from the small pellets required for an alloy junction of only 100 μ diameter poses difficult problems with respect to handling and weight control of the pellets. Alloy junctions of such small dimensions are highly desirable for high-frequency transistors, particularly in the case of electrochemical transistors in which control of the web thickness is achieved by electrochemical etching (2), and an alloying depth small compared with the web thickness is desirable in order to maintain the excellent control of web thickness achieved by electrochemical means.

A frequent problem encountered in pellet alloying is the spreading of the alloy contact along the surface of the semiconductor, resulting in an uncontrolled contact area. One method of restricting this spreading is to plate the desired contact area with a metal, such as gold, which is preferably wet by the alloying pellet (3). This imposes an additional process step which is difficult to control without elaborate means. Another method has involved the use of jigs made from an inert material, usually graphite, into which the pellets are loaded and which restrict the spread of the pellet through close contact of the jig and wafer. A plunger is frequently used in conjunction with such jigs to improve the uniformity of the wetting by exerting pressure on the liquid alloy. Difficulties in this procedure arise from handling of small pellets and wear of the jig which must be machined to extremely close tolerance. An additional disadvantage where very small alloy (not elemental) pellets are used is the lack of control of the chemical composition. The phase diagram of the alloy may indicate a mixture of several phases, and the composition of the alloy can then vary from pellet to pellet unless the grain size of each phase in the ingot from which the pellets have been made was small compared with the pellet diameter. A new technique disclosed elsewhere (4, 5) and described in detail in the present paper avoids the handling of individual pellets and prevents the formation of oxide on the liquid metal surface with a resulting improvement in the uniformity of wetting of the semiconductor by the metal.

Independent of us, Ingraham and Hunt (6) also emphasized the great advantage of the liquid column alloying method compared to pellet alloying. While their paper dwelt principally on production engineering aspects of liquid column alloying, the present paper is concerned primarily with the metallurgical aspects of the alloy contact made by liquid column alloying.

Liquid Column Alloying Method

Figure 1 shows a capillary from which a droplet of liquid alloy is ejected. Figure 2 shows a wafer placed on the orifice of the capillary. The wafer is held by a quartz rod to prevent excessive cooling by conduction. The quartz rod is affixed to a micromanipulator, permitting controlled motion in three dimensions. Our equipment permitted control of the atmosphere in which the alloying process takes place. The equipment used in our studies consists of a glass capillary through which the alloy in the form of a liquid column is channeled from a large reservoir. The equipment has an elaborate loading mechanism to insure against contamination in the alloying chamber during insertion of the wafer. The alloying procedure is as follows.

After a fresh, pure surface of the liquid alloy has been exposed, by ejecting a droplet from the orifice of the capillary, a semiconducting wafer is placed

Fig. 1. Capillary with a droplet of liquid alloy

Fig. 2. Capillary with wafer placed on the orifice

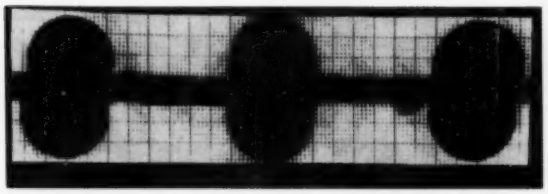

Fig. 3. Wafer with six alloyed dots

on the top of the capillary and the liquid alloy is raised until it contacts the semiconducting wafer. The system is then maintained in this configuration for a predetermined time, after which the liquid alloy is lowered, leaving a droplet of alloy in contact with the semiconducting wafer. The wafer is then removed from the top of the capillary and may or may not be placed into a heating chamber to permit further alloying.

The wafer may then be turned over and placed again on top of the capillary in order to deposit an alloy dot on the wafer surface opposite to the surface already alloyed. The system may also be used to "print" several dots on the same wafer, as shown in Fig. 3 with obvious possibilities for microminiaturization.

Theoretical Analysis of Liquid Column Alloying

Let us first consider the dissolution rate of the semiconducting wafer in the liquid column. Considering the liquid column as a one-dimensional infinite system, one may visualize the limiting case of a dissolution rate determined by the diffusion of dissolved semiconducting material from the semiconducting wafer into the liquid column. This problem can be formulated mathematically by assuming that the concentration of the semiconducting material in the liquid adjacent to the solid wafer is equal to the saturation concentration at the particular alloying temperature, in other words, that quasi-equilibrium is maintained at the boundary between the solid semiconductor and the liquid alloy. Strictly speaking, the resulting diffusion problem is one of a receding boundary, since the position of the solid-liquid interface changes with time as the wafer is dissolved. However, since the diffusion length of the dissolved semiconductor is usually large compared to the depth of removal of semiconducting material from the wafer, the error introduced by neglecting the motion of the boundary becomes negligible. We then obtain as an approximation the well-known equation of diffusion in a linear infinite system with a constant boundary concentration, and the distribution of diffusing atoms in the liquid column is a complementary error function

$$C = C_s \operatorname{erfc}\ (x/L_D) \qquad [1]$$

where x is the distance along the capillary counted from the boundary of the dissolving solid; C_s is the saturation concentration of the dissolved solid at the interface, $x = 0$; and $L_D = 2(Dt)^{1/2}$ is the diffusion length, with D the diffusion constant and t the diffusion time. Consider the alloy pit which results from the solution of germanium to be of cylindrical shape of area A_s and depth h, and let the number of atoms per cubic centimeter in the (elementary) solid be N_1. Equating the number of atoms removed from the solid with those in the liquid column of area A_c provides

$$A_s h N_1 = A_c \int_0^\infty c\,dx \qquad [2]$$

and a normalized alloying depth, h^*, can be formulated as follows

$$h^* = h A_s/A_c = 2(C_s/N_1)\ (Dt/\pi)^{1/2} \qquad [3]$$

The contact area, A_s, of the alloyed pit differing from the area of the capillary orifice, A_c, can be obtained by alloying with the wafer at a small distance from the capillary; this will be discussed in a later section of this paper in more detail.

In order that the alloying depth should comply with Eq. [3], the length of the capillary should be at least three times the diffusion length, so that the condition of a semi-infinite cylinder into which the diffusion takes place is fulfilled.

Normalized alloying depths were determined by measuring h, A_s, and A_c on a number of germanium wafers alloyed at a liquid indium column. The alloyed samples were cross sectioned and then etched for junction delineation. Since no appreciable solid-state diffusion of the alloy into the semiconducting material takes place under our alloying conditions, the junction coincides with the boundary up to which the liquid indium moved during the alloy process. Therefore, the distance between delineated junction and original surface of the wafer provides the alloying depth, h.

In Fig. 4 the square of the normalized alloying depth is plotted *vs.* alloying time at 360°C. The points can be connected by a straight line through the origin as expected from Eq. [3]. In order to evaluate the diffusion constant from the measured normalized alloy depth, h^*, Eq. [3] is used in conjunction with published data of the solubility of germanium in indium. The saturation concentration, C_s, was calculated from the atom fraction, χ, of dissolved material taken from the phase diagram (7) and from the number of indium atoms, N_2, per cm^3 of liquid indium

$$C_s \simeq \chi \cdot N_2 \qquad [4]$$

This neglects the changes of density in the liquid due to the dissolved germanium, which is permissible in view of the small atom fractions of dissolved

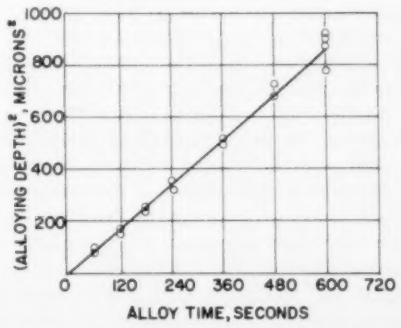

Fig. 4. Square of alloying depth vs. time at 360°C

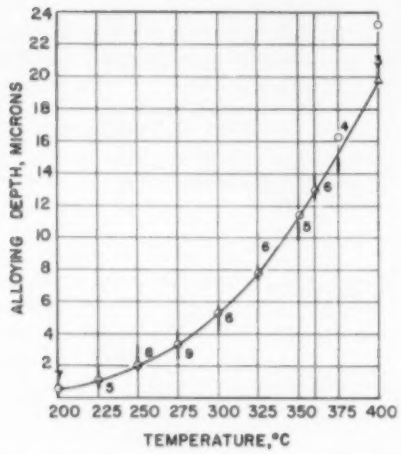

Fig. 5. Alloying depth vs. temperature at 2 min

germanium. In computing N_2, the density change of liquid indium with temperature is taken into consideration (8). The density of solid germanium (9) is taken as 5.33 g cm^{-3} to compute N_1. From the slope of the line in Fig. 4 the diffusion coefficient $D = 4.9 \times 10^{-5}$ cm^2 sec^{-1} is obtained which is in the range generally observed for diffusion in liquid metals (10).

A plot of the normalized alloying depth *vs.* temperature at the constant alloying time of 2 min is shown in Fig. 5. The spreading of the values is indicated by line segments. The number at each line segment indicates the number of samples used for the evaluation.

The circles in Fig. 5 are theoretical values of the normalized alloying depth calculated from the right-hand side of Eq. [3] and using the data by Keck and Broder (7) for the solubility of germanium in indium and the diffusion coefficient mentioned above. The point designated by a triangle has been calculated in the same manner by using the data by Thurmond and Kowalchik (11) for the solubility. In calculating the theoretical points we have neglected a possible temperature dependence of the diffusion constant. The good fit of the theoretical and the experimental data justifies this neglect. The agreement between theoretical data and observed data at 360°C is a consequence of our choice of the diffusion constant. Observed data at 400°C agree better with the theoretical data derived from Thurmond and Kowalchik, supporting their value in preference to Keck and Broder. However, if the diffusion constant would decrease with temperature between 360° and 400°C significantly, better agreement with Keck and Broder than with Thurmond and Kowalchik would result. Since diffusion constants in liquid metals appear to increase slightly rather than decrease, and good agreement between observed data and theoretical data based on a temperature independent diffusion constant is obtained below 360°C, a decrease of diffusion constant with temperature between 360° and 400°C is unlikely.

Equation [3] indicates that the important variables for controlling the amount of removed material are the two parameters temperature (which determines the satuation concentration C_s) and time. This should be contrasted to the pellet alloying process where the two main parameters are temperature and weight of the pellet, assuming that sufficient time is permitted to approach equilibrium conditions (12, 13). Obviously, time in capillary alloying is much easier to control than weight of the pellet in pellet alloying, particularly in case of small pellets as used for high-frequency transistors.

After each alloying experiment the top part of the liquid column (several diffusion lengths deep) is ejected in order to start with the same initial condition for the next wafer, namely, a liquid alloy free from dissolved semiconducting material. Obviously, the rate of alloying can be modified also by having a certain amount of semiconducting material dissolved in the liquid alloy previous to the liquid column alloying, much in the same manner as alloy pellets containing a certain amount of semiconducting material are being used in ordinary pellet alloying. The addition of semiconducting material to the alloy effects an alloying near the equilibrium point and has a favorable effect on the flatness of the bottom. This state of near equilibrium alloying has been described by Mueller (14).

If the contact between the liquid column and the semiconducting wafer is interrupted subsequent to alloying, a droplet of alloy as already mentioned remains attached to the wafer. This droplet was a part of the liquid column, before the interruption was carried out, and therefore the concentration distribution of dissolved semiconductor material throughout this droplet is close to the distribution of that part of the liquid column from which the droplet was formed. This situation is illustrated in Fig. 6. In this figure the concentration $C(x)$ of germanium in a liquid column (indium) is plotted *vs.* the length x of the column. C_s is the saturation concentration at the interface $x_1 = o$ between the solid germanium and the liquid column. The concentration of the germanium in the indium decreases with increasing distance from the interface. The shaded area represents the amount of germanium dissolved in the indium after a certain time. If we would alloy for an infinitely long time, the concentration of germanium throughout the liquid column would be uniform and would be equal to C_s. If after a short time the liquid column is interrupted at a distance of, for example, $x_2 = 160$ μ, the indium droplet which adheres to the germanium wafer is not saturated with germanium. It still could dissolve an additional amount of germanium, which is represented by the unshaded area between x_1 and x_2. Be-

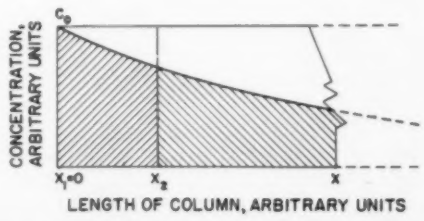

Fig. 6. Illustration of the concentration profile of semiconducting material dissolved in a column of liquid alloy.

cause the droplet is not saturated with germanium it is possible to dissolve more germanium by after-annealing the wafer at a temperature which is equal to that of the liquid column. By this after-annealing procedure the alloying depth would be increased, but only to a slight extent, since the droplet is already nearly saturated. Therefore alloying near the equilibrium point can be carried out by separation from the liquid column and subsequent annealing.

The change of depth obtained by subsequent annealing depends, among other factors, on the volume of alloy in the droplet and its contact area with the semiconducting wafer. While the contact area on the capillary is well defined by the diameter of the capillary, the volume of the liquid alloy droplets is a complicated function of the design of the capillary orifice. By utilizing different capillary designs, we have been able to produce almost hemispherical droplets as shown in Fig. 3, while with other capillaries quite flat droplets have been obtained. Unless a ratio between the alloy volume in the droplet and the contact area is properly chosen to produce the equilibrium contact angle (13) between the liquid alloy and the semiconductor surface, there may be changes of the contact area by subsequent annealing off the capillary. Another factor which tends to change the boundary of the contact area by subsequent annealing is the preferential wetting along certain crystallographic directions as pointed out by Roschen and co-workers (15).

Flatness of the Bottom of Alloyed Contacts

The alloy junctions to be discussed in what follows have been obtained with germanium by alloying with either indium or a lead-arsenic eutectic alloy. Cooling conditions after alloying have been chosen in such a manner as to obtain only a small recrystallized layer on the semiconducting wafer. This is demonstrated by Fig. 7, which shows a magnified section of the alloy-germanium interface on which the junction has been delineated by chemical etching. It is seen that the upper junction follows very closely the alloy-germanium interface. The distance here was determined to be only 0.5 μ. Also illustrated are the extremely uniform width of the recrystallized layer and the flatness of the junction.

Having established that the width of the recrystallized layer is quite uniform and small compared to the web thickness, we may utilize the interface between recrystallized layer and alloy dot as an indication of the flatness and position of the junction. This is done by etching off the alloyed droplet and then inspecting the sample either in cross-section as shown in Fig. 8, or by interferometric techniques, Fig. 9. By utilizing germanium wafers whose surface is parallel to one of the crystallographic {111} planes, extremely flat junctions can be obtained. (This set of planes is dissolved much more slowly during the alloying than the other crystallographic planes.) Figure 8 shows an example of a cross section where a base width of only 2.5 μ over a distance of approximately 250 μ has been achieved. In the case of Fig. 8 the average alloying depth from each surface of the wafer was of the order of 10 μ. It will be noted that the upper part of the wafer is curved; this will be discussed in more detail in a later section. Figure 9 shows a successful attempt to alloy uniformly to a depth of only 0.25 μ (this is equivalent to the distance between 2 adjacent interference fringes obtained by illumination with sodium light). By following the fringes from the outside of the alloy pit to the inside of the alloy pit, a displacement by approximately 1 fringe will be noted. The sample shown in Fig. 9 has been alloyed with lead-arsenic and the diameter of the alloy contact was approximately 230 μ. Multiple reflection interferometric methods have been used to increase the sharpness of the fringes.

Figure 10 shows the bottom of an alloy pit obtained with indium using an alloying depth of approximately 8 μ. In this case a wafer has been selected which has a surface roughness corresponding to approximately 5 fringes. Note that the surface structure has completely disappeared at the bottom of the etch pit as indicated by the uniform and broad fringe system there. The spacing of the fringes at the bottom of the alloy pit is an indication

Fig. 7. Delineated junction of a transistor

Fig. 8. Cross-section of an alloyed transistor. (The dots have been etched off.) The base is 2.5 μ wide.

Fig. 9. Very shallow alloyed pit with a depth of about 0.3 μ.

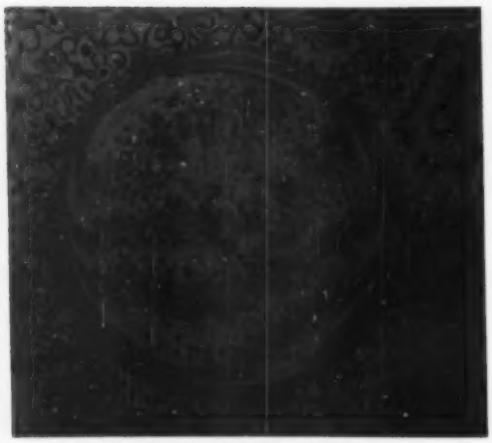

Fig. 10. Bottom of an alloyed pit. The interference fringes inside the pit are uniform and broad and indicate the extreme flatness of the bottom.

that the (111) plane was not quite parallel to the surface of the wafer. The diameter of the alloy contact in this case was 760 μ.

Boundary of Alloyed Region when the Capillary is not in Contact with the Wafer

We have been interested in alloying to the bottom of a jet-etched indentation of a germanium wafer. The advantage of this procedure consists in utilizing the excellent control of electrochemical etching for obtaining well-defined base thickness of a transistor. As the bottom of a jet-etched indentation is slightly curved, there would be a space between the orifice of the capillary and the germanium wafer. When pushing the liquid alloy through the capillary to contact the wafer surface, some of the liquid alloy may squeeze laterally out of the gap between the top of the capillary and the wafer to an extent depending on the pressure on the liquid alloy column, the surface tension of the liquid alloy, and the wetting characteristics between the germanium wafer and the alloy. Since this wetting partially depends on the crystallographic direction, it could be observed that the contact area tends to align along certain crystal directions when a gap between capillary and wafer surface was present during liquid column alloying. Figures 11 and 12 show examples of alloyed structures produced on germanium surfaces, parallel to a (111) and (110) plane, respectively. The alloying metal was indium and the gap between the orifice of the capillary and the germanium surface was approximately 25 μ (this is a tenth of the diameter of the orifice). The alloying region is bounded by the intersection of part of a set of {111} planes with the wafer surface.

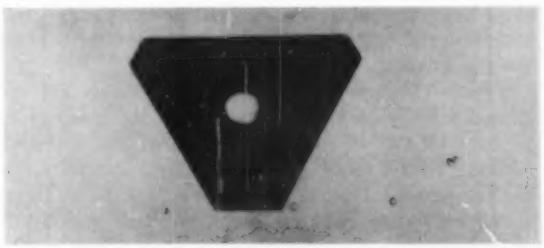

Fig. 11. Structure of indium alloyed to a (111) oriented germanium wafer.

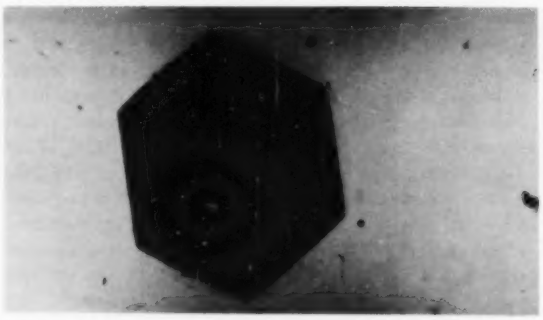

Fig. 12. Structure of indium alloyed to a (110) oriented wafer.

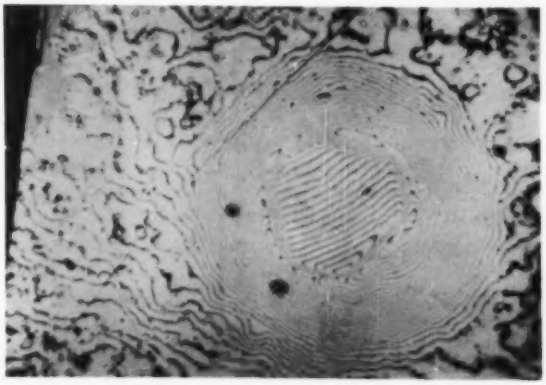

Fig. 13. Bottom of an alloyed pit, situated in the bottom of a jet-etched indentation.

Figure 13 shows an interference fringe photograph of an alloyed pit, situated at the bottom of a jet-etched indentation. The curvature of the jet etched indentation can be evaluated from the circular fringe system outside of the alloy pit. The boundaries of the alloy pit are a regular triangle with rounded off corners. These boundaries are a compromise between the tendency of the alloy to wet along {111} planes which would lead to a regular triangle and the tendency to comply with the circular orifice of the capillary, which was at the level of the original flat part of the wafer at some distance above the bottom of the indentation.

Returning to Fig. 8, it is seen that the depth of alloying at the edges of the alloy pit is somewhat deeper in the case of the curved surface than in the case of the flat surface. The difference in alloying depths results from the difference in curvatures of the two wafer surfaces. Since the alloying proceeds to a crystallographic (111) plane, the depth of alloying to a curved surface must vary with position, the maximum depth occurring at the boundary of the pit in the case of alloying to an indentation on a (111) oriented wafer. If the jet-etched indentation had the shape of a rotational paraboloid and the depth of alloying at the center were zero, the alloy depth at the cylindrical boundary of the alloy pit

would be exactly twice the average alloy depth. Note that the ratio of alloy depth at the boundary of the curved surface and at the flat surface in Fig. 8 is approximately 2:1.

Summary

Alloying from a liquid column to a semiconductor wafer has been investigated. This method provides excellent wetting due to the oxide-free alloy surface and a good definition of the boundary of the alloy pit. In addition to obvious device applications this liquid column alloy method enables basic studies of the equilibrium boundaries of pits alloyed on wafers which are slightly off the capillary. Furthermore, liquid column alloying appears to be a convenient tool for measuring diffusion coefficients in liquids or else, knowing the diffusion coefficient, determining solubilities.

Manuscript received July 25, 1960. This paper was prepared for delivery before the Columbus Meeting, Oct. 18-22, 1959.

Any discussion of this paper will appear in a Discussion Section to be published in the December 1961 JOURNAL.

REFERENCES

1. J. S. Saby and W. C. Dunlap, Jr., *Phys. Rev.*, **30**, 630 (1953).
2. W. E. Bradley, *Proc. I.R.E.*, **41**, 1702 (1953).
3. L. D. Armstrong, *ibid.*, **40**, 1341 (1952).
4. K. Lehovec, U. S. Pat. 2,893,901 (July 7, 1959).
5. K. Lehovec, U. S. Pat. 2,779,877 (January 29, 1957).
6. R. C. Ingraham and R. E. Hunt, IRE Wescon Convention Record (July 1959).
7. "Gmelins Handbuch der anorganischen Chemie," Verlag Chemie, G.M.B.H., Weinheim, Bergstrasse, 83 (1958).
8. M. F. Culpin, *Proc. Phys. Soc. (London)*, **70-B**, 1069 (1957).
9. P. H. Keck and J. Broder, *Phys. Rev.*, **90**, 521 (1953).
10. W. Jost, "Diffusion in Solids, Liquids, Gases," 1st ed., p. 465, Academic Press Inc., New York (1952).
11. C. D. Thurmond and M. Kowalchik, *Bell System Tech. J.*, **39**, 169 (Jan. 1960).
12. L. Pensak, "Transistors I," 1st ed., pp. 112-120, RCA Laboratories, Princeton, N. J. (1956).
13. A. P. Viatkin, *Soviet Physics. Technical Physics*, **2**, 1092 (June 1957).
14. C. W. Mueller, *RCA Rev.*, **18**, 210 (1957).
15. J. Roschen, T. J. Miles, and C. G. Thornton, Semiconductor Products, pp. 41-45 (August 1959).

Photovoltages in Silicon and Germanium Layers

H. Kallmann, B. Kramer, and E. Haidemenakis[1]

Department of Physics, New York University, New York, New York

W. J. McAleer, H. Barkemeyer, and P. I. Pollak

Electronic Chemicals Department, Merck Sharp & Dohme Research Laboratories, Division of Merck & Co., Inc., Rahway, New Jersey

ABSTRACT

Photovoltages up to a few hundred volts at room temperature and up to a few thousand at liquid nitrogen temperatures were observed under strong illumination in silicon and germanium layers with a distance of about 1 cm between electrodes. Only samples with a thickness gradient of evaporated material exhibited these photovoltages. In both the Ge and the Si layers the photovoltage showed an almost linear relationship with illuminating intensity. Both the magnitude and sign of the voltage depended on which side of the film was irradiated, the wave length of incident light, and the temperature. The dark resistance of these layers varied between 10^{11} and 10^{14} ohms. A theoretical interpretation of the origin of these voltages is given.

Since the discovery of larger than band gap photovoltages in evaporated CdTe layers by Pensak (1) a number of papers (2) appeared which dealt with similar effects in ZnS crystals. The explanations offered were based on the assumption that small photovoltaic elements in the evaporated layers combined in a kind of series effect, while in crystals the barriers due to crystallographic asymmetries added up in a similar way. The present investigations with Si and Ge layers indicate that photovoltages far exceeding the band gap are not limited to the above materials. Silicon and Ge layers show photovoltages up to several hundred volts at room temperature and up to a few thousand in liquid nitrogen. In addition, some samples show a reversal of polarity on irradiating from the opposite side, using various wave lengths, and at liquid nitrogen temperatures.

The first part of the paper includes a presentation of the methods of evaporation and the measurement of the photovoltages and dark resistances under various conditions of excitation. In the second part the results are discussed from a theoretical viewpoint.

Experimental Procedure and Results

Evaporation of the Layers.—Method A.—The evaporation was carried out in the bell chamber of a typical PW-400 Kinney vacuum assembly. Pieces of freshly cleaned quartz[2] (1.5 x 0.5 x 0.2 cm) were

[1] Present address: Advanced Rd D, Semiconductor & Materials Div., RCA, Somerville, N. J.

[2] In both methods the substrates were cleaned first with a detergent, then with acetone, and finally washed with high resistivity water and air dried.

arranged in three rows of four each under the emitter in such a manner that the center row was directly below the emitter approximately 3 cm away. The other two rows were at about 60° to the emitter. The emitter, a spiraled tantalum wire (0.025 in. diameter) clad with elemental high-purity Si (prepared by thermally reducing trichlorosilane in H_2 on a hot Ta wire) was mounted between the electrodes in the vacuum chamber so that the wire could be heated by resistance heating. When the assembly was completed, the chamber was evacuated to 10^{-5} mm Hg and the emitter brought to ~1250°C. (Temperature was measured with an optical pyrometer.) Evaporation was carried out for 2 hr. The entire system was allowed to cool to room temperature while still at 10^{-5} mm Hg pressure. Finally, air was admitted to the system.

Method B.—In this method one film at a time was prepared. The vacuum chamber was a cylindrical quartz test tube 2.8 cm in diameter and 28 cm long which connected to the vacuum manifold through a ground glass joint. Vacuum was provided with a Duo-seal mechanical pump and an oil diffusion pump.

The emitter, usually a wafer of single crystal 30Ω cm p-type Si 2.5 cm in diameter and 5 mm thick, was cleaned by first etching in $HF \cdot HNO_3$ composition mixture, washing with high resistivity water, acetone, and again with high resistivity water and air dried. The Si piece was then mounted on a quartz shelf about half-way up the quartz tube and the freshly cleaned quartz substrate (1 by 0.5 cm) placed on another ledge 1 cm above the emitter.

With the pieces in place the tube was connected to the vacuum manifold and the system evacuated to 10^{-6} mm Hg.

The Si emitter was heated in an RF field. A 3 cm diameter pancake coil encircled the quartz tube and power was provided by a 5 kw Lepel radio-frequency generator. Initial coupling was attained through a small wafer of molybdenum inserted between the Si piece and its quartz shelf. The emitter was heated to ~1250°C (optical pyrometer), and the substrate warmed to ~500°C as a result of the proximity of the radiating emitter. Evaporation was continued for 20 min, the heat was turned off and the system cooled to room temperature while still *in vacuo*. Finally, hydrogen was bled into the system.

The Ge layers were made by evaporating high resistivity p-type material[a] (15Ω cm) in a ceramic cylinder onto substrates which were not placed directly above the cylinder but in such a position that the evaporation was at an angle of about 20° to the normal to the quartz, Vycor, and Pyrex substrates, which were kept at a temperature of about 400°C during the evaporation. These layers were of brownish appearance and of a color slightly darker than that of the Si layers. The vacuum was maintained around 1 x 10^{-4} mm Hg during evaporation.

Measurements and results.—The photovoltages were measured by using an electrometer (G.R. No. 1230A) as a null indicator in conjunction with an external biasing d-c circuit. The dark resistances were measured directly with the electrometer. An ordinary 750 w slide projector with an infrared absorbing filter was used as the light source, giving an intensity of a few tenths of a w/cm^2 while a blower kept the samples at about room temperature. The illumination was directed either onto the evaporated layer or through the transparent substrate. Contacts were made by pressing clips to the ends of the evaporated layers, by applying silver paint onto the layers, or in the case of Ge, in addition to the other two, by baking Pt or Au electrodes onto the substrates prior to evaporation. The method of applying contacts had no essential influence on the resulting photovoltages. For measurements involving variation of the light intensity, wire mesh filters of 40% transmission were used.

Results are given in Tables I and II. Results with many samples are given in order to show that various samples exhibit different photovoltages under different conditions of illumination. Table I contains results for nine samples of evaporated Si layers, at both room (V) and liquid nitrogen (V_{l_N}) tempera-

[a] Results similar to those discussed in this paper have since been obtained with n-type Ge.

Table I. Photovoltages of evaporated Si layers at near room and at liquid nitrogen temperatures, under various conditions of illumination

No. Si	11	12	13	14	15	16	17	18	19
V	20.0	28.0	280.0	3.5	50.0	10.0	6.0	88.0	175.0
V_{l_N}	75.0	160.0	80.0	−55.0	−60.0	130.0	−20.0	300.0	250.0
V*	55.0	85.0	303.0	0.4	11.0	42.0	2.0	−25.0	−11.0
$V^*_{l_N}$	155.0	160.0	2.0	−230.0	−250.0	150.0	15.0	80.0	1.0
R	3×10^{12}	5×10^{12}	1×10^{13}	3×10^{11}	3×10^{12}	4×10^{11}	5×10^{11}	4×10^{11}	2×10^{12}
V_{12}		6.0		−0.2	31.0	0.6	0.1	33.0	−62.0
R_{12}		2×10^{12}		6×10^{10}	4×10^{12}	9×10^{11}	4×10^{13}	3×10^{11}	3×10^{11}
$V_{\beta-\alpha}$		102.0		2.0	21.0	7.0	0.3	−0.7	6.5
$V_{\delta-\gamma}$		120.0		1.0	30.0	−6.0	3.8	63.0	110.0
V_1		167.0		1.5	33.0	6.5	2.6	40.0	80.0
V_2		75.0		0.6	18.0	2.0	1.0	12.0	26.0
V_3		30.0		0.2	7.0	0.6	0.4	3.5	8.0
V_A		130.0		3.0	45.0	3.0	4.5	62.0	
V_B		180.0		0.5	5.0	7.0	1.9	34.0	
V_β		180.0		4.5	37.0		3.9	45.0	
$V_{\alpha\gamma}$		140.0		0.4	17.0		1.9	40.0	

V_A refers to the photovoltage when section A is covered and section B only is illuminated. Similarly $V_{\alpha\gamma}$ refers to the photovoltage when sections α and γ are covered, etc. (see Fig. 1). See text for meaning of other subscripts.

Table II. Photovoltages of evaporated Ge layers at near room and at liquid nitrogen temperatures, under various conditions of illumination

No. Ge	1	3	4	5	7
V	4.4	42.0	36.0	2.0	11.0
V_{1a}	18.0	260.0		1700.0	15.0
V*	5.3	11.0	6.0	68.0	4.0
V^*_{1a}	31.0	160.0		3000.0	9.0
R	8×10^{12}	3×10^{12}	7×10^{12}	2×10^{12}	4×10^{11}
V_1	2.3	18.0	18.0	41.0*	5.0
V_2	0.7	7.5	8.5	22.0*	1.8
V_3	0.2	3.5	4.0	11.0*	0.5
$V_{2-64}(\lambda>0.64)$	2.5	8.0	15.0	38.0*	2.0
$V_{2-62}(\lambda>0.62)$	3.3	13.0	19.0	43.0*	2.5
$V_{2-57}(\lambda>0.54)$	4.0	32.0	30.0	62.0*	7.0
$V_{2-70}(\lambda>0.49)$	3.3	39.0	33.0	66.0*	9.2
$V_{2-72}(\lambda>0.44)$	3.6	40.0	34.0	67.0*	9.5
$V_{2-75}(\lambda>0.37)$	4.1	41.0	35.0	68.0*	9.8

* In No. 5 Ge the voltages V_1 to V_{2-75} are obtained from underside illumination.

tures. The first row gives the photovoltages obtained under full illumination. It varies from 3.5 v for sample No. 14 to 280 v for sample No. 13. The dark resistances (R) are given in the fifth row; they vary in value, but in general they are extremely high. V* refers to the voltage obtained when the sample was irradiated from the opposite side, viz., through the transparent substrate. Under these conditions, samples No. 19 and 18 show a smaller voltage but with a negative polarity, whereas samples No. 16, 13, 12, and 11 show a larger voltage with no change in polarity. The absolute value of the photovoltages was larger at liquid nitrogen temperatures in all layers except No. 13, and for several layers the polarity of the voltage was changed, as can be seen from the second and fourth row of the table (V_{1a} and V^*_{1a}). Rows 6 and 7 give the photovoltage (V_{12}) and dark resistance (R_{12}) measured across the smaller dimension of the layer (see Fig. 1).

Using wave lengths between 0.64μ and 4.5μ, which are only slightly absorbed in the thin layers, rather than the full spectrum, the photovoltages dropped considerably in all but sample No. 13, and went to a negative value in sample No. 18 as can be seen in the 8th row of Table I (V_{2-64}). With $0.32\mu < \lambda < 0.7\ \mu$ the photovoltage (V_{4-70}) also decreased, but by a smaller amount, except for sample No. 14. The polarity was reversed in sample No. 16 (row 9). Using 1, 2, and 3 wire mesh density filters, the photovoltage was found to be roughly linear with illuminating intensity (V_1, V_2, V_3, rows 10, 11, and 12).

The direction of the photovoltage was found to follow the thickness gradient, with the thicker side exhibiting a positive polarity under full illumination on the evaporated layer. The part of the layer exhibiting the maximum photovoltage varied from

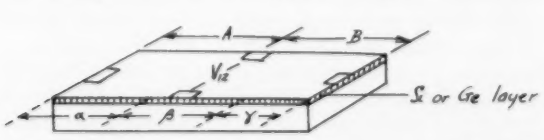

Fig. 1. Schematic diagram of an evaporated Si or Ge layer with electrode configuration.

Table III. Short-circuit currents, open-circuit voltages, and maximum power at room and at liquid nitrogen temperatures; input power is 0.2 w

**	Thin Si	Thick Si	Ge
I_{rt}	2×10^{-10}	6.5×10^{-9}	6×10^{-10}
I_{lt}	1×10^{-11}	3×10^{-9}	5.5×10^{-10}
V_{rt}	50.0	36.0	43.0
V_{lt}	10.0	1200.0	350.0
P_{rt}	1×10^{-8}	2.3×10^{-7}	2.6×10^{-9}
P_{lt}	1×10^{-10}	3.6×10^{-6}	1.9×10^{-7}
Sample No.	18	3	5

sample to sample, but it was always the thickest part. This was found by successively covering different portions of the sample (see Fig. 1 and the last 4 rows of Table I).

In addition to the photovoltages, short circuit photocurrents were also measured both at room and low temperatures using high external resistances in series with the input resistances of the electrometer. The currents for these thin Si layers were found to be of the order of 10^{-11} and 10^{-10} amp at room and liquid nitrogen temperatures, respectively, as can be seen from Table III. Silicon layers of greater thickness than those discussed above exhibited similar voltages at room temperature, and up to 1250 v at liquid nitrogen temperatures. Their dark resistances were lower than those of the thinner layers by a factor of about 100; as a consequence of this the rise time of the photovoltages of these thick samples was appreciably below 1 sec, while the thin samples exhibited rise times of the order of several seconds. Currents as high as 5.5×10^{-9} and 3×10^{-9} amp at room and low temperatures were observed. These thick layers displayed only small photovoltages when illuminated through the substrates, which indicates that the upper layer is responsible for the appearance of photovoltages (see Discussion).

Table II gives the photovoltages obtained for the Ge evaporated layers under conditions of excitation similar to those for the Si layers. The dark resistances are in the same range as those of the Si layers, but the photovoltages are much larger at low temperatures, exceeding 3000 v as can be seen with sample No. 5. The voltages again are nearly proportional to the light intensity, and only in the case of the very large voltages is the increase with intensity less than linear. A study of the dependence of the voltage on wave length showed that there was a strong response in the yellow-green to red region. No change in polarity was observed in the Ge layers at low temperatures or when they were irradiated through the substrates. Contrary to the results with Si, the thicker side was found to have the negative polarity. Currents up to 6×10^{-10} amp were observed in these layers. Generally the dark resistances of the Ge and the Si layers at liquid nitrogen temperature were slightly above those at room temperature.

Finally, Table III shows the short circuit currents and the approximate power output of some typical samples at both room and liquid nitrogen temperatures; up to $\sim 3.6 \times 10^{-6}$ w/cm^2 were obtained at low temperatures with thick Si layers. These layers consist of many grains as is borne out by their high

resistances. Even the purest Si, when in a layer 1μ in thickness, would exhibit a much smaller resistance than that observed. The same is true for Ge. Photographs of the thicker layers taken with an electron microscope showed definite structural differences between those samples which gave large photovoltages and those which did not. The samples with the larger photovoltage showed larger plateaus in the structure and a greater ordering. X-ray diffraction measurements showed greater crystallinity for the samples with larger voltages.

Discussion

Although no exact mechanism for the creation of these photovoltages can be given at this time, some observations can be made. It is quite obvious that these large photovoltages do not originate at the electrodes. This is indicated by the independence of the effect on change of electrodes and is directly shown by measurements in which parts of the layers are covered. These latter measurements also show that the photovoltage is approximately proportional to the distance between electrodes. There is another difference between these photovoltages and those obtained with p-n junctions or through diffusion effects (3); the voltage increases roughly linearly with the illuminating intensity.

The results with underside illumination and at liquid nitrogen temperatures sometime show a complete reversal of polarity in the thin Si layers. This seems to indicate that two competing processes are involved, one of which shows a polarity change depending on which surface is illuminated. The results further show that in most of the layers the main effect is due to wave lengths in the visible range. This seems at variance with the fact that the absorption edges of these materials lie beyond 1μ. But this can easily be understood if one recalls that these layers are rather thin, and that the absorption curves of these materials have a relatively gentle slope. Since these layers are of the order of 1μ thick, infrared light is barely absorbed, and only light of much shorter wave length is absorbed in any quantity. This was verified by absorption measurements.

These voltages may originate in a manner somewhat similar to that proposed by Pensak. The evaporation produces single crystallites, which are not oriented completely perpendicularly to the surfaces of the support. Along each crystallite a photovoltage may develop because of inhomogeneous absorption of the incident light and/or differences between the upper and lower crystallite surface, *i.e.*, the upper layer may be oxidized to some extent. This voltage has a component parallel to the surface if the crystallites are stacked at an angle. A larger recombination rate at one surface is enough to produce a photovoltage when the mobilities of the two carriers are different. If two neighboring crystallites have about the same voltage and these voltages were to be added in series, they would be cancelled across the contact between the crystallites. This cancellation is only partial when the conductivity properties of the gap, especially the mobility with which the carriers cross the gap, are different from those in the crystallites. The latter condition is essential. With a homogeneous material the voltages of the crystallites would not add up, but would cancel entirely, and the voltage between the ends of the layer would be of the order of kTln n_1/n_2 where n_1 and n_2 are the carrier concentrations at the ends of the layer. With potentials of more than 100 v this would lead to physically impossible ratios for n_1/n_2. In order to get more reasonable ratios for n_1/n_2 one must assume that regions of different electrical properties exist between the crystallites.

If the observed voltages are caused by inhomogeneous excitation (due to inhomogeneous absorption), the sign of the voltage should depend on whether the light is incident on the support side or on the sample surface. That is the case only in some Si samples. If only surface differences are responsible for the voltage, the sign should not reverse when the illumination is directed through the substrate, at least not while the layers remain rather transparent. Since such reversals do occur it seems that in thin Si samples both effects contribute to the production of a voltage and compete with each other. For the thick Si layers, on the other hand, apparently the outer layer is responsible for the large photovoltages since only small voltages were observed when the illumination was through the substrate.

The almost linear dependence on light intensity indicates that the difference in carrier concentration between the two surfaces is not very large. If it were, the logarithmic dependence of voltage on intensity would become manifest. One can make a crude estimate of the number of "cells" which combine to produce the large voltage, in the following way. The expression for the photovoltage is

$$V_{ph} = \frac{kT}{e}\int_{1}^{2}\frac{w^{+}dn^{+}-w^{-}dn^{-}}{w^{-}n^{+}+w^{-}n^{-}}$$

where the change in concentration of the carriers n^+ and n^- is essentially brought about by the irradiation, and w^+ and w^- are the respective mobilities. This expression leads to $V_{ph} = (kT/e)\ \ln\ (n_1/n_2)$ when one of the mobilities is rather small. The experiments show that in the range between 1000 and 3000 v an intensity change by a factor of ten increases the voltage by only a factor of two. Therefore the carrier concentration ratio n_1/n_2 cannot be greater than 100. This gives 20-30 mv/single element at low temperatures. To obtain a potential of 3000 v for Ge and 1250 for Si one must assume a series of about 10^5 such elements/cm. This figure does not seem unreasonable, and, indeed, the electron microscope photographs disclosed "grain" sizes of about 0.5×10^{-5} cm.

The considerable increase in photovoltage obtained with a decrease in temperature, while the current does not increase, may be explained by the following model. The photovoltaic elements may be looked on as small batteries each with a high internal resistance and all in series. At room temperatures these are shunted by a lower resistance (which may be some surface impurity of the sample). At low temperatures this shunting resistance becomes very high. Thus the voltage can go up at low temperatures, while the current does not, because the

current is determined by the high internal resistance of the battery cells themselves at both temperatures.

Manuscript received June 10, 1960; revised manuscript received Oct. 27, 1960. This paper was prepared for delivery before the Chicago Meeting, May 1-5, 1960. The work on this paper was supported by the Air Force Cambridge Research Center, Bedford, Mass.

Any discussion of this paper will appear in a Discussion Section to be published in the December 1961 JOURNAL.

REFERENCES

1. L. Pensak, *Phys. Rev.*, **109**, 601 (1958); B. Goldstein, *ibid.*, **109**, 601 (1958); L. Pensak and B. Goldstein, *J. A. P.*, **30**, 155 (1959).
2. S. G. Ellis, *et al.*, *Phys. Rev.*, **109**, 1860 (1958); G. Chernoff and P. Keller, *ibid.*, **111**, 98 (1958); W. J. Mertz, *Helv. Phys. Acta*, **31**, 625 (1958).
3. H. Kallmann, B. Kramer, J. Shain, and G. M. Spruch, *Phys. Rev.*, **6**, 1482 (1960).

The Preparation and Floating Zone Processing of Gallium Phosphide

C. J. Frosch and L. Derick

Bell Telephone Laboratories, Incorporated, Murray Hill, New Jersey

ABSTRACT

A procedure is described for producing large solid multicrystalline ingots of gallium phosphide. Bars cut from these ingots are being employed in the investigation of the floating zone technique for growing single crystals under controlled conditions. Methods are described for producing stable melted zones in gallium phosphide bars which demonstrate the feasibility of growing large single crystals. Gallium phosphide crystallites are described which grow from the vapor on the bar surfaces above the melted zone during the floating zone processing. These are shown by x-ray analysis to be continuous with and oriented with respect to the underlying bar crystals.

The III-V compounds were investigated first by Welker (1). They are of considerable interest in the semiconductor field because of their wide range of electrical characteristics. Some of the phosphides and nitrides including gallium phosphide are of particular interest because of their capabilities for high-temperature operation in electrical devices and their transparency to visible light. The latter permits the examination of impurity effects in these materials by ordinary optics.

The preparation and properties of gallium phosphide are reported extensively in the literature especially in the papers of Folberth (2), Wolff (3), and their co-workers. However, these papers generally are concerned with relatively small single crystals grown at low phosphorus pressures below the melting point or cut from multicrystalline ingots produced at higher phosphorus pressures near the melting point of gallium phosphide. These procedures generally are not suitable for producing the large single crystals of high purity and controlled impurity concentrations which are required for characterization and device applications.

The high phosphorus pressure at the melting point of gallium phosphide, which will be discussed later, requires changes in the usual techniques for producing large single crystals under controlled conditions. The usual apparatus must be modified to permit operation at high phosphorus pressures. Except for these modifications, which are dictated by the high-pressure requirements, the apparatus and techniques used here are similar to those described by van den Boomgaard (4) and by Whelan and Wheatley (5).

The first part of this paper describes a pressure chamber for producing large multicrystalline ingots of gallium phosphide at high phosphorus pressures. The second part describes the floating zone processing of bars cut from these ingots. Developments in the floating zone investigation are described which demonstrate the feasibility of growing large single crystals of gallium phosphide under controlled conditions. The properties of these materials will be reported in another paper (6).

Multicrystalline Ingots

Because of the ability of fused silica tubes to withstand fairly high internal pressures, it is possible to produce gallium phosphide ingots at fairly high phosphorus pressures without a pressure chamber. However, adequate protective shields must be provided since severe explosions are very likely to occur. Such explosions can be a serious hazard in the ingot preparations because of the fairly large fused silica tubes and large amounts of phosphorus which are involved. For these reasons, a pressure chamber is employed for the preparation of the ingots in this work. The basic principle of the pressure chamber is the application of an external gas pressure on the fused silica reaction vessel during the ingot preparation.

Pressure chamber.—The pressure chamber is shown schematically in Fig. 1. It consists of a 75 cm long stainless steel tube with a 25 cm ID and a 5 cm wall. Five cm thick stainless steel flanges with O-ring seals are bolted to each end of the tube to provide the pressure chamber. One of the end flanges is fitted with soapstone electrical pressure

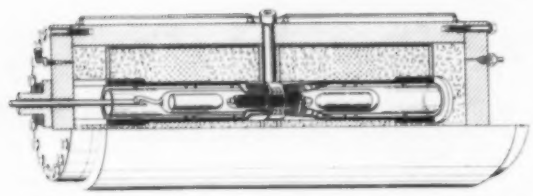

Fig. 1. A pressure chamber and reaction vessel for producing gallium phosphide under pressure.

seals for bringing the temperature control thermocouples and electrical power leads into the chamber. The same flange is fitted in the center with a triple O-ring seal to accommodate a 1.25 cm fused silica drive rod. This, in conjunction with a speed control drive provides the means for moving the reaction vessel or floating zone sample under pressure. The other flange is fitted with two high-pressure valves for increasing or decreasing the gas pressure in the system. Four 22 mm diameter holes spaced 90° apart are drilled through the center of the side wall of the steel tube. These are fitted with suitable O-ring closures to accommodate three clear fused silica viewing windows and the coaxial conductor for introducing the RF into the chamber. The steel tube and end flanges are water jacketed to avoid overheating of the chamber walls. The drive mechanism and pressure chamber are mounted on a swivel support (not shown in Fig. 1) to permit either horizontal or vertical operation.

The pressure chamber contains two identical 35 cm long furnaces with a separation of about 38 mm in the center for the RF zone. Three separately controlled nichrome windings in each furnace provide the necessary control for the two minimum temperature zones. The end furnace windings are covered with a low heat loss insulation. The center windings are covered with quartz sand and pebbles to provide a higher heat loss in this region. This is found necessary to compensate for the high rate of heat transfer from the high-temperature RF zone which otherwise causes the minimum temperature zones to rise above their control settings. All of the unnecessary void space is filled with fibrous insulation and finely divided blown mica to reduce convection currents which can otherwise seriously upset the temperature controls especially at the higher pressures.

Two thermocouples completely shielded with grounded platinum foil are cemented to opposite sides of the inner walls of the furnace cores at the approximate center of each winding. Two additional shielded thermocouples are cemented to the opposite inner walls of each furnace core at the minimum temperature locations which were established with a probe thermocouple with the furnaces in operational control. The thermocouples and power leads extending through the pressure chamber are enclosed in grounded stainless steel ducts. The minimum temperature zones can be controlled to about ±3°C over the pressure range studied.

Reaction vessel.—The reaction vessel for preparing gallium phosphide ingots is shown within the pressure chamber in Fig. 1. It consists of an approximately 50 cm long by 25 mm ID fused silica tube. This length is designed to keep a portion of the reaction vessel in one of the minimum temperature zones throughout the preparation of the ingot. A fused silica boat supports the one containing the gallium to protect the outer shell against excessive heating or breakage. Two fused silica test tubes are inserted with their closed end adjacent to the gallium boat as heat shields. A 50 g charge of 99.999 Ga (Aluminum Company of America) is contained in fused silica, graphite coated fused silica or purified graphite (National Carbon Company) boats. The sample boats are approximately 15 cm long by 12 mm deep by 18 mm wide with a wall thickness of about 1.5 mm.

The weight of the phosphorus charge is in excess of that required to react with all of the gallium and to maintain the phosphorus pressure calculated as P_4 at a value established by the minimum temperature zones in the pressure chamber. Purified white phosphorus (The American Agricultural Chemical Company) is available in fused silica ampoules with breakaway seals. The reaction vessel containing the gallium charge is evacuated to at least 5×10^{-4} mm Hg before introducing the phosphorus. This is accomplished under vacuum by flame melting the phosphorus after breaking the ampoule seal with a fused silica coated steel bar and a magnet. The reaction vessel is sealed off under a dynamic vacuum of at least 5×10^{-6} mm Hg. A fused silica hook is attached to one end to mate with the hook on the drive rod in the pressure chamber.

Ingot preparation.—Several variables such as boat material, reaction temperature, phosphorus pressure, feed rate, and number of passes were investigated to develop suitable techniques for producing large solid ingots of gallium phosphide. All of the ingot preparations were carried out in the pressure chamber illustrated in Fig. 1 with an argon pressure of 10 atm above the phosphorus pressure in the reaction vessel being maintained throughout the run. One end of the sample boat first is raised to about 900°C to prevent the deposition of the phosphorus in this region. A two turn RF coil with a 10 kw generator tuned to about 5 or 12 Mc is employed in these experiments.

The furnaces are heated slowly to their control settings with the end zones being controlled at least 50°C higher than the minimum temperature zones. When temperature control is established, the sample boat is brought to the desired reaction temperature. The sample boat is then moved slowly through the RF coil by means of the controlled feed mechanism. Multiple passes are made by returning the boat to the starting position after the boat temperature has been dropped to about 900°C. When the run is completed, the boat temperature is dropped to about 600°-700°C before reducing the phosphorus pressure in order to avoid decomposition of the gallium phosphide.

Ingots 15 cm long generally were not produced in fused silica or graphite coated fused silica boats by any of the processing conditions investigated.

The ingots as well as the fused silica boats usually developed cracks during the processing operations. The graphite coating probably is not effective since it tends to separate from the fused silica boat during the heating operation. This is true even when the boat is sandblasted before coating with graphite. The adherence of some of the fused silica boat sections to the gallium phosphide is sufficiently strong to require etching in HF for its removal. The cracking of the fused silica boats also increases the explosive hazard in a second high-temperature zone pass which seems desirable for producing solid ingot. However, several large uniform sections of solid multicrystalline gallium phosphide were produced in fused silica boats for experimental studies. These larger sections were obtained from single zone pass runs usually at feed rates of 0.5 mm/min or less, phosphorus pressures from 6 to 35 atm, and reaction temperatures of about 1500°C or higher.

Solid ingots 15 cm long of multicrystalline gallium phosphide now are produced consistently in graphite boats over a phosphorus pressure range of 6-35 atm and reaction temperatures of at least 1500°C. These also require a first pass of 0.5 mm/min or less followed by a second zone pass of 0.75 mm/min or less. A second zone pass of 0.1 mm/min did not show a significant increase in the crystal sizes. A photograph of a typical ingot is shown in Fig. 2. These ingots are transparent except for the last 6-25 mm of their length which usually contains free gallium in varying amounts.

Temperatures of at least 1500°C generally are required in the final zone pass to produce the solid ingots of uniform cross section shown in Fig. 2. This is shown by the preparation of a series of ingots at 20 atm phosphorus pressure over a temperature range from 1450° to 1550°C in 25°C intervals. At preparation temperatures below 1500°C, the ingots were corrugated or pitted in appearance with a variable cross section. On the other hand, ingots prepared at 1500°C and above were smooth in appearance and uniform in cross section. These results suggest that gallium phosphide melts near 1500°C at 20 atm phosphorus pressure. A stoichiometric melting point close to 1500°C at an undetermined equilibrium phosphorus pressure has been measured by Richman (7).

In the preparation of gallium phosphide ingots, the explosive hazard can be reduced by making the first zone pass at a low phosphorus pressure and the second zone pass at the required higher phosphorus pressure. This reduces the amount of free phosphorus during the higher pressure operation. There is no apparent difference in the ingots which are prepared by these two methods.

Fig. 2. Typical 15 cm long multicrystalline gallium phosphide ingot which was prepared in a graphite boat in the pressure chamber.

The ingots prepared in graphite boats by these procedures are transparent, with colors ranging from deep amber to light yellow. However, some of the ingots sections produced in fused silica boats were opaque. Laminar crystalline patterns also are observed in most of the ingots. The ingot material generally is p-type but in some cases is n-type or a mixture of both n- and p-type. The resistivities vary between about 0.01 to above 20 ohm-cm. The free-carrier concentrations at room temperature generally fall between 10^{16} to 10^{19} electrons or holes/cc. However, the temperature dependence of the Hall coefficient indicates that the ingot material is compensated.

Vapor deposits during ingot preparation.—The wall of the reaction tube, while passing through the high-temperature zone, becomes coated with a light orange or black film during the ingot preparation. The deposited films are light orange in color at processing temperatures below about 1500°C, but are usually black in color at higher processing temperatures. A black film (8) of gallium arsenide is deposited during the preparation of gallium arsenide ingots. Since the film deposits begin almost immediately and the film thickness increases at a rapid rate at the gallium phosphide processing temperatures, the optical pyrometer temperature is observed to fall rapidly for a given power level. In other words, the true boat or reaction temperature must be established quickly at the beginning of the run. In addition, a constant processing temperature throughout the run must depend on the stability of the RF generator and the uniformity of the sample impedance.

The orange films deposited during the ingot preparations are composed of small overlapping crystalline dendrites of gallium phosphide. Loose dendrites also generally cover the surface of the ingot. These may have been dislodged from the wall during the processing or on release of the vacuum. The orange deposits are believed to result largely from an appreciable vapor pressure of gallium phosphide at these processing temperatures. However, they also could be explained by an appreciable vapor pressure of gallium at these temperatures.

The black films formed at the higher processing temperatures are composed largely of gallium phosphide crystallites, but also are found to contain carbon in concentrations as high as 10% by weight. The carbon in the films must result from a volatile carbide which dissociates upon deposition on the cooler walls. A volatile CP compound is reported (9) which is stable only at high temperatures. While appreciable concentrations of carbon are known to be present in the phosphorus employed in these experiments, the carbon in the films originates largely from the graphite boats. This is illustrated by the presence of a high concentration of C^{14} in a film which was deposited during the preparation of an ingot in a C^{14} coated graphite boat. The coating was applied by cracking C^{14} acetylene vapor on the graphite boat which was heated in an RF field to 900°-1000°C in a vacuum. A radiograph of the film showed the presence of an appreciable con-

centration of C^{14}. The film was taken from the reaction vessel at a position where splashing of the reactants could not occur, and vapor transfer alone could account for the presence of C^{14}.

Floating Zone Investigation

While relatively large single crystals generally can be cut from the multicrystalline ingots described above, these are not sufficiently reproducible for the characterization of this material. This requires single crystals of high purity and controlled concentrations of known impurities. The floating zone technique is a possible procedure for producing such crystals. This part of the paper is concerned with the investigation of the floating zone technique for growing and purifying single crystals of gallium phosphide.

Floating zone passes in gallium phosphide bars were produced first using a modified 120 Mc, 1 kw generator with single and two turn RF coils. The modification consisted essentially in the addition of a tunable transmission line to the heating circuit. The other equipment and the sample mounts are the same as those which are described later for 12 Mc. The 120-Mc frequency proved to be less satisfactory than the 12-Mc frequency for producing stable floating zones and was abandoned. However, a number of floating zone runs were made at 120 Mc at phosphorus pressures from 6 to 35 atm which served as a starting background for this investigation. The important results may be listed briefly as follows: (*a*) phosphorus pressure at the stoichiometric melting point of gallium phosphide is above 20 atm; (*b*) impurity concentrations are reduced appreciably by floating zone processing; and (*c*) a large single p-type crystal, about 2 cm long by 5 mm in cross section, was grown during a single floating zone pass at 35 atm phosphorus pressure and a feed rate of 0.15 mm/min.

Sample mounts.—Bars about 6-7 mm square by 7-15 cm long are cut from the multicrystalline ingots. In these experiments the bars are further machined to an octagon shape to reduce caging effects. As shown in Fig. 3, the bars are mounted in 12 mm ID by 15 mm OD evacuated fused silica envelopes containing phosphorus. The support and centering mounts for the bars are fused silica tubes which nest closely in the container envelope. A short length of the top and bottom of the bars is ground to a cylindrical shape which fits tightly into the small center tubes. The upper center tubes and the inserted portion of the bars are notched to accommodate a tight fitting fused silica pin. The upper assemblies are fixed in position for supporting the weights of the bars by dimpling the outer envelope into the small center tube. During the floating zone operations the envelope assemblies are supported vertically on a fused silica drive shaft with standard tapered joints.

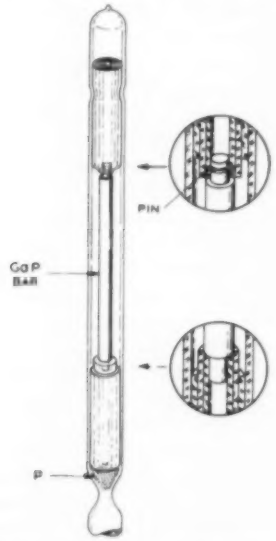

Fig. 3. Container and mounting arrangement for gallium phosphide bars for floating zone processing.

Apparatus.—The pressure chamber is not employed in the floating zone operations described in this paper. The explosive hazard is not as great as in the ingot preparation since smaller tubes and smaller amounts of phosphorus are involved. Moreover, the more flexible design and better visibility in an open system as compared to the pressure chamber is more desirable for the study of processing parameters. Floating zone runs up to 35 atm phosphorus pressure have been made without a pressure chamber.

The apparatus consists of a 10 kw generator tuned to 12 Mc which is provided with a one-half power control switch. The tank circuit is located as close as possible to the RF coil. Platinum wound temperature-controlled furnaces are located at a distance of about 10 mm above and below the RF heating coil. The furnaces are provided with heavy walled Inconel tube inserts for better heat transfer and temperature control along the sample container. The Inconel tube ends adjacent to the RF coil are slotted for about 2 cm to reduce coupling effects. This furnace arrangement provides the temperature control for the phosphorus pressure, but also permits the heating of the sample container walls to high temperatures. The fogging of the envelope walls during a floating zone run is found to decrease with increasing wall temperature. However, the strength limitations of fused silica tubes under pressure restrict the maximum furnace temperatures to about 1100°C. The phosphorus pressure calculated as P_4 is controlled by the complete volatilization of an exact weight of purified red phosphorus which is based on the furnace temperatures, void volume within the sample container and the desired pressure. A speed controlled drive mechanism completes the essential floating zone apparatus.

Initiation of the melted zone.—The generator power is increased slowly with close observation of the bar in the RF field. At first the temperature of the bar rises very slowly with increasing power. However, at a particular power level the temperature of the bar begins to rise at a very rapid rate. At this point the power must be reduced very quickly to approximately one-half of this value. This is most conveniently accomplished with the one-half

power control switch. If this power adjustment is not made quickly, the melted zone length will increase rapidly until it can no longer be supported by the surface tension. The desired zone length then is established by adjusting the voltage with the generator operating on the one-half power control. It may be desirable to operate some generators on the full power control because of better stability in the output power. This can be accomplished by manipulating the one-half power control switch on and off during the voltage adjustment with close observation of the melted zone.

Floating zone runs.—Several floating zone runs were made by the above procedure with two RF coil designs. These were made at 25 atm phosphorus pressure at feed rates of 0.15 to 0.5 mm/min with the furnaces controlled at 1050°C. At the end of each run the melted zone was solidified quickly by turning off the RF generator with the bar moving at the prescribed feed rate. The processed bars then were cut in half in the lengthwise direction. This gives a good estimate of the length and shape of the zone as well as the size and shape of the crystals in the processed portion of the bar. The quenched region also gives some indication of the melt composition.

An example of one of the bars processed by moving the melted zone upward is illustrated in Fig. 4 before sectioning. Note the uniformity of the cross section and the transparency which is illustrated by the interposition of a key between the bar and the light source. The bar is very light yellow in color. On the other hand, bars processed by moving the melted zone downward are covered with gallium phosphide crystals which grow from the vapor. Two examples are illustrated in Fig. 5. These were processed by the same procedure except for a shorter melted zone length in (a) as compared to (b). Note the feather-like growths on (a) and the rows of protrusions on (b). These vapor deposits are discussed more fully in a later section.

Zone length and shape.—The photographs in Fig. 6 illustrate two quenched melted zones which were produced with a single turn RF coil. The one in (a) was produced from a shorter melted zone than the one represented by the other three figures. Note the failure to melt through and the shallow necking down of the bar in (a). On the other hand, melt-through was just attained in Fig. 6b. Note the more pronounced necking-down of the bar in (b) as compared to (a). This is more clearly illustrated by the transmission photograph in Fig. 6c. The dark band is due largely to the effect of the disturbed quenched region on the light transmission. However, free gallium is present in appreciable quantities in this dark region. This indicates that phosphorus pressures above 25 atm will be required for a stoichiometric melted zone under these processing conditions. Note also in Fig. 6b the curvature of both frozen meniscuses with convergence or narrowing of the zone toward the center of the bar. This is more clearly illustrated in Fig. 6d, which is the same surface as (b) after etching in aqua regia. These meniscus shapes are not desirable for melt-through of the bars and the growth of single crystals. However, note the large crystals in Fig. 6b which grew during a single floating zone pass.

While the results with a single turn RF coil were encouraging, a more suitable meniscus shape, espe-

Fig. 4. A 7.5 cm long gallium phosphide bar after a single floating zone pass with the melted zone moving upward.

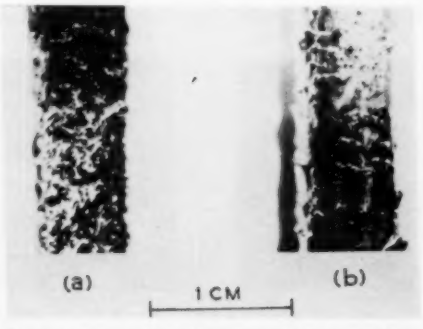

Fig. 5. Appearance of gallium phosphide bars after a floating zone pass is moved downward.

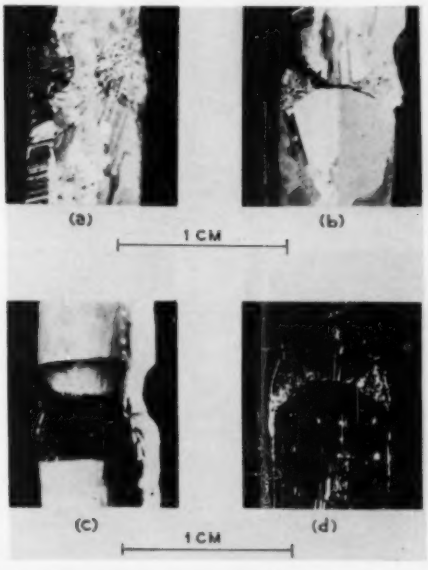

Fig. 6. Appearance after quenching of a melted zone which was produced with a single turn RF coil.

cially for the crystallizing interface, was believed necessary for the controlled growth of single crystals of gallium phosphide. The curvature of the meniscuses is believed to result largely from a gradual decrease in the field strength on either side of the RF coil. Thus, flatter meniscuses should result if the field was terminated at a finite distance from the RF coil. This is accomplished most conveniently with reverse turns in the RF heating coil. A reverse coil design was employed by Comentz and Salatka (10) for melting 10-g charges of metals. Reverse turn coils also are being employed in the floating zone processing of some semiconductors (11).

Several floating zone runs were made with a 3-turn RF coil with the lower turn wound in a reverse direction to the other two turns. A typical effect of this coil design on the shape of the melted zone is illustrated in Fig. 7a by a cross-sectional view of the quenched zone. Note the flatness of both frozen meniscuses and the large crystals which grew as a result of a single floating zone pass. The extent of the crystal growth is shown by Fig. 7a, b, and c in consecutive order from top to bottom and at a lower magnification in Fig. 7d. While extensive twinning is evident in these large crystals, these results are believed to demonstrate the feasibility of growing large single crystals of gallium phosphide under controlled conditions by the floating zone technique.

Vapor deposits and fogging.—It is evident from the temperatures and phosphorus pressures involved that convection currents are present in the sample container during a floating zone run. These would originate at the high-temperature melted zone with an upward movement along the bar and a downward movement near the tube wall. Vapor species originating at the high-temperature melted zone will form deposits on contact with a cooler surface. This may be the bar surface or the tube wall above the melted zone. The location of the vapor deposits forming on the tube walls just above the melted zone level during the runs indicates mixing of the vapor laden upstream with the downstream. These vapor deposits on the tube walls decrease the visibility of the melted zone with increasing zone length and decreasing feed rate. The deposits are quite opaque for a short time after the initiation of the melted zone, but then gradually become more transparent. This constantly changing transmission characteristic of the tube walls prevents accurate measurements of the melted zone temperature with an optical pyrometer. The wall deposits also create a serious observational problem especially where a number of floating zone passes are desired.

During the floating zone runs a visible bluish-green light is observed to stream upward along the bar until it disappears into the upper furnace. The intensity of the light increases with increasing zone length. The light emission is believed to result from a gas discharge which is initiated by the high-intensity electrical field at the RF coil. However, if the P_4 molecules alone were responsible for the gas discharge, some visible light should also be observed below the RF coil. Since this is not observed, the gas discharge probably results from other molecular species which are generated at the high-temperature melted zone. For example, these might be P_2 molecules which are produced in appreciable concentrations at the melted zone temperature.

As previously mentioned, the upward convection currents during a floating zone run cause crystals of gallium phosphide to grow from the vapor on the bar surface and tube wall above but not below the melted zone. Thus the direction of the melted zone results in bars of different surface appearance as shown in Fig. 4 and 5. Some of the crystallites grow in a loose structure on the bar surface or tube wall. These are crystal dendrites of gallium phosphide which have the general structure illustrated by Fig. 8. On the other hand, tightly adherent crystal growths are found on the immediate surface of the bars. These give the bar a sandblasted appearance with the crystallite growths being aligned in a manner which almost exactly maps the size and shape of the underlying bar crystals The latter is confirmed by etching or sandblasting the bars. This is believed to result from the vapor phase growth of

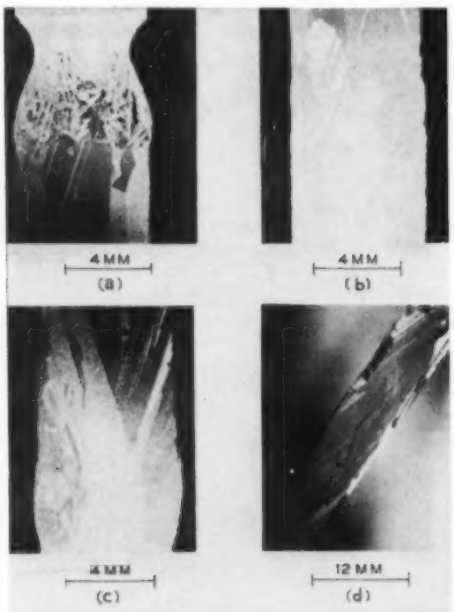

Fig. 7. Appearance after quenching of a melted zone which was produced with a three turn RF coil with the lower turn wound in a reverse direction to the other turns.

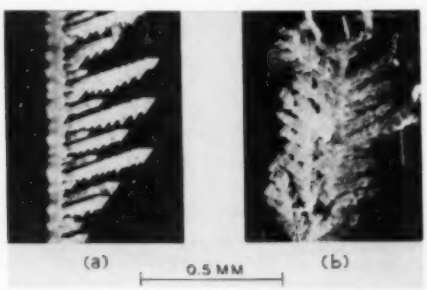

Fig. 8. Crystalline dendrites of gallium phosphide grown from the vapor.

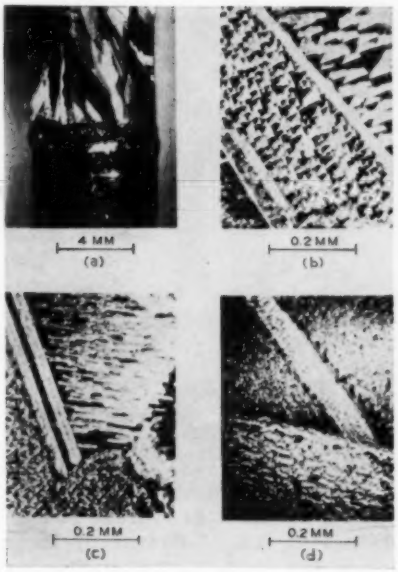

Fig. 9. Gallium phosphide crystallites which grow from the vapor on the bar surface above the melted zone.

gallium phosphide crystals. These crystal growths are illustrated in Fig. 9. Figure 9a illustrates a partially processed octagon shaped bar in which a narrow zone was moved upward. By this procedure flat surfaces were retained for photomicrographs of the vapor deposits. Note the visible patterns above the zone which index with the underlying crystals. Some of these regions are shown at a higher magnification in Fig. 9b, c, and d. Note the continuity in the shape and alignment of the crystal growths in a particular area as well as the difference between areas. These crystal growths are found to be continuous with the underlying bar crystals by x-ray analysis. Some fairly large areas, not shown in Fig. 9, were observed which appeared to be a single crystal growth close to the (111) direction.

Conclusions

Large multicrystalline ingots of gallium phosphide can be grown from the melt over a range of phosphorus pressures. Bars cut from these ingots are suitable for floating zone processing. Stable melted zones can be produced with RF heating coils which are designed to concentrate the field. Large crystals of gallium phosphide can be grown with these stable melted zones.

Crystal deposits of gallium phosphide grow from the vapor on the bar surfaces above the melted zone during the floating zone operation. This suggests a possible procedure for producing epitaxial films of gallium phosphide under controlled conditions.

Acknowledgments

The authors wish to thank Mrs. E. A. Wood and Mrs. M. H. Read for the x-ray analysis; Mr. D. Gibbs for the preliminary work at 120 Mc; Messrs. F. S. Boyle, C. D. Thurmond, M. Tanenbaum, R. L. Wallace, Jr., and J. M. Whelan for their many helpful suggestions and encouragement; and especially Mr. E. Buehler for his extensive contributions to the design of the high-pressure equipment.

Manuscript received Sept. 7, 1960. Portions of this paper were presented at a symposium at Battelle Memorial Institute, November 1959, and at the Chicago Meeting, Electrochemical Society, May 1-5, 1960.

Any discussion of this paper will appear in a Discussion Section to be published in the December 1961 JOURNAL.

REFERENCES

1. H. Welker, *Z. Naturforsch.*, **7a**, 744 (1952).
2. O. G. Folberth, *J. Phys. Chem. Solids*, **7**, 295 (1958).
3. G. Wolff, P. H. Keck, and J. D. Broder, *Phys. Rev.*, **94**, 753 (1954).
4. J. van den Boomgaard, and K. Schol, *Phillips Research Repts.*, **12**, 127 (1957).
5. J. M. Whelan and G. H. Wheatley, *J. Phys. Chem. Solids*, **6**, 169 (1958).
6. M. Gershenzon and R. M. Mikulyak, To be submitted for publication.
7. D. Richman, R.C.A. at Princeton, Private communication.
8. J. M. Whelan, Private communication.
9. J. R. van Wazer, "Phosphorus and Its Compounds," p. 149, Interscience Publishers Inc., New York (1958).
10. G. Comentz and J. W. Salatka, *This Journal*, **105**, 674 (1958).
11. W. C. Erdman, R. A. Porter, and S. J. Silverman, Private communication.

Anisotropic Segregation in InSb

W. P. Allred[1] and R. T. Bate

Battelle Memorial Institute, Columbus, Ohio

ABSTRACT

The anisotropic segregation of Se in InSb has been studied using radioactive Se as a tracer element. A core consisting of a high concentration of Se has been found in the center of crystals pulled in the [111] direction. This phenomenon is thought to result from an extremely rapid lateral growth occurring on the (111) facet. Well-defined striations were also observed. Crystals grown from seeds oriented in directions other than the [111] are found to have high concentrations of Se in the (111) facets near the edge of the crystal, thus removal of the edges leaves the major portion of the crystal relatively homogeneous and with lower impurity content.

Several investigators have studied the segregation of impurities in InSb (1-4) with widely varying results. Mullin reports that the segregation coefficient of Te varies from 0.5 to 3.0 (4) depending on the section of the crystal measured. Crystals pulled in a [111] direction exhibit a high concentration of Se and Te (4) along the central axis. It has been established that the high impurity concentration area in the center of the [111] grown crystals is associated with the formation of a (111) facet at the liquid solid interface. This paper reports the results of autoradiographic and selective etching studies of these and related phenomena in selenium doped InSb.

The observations tend to confirm Mullin's postulate that this phenomenon could be caused in part by rapid lateral growth on the (111) facet. A description of the probable growth mechanism is included in this paper.

Experimental Observation

The single crystals of InSb used in these experiments were grown by the Czochralski technique in the apparatus illustrated in Fig. 1. The inner crucible was a device used to eliminate an oxide scum which is sometimes found on the melt surface. The inner crucible was inserted into the melt after the InSb was molten. Liquid flowing up through the small hole in the center of the crucible originated beneath the surface of the melt and was, therefore, free from oxide particles. The crucible was rotated in a counterclockwise direction at a rate of 6 rpm while the seed was rotated clockwise at the same rate. The net rotation rate was, therefore, 12 rpm with respect to the melt.

Single crystals doped with radioactive Se were pulled in both the [111] and the [110] directions. The major radioactive isotope of the Se was Se^{75} which decays by K capture emitting a soft x-ray as well as a gamma ray.

[1] Present address: Bell and Howell Research Center, Pasadena, Calif.

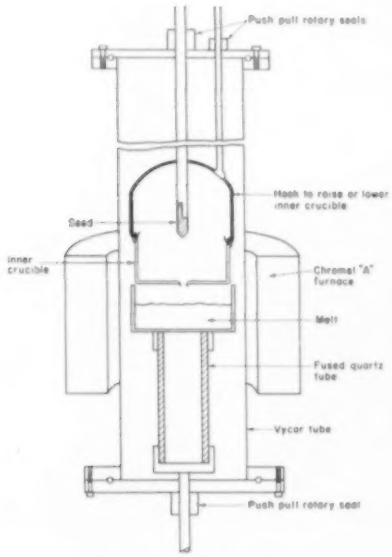

Fig. 1. InSb crystal puller

Discussion

As can be seen from Fig. 2, the greatest concentration of Se is found in the center of the ingot. The outline of the bright area in the autoradiograph corresponds to a (111) facet formed on the bottom of the crystal during the growth process. The striations across the center portion of the radiograph are of particular interest. Most of the Se incorporated in the (111) facet appears to be concentrated in these striations. Since the average penetration depth for Se^{75} gamma radiation is approximately 0.7 cm, it is expected that gamma radiation from the entire slice would contribute to the darkening of the plate. The soft x-rays, however, which could only originate near the surface of the material give rise to the fine structure which indicates the distribution of Se at the surface. It has been determined that the stria-

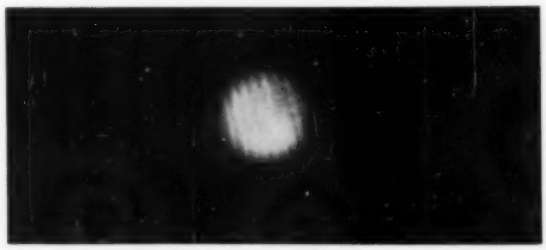

Fig. 2. Autoradiograph of cross-sectional cut from InSb crystal grown normal to the (111) plane.

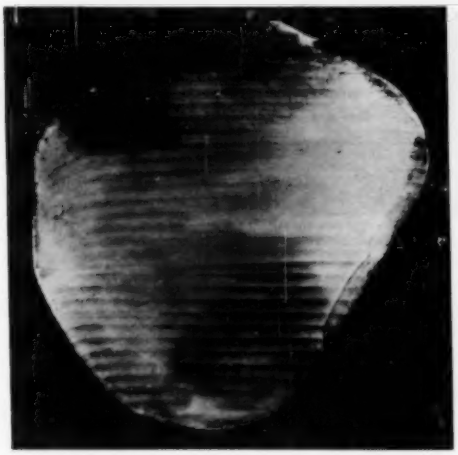

Fig. 3. Etched slice of InSb crystal cut at a 6° angle from the plane of growth.

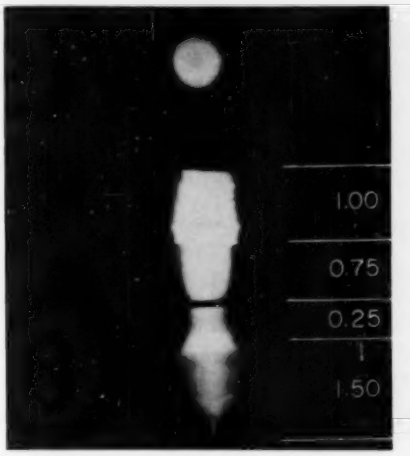

Fig. 5. Autoradiograph of Se doped crystal, pull rate in./hr. The crystal was grown normal to the (111) plane.

tions are related to the growth spirals which are observed on rotated crystals.

Striations observed in longitudinally cut crystals have been reported previously (5, 6). The striations are produced only in rotated crystals and are caused by nonuniform temperature gradients across the melt (7). The crystals rotate through hotter and cooler regions as they are withdrawn, causing a threaded appearance on the surface of the ingot. The depth of the thread is proportional to the magnitude of the horizontal temperature gradient, and the outer periphery of the thread is grown as the crystal is ratated through the lowest temperature. For each full rotation of the crystal with respect to the melt gradient, a cycle of slow and rapid growth is completed. This effect extends completely through the crystal and can be observed by proper decoration.

Figures 3 and 4 are etched samples of InSb. The crystal was pulled normal to the (111) plane. Figure 3 shows striations similar to those seen in the autoradiograph of Fig. 2, with the exception that the etched striations extend completely across the sample and the slice was cut at a larger angle with respect to the growth plane. Figure 4 shows striations near the center of the crystal similar to the external growth rings. This figure was obtained by cleaving the disk shown in Fig. 3, then etching and photographing the edge. The etch used on these samples was a standard CP4 etch of 5 parts HNO_3, 3 parts HF, and 3 parts CH_3COOH.

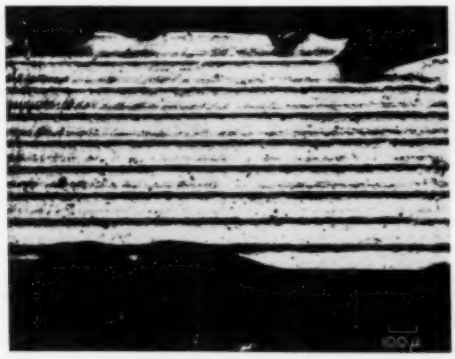

Fig. 4. Edge of sample shown in Fig. 3. Sample was cleaved through the center and etched with a CP4 etch. 65X magnification before reduction for publication.

The striations seen in the surface of the autoradiograph are thought to be the same phenomenon observed by Tanenbaum (5) and Edward (6) in Si. Strauss (8) has further substantiated this conclusion by lapping the surface at various angles with respect to the [111] axis. As would be expected, the striations across the surface of the slice change directions as the direction of the cut with respect to a [111] axis changes. The number of striations observed also changes with the magnitude of the angle.

The amount of Se incorporated into the (111) facet does not appear to change drastically as the growth rate of the crystal changes. Figure 5 is an autoradiograph of a crystal cut longitudinally. The crystal was pulled on the [111] axis at a growth rate which was varied from 0.25 to 1.50 in./hr. As long as the facet remained, the amount of Se incorporated remained relatively constant. Only the size of the facet appears to change as the growth rate changes. At the higher growth rate (1.50 in./hr) the ingot necked in and the facet was eliminated. The effects of the curvature of the liquid solid interface can be observed easily in the autoradiograph. The facet region is seen as a straight line across the center of the ingot. The interface near the edge of the crystal is curved with the gradient of the melt.

It has been shown that crystals tend to grow in steps or layers (9, 11). Figure 6 is a set of photographs of the surface of an InSb crystal orientated in the (113) plane. The melt was decanted leaving the surface as near as possible to that under growing conditions. The lines across the face of the facet are growth steps. Points marked X are low angle twins within the facet. The photograph to the right is from the center of the crystal; this portion of the interface was growing in the [113] direction. From comparison of the two prints the growth steps on the (113) plane can be seen to be much closer together than the steps on the (111) facet. The width

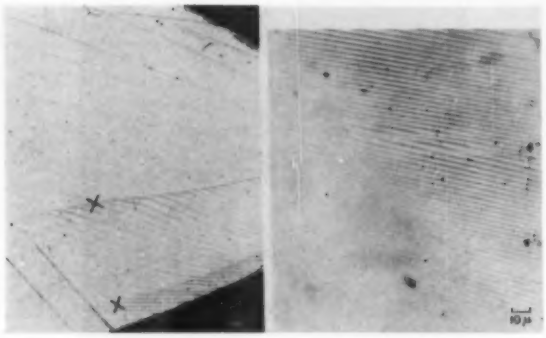

Fig. 6. A (left). (111) facet showing growth steps and low angle twins. Magnification 65X before reduction for publication. B (right). (113) growth surface showing growth steps. Magnification 250X before reduction for publication.

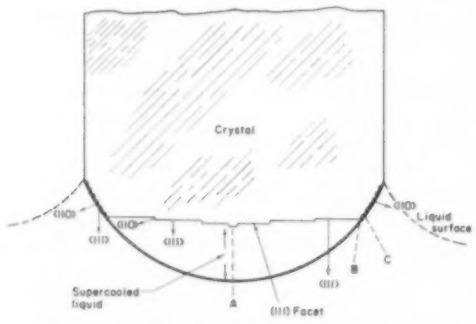

Fig. 7. Drawing of liquid solid interface of growing crystal

of the growth steps on the (111) facet are approximately 500 times as wide as those on the (113) face. Figure 7 is a cross-sectional drawing of the growth pattern of a crystal grown on the (111) facet. The heavy line represents an isotherm at the liquid solid interface. At the center of the (111) facet (point A) the melt has the largest degree of supercooling. Eventually, however, point A growth is initiated probably by a dislocation and is enhanced by supercooling. Since the facet is a (111) face, it has the most unfavorable chance of nucleation of any of the three major planes (10). A (113) surface, however, which is alternate (110) and (111) steps, is one of the easiest growing surfaces (10). After point A has begun to grow the surface grows rapidly from point A to B with very little growth normal to the (111) plane. During this period of growth the growing interface between the facet and the edge of the crystal only grows from point B to C. The relative rates of growth are, therefore, very high on the (111) facet as compared to that portion of the crystal growing at angles not on the (111) face. The impurities in front of the advancing face, along the (111) facet, are incorporated into the crystal, whereas the impurities outside the facet have a greater chance to diffuse away from the advancing interface. The lower concentrations (dark area) of Se in the center of Fig. 2, and seen in all of the autoradiographs of crystals grown on the (111) facet, is probably caused by the mechanism of growth near the center of the crystal. This growth would be, of necessity, normal to the (111) face (controlled by the pulling rate of the crystal) and thus much slower than that of the lateral growth of the rest of the (111) facet.

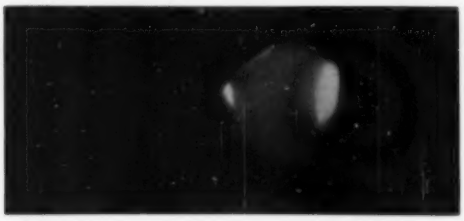

Fig. 8. Autoradiograph of Se doped crystal grown normal to the (110) plane.

Crystals grown on other major planes would not be expected to behave in this manner, as the probability of nucleation is considerably greater on the (110) and (100) planes (9). Figure 8 is an autoradiograph of a crystal doped with radioactive Se and pulled in a direction normal to the (110) plane. As would be expected, the high concentration of Se is in the two (111) facets which now are located near the edge of the crystal. Autoradiographs of crystals pulled in the [100] direction show four (111) facets near the edge of the crystal. These facets also possess a high concentration of Se.

If it is assumed that there is no adsorption of Se or Te atoms on the surface of the growing crystals, the effective segregation coefficient can vary from a value less than one off the (111) facet to a value approaching unity within the facet area. If there are atoms of Se or Te adsorbed on the surface of the solid, the effective segregation coefficient could vary from less than one off the (111) facet to a value greater than one on the facet.

Conclusion

The striations observed in the (111) facet which are caused by the rotation of the crystal are not directly related to the incorporation of high quantities of Se and Te into the (111) facet. The rapid growth region caused by the rotation changes the degree of supercooling at the interface and, therefore, only causes the growth rate to vary in magnitude. Both Se and Te are found in high concentrations in the (111) facet region of nonrotated crystals.

The high concentration of Se and Te found in the (111) facet region is incorporated into the crystal by a process of rapid growth. A high concentration of impurities adsorbed on the surface of a growing crystal can cause the effective segregation to vary from less than one outside the (111) facet to a value greater than one in the facet, only if a difference in growth rate exists.

The zone purification of an InSb crystal is much more effective if the crystal is orientated in a direction other than normal to the (111) plane. This mechanism could also account for the large discrepancies of effective segregation coefficient for other 111-V compounds.

Acknowledgments

The authors wish to thank Dr. H. L. Goering, J. F. Reid, J. J. Duga, and Dr. A. C. Beer for helpful sug-

gestions. They are especially indebted to T. H. Franklin and S. E. Miller for their assistance in growing the crystals, and to Dr. L. W. Aukerman for assistance with the radioactive materials. This research was supported by the Electronic Components Laboratory, Wright Air Development Division and in part by the Air Force Office of Scientific Research.

Manuscript received Sept. 6, 1960. This paper was prepared for delivery before the Chicago Meeting, May 1-5, 1960.

Any discussion of this paper will appear in a Discussion Section to be published in the December 1961 JOURNAL.

REFERENCES

1. T. C. Harman, *This Journal*, **103**, 128 (1956).
2. J. B. Mullin, *J. Electronics and Control*, **4**, 358 (1958).
3. A. J. Strauss, *J. Appl. Phys.*, **30**, 559 (1958).
4. J. B. Mullin, Electrochem. Soc. Abstracts, **9**, 176 (1960).
5. M. Tanenbaum, L. B Valdes, E. Buehler, and N. B. Hannay, *J. Appl. Phys.*, **26**, 686 (1955).
6. W. D. Edwards, *Can. J. Phys.*, **38**, 439 (1960).
7. P. R. Camp, *J. Appl. Phys.*, **25**, 459 (1954).
8. A. J. Strauss, Personal conversation.
9. W. A. Tiller, *J. Appl. Phys.*, **29**, 611 (1958).
10. R. C. Sangster, Electrochem. Soc. Abstracts, **9**, 172 (1960).
11. Burton, Cabrera, and Frank, *Phil. Trans. Roy. Soc. (London)*, **A243**, 299 (1957).

The Formation of Chromium or Molybdenum Stabilized Tungsten Silicon Carbide

V. I. Matkovich and H. H. Rogers

Research Laboratories, Allis-Chalmers Manufacturing Company, Milwaukee, Wisconsin

ABSTRACT

The formation of W_4Si_3C was investigated. It was found that it forms readily in the presence of about 4.6 atom percent (a/o) of chromium or 11.5 a/o of molybdenum. No evidence of formation of pure W_4Si_3C was found. The unit cell size of W_4Si_3C was found by extrapolation from the series of W_4Si_3C-Cr_4Si_3C solid solutions.

The existence of a compound of the chemical formula Mo_4Si_3C was reported by Nowotny, *et al.* (1) and Brewer and Krikorian (2). Parthé, Schachner, and Nowotny (3) investigated the formation of similar compounds by the use of metals other than molybdenum and reported the existence and x-ray data on isostructural chromium and tungsten silicon carbides. Since the compositions are not necessarily stoichiometric they introduced a general formula $Me_{5-x}Si_{3-y}C_{x-y}$. While compounds of Mo and Cr form readily, the formation of tungsten silicon carbide is reported to be very difficult, and the use of a considerable excess of carbon is required (4).

Experimental

Since atomic proportions corresponding to Me_5Si_3C may be considered ideal, all samples were mixed in proportions in accordance with the formula even if more than one metal was used. Molybdenum, −325 mesh, and tungsten, type 427, powders were obtained from Fansteel Corporation. Electrolytic chromium powder, −325 mesh, was obtained from Charles Hardy, Inc. Spectroscopic graphite powder, grade UCP-1, was obtained from United Carbon Products Company. Silicon, which was obtained from the Electro Metallurgical Company was purified (5), to contain, spectrographically, only the trace impurities of Cu, Fe, and Al. Samples were mixed in a mortar, placed in a graphite crucible, and fired to 1930°C for 5 min in a He atmosphere. All samples melted between 1900°-1930°C. Well-developed single crystals were obtained in many cases. Samples were examined by x-ray single crystal and powder methods.

The chemical composition of prepared solid solutions was based on proportions mixed during preparation of samples. Chemical analysis of samples analyzed before and after firing have shown no noticeable change in composition at a molar ratio of 8.

Anal. Calcd. for $(WCr)_5Si_3C$, (W:Cr = 8:1):W, 84.56; Cr, 2.99; Si, 10.90; C, 1.55. Found: (before firing) W, 84.73; Cr, 2.88; Si, 10.31; C, 1.54. Found: (after firing) W, 84.89; Cr, 2.87; Si, 10.31; C, 1.48.

Mixtures containing only W, Si, and C in proportions to form W_5Si_3C were found to contain WSi_2, WC, and W_5Si_3 after being fired. No indication of W_5Si_3C was found even when samples containing up to 22 a/o of carbon were fired.

$W_4Si_3C - Cr_4Si_3C$

The formation of a solid solution of W_5Si_3C and Cr_5Si_3C was attempted in the following W:Cr molar ratios: 2:1, 4:1, 6:1, 8:1, 10:1, and 12:1. Solid solutions of the two compounds were found to form readily from mixtures containing over 4.6 a/o (W:Cr = 10:1) Cr. Such samples contained no tungsten silicides although the presence of trace tungsten carbide was found on all x-ray powder photographs. When less than 4.6 a/o Cr was used WSi_2 and W_5Si_3 appeared besides WC and the solid solution.

X-ray examinations of samples have shown an increase of unit cell dimensions as the amount of Cr was decreased. From the data the unit cell dimensions of W_5Si_3C were obtained by extrapolation to zero Cr content. Data are presented in Table I.

$W_4Si_3C - Mo_4Si_3C$

The formation of solid solutions of W_5Si_3C and Mo_5Si_3C was attempted in the following W:Mo molar

Table I. Extrapolation of unit cell sizes of W_2Si_3C from W_2Si_3C—Cr_2Si_3C solid solutions

Molar ratio W_2Si_3C:Cr_2Si_3C	Wt % Cr	Atomic %	a	c
2:1	10.57	16.6	7.182	4.821
4:1	5.73	10.0	7.204	4.834
6:1	3.93	7.2	7.212	4.840
8:1	2.99	5.6	7.223	4.846
10:1	1.53	4.6	7.237	4.856
Extrap.	0.00	0.0	7.252	4.865

ratios: 10:5, 10:4, 10:3, 10:2, and 10:1. This system was found to behave very much like W_2Si_3C — Cr_2Si_3C system forming a series of solid solutions. However, the formation of tungsten silicides appears at Mo contents under about 11.5 a/o (W:Mo = 10:3).

Discussion

It was found that tungsten silicon carbide readily forms solid solutions with molybdenum silicon carbide and chromium silicon carbide. The stability of W_2Si_3C as a ternary phase is questionable because the experimental results indicate, in agreement with Brewer and Krikorian (2), that a pure tungsten silicon carbide does not form. The systems may therefore be considered as either a solid solution of tungsten in Cr_2Si_3C and Mo_2Si_3C or as that of chromium and molybdenum in W_2Si_3C. The $W_{5-x}Si_{3-y}C_{x+y}$ reported in the literature (4) may have had either a composition with a W/Si ratio different than 4/3 or contained impurities of elements which stabilized the tungsten silicon carbide phase.

The solid solutions appear at the W/Cr and W/Mo atomic ratios of 10/1 and 10/3, respectively. At higher ratios or when the stabilizing component is not present, the formation of WSi_2 along with W_5Si_3 and WC was found to take place. In this respect our findings differ from those of Brewer and Krikorian (2) who observed the presence of WC, SiC and W_5Si_3 in the same composition range in samples heated for 1 hr at about 1830°C.

Manuscript received Aug. 22, 1960.

Any discussion of this paper will appear in a Discussion Section to be published in the December 1961 JOURNAL.

REFERENCES

1. H. Nowotny, E. Parthé, R. Kieffer, and F. Benesovsky, *Monatsh.*, **85**, 255 (1954).
2. L. Brewer and O. Krikorian, *This Journal*, **103**, 39 (1956).
3. E. Parthé, H. Schachner, and H. Nowotny, *Monatsh. Chem.*, **86**, 182 (1955).
4. H. Nowotny, B. Lux, and H. Kudielka, *ibid.*, **87**, 447, (1956).
5. N. P. Tucker, *J. Iron Steel Inst. (London)*, **115**, 412 (1927).

Electrolytic Micromachining of Iron Whisker Surfaces

B. C. Banerjee and P. L. Walker, Jr.

Division of Mineral Technology, The Pennsylvania State University, University Park, Pennsylvania

ABSTRACT

An electron microscopic study of etch patterns of iron whiskers suggests that contamination films which were formed on the whisker edges during the growth process can be removed effectively by hydrochloric acid solutions (pH 0.2-2.0), resulting in the formation of a highly active and smooth surface. At higher pH, however, such a surface cannot be produced. This may be either a result of the insolubility of the original film or the formation of a new protective film on removal of the original film from the whisker surface. Additives such as chromic acid, cupric chloride, ferric chloride, and nitrate ions, present in appropriate concentrations in hydrochloric acid solutions, are found to produce a very smooth surface with pointed tips. Based on the above experimental results a growth mechanism for metal whiskers has been suggested.

Investigations on the physical properties and crystallographic structure of metal whiskers have been conducted by various workers (1, 2). However, very few studies have been reported on the chemical properties of whiskers, especially on the activity of their surfaces in a corrosive environment. This is important since the sides of whiskers are supposed to consist of faces of high density and low surface energy and to be free from dislocations (1, 2). Since different faces of a single crystal possess widely different activities in a corrosive liquid or gas (3, 4), it is also desirable to give due allowance to the orientation of crystal faces developed at the sides of a whisker with respect to its fiber axis. In order to test the reactivity of whisker surfaces, some dissolution experiments in acid solutions were carried out with iron whiskers. Electron micrographs were taken to study the smoothness of whisker surfaces resulting from etching. Since dissolution processes are often a measure of growth processes in reverse, the present investigation sheds some light on the mechanism of whisker formation itself.

Experimental

The iron whiskers, prepared by reduction of halide vapors with hydrogen in the usual way (1, 2, 5, 6), were 5-10μ in diameter and 10-12 mm in length. They were carefully spot-welded on 4-mil tungsten loops for ease of handling during etching. Electrolytic etching was conducted at 25°C in HCl solutions

Table I. Summary of electrolytic micromachining results

Nature of corrosive medium	pH of the medium	Impressed voltage, a.c.	Remarks about surface after etching	Electron micrograph, 5000X
Conc. HCl diluted 10 times	0.15	0-0.1	Irregular surface and no sharp tip	Fig. 1
Conc. HCl diluted 20 times	0.4	0.1-0.2	Smooth surface	Fig. 2
Conc. HCl diluted 30 times	0.5	0.2	Smooth surface and sharp tip	Same as Fig. 2
Conc. HCl diluted 40 times	1.0	0.4	Smooth surface and sharp tip	Same as Fig. 2
Conc. HCl diluted 80 times	2.0	0.6	Tolerably smooth surface with extremely sharp tip	Fig. 3
Conc. HCl diluted 120 times	3.0	0.8	Poor tip and surface starts showing unevenness	Fig. 4
Conc. HCl diluted 150 times	4.0	1.2	Poor tip and the surface is rough	Fig. 5
Conc. HCl + conc. HNO_3 (3:1), saturated with $CuCl_2$	<0.1	0.8	Tolerably sharp tip but surface is rather rough	Fig. 6
Conc. HCl + conc. HNO_3 (3:1), diluted one time, and saturated with $FeCl_3$	<0.1	0.6	Tolerably smooth surface but no sharp tip	Fig. 7
Conc. HCl + conc. HNO_3 (1:10), diluted one time	<2.1	0.4	Growth of spiral showing crossed screw dislocation, which on further etching gives tolerably smooth tip surfaces	Fig. 8, 9
Conc. HCl diluted 10 times with 0.05% chromic acid	<0.2	0.6	Tolerably smooth surface	Same as Fig. 3
Conc. HCl diluted 10 times with 0.1% chromic acid	<0.2	0.6	Rough surface	Same as Fig. 5

of pH values ranging from 0.1 to 4 at externally impressed voltages (a.c.) of 0-1.2, in general. Some runs were conducted at pH 5 and externally impressed voltages up to 8. The acid, of A. R. grade, was diluted with distilled water to give the desired pH conditions. The solutions were held in a 50 ml Pyrex beaker open to the atmosphere. A carbon rod was used as the cathode during dissolution experiments. The electrolytic etching was carried out for a few seconds at an angle with the normal to the liquid surface, since, in general, vertical immersion did not lead to a sharp tip. The angle of inclination for etching was not very critical, any value ranging from 15° to 60° leading to satisfactory results. This procedure was found to give a whisker tip of radius 10^{-4} to 10^{-5} cm, which is suitable for use in field emitters. The electron micrographs were taken at a magnification of 5000X. Results are summarized briefly in Table I.

Results and Discussion

It is seen from the electron micrographs that acid solutions of pH values from 0.2 to 2, with an appropriate externally applied voltage on the whiskers, favor a smooth surface with a pointed tip. At a pH of 3, a rather uneven surface is obtained, even when using higher anode voltages during etching. At a pH of 4, it is difficult to etch a tolerably smooth surface even at voltages between 1.2 and 3.0. At still higher pH values, the whisker retains its original cylindrical filamentary structure, even at impressed voltages up to 8. The behavior at or below a pH of 3 may be attributed to the dissolution of a protective coating on the original whisker surface, followed by progressive dissolution of metal. The insolubility of the original protective film or the instantaneous formation of a highly protective coating on the whisker surface after dissolution of the original film may lead to progressive resistance to corrosion of whisker surfaces at higher pH conditions. When the HCl solution is too highly acidic, the dissolution of the original film as well as the metal is very fast and this leads to an irregular type of surface, as can be seen from Fig. 1. It is also possible that such a rough surface may result due to the more pronounced interaction of whisker surfaces with impurities present in higher concentration in more concentrated acid solutions.

It is noted from Table I that iron whiskers (insoluble in conc. HNO_3) are soluble at impressed voltages of 0.6-0.8, when 3 parts by volume of conc. HCl are added to 1 part by volume of conc. HNO_3 and the resulting solution is saturated either with cupric or ferric chloride at room temperature. The result is a tolerably good surface, as can be seen from Fig. 6 and 7. The above mixture of acids, in the absence of cupric or ferric chloride, results in an immeasurably fast dissolution rate, which does not favor a controlled action. Cupric or ferric ions present in appropriate amounts in acid solutions tend to suppress the hydrogen discharge reaction at cathodic sites of the whisker surface, thereby controlling the rate of dissolution of metal which leads to an effective micromachining of the surface.

By comparing Fig. 3 with Fig. 5, it is seen that addition of chromic acid in appropriate amounts to conc. HCl solution leads to smooth micromachining, whereas additions in too high a concentration result in roughness of the whisker surfaces. This result probably can be attributed to adsorption of chromic acid at various active sites on the surface and its subsequent desorption by chloride ions as discussed in previous communications (7, 8).

Fig. 1

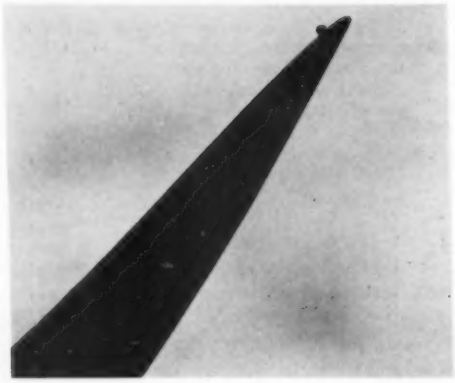

Fig. 2

Fig. 3

Etching of an iron whisker at 25°C and 0.4 v from a twice diluted solution consisting initially of conc. HNO_3 and conc. HCl in a proportion of 10 to 1 reveals a crossed screw type of dislocation (Fig. 8). This surface on subsequent etching, however, becomes moderately smooth and possesses a sharp tip. This can be seen from Fig. 9. Such a dislocation results from a twist grain boundary when two whiskers, most probably originating from two adjacent sites in a parent whisker, cross each other at an angle.

Fig. 4

Fig. 5

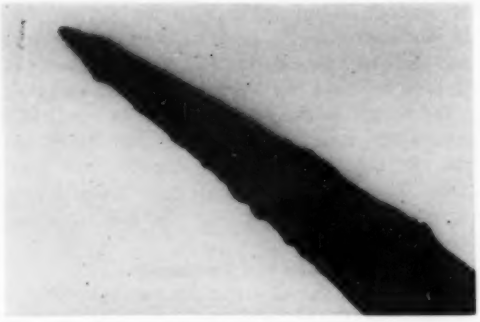

Fig. 6

This is a direct verification of the presence of axial screw dislocations in iron whiskers (9). However, this phenomenon is not general and was found only in a few isolated whisker samples.

Freshly etched whisker surfaces when preserved under vacuo (10^{-5} mm Hg) or kept in a desiccator containing dry air for a few hours become highly inert to the corrosive solutions from which they were etched previously. The whiskers do go into solution at considerably higher voltages but a smooth surface and pointed tip is not obtained. This finding shows that the whisker surfaces are very active, picking up contaminants after etching (probably from vac-

Fig. 7

Fig. 8

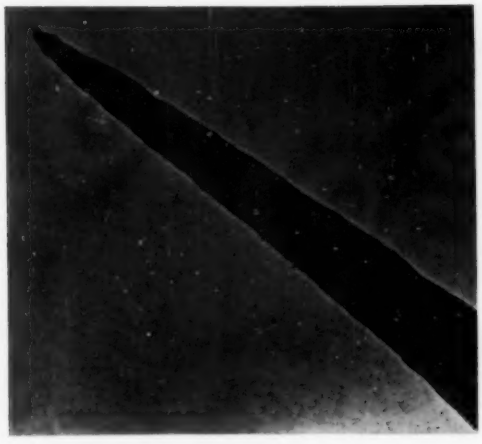

Fig. 9

uum pump oil or residual oxygen when they are preserved under vacuo or oxygen from the air when kept in a desiccator) to give a highly homogeneous and protective coating. This leads to the conclusion that the iron whisker surfaces were very active during formation and quickly picked up contaminants (2, 10). The adsorption of contaminants at the sides of whiskers during their formation might suppress all the active centers which contribute to their lateral spread, resulting in subsequent inertness to corrosive environments. This reasoning is in substantial agreement with the results of Van der Meulen and Linstrom (11) and Coleman and Sears (10). Probably the conclusion of Green and Wolf (12) that silver whiskers are comparatively inert in nitric acid solution is a result of the inability of nitric acid to remove quickly the homogeneous contaminating film formed on the silver surface during the growth process.

Our present knowledge of the mechanism of metal deposition on unclean surfaces either by electrodeposition or by reduction of halide vapors by hydrogen is inadequate to explain satisfactorily whisker formation. It has been suggested that the active centers for deposition of metal atoms or ions on the sides of a whisker might be blocked by contaminants, saturating the surface forces which would have otherwise contributed to lateral spread of the whisker (11, 13, 14). As a result, metal atoms or ions will have an unusually high mobility on such surfaces, since the weak Van de Waals' forces are incapable of incorporating them into the lattice from the sides of a whisker. The atoms, consequently, will be incorporated into the crystal lattice only after reaching the bare surface at the tip, where, probably owing to the higher rate of condensation of metal atoms, contaminants cannot spread during the growth process. Termination of growth should occur only when the rate of condensation of metal atoms on the tip is slow compared with the rate of spread of impurities on the whisker surface. Our experiments which show the high activity of whisker surfaces in suitable etching media, after the initial protective film is removed by dissolution, thus partly explains the mechanism of whisker formation.

Acknowledgment

The authors are indebted to the Physics Dept., The Pennsylvania State University for supplying the iron whiskers. This work, in part, has been supported by the Atomic Energy Commission, Contract No. AT(30-1)-1710.

Manuscript received May 26, 1960.

Any discussion of this paper will appear in a Discussion Section to be published in the December 1961 JOURNAL.

REFERENCES

1. S. S. Brenner, *Acta Met.*, **4**, 62, 157 (1956).
2. F. R. N. Nabarro and P. J. Jackson, "Growth and Perfection of Crystals," p. 14, John Wiley & Sons, New York (1958).
3. A. T. Gwathmey and R. E. Cunningham, "Advances in Catalysis," X, p. 57, Academic Press, New York (1958).
4. B. C. Banerjee, *This Journal*, **107**, 80 (1960).
5. R. Bacon and J. C. Bowman, *Bull. Am. Phys. Soc.*, **2**, 31 (1957).
6. E. R. Johnson and J. A. Amick, *J. Appl. Phys.*, **25**, 1204 (1954).
7. B. C. Banerjee and A. Goswami, *This Journal*, **106**, 590 (1959).
8. B. C. Banerjee and A. Goswami, *J. Sci. Ind. Research*, **16B**, 144 (1957).
9. G. W. Sears and R. V. Coleman, *J. Chem. Phys.*, **25**, 635 (1956).
10. R. V. Coleman and G. W. Sears, *Acta Met.*, **5**, 131 (1957).
11. P. A. Van der Meulen and H. V. Lindstrom, *This Journal*, **103**, 390 (1956).
12. J. F. Green and A. A. Wolf, *Research*, **11**, 38 (1956).
13. J. Franks, *Acta Met.*, **6**, 103 (1958).
14. L. Meyer, *Proc.* Third Conf. on Carbon, p. 451. Pergamon Press, New York (1958).

Anodic Behavior of Copper in Phosphoric Acid

F. H. Giles[1] and J. H. Bartlett

Department of Physics, University of Illinois, Urbana, Illinois

ABSTRACT

The anodic behavior of copper has been studied up to about 1.5 v above the floating potential, mainly in 50% orthophosphoric acid. The floating potential is at about −0.16 v (with respect to 0.1*N* calomel). Characteristic potentials occur at $\epsilon_I = -0.01$ v and $\epsilon_{II} = 0.16$ v. Electropolishing is found between these two potentials and above 0.8 v. The limiting current appears to be governed by the convection of the reaction products away from the electrode, and there seem to be at least two low-resistance layers which can form on the surface, one associated with ϵ_I and the other with ϵ_{II}. Below ϵ_{II}, the cation is primarily Cu^+; above ϵ_{II} it is primarily Cu^{++}.

In two earlier papers, Bartlett and Stephenson describe the use of special electrical and optical methods for the study of the anodic behavior of iron in H_2SO_4 (1), and of copper in HCl (2). These methods have been expanded and employed in the study of the anodic dissolution of copper in H_3PO_4, with some reference to the phenomena of electropolishing (3).

In the present article, the results found for copper in phosphoric acid are summarized, and an attempt is made to interpret them in a consistent way. It is shown that at least two different types of film occur on the anode surface, and that these have a rather low resistance. Interruption experiments indicate that capacitative effects are of importance, but the determination of the detailed electrical behavior of the surface films will require separate investigation. The complete analysis of the transients for copper in phosphoric acid probably will be rendered easier when one has developed the principles with other systems, such as iron in sulfuric acid. (This system is now being studied very intensively.)

Experimental Procedure

The circuitry and nomenclature defined and used in the papers referred to in the introduction have been practically unchanged. For convenience, a diagram of the basic circuit is shown in Fig. 1.

Aqueous orthophosphoric (H_3PO_4), 50% by weight (sp. gr. 1.415), was chosen because it is in the range which leads to good electropolishing, while still yielding a limiting current which is sufficiently high to be handled easily with the equipment.

The copper anode, the platinized platinum cathode, and the calomel (0.1N) reference electrode were all put directly into the acid. The copper anode was constructed of a piece of copper wire approximately 1 cm in length, soldered so as to protrude at right angles from the end of a 4 in. brass rod. The anode face was a cross section of the wire; an area of 2.1 mm². The entire anode assemblage was coated initially with Unichrome 218X, then, first with a file, and finally with 0000 polishing paper (Norton), a surface was prepared. Upon mounting, the anode face was vertical and set so as to be visible readily through the cell wall.

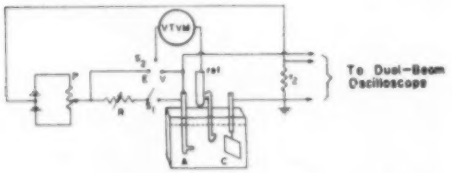

Fig. 1. Basic circuit. P, potential divider; R, 200 ohm helipot; VTVM, vacuum-tube voltmeter; A, anode; C, cathode; ref, calomel reference cell; r_s, current resistor.

General Experimental Results

Throughout the experiments, the calomel-cathode voltage remained constant at 0.42±0.01 v. The anode-calomel potential V varied:

(*A*) as a function of the internal parameters of the system. When capacitative effects are not important, then $V = \epsilon + ir$, where ϵ is the potential of the anode at zero current, i is the current and r is the resistance between the anode and the calomel. This resistance r will be regarded as composed of two parts: (*a*) a leakage or self-discharge resistance r_p effectively operating across the surface layer capacity C and (*b*) a resistance r_s in series with the above leaky condenser. (For a discussion of capacity effects, see Appendix.)

(*B*) as a function of the external parameters E and R. At all times: $V = E - iR$ where R is the external resistance and E is the applied potential minus the calomel-cathode voltage. In any given experiment, E is constant.

With no current flowing, a potential of approximately −0.125 v was observed immediately on contact of the acid and the copper anode. As the metal ions went into solution, the potential decreased to the average steady value of $V_f = -0.16$ v. Slight variations occurred. No anode was used if V_f was not between −0.14 and −0.17 v. However, it was found that this initial floating potential had little or no effect on the transients which followed the initiation of current flow.

Within 10^{-5} sec after the circuit was closed, the current jumped to a definite value i_0, equal to

[1] Present address: Department of Physics, University of South Carolina, Columbia, South Carolina.

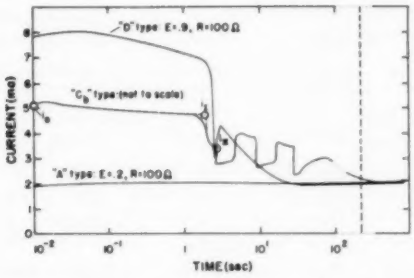

Fig. 2. Typical transients. Plots of current vs. time. E is the applied voltage and R the external resistance. While the C_b plot is not to scale, the abscissa is approximately proportional to the time (not its logarithm) and the duration of the plateau is about 3 sec. A typical B type transient, not shown, has plateau of about 20 sec duration (E = 0.3, R = 80 ohms).

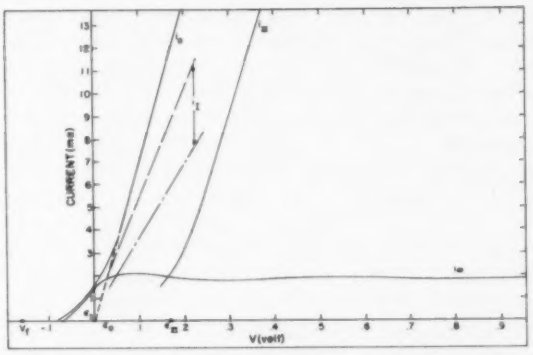

Fig. 3. Characteristic curves. Plots of currents i_o, i_I, i_{II} and i_s in milliamperes vs. anode-calomel voltage, V in volts.

$(E - \epsilon)/(r_p + r_s + R)$ (see Appendix). Throughout the experiments, the observed values of i_o ranged from 0.2 ma up to 40 ma, and the resulting i_o, V_o locus is shown in Fig. 3. The maximum deviation from this line, of any single datum point, was less than 0.02 v. Above $i_o = 5$ ma, the data are represented by a straight line with a voltage intercept at $\epsilon = \epsilon_o = 0.00$ v, and a slope corresponding to $r = r_o = 14.5$ ohms. The fact that all the i_o, V_o data fall on a single line indicates that ϵ_o and r_o are functions of the system alone and are not dependent upon the external parameters or the history of the system (3).

Transient types.—Subsequent to i_o the current rose slightly to a maximum. The manner and rate at which the current then varied with time depended on the external parameters. Four general forms of the current transient have been observed, the A, B, C, and D forms, with two variations of the C type (Fig. 2). The A form of transient is the simplest. The current rises slowly from i_o, and then, after reaching the maximum, falls even more slowly to a steady-state value. The B type occurred with somewhat higher currents. It is distinguished from the A form by the presence of an initial plateau which is terminated by a marked change in the slope of the current-time line. The B type transient is relatively slow: the plateau extended for at least 5 sec, and generally more than 10 sec.

The C forms of the transient display periodic activity. In the C_a variation, as in the B transients, the current goes through an initial plateau, but falls in two steps. The second (sharp) drop initiates periodic activity which is sustained indefinitely. In the C_b variety, the pulsing is begun with the drop in current from the initial plateau. After several cycles, the oscillations cease, and the current takes on a single steady value.

The fourth general form of the transient, designated as D, occurs at the highest initial currents. Following an initial plateau, the current falls very abruptly, rises to a maximum, and then decreases smoothly toward a steady-state value. No periodic activity is observed. The plateau of the D transient is relatively short, the maximum recorded length being 7 sec.

Characteristic curves.— Analysis reveals certain points which are characteristic of the various transients. When the current and potential values at these points were plotted on an i *vs.* V chart, the result was a family of curves, the "characteristic curves" of the system. The four points i_o, i_I, i_{II}, and i_s are shown in Fig. 2 and the resulting characteristic curves are shown in Fig. 3. i_o occurred in all forms of the transients, i_s in all types except "C_a", i_I only in B and C type transients, and i_{II} only in the C and D forms.

The current was considered at its steady-state value i_s when the rate of decrease of i was less than 10^{-2} ma/min. Usually 5 min was ample time for the steady state to be well established.

The locus (i_s, V_s) rises monotonically as V_s increases from −0.1 to approximately 0.05 v. For steady-state potentials in the range between 0.05 and 1.2 v, the current was very nearly constant. The highest value of i_s occurred when $V_s = 0.1$ v, and at that point, the steady-state current was 2.0 ma. Between 0.2 and 1.2 v, the value of i_s remained within 0.05 ma of 1.85 ma. Above $V_s = 1.2$ v, oxygen evolution occurred at the anode, and any rise in potential caused a corresponding rise in current.

Though the value of i_s is independent of the external parameters, it is very sensitive to changes in acid concentration. When the concentration of the H_3PO_4 was decreased, i_s rose rapidly. In the three concentrations, 15% acid (sp. gr. 1.131), 25% acid (sp. gr. 1.213), and 50% acid (sp. gr. 1.413) the steady-state current was 5.23 ma, 3.74 ma, and 1.85 ma, respectively. For higher concentrations, the limiting current dropped much lower.

Upon breaking the current flow, the value of V immediately after the "break" will be equal to $\epsilon_1 = \epsilon + v$ (v As in Appendix). By using a special switch (Western Electric Relay: 275C) and Tektronix, model 512, oscilloscope, the magnitude of ϵ_1 was measured within 10^{-5} sec after the current was stopped. The results of break experiments in the steady state are plotted in Fig. 4. It is apparent that the value of the resistance r_s remained constant at less than 23 ohms.

Experiments in Different Regions

Each of the four transient forms arise under particular applied conditions and are associated with

Table I. Characteristics of the copper anode for various applied voltages

Region	A Low-voltage region	B Intermediate range	C Transition, unstable range C_a	C Transition, unstable range C_b	D High-voltage region
i_a (ma)	<2.5	$2.5 \rightarrow 8.5$	$2.8 \rightarrow 8.0$	$3.8 \rightarrow 22.0$	>4.7
V_a (v)	<0.17	$0.1 \rightarrow 0.27$	$0.23 \rightarrow 0.4$	$0.3 \rightarrow 0.65$	>0.6
E (v)	<0.5	$0.15 \rightarrow 0.5$	$0.35 \rightarrow 0.6$	$0.4 \rightarrow 0.9$	>0.8
ϵ_i (v)	$<\epsilon_I = 0.01 \pm 0.01$	$\epsilon_I < \epsilon_i < \epsilon_{II}$	—	$>\epsilon_{II}$	$>\epsilon_{II} = 0.16 \pm 0.02$
r_a (ohms)	Approximately 23 ohms	Approximately 23 ohms	Approximately 23 ohms		Approximately 23 ohms
Extent of initial plateau in current transient $= t$	—	>5 sec	$8 \rightarrow 25$ sec	$0.3 \rightarrow 8$ sec	<5 sec
Charge transferred during initial plateau: $Q = \int_0^t i dt$ (Q in millicoulombs)	—	$Q = 2.12t + 15$		$Q^2 = 137t$	
Cation	Cu^+	Cu^+	—	—	Cu^{++}
Electropolishing (?)	No	Yes	No		Yes ($V_a > 0.8$)
ϵ decay following the break from steady state	Slow: $\epsilon_i \rightarrow V_f$ (about 5 min)	Fast: $\epsilon_i \rightarrow \epsilon_I$ (<0.003 sec) Slow: $\epsilon_I \rightarrow V_f$ (about 5 min)	Fast: $\epsilon_i \rightarrow \epsilon_I$ (>0.005 sec) Slow: $\epsilon_I \rightarrow V_f$ (about 5 min)		Fast: $\epsilon_i \rightarrow \epsilon_I$ (>0.01) <0.15 sec, Slow: $\epsilon_I \rightarrow V_f$ (about 5 min)

distinct optical and electrical phenomena. It is therefore convenient to divide the descriptions of the Cu-H_3PO_4 system into four sections: each section dealing with activity commensurate with one of the transient forms. Characteristics of the four regions of observations are tabulated in Table I.

Low-voltage region (region A).—During and following an A-type transient, the surface of the anode was covered with a reddish brown layer which remained attached to the surface throughout electrolysis. At the high voltage end of the A region, the layer occasionally peeled off. The resulting exposed surface was very badly etched, but had a metallic luster.

In this region, the plot of steady-state current (i_a) *vs.* voltage (V_a) shows a monotonic rise of current with voltage. Interruptions in current flow during an A transient indicated that ϵ rises slowly from its initial value to a steady-state value which is always less than -0.01 v. With the cessation of current flow, ϵ drops slowly, (of the order of 5 min) to the floating potential V_f (Fig. 6).

Intermediate-voltage region (region B).—When the load-line (the line, $V = E - iR$, determined by the external parameters) crossed the (i_a, V_a) locus above the knee of the curve, or more precisely, between 0.1 and 0.26 v, a B transient occurred. The duration of the initial plateau, which characterizes the B transient, ranged from 115 sec for the lowest potentials to 5 sec for the highest. The plateau terminated at time t_i, with current i_i, and, according to the characteristic curves (Fig. 3), with an $\epsilon_i = -0.01$V and $r_i = 22\ \Omega$. Throughout the B region, i_a was very nearly constant, falling slightly from 2 ma down to 1.85 ma.

By interrupting the current at various points along the transient, the accompanying potential changes were measured directly. During the initial plateau, the value of ϵ rose slowly from its minimum value at i_{max} to the value ϵ_I. If allowed to decay, ϵ was observed to fall slowly to the resting potential of the anode. If the interruption occurred after time t_i, a very rapid, (less than 0.003 sec) fall in potential from ϵ down to ϵ_I became apparent (Fig. 5). From ϵ_I to the floating potential, the decay was very slow, ending at V_f (Fig. 6). The end of the initial plateau in the B transient occurred when the open-circuit potential reached a maximum value, ϵ_I. This

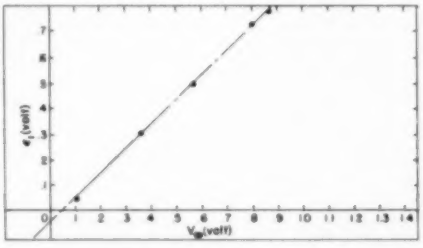

Fig. 4. Open-circuit potential. Plot of the open-circuit potential ϵ_i immediately after break from the steady state with anode-calomel potential V_a.

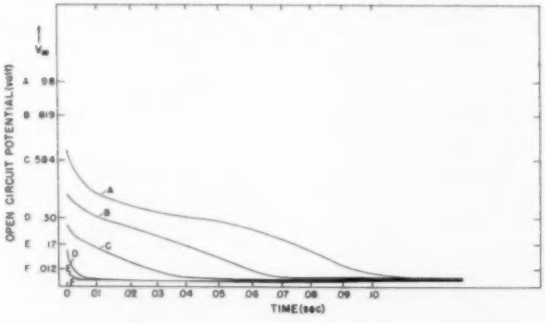

Fig. 5. Break transients. Plot of open-circuit potential vs. time. For run A, E = 1.2 v and R = 130 ohms; for B, E = 0.9, R = 60; for C, E = 0.6, R = 10; for D, E = 0.4, R = 60; for E, E = 0.3, R = 70; and for F, E = 0.2, R = 100.

ϵ_i, measured indirectly from the characteristic curves and directly from the break experiments (Fig. 4) has the value $\epsilon_i = -0.01 \pm 0.01$ v.

Schlieren photographs indicate that the slow decay of ϵ runs parallel with the relaxation of the thick, viscous layer near the anode surface (Fig. 6). However, no immediate change in the anolyte was apparent when current flow was stopped and reflectivity measurements did not show any rapid changes on the metal surface, in spite of the very rapid decay of potential from ϵ_s to ϵ_i.

During the plateau of a B transient the anode surface was covered with a red-brown layer. Upon termination of the plateau, the layer began to split and slide away, revealing an electropolished surface. The surface remained polished during steady-state conditions, but the system was very sensitive to mechanical agitation. A slight jar caused the current to rise, ϵ to fall, and the surface to etch. On re-establishment of ϵ_i the anode was again polished.

The unstable or transition region (region C).—In the unstable, or transition region, the C_a transients began as did the B transients; the end of the initial plateau occurred at current i_i and potential ϵ_i. The current decreased more rapidly until it reached the value i_{II}, when it fell abruptly and then began to oscillate. The locus of (i_{II}, V_{II}) is a straight line having a slope corresponding to $r = r_{II} = 15.5$ ohms and an intercept indicating an $\epsilon = \epsilon_{II} = 0.16$ v.

In C_a transients, the current pulsations persisted indefinitely. Interruption experiments showed these oscillations to be associated with variations of ϵ. If the current flow was broken between the times of occurrence of i_i and i_{II}, or if during the oscillation, the break occurred when the current was high (during a low ϵ part of the cycle) the value of ϵ decayed to ϵ_i in less than 0.003 sec and was qualitatively the same as that which occurred from the steady state of a B transient. When the interruption occurred after i_{II}, and during a low current section of a cycle (during the high ϵ part of the pulse), ϵ decayed smoothly, but more slowly to ϵ_i; ϵ never reached ϵ_i in less than 0.005 sec. This decay resembled that from the steady state after a D transient.

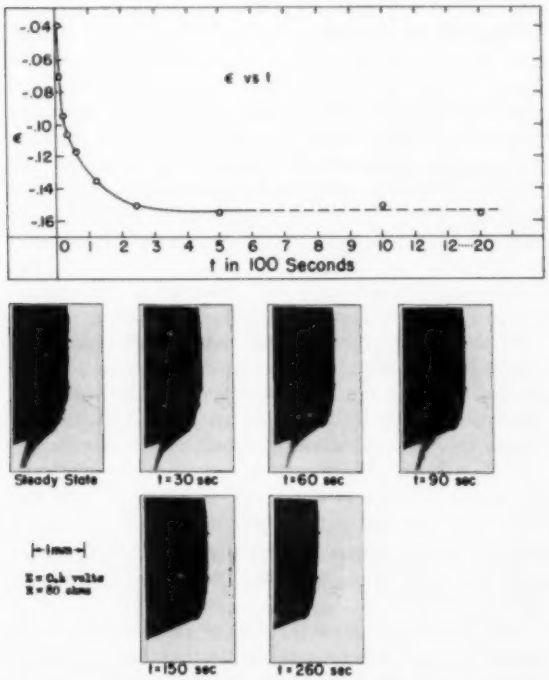

Fig. 6. Long time potential decay. Potentiometric and Schlieren study of the long-time potential decay, following interruption of the steady-state current.

As i_a was increased, the time interval between i_i and i_{II} lessened. Ultimately, in the C_b transients, the current and voltage at the end of the initial plateau fell along the i_{II}, V_{II} locus, and no point corresponding to i_i, V_i was discernable on the transient. ϵ rose to ϵ_{II} during the initial plateau. Upon interrupting the current flow during the plateau, ϵ appeared less than ϵ_i, and decayed slowly to V_f. Upon breaking the current immediately after the plateau, ϵ fell quickly (but always in a time greater than 0.005 sec) to a slowly decaying value of ϵ which was less than ϵ_i.

The oscillations in a C_b transient were always short lived: usually less than 5 cycles occurred. In the steady state following a C_b transient, i_s was constant at 1.85 ma. The value of ϵ_s and the shape of the ensuing ϵ decay were found to depend upon V_s. The decay consisted of a short-time portion and a long-time one (this of the order of 5 min). At no time, following a current drop from i_{II}, did the short-time decay become complete in less than 0.005 sec. This is true for both C and D regions, although in the D region, the time needed for ϵ_s to decay to ϵ_i might be as much as 0.15 sec. When compared to the short-time decay, the slowly falling potential appeared practically constant.

Throughout the transition region, no electropolishing occurred. Schlieren studies, in which the anolyte was studied down to within 0.001 cm of the anode surface, showed no variations in refractive index during oscillations. Measurements of surface reflectivity did, however, show variation with the oscillations, the apparent brightness falling with the current at i_{II}, and at the end of every high current cycle during oscillations. When ϵ was above ϵ_{II}, the reflectivity also revealed a definite change in surface brightness upon breaking current flow; at the instant of the break and again at the end of the decay of ϵ to ϵ_i.

The high-voltage region (region D).—The characteristic curves indicate that the plateau in a D transient ends at i_{II}. The plateaus were always short—the maximum duration being approximately 5 sec, and the minimum 0.2 sec. The current dropped rapidly from i_{II}, rose to a maximum, and then fell steadily to i_s. Throughout the D region, the current in the steady state was 1.85 ± 0.05 ma.

When the steady-state current was broken, the short-time ϵ decay appeared to consist of two parts: (*a*) an approximately exponential fall, and (*b*) a more or less well-defined plateau terminated by an S-curve fall to the value ϵ_i.

The first part is probably a decay of activation overpotential, but it will be sufficient for the present

purpose to treat it as the discharge of a capacity C through a shunting resistance r_p. Since the change of potential during the discharge, $-i_s r_p$, increases with V_s, and i_s is roughly constant, the resistance r_p must increase with V_s. The time constant $r_p C$ also increases with V_s, which could be consistent with a value of C independent of V_s. However, the detailed knowledge of the behavior of the capacity C and its shunting (probably nonohmic) resistance can only be had by further experiments, coupled with an appropriate analysis of activation decay curves.

The second part of the decay curve is similar to the decay curves previously found for Cu in HCl (2), and has a definite plateau, the length of which is a linear function of V_s. The height of the plateau varies with V_s, probably indicating the presence of a concentration overvoltage. Decays such as these have been found by Giner also (14) for Pt in 1N H_2SO_4, 10^{-3}M H_2O_2.

On interruption, no immediate change in the anolyte was visible in the Schlieren microscope. There was, however, a definite break in the reflectivity *vs.* time trace at both ends of the rapid decay curve.

Also the make transient was interrupted at various points along its final falling portion, and it was observed that the resulting break transients resembled those from the steady state, with a late break being similar to a break from a high voltage. This means, following the argument above, that the resistance r_p is increasing, and concentration effects are also entering, as the current falls during the final stage of a D transient.

During a given transient, the time needed for ϵ to fall to the slowly decaying potential[2] increased from approximately 0.005 sec just after the establishment of ϵ_{II}, to the steady-state duration associated with V_s. If one interrupted the current flow briefly, and if during the off-time the intermediate potential had sufficient time to decay to the slowly decaying potential, the values of i and V immediately after the circuit was remade fell on the (i_I, V_I) locus. The current then went through a plateau and dropped rapidly from an i_{II}. If, however, the current was switched back on before the potential had decayed to ϵ_I, the recovery current merely spiked and fell smoothly toward i_s.

Comparison with Other Work

The pioneer work on the behavior of copper in orthophosphoric acid solution was done by Jacquet and co-workers (4, 5). Working at essentially constant current, they observed a plateau in the current-voltage curve and stater that "within the voltage range corresponding to the horizontal section of (the) curve we get a bright surface." We have looked at this section in more detail (which was possible because of our low external resistance) and find that (*a*) the behavior does depend on the voltage, and (*b*) electropolishing occurs in two voltage regions which are separated from each other.

[2] It took at least 2 sec for the slowly decaying potential to rise to ϵ_I. In D transients, ϵ_{II} was established before the slowly decaying potential reached its limiting value. Interruptions in current flow occurring after i_{II}, but less than 2 sec from the initial "make," manifested short-time potential decay to a slowly decaying potential which was less than ϵ_I.

Our experimental work resulted in the first good current-voltage curve to be reported. This part of it has been reported later by Lorking (7), and the results are quite similar.

The present work goes beyond any previously reported in that it attempts to analyze the time behavior of the make and break transients. Lorking (7c) did speculate on the cause of the periodic oscillations, as did Bonhoeffer, *et al.* (12), but we hold different views which will be mentioned below.

Discussion

In the low-voltage region (region A), the rise of ϵ during a make transient seems to run parallel with the establishment of the convection layer, and the time necessary to attain ϵ_I is at least 2 sec. If, in any region, the circuit is broken before this period is over, there is a rapid decay to a voltage lower than ϵ_I. This rapid decay is probably symptomatic of a breakdown of a layer at the surface, while the slow decay is associated with the ironing out of concentration gradients due to convection and diffusion. The slowly decaying potential, the maximum value of which is ϵ_I, may be regarded as a measure of the concentration at the interface between surface layer and convection layer.

In the B region, when ϵ reaches ϵ_I during a make transient, $d\epsilon/dt$ increases rapidly, as is the case when a layer is completed. Break transients from the steady state show a very rapid ϵ decay (less than 0.003 sec) superimposed on the long-time decay mentioned above. If this rapid decay be regarded as the same sort of process as the slow one, except with a much shorter time constant, it would reflect the ironing out of concentration gradients in the pores of a thin layer. Another mode of representation would be in terms of a capacitative layer model, and this serves admirably in the description of the break curve for passive iron (see Appendix). Further experimentation is needed to decide which description is the more appropriate. In any case, it seems that (*a*) the small time constant, the marked change in $d\epsilon/dt$, and the alteration of surface reflectivity indicate the presence of a layer on the surface for $\epsilon > \epsilon_I$, and (*b*) the resistance of the layer is small.

If we try to account for the shape of the slow decay curve by assuming a diffusion model, certain difficulties arise, but can apparently be overcome by refining the model. If in the steady state the concentration c of the potential-determining ion increases linearly across the diffusion layer, and if during the break this concentration gradient levels out in accordance with the diffusion equation, the concentration at the metal will be $c = c_s + a\sqrt{t}$, and the slope *vs.* t will be infinite at $t = 0$. However, Fig. 6 shows the initial slope to be just large rather than infinite, and Fig. 5 indicates that the drop during 0.01 sec is not great.

The explanation seems to be connected to the circumstance that the solution at the anode actually is saturated with reaction products, which cannot move away very rapidly. The anion moving in will continue to react with the surface layer until

there is no more layer left, and so its concentration will stay low for a fairly long time. Consequently, the slow change of ϵ is to be expected, and may be taken to be further evidence for the existence of a layer associated with ϵ_I.

In the D range, the initial high current evidently saturates the anolyte adjacent to the anode very rapidly, and the current falls. The occurrence of ϵ_{II} indicates a new type of layer on the surface, this layer being less sensitive to mechanical agitation than any previous layer. The rapid ϵ decay (Fig. 5), with its increased duration and plateau-like form, is of the same general shape as was found previously in HCl, where the plateau becomes more pronounced the higher the voltage from which the break occurs. This is particularly so for break transients from the passive state in iron, where the ϵ decay plateau may last for many seconds.

Several observations may be adduced as evidence that ϵ_{II} is associated with a new reaction, namely: (*a*) a new hazy whitish film usually can be observed over the anode surface following the establishment of ϵ_{II}, (*b*) both ϵ_I and ϵ_{II} can occur during the same transient. The fact that oscillations occur can be taken as prima facie evidence of the existence of two states, (*c*) Faradaic experiments indicate that in the B region the cation is primarily Cu^+, whereas in the D region it is primarily Cu^{++}, (*d*) the break transients following the establishment of ϵ_{II} appear qualitatively different from those arising under conditions of lower voltage.

Periodic activity.—Although periodic oscillations are found in the experiments reported here, they do not differ in nature from those found generally elsewhere, and no new light is shed on the mechanism involved.

Bonhoeffer and Gerischer (12) proposed a theory of periodic behavior for copper in HCl, where it was assumed that cuprous oxide was involved, even though none is detected experimentally. Lorking (7c) discussed briefly the behavior of copper in phosphoric acid, attributing the rise of potential to a dearth of OH^- ions, and the fall to dissolution of the oxide film. He did not give any reasons why the system should continue to oscillate rather than settle down to a steady state.

Cooper and Bartlett (13) suggested an alternative theory of oscillatory behavior for copper in HCl, based mainly on the idea that (*a*) concentration changes in the pores are important, and (*b*) layer formation will not occur below a certain electrode potential. This theory may also be valid for copper in phosphoric acid, but the verification of this would require a special investigation.

Summary and Conclusions

At low voltages, the current-potential curve of a copper anode in 50% orthophosphoric acid consists of two parts. The first part rises from zero current at −0.16 v to a current density of about 100 ma/cm^2 at −0.01 v. In this region the current appears to be activation controlled, and the copper enters the solution in the cuprous form. The second part of the curve is rather flat up to about 1.1 v, where oxygen evolution begins. The value of the current on this plateau apparently is controlled by the convection of the reaction products away from the anode. Below +0.16 v, copper goes into solution primarily as cuprous ions, while above +0.16 v it enters primarily as cupric ions.

Just above −0.01 v, the anode surface appears bare to the eye, but evidence adduced here indicates that there is a low-resistance layer on the surface. In this region, electropolishing occurs, and Hoar and Farthing (8) have inferred the existence of a film from their mercury-drop experiment.

Above +0.16 v a hazy whitish film is observed, and this is not greatly sensitive to mechanical agitation. The surface appears etched until the potential reaches a value of about 0.8 v, when the white layer slides off from the anode face and electropolishing begins.

In the neighborhood of +0.16 v, there can be two possible states of (films on) the electrode, and the system oscillates between them. The periodic variation of the current is of the same general nature as has been observed for other systems, and for which there have been various theories (12, 13). No special investigation of the detailed mechanism for copper in phosphoric acid has been made, but it is probable that this mechanism is similar to that postulated for the other systems.

Acknowledgment

The authors express their grateful appreciation to the Office of Ordnance Research for the provision of funds which made this work possible.

Manuscript received May 26, 1960; revised manuscript received Nov. 14, 1960. This article is based on experimental results contained in OOR Technical Report No. 2, Contract No. DA 11-022-ORD-939, June 15, 1955. This paper was prepared for delivery before the Columbus Meeting, October 18-22, 1959.

Any discussion of this paper will appear in a Discussion Section to be published in the December 1961 JOURNAL.

REFERENCES

1. J. H. Bartlett and Lee Stephenson, *This Journal*, **99**, 504 (1952).
2. Lee Stephenson and J. H. Bartlett, *ibid.*, **101**, 571 (1954); R. S. Cooper and J. H. Bartlett, *ibid.*, **105**, 109 (1958).
3. F. H. Giles and J. H. Bartlett, Office of Ordnance Research, Contract No. DA-11-022-ORD-939, Technical Report No. 2 (138 pp.) June 15, 1955.
4. P. A. Jacquet, *Nature*, **195**, 1076 (1935); *Trans. Electrochem Soc.*, **69**, 629 (1936); *Rev. met.*; **37**, 210, 244 (1940); *ibid.*, **42**, 133 (1945).
5. P. A. Jacquet and M. Jean, *Compt rend.*, **230**, 1862 (1950); *Rev. met.*, **48**, 537 (1951).
6. J. K. Higgins, *This Journal*, **106**, 999 (1959).
7. K. F. Lorking, (a) *Trans. Australian Inst. Met.*, **5**, 109 (1952); (b) *Trans. Inst. Met. Fin.*, **32**, 119 (1955); (c) Australia, Department of Supply, ARL Report 18 (1956); (d) Australia, Department of Supply, ARL Report 24 (1957); (e) *J. Australian Inst. Met.*, **4**, 22 (1959).
8. T. P. Hoar and T. W. Farthing, *Nature*, **169**, 324 (1952).
9. F. Bouillon, Y. Bouillon-Nyssen, and A. Delplanche, *Bull. soc. chim. Belges*, **59**, 660 (1950), and **65**, 245 (1956).
10. E. C. Williams and M. A. Barrett, *This Journal*, **103**, 363 (1956), and **104**, 393 (1957).
11. D. Laforgue-Kantzer, *J. Chim. Phys.*, **52**, 314 (1955).

12. K. F. Bonhoeffer and H. Gerischer, *Z. Elektrochem.*, **52**, 149 (1948).
13. R. S. Cooper and J. H. Bartlett, *This Journal*, **105**, 115 (1958).
14. J. Giner, *Z. Elektrochem.*, **64**, 491 (1960).

APPENDIX

As a model for the capacitative properties, consider an idealized electrode as shown in Fig. 7. There are

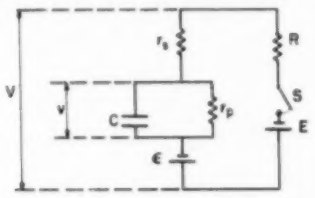

Fig. 7. Idealized equivalent circuit. Series resistance r_s, capacity C shunted by resistance r_p, electrode potential ϵ, and the anode-calomel potential V.

three elements in series, namely: (*a*) a series resistance r_s, which could be composed of a layer resistance and a solution resistance, (*b*) a capacity *C* shunted by a resistance r_p, and (*c*) an electrode potential ϵ, which may include concentration overpotentials among other types. Denote the impressed emf by *E*, the external resistance by *R*, the anode-calomel potential by *V*, the potential across the condenser by *v*, and the steady-state current by i_s.

Upon closing the switch, the differential equation for the potential across the capacitor is

$$C(dv/dt) + (v/r_p) = (E - \epsilon - v)/(r_s + R) \quad [1]$$

or

$$C(dv/dt) + [1/r_p + 1/(r_s + R)]v = (E - \epsilon)/(r_s + R) \quad [2]$$

If $v = 0$ at the start, the initial current will be $(E - \epsilon)/(r_s + R)$, and this serves to charge up the condenser. When the condenser has been charged, the current will be $(E - \epsilon)/(r_s + r_p + R)$. The time constant, if ϵ is fixed, is $r_p(r_s + R)C/(r_s + r_p + R)$. If $r_p >> r_s + R$, as is the case for passive iron, the time constant is approximately $(r_s + R)C$, so that the make constant in this case is just that for charging the condenser *C* through the resistance $r_s + R$. In our present work, the charging seems to be all over in less than 10^{-5} sec, the current having reached a definite value i_s, equal to $(E - \epsilon)/(r_s + r_p + R)$ on this model.

When we break from the steady state, there will be a sudden change of potential $\Delta V = i_s r_s$. The condenser then will discharge through the resistor r_p with a time constant r_pC. At the beginning of this discharge, $-C(dV/dt) = i_s$, so that a measurement of the initial slope enables us to calculate *C* from this equation. If *C* does not vary, the time constant of the decay is r_pC, so that we may now calculate r_p. If the quantities r_p, ϵ, and *C* vary with time, it becomes more difficult to determine them experimentally.

Measurements for passive iron indicate that such an idealized electrode is of use as a model. The corresponding experiments have not been made as yet for the system under discussion in the present article, but one can make some inferences on the basis of the above analysis, especially if the transients have roughly exponential character. When *C* does turn out to be a significant parameter, we must, if possible, ascertain its physical meaning, in terms of properties of the layers on the electrode.

In the steady state, $v_s = i_s r_p$. If the resistance r_p remains constant during the exponential decay, then, at the instant of break, it is given by v_s/i_s. If $v_s = 0.1$ v and $i_s = 2$ ma, which would be typical for Cu in H_3PO_4, then $r_p = 50$ ohms. However, if $v_s = 0.1$ v and $i_s = 5$ μa as for passive iron, then $r_p = 20{,}000$ ohms. If high resistivity be regarded as a criterion for passivity, then the copper electrode is not passive, even when covered by a layer.

A Precision Conductance Bridge of New Design

George J. Janz and James D. E. Mc Intyre

Department of Chemistry, Rensselaer Polytechnic Institute, Troy, New York

ABSTRACT

A conductance bridge in which the essential component is a precision impedance comparator and which combines speed, wide range, and high accuracy in measurements is described. While fundamentally similar in design and operation to the precision a-c conductance bridges known today, the present design has the attractive features of simplicity of construction from unitized components available on the market and provision for use of the "four-leads" cell technique to eliminate connecting lead effects in remote conductance measurements.

The conductance bridge described in this paper combines the features of speed, wide range, and high accuracy in measurements. While nothing original is claimed for individual portions of the circuit, the design of a bridge that may be readily assembled from commercially available components at moderate cost and capable of the precision of the best bridges for the purpose (1-5) is of interest. The central component is an impedance comparator (General Radio Co., Type 1605-AS5), a modified version of the comparator widely used for rapid production testing as well as laboratory measurements. A complete list of parts and components is included as a practical feature.

This bridge has proved particularly valuable for eliminating time-temperature, polarization, and leads resistance effects from conductance measurements on high-temperature molten salt systems in this laboratory.

Design

The theoretical and practical conditions for attaining high accuracy in electrolytic conductivity measurements have been discussed in detail by Jones and Josephs (1), Shedlovsky (2, 6), Luder (7), and Feates, Ives, and Pryor (8). The present conductance bridge was designed and constructed with these requirements in mind.

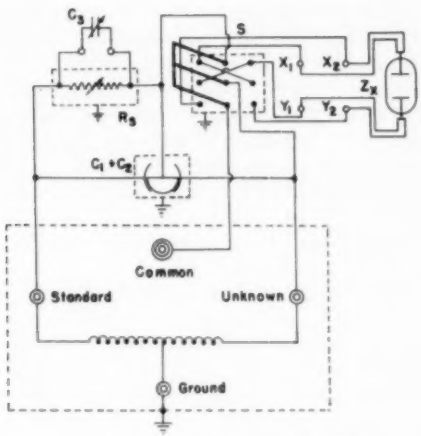

Fig. 1. Schematic diagram of bridge circuit

A schematic diagram of the bridge circuit is shown in Fig. 1. R_s is the variable resistance standard, C_1 and C_2 are balancing capacitors, C_3 is an auxiliary capacitor, S is a 3-pole reversing switch, and X_1, X_2 and Y_1, Y_2 are binding posts to which the four leads from the cell are connected. L_1 and L_2 are the halves of the center-tapped transformer of the impedance comparator which constitute the unity-ratio arms of the bridge. The standard, unknown, common, and ground terminals are binding posts on the comparator. Dotted lines about the individual components indicate grounded shields; for simplicity, wiring shields are not indicated. The impedance comparator is outlined as a dash-line rectangle in this illustration. Binding posts on the front panel of the bridge cabinet are indicated by open circles.

The entire bridge is enclosed in a standard steel cabinet rack. The resistance decade units are mounted at the bottom of the removable front panel in order to maintain their temperature within 2°C of room temperature.

Shielded polyethylene insulated wire and Teflon insulated wire are used for all internal connections in order to minimize dielectric losses and stray coupling effects. Polystyrene sheet is used for the balancing capacitor mounting brackets.

All bridge components are shielded, according to Shedlovsky's recommendations, in order to minimize external electrical interference and to fix definitely and control possible interbranch capacitances. Connections to the cell leads are made with two twin-conductor transmission cables. The shields of these cables are connected to the shield terminal on the front panel; this terminal is in turn connected to the guard point of the impedance comparator. The bridge cabinet, internal component and wiring shields, and the ground terminal of the comparator are connected to a suitable external ground.

Bridge Components

Three basic components, a precise impedance comparator, an adjustable resistance standard, and a set of balancing capacitors are the essential units of this bridge. A brief description of each follows. A complete list of parts and components is summarized in Table I.

Table I. Components and parts for conductance bridge

Item	Description	Source*
Impedance comparator	G. R. Type 1605-AS5	GR
Resistance units	G. R. Type 510-A 1 ohm decade	GR
	G. R. Type 510-B 10 ohm decade	GR
	G. R. Type 510-C 100 ohm decade	GR
	G. R. Type 510-D 1,000 ohm decade	GR
	G. R. Type 510-E 10,000 ohm decade	GR
Switch	4 PDT, Federal Anti-Capacity, No. 1424	T
Capacitors	Johnson Differential; No. 167-31, Type No. 10LA15; max. cap./section 11 mfd	T
	Hammarlund Double Section Transmitting; No. HFBD-100-C. max. cap./section 105 mfd	T
Cabinet rack	Bud Deluxe; No. CR-1743; 19-5/16 × 17-1/2 in.	T
Rack panel	Bud Aluminum; 19 × 10-1/2 in., No. PA-1106	T
Angles	Bud, Chassis Supporting; No. 5A-1350	T
Shields	Bud, Aluminum Minibox, 8 × 6 × 3-1/2 in.; No. Cu 3009	T
	Bud, Aluminum Minibox, 4 × 2 × 2-3/4 in.; No. Cu 3015	T
	Premier Aluminum Miniature Case; 17 × 5 × 4 in.; No. AMC-1012	T
Binding posts	Grayhill	T
Wiring	Belden RG 58/U Transmission Line, No. 8240 Alpha Type "E" Teflon Insulated Hook-up Wire, MIL-W-16878B	GR, T
	Belden Shielded Cable, No. 8227	

* GR, General Radio Co., Cambridge, Mass.; T, Electronic Supply House.

Impedance comparator.—The General Radio Type 1605-AS5 impedance comparator is basically the same instrument as the more widely used Type 1605-A (9, 10), the chief difference being that the combination of four decade frequencies from 100 cps to 100 kc in the latter has been replaced by the frequencies, 1, 2, 5, and 20 kc to cover a range of more practical value for electrolytic conductance measurements.

The impedance comparator is a special self-contained impedance measurement system, its variable oscillator, bridge transformer, amplifiers, and sensitive detectors constituting basic parts of the bridge circuit.

The stabilized internal oscillator is an R.C. oscillator of the Wienbridge type that uses a thermistor for amplitude control. The push-pull output is fed

from the oscillator to a cathode follower output stage to drive the bridge transformer. The latter is a toroidal transformer in which the halves of a center-tapped secondary winding act as two highly precise unity-ratio arms of the bridge circuit. The inner primary winding is a modified banked winding and completely covers the high permeability wound-ribbon core. Electrostatic coupling with the secondary is prevented by two copper cups covering the primary winding. The secondary windings consist of a twisted pair of identical wires wound around the core so that they occupy equal volumes, thereby producing identical flux linkage, unity coupling, and equal output voltages. The amplifier input circuit in the impedance comparator is a cathode follower of high input impedance, constant gain, and two output impedance ranges selected by the "operate guarded" and "operate unguarded" positions of the function selector switch. In the "guard" circuit, the outer conductor of the General Radio Company coaxial connector is driven at nearly the same potential as the inner (detector input) conductor. Its low impedance output thus provides a marked reduction in input capacitance and thereby facilitates remote high impedance measurements where added input capacitance due to a grounded shield would cause measurement errors. With the selector switch in the "unguarded" position, the outer conductor of the coaxial connector is grounded.

Any unbalance voltage resulting from an inequality of standard and unknown impedances is amplified by the internal signal amplifier of the comparator and separated into its in-phase and quadrature components by the phase-sensitive detector circuit. The orthogonal voltage components are amplified and indicated directly by meters reading, respectively, impedance magnitude difference (ΔZ) in per cent and phase-angle difference ($\Delta\theta$) in radians. These meters are protected by a relay circuit which opens the meter circuits when the unbalance voltage is outside the range of the instrument. Full-scale deviation ranges of 0.3, 1, 3, and 10% for ΔZ and 0.003, 0.01, and 0.1 radian for $\Delta\theta$ are provided with the Type 1605-AS5 comparator.

Since the standard elements, R_s, C_1, C_2, and C_3 (Fig. 1) are relatively pure, the ΔZ meter indication may be interpreted as a ΔR difference, with negligible error, when the $\Delta\theta$ meter is nulled by adjustment of the balancing capacitors. The ΔZ meter may be calibrated with an internal calibration circuit in the comparator.

The inductively coupled ratio arms are equal to within one part in 10^6, and the detector sensitivity permits impedances to be matched with a precision of 0.002% when the instrument is nulled with a variable standard. The accuracy of impedance measurement, therefore, depends primarily on the precision of the external standard. The impedance comparator may be employed for impedance measurements over a range of 2 ohms to 20 megohms.

Resistance standard.—The variable resistance standard, R_s, (Fig. 1), consists of five General Radio Company Type 510 Decade-Resistance Units, connected in series to give a total resistance of 11,111 ohms in steps of 0.1 ohm. The 10, 100, and 1000 ohms per step units are certified to be exact within 0.05%; the 1 and 0.1 ohm per step units have a certified accuracy of 0.15 and 0.5%, respectively. The decade units have a temperature coefficient less than 0.002% at 23°C, have a negligible thermal emf to copper, and exhibit virtually no frequency dependence in the audio range. They are enclosed in an aluminum shielding box and are mounted behind the front panel of the bridge cabinet. Insulated shafts on the switching knobs make the readings insensitive of operator position.

Balancing capacitors.—Reactance of the conductance cell due to electrode polarization is balanced out by means of two differential air capacitors, C_1 and C_2 (Fig. 1), connected in parallel. Coarse balance is obtained by adjustment of a double section transmitting capacitor, C_1, with a maximum capacity of 105 $\mu\mu$f per section, reconstructed in the form of a differential capacitor. Fine balance is obtained with a micro differential capacitor, C_2, with a maximum capacity of 11 $\mu\mu$f per section. The capacitors are fitted with insulated shafts and knobs and are mounted in an aluminum shielding box on the rear of the front panel.

Terminals are provided to allow an auxiliary variable capacitor, C_3, (Fig. 1) to be connected in parallel with the resistance standard if necessary. An Electronic Instrument Company Model 1180 capacitance decade box has been found satisfactory for this purpose.

Conductance Measurements

Electrostatic coupling effects.—Capacitive coupling between individual elements of the bridge circuit, or between these parts and surrounding objects, effectively introduces stray paths through which an alternating current can flow and may lead to a false balance of the bridge. These effects may be defined more accurately by shielding the individual bridge components. Each component then has a distributed capacity to its surrounding shield. If, for simplicity, a conductor of resistance R is considered to have its total capacity to its grounded shield, C_s, concentrated at its midpoint, as shown in Fig. 2a, it can readily be shown[1] that this network is equivalent to the three terminal network shown in Fig. 2b, where

$$Z_x = R + (j\,w\,C_s\,R^2)/4$$

and

$$Z_a = Z_b = R/2 + 1/(j\,w\,C_s/2)$$

In order to measure the impedance, Z_x, between the two terminals X and Y, it is necessary to make the effect of the other two, Z_a and Z_b, negligible. Such a measurement is possible with the impedance comparator bridge without employing a Wagner Earth circuit. Due to the tight coupling of the bridge transformer and its low resistance, impedance shunting to ground of one of the transformer secondary windings has so little effect that one of the unwanted impedances, *e.g.*, Z_a, may usually be placed across it with negligible error. When the bridge is nulled with the variable standard, Z_s (refer Fig. 2c), the

[1] A detailed discussion of electrostatic coupling effects and shielding in conductance bridges is given in Shedlovsky's original paper (2) and his more recent review article (6).

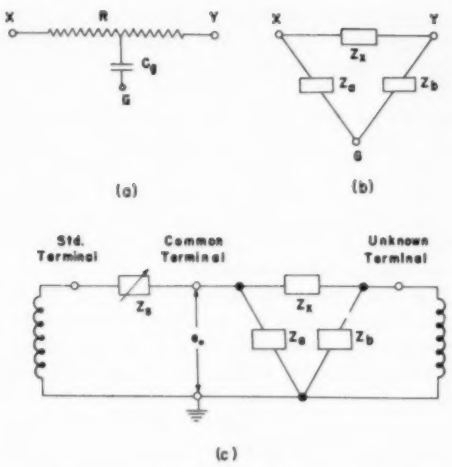

Fig. 2 (a). Resistor with capacity of shield concentrated at mid-point; Fig. 2 (b). equivalent three-thermal circuit; Fig. 2 (c). direct impedance measurement using variable standard.

only effect of the other unwanted impedance, Z_b, across the detector, is to reduce the latter's sensitivity.

Electromagnetic coupling.—Stray electromagnetic couplings with the elements of the bridge circuit may also produce a false bridge balance. In the present bridge, these mutual inductive effects are minimized by the use of an R-C oscillator, high degree of coupling (greater than 0.9999) of the bridge transformer, and shielding around the bridge components.

Leads resistance.—Conductance measurements, by virtue of the fact that the conductance cell must be maintained in a thermostatted chamber, necessitate the determination of an external impedance at some position remote from the bridge. When making measurements of extreme precision, or in a case where a conductance cell of suitably high cell constant cannot be employed (as, for example, with the molten alkali carbonates), the resistance of the connecting leads may be significant.

With the present bridge, provision has been made to eliminate leads resistance from the measurements by use of the "four leads method" (8). Two leads from each electrode of the conductance cell are connected to the bridge binding posts X_1, X_2, and Y_1, Y_2, respectively (Fig. 1). The latter, in turn, are connected to the poles of a shielded 3-pole double-throw anticapacity switch, S, in such a way that reversals of connections may be made as shown in Fig. 1.

The principle of the "four leads method" is, briefly, as follows. If the impedances x_1 and y_1 represent the impedances of the current-bearing leads to the cell electrodes plus any contact impedances in the reversing switch, Z_x is the cell impedance, Z_1 and Z_2 are the impedances of the inductively coupled ratio arms, and Z_s is the variable standard impedance, then the fundamental conditions for balance of the bridge are:

$$\frac{Z_s' + x_1}{Z_1} = \frac{Z_x + y_1}{Z_2}$$

and

$$\frac{Z_s'' + y_1}{Z_1} = \frac{Z_x + x_1}{Z_2}$$

where Z_s' and Z_s'' are the values of Z_s in the alternative bridge arrangements. Since the impedances of the ratio arms are identical, then

$$Z_s' + x_1 = Z_x + y_1$$

$$Z_s'' + y_1 = Z_x + y_1$$

and hence

$$Z_x = \frac{Z_s' + Z_s''}{2}$$

The extraneous impedances are thus cancelled by this technique.

Operating Procedure

The following procedure has been employed in making conductance measurements with the impedance comparator bridge in this laboratory.

Before making a series of measurements, the comparator is allowed to warm-up for about 15 min in order to stabilize the oscillator and meter circuits. The detector meters are initially zeroed[2] with the thumb adjustments for very precise measurements, the meter zeroes are checked frequently for the most sensitive range settings, particularly when the test frequency is changed. The ΔZ meter is calibrated by setting the "impedance difference per cent" switch to position 1 and the "function" switch to CAL 1%. With the CAL control adjusted to give a 1% (full scale) indication, the bridge input voltage is approximately 0.15 v.

The desired deviation ranges are selected with the "impedance difference per cent" and "phase angle difference radians" switches. These switches indicate the full-scale deflections of the meters. Wider ranges are attainable if the bridge is calibrated at lower oscillator levels.

With the instrument zeroed on the most sensitive ranges and calibrated, the range switches set at their maximum value of 10% and 0.3 radian, the frequency switch at the desired test frequency, and the reversing switch, S, at position 1, the function selector switch is turned from zero to "operate unguarded." If the impedance to be measured differs from the standard impedance by more than the above limits, the protective relays are actuated and the meter circuits opened; the "off scale" condition is indicated by a red panel light.

The bridge is brought to a coarse balance by alternate adjustment of the variable resistance decade units and the variable capacitors C_s and C_1. The ΔZ and $\Delta\theta$ range switches are then set to their most sensitive positions, 0.3% and 0.003 radian, respectively, and both meters are nulled by adjustment of R_s, C_1, and C_2. A slight unbalance indication on the calibrated ΔZ meter may be used to extend the precision of the measurement when required. The balancing resistance value is recorded and the function switch is then turned to the "operate guarded" position. The bridge is rebalanced and the new bal-

[2] The detailed operating procedure for the General Radio Company Type 1605-AS5 impedance comparator is given in the operating instructions (9) for this instrument. Only the basic procedure is described here.

Table II. Calibration of bridge resistors

Test frequency, kc	Jones Bridge Resistor: Nominal value, ohms	Jones Bridge Resistor: D.C. calibration value, ohms	Impedance comparator bridge R_s, ohms
1			100.00$_0$
2	100	99.999	100.00$_0$
5			100.00$_0$
20			100.00$_0$
1			1000.0$_0$
2	1000	1000.113	1000.0$_7$
5			1000.0$_5$
20			1000.0$_0$
1			10,001.8
2	10,000	10,000.09	10,001.9
5			10,002.2
20			10,001.7

ancing resistance value noted. Usually the difference in these readings is extremely small, even for the 20 kc test frequency.

Lead resistance is eliminated from the measurements by balancing the bridge with the reversing switch, S, first in position 1 and then in position 2. The average of the readings yields the true cell resistance. The polarization-free electrolyte resistance at infinite frequency may then be extrapolated conveniently from a plot of resistance vs. the square root of the reciprocal frequency.

Discussion

The precision of the bridge was tested by measuring the resistance of the coils of a Jones-Josephs Bridge (1, 3) available in this laboratory. The resistance coils of the latter had been calibrated accurately on direct current with a Mueller Bridge against National Bureau of Standards certified resistance standards. Results are summarized in Table II for the 100, 1000, and 10,000 ohm calibration standards at the four test frequencies The resisances of all the General Radio Company decade units were found to lie well within their stated tolerance values.

Since the ratio arms of the impedance comparator are equal to one part in 10^5, the accuracy of the measurements depends largely on the precision of the external resistance standard. The preceding calibration showed that the external decade resistance units have excellent characteristics over the audio frequency range; the maximum percentage charge in effective series resistance is less than 0.01%.

The bridge has been used in this laboratory for studies of the electrical conductances of high-temperature molten inorganic salt systems (240°-1000°C), and solutions of electrolytes in aqueous and organic solvents in the more conventional temperature range (0°-45°C). Details of these results will be published elsewhere.

While fundamentally similar in principle of design and operation to the precision a-c conductance bridges in current use (1-5), the attractive features of the present bridge lie in its simplicity of construction from readily available unitized components, in its wide impedance measurement range, rapidity of balance, and in its provision for use of the "four leads method." Polarization effects are minimized by the low bridge input voltage (0.15 v) and the wide test frequency range (1-20 kc).

Acknowledgments

This work was made possible in part by support, received from the U.S. Air Force, ARDC, Office of Scientific Research, Chemistry Branch and U.S. Department of the Navy, Office of Naval Research, Chemistry Branch, Washington, D. C.

Manuscript received June 20, 1960.

Any discussion of this paper will appear in a Discussion Section to be published in the December 1961 JOURNAL.

REFERENCES

1. G. Jones and R. C. Josephs, *J. Am. Chem. Soc.*, **50**, 1049 (1928).
2. T. Shedlovsky, *ibid.*, **52**, 1793 (1930).
3. P. H. Dike, *Rev. Sci. Instruments*, **2**, 379 (1931).
4. W. F. Luder, *J. Am. Chem. Soc.*, **62**, 89 (1940).
5. H. Eisenberg and R. M. Fuoss, *ibid.*, **75**, 2914 (1953).
6. T. Shedlovsky, "Technique of Organic Chemistry," Vol. I, p. 1651, "Physical Methods" (Editor Weissberger), Interscience Publishers, New York (1949).
7. W. F. Luder, E. F. McCarren, and A. A. Vernon, *J. Chem. Ed.*, **34**, 190 (1957).
8. F. S. Feates, D. J. G. Ives, and J. H. Pryor, *This Journal*, **103**, 580 (1956).
9. General Radio Co. Type 1605-AS5 Impedance Comparator Operating Instructions, General Radio Co., Cambridge, Mass., 13 (1957).
10. H. Painter, *General Radio Experimenter*, Vol. 34, No. 4 (1960).

December 1961 Discussion Section

A Discussion Section, covering papers published in the January-June 1961 JOURNALS, is scheduled for publication in the December 1961 issue. Any discussion which did not reach the Editor in time for the June 1961 Discussion Section will be included in the December 1961 issue.

Those who plan to contribute remarks for this Discussion Section should submit their comments or questions in triplicate to the Managing Editor of the JOURNAL, 1860 Broadway, New York 23. N. Y., *not later than September 1, 1961.* All discussion will be forwarded to the author(s) for reply before being printed in the JOURNAL.

Characteristic Functions and Parameters in the Theory of Hydrogen Overpotential

I. Theoretical

Gilbert W. Castellan[1]

U. S. Naval Research Laboratory, Washington, D. C.

ABSTRACT

It is shown that the current density-overpotential relationship for several mechanisms of the hydrogen evolution reaction can be expressed conveniently in terms of one or the other of two characteristic functions: $g_1 = \left\{\exp\left[\left(\alpha - \frac{1}{2}\right)\eta\right] \sinh\left(\frac{1}{2}\eta\right)\right\} \Big/ i$, $g_2 = \left[\tanh\left(\frac{1}{2}\eta\right) \Big/ i\right]^{1/2}$. The following parameters are convenient: α, the transfer coefficient for the oxidation reaction; θ_0, the fraction of the surface covered by H atoms at equilibrium, $i_0 = (di/d\eta)_{\eta=0}$; and $\rho = \{d \ln [\theta/(1-\theta)]/d\eta\}_{\eta=0}$. In the important special cases, the appropriate characteristic function is a simple function of the overpotential over the entire range of anodic and cathodic values. The evaluation of the parameters involved is discussed.

Many formulations of the current-potential relation at a hydrogen electrode have been given (1). The complex expressions involve several parameters which are generally evaluated in certain limiting cases. The present study is an attempt to develop graphical methods for treating the potential-current data which will yield values for all of the parameters involved. This attempt has its best success for the electrochemical mechanism. Useful expressions for the combination mechanism are derived, but the evaluation of the parameters is simple only in the limiting cases.

The Elementary Reactions

Although many elementary steps (2) have been suggested as possible contributors to the over-all reaction, the treatment here will be limited to a consideration of only three of these.

Reaction 1: $H_{ad} = H^+ + e^-$

Reaction 2: $H_2(g) = H_{ad} + H^+ + e^-$

Reaction 3: $H_2(g) = 2\,H_{ad}$

Reaction 1 together with reaction 2 will be referred to as the "electrochemical" mechanism, while reaction 1 with reaction 3 will be called the "combination" mechanism.

The relations between current density and overpotential for the elementary steps can be developed by the method of Vetter (3). The rate of the forward (anodic) reaction is written as a positive current density i_+; the reverse, as a negative current density i_-. The net forward rate is then

$$i = i_+ + i_- \qquad [1]$$

The fraction of the surface covered by adsorbed H atoms is denoted by θ, the fraction of vacant surfaces sites by $1-\theta$. The pressure of gaseous H_2 is p, the activity of H^+ ion in the solution a. Symbols with a zero subscript denote the quantity at equilibrium, *i.e.*, at $i = 0$. The Galvani potential difference electrode minus solution is ϵ, expressed in units of RT/F. The overpotential η in the same units is defined by

$$\eta = \epsilon - \epsilon_0 \qquad [2]$$

The sign of ϵ is chosen so that a cathodic current corresponds to a negative overpotential; k is used for rate constants; α is the transfer coefficient for the *oxidation* reaction.

For reaction 1, an adsorbed H atom is required for the forward reaction, and a vacant site for the reverse; consequently[2]

$$i_{1+} = k_1 \theta \exp(\alpha_1 \epsilon) \qquad [3]$$

$$i_{1-} = -k_{-1}(1-\theta)\, a \exp[-(1-\alpha_1)\epsilon] \qquad [4]$$

the net forward (anodic) current density is $i_1 = i_{1+} + i_{1-}$. At equilibrium $i_{1+} = -i_{1-} = i_{10}$, and $\epsilon = \epsilon_0$ so that

$$\exp(\epsilon_0) = (k_{-1}/k_1)\, a_0\, (1-\theta_0)/\theta_0 \qquad [5]$$

a form of the Nernst equation. With the abbreviation

$$K_1 = k_1/k_{-1}$$

$$i_{10} = k_1 K_1^{-\alpha_1} \theta_0^{1-\alpha_1} (1-\theta_0)^{\alpha_1} a_0^{\alpha_1} \qquad [6]$$

The expression for the net current density then becomes

$$i_1 = i_{10}\, e^{\alpha_1 \eta} \{\theta/\theta_0 - [(1-\theta)/(1-\theta_0)]\, (a/a_0)\, e^{-\eta}\} \qquad [7]$$

In reaction 2 a vacant site is required for the forward reaction and adsorbed H atom for the reverse; consequently

$$i_{2+} = k_2 (1-\theta) p \exp(\alpha_2 \epsilon) \qquad [8]$$

$$i_{2-} = -k_{-2}\, \theta\, a \exp[-(1-\alpha_2)\epsilon] \qquad [9]$$

Then the net forward (anodic) current density is $i_2 = i_{2+} + i_{2-}$. At equilibrium $i_{2+} = -i_{2-} = i_{20}$ so that

[1] Regularly at The Catholic University of America, Washington, D. C.

[2] In all that follows, the assumption is implicit that the ionic strength of the solution is high enough so that the effects due to the changes in the structure of the diffuse double layer can be ignored.

$$\exp(\epsilon_0) = (k_{-2}/k_2)(a_0/p_0)\,\theta_0/(1-\theta_0) \quad [10]$$

With the abbreviation $K_2 = k_2/k_{-2}$

$$i_{20} = k_2 K_2^{-\alpha_2}\,\theta_0^{\alpha_2}\,(1-\theta_0)^{1-\alpha_2}\,a_0^{\alpha_2}\,p_0^{1-\alpha_2} \quad [11]$$

This yields for the net current density

$$i_2 = i_{20}\,e^{\alpha_2\eta}\{[(1-\theta)/(1-\theta_0)]\,(p/p_0) - (\theta/\theta_0)\,(a/a_0)\,e^{-\eta}\} \quad [12]$$

For reaction 3, it will be assumed that the rate of adsorption on a dual site is slow in comparison to the rate of dissociation and in comparison to the jumping rate from one site to another (5). Then

$$i_{3+} = k_3\,(1-\theta)^2 p \quad [13]$$

$$i_{3-} = -k_{-3}\,\theta^2 \quad [14]$$

while the net forward (anodic) current density is $i_3 = i_{3+} + i_{3-}$. At equilibrium, $i_{3+} = -i_{3-} = i_{30}$, and, setting $K_3 = k_3/k_{-3}$, we obtain

$$\theta_0/(1-\theta_0) = K_3^{1/2}\,p_0^{1/2} \quad [15]$$

The final expression for the net current density is

$$i_3 = i_{30}\{[(1-\theta)/(1-\theta_0)]^2\,(p/p_0) - (\theta/\theta_0)^2\} \quad [16]$$

Equations [7], [12], and [16] are the fundamental rate equations for the three reactions. The form of the rate laws and the exchange currents is the same as that of Gerischer (4).

For the present, the complication of a concentration polarization of H^+ ion or H_2 gas will be ignored. This is done by setting

$$a/a_0 = 1, \qquad p/p_0 = 1 \quad [17\text{-}18]$$

These qualifications reduce the rate expressions to

$$i_1 = i_{10}\,e^{\alpha_1\eta}\{\theta/\theta_0 - [(1-\theta)/(1-\theta_0)]\,e^{-\eta}\} \quad [19]$$

$$i_2 = i_{20}\,e^{\alpha_2\eta}\,[(1-\theta)/(1-\theta_0) - (\theta/\theta_0)\,e^{-\eta}] \quad [20]$$

$$i_3 = i_{30}\{[(1-\theta)/(1-\theta_0)]^2 - (\theta/\theta_0)^2\} \quad [21]$$

The Electrochemical Mechanism

The electrochemical mechanism consists of reaction 1 followed by reaction 2.

If i is the total current density,

$$i = i_1 + i_2 \quad [22]$$

and, in the steady-state

$$i_1 = i_2 \quad [23]$$

This condition is required if θ is to have a steady value. Equation [23] determines θ as a function of η.

It is convenient to introduce two parameters at this point: i_0, the over-all exchange current, and ρ.

$$i_0 = (di/d\eta)_{\eta=0} \quad [24]$$

$$\rho = \{d \ln [\theta/(1-\theta)]/d\eta\}_{\eta=0} \quad [25]$$

Both i_0 and ρ can be evaluated in terms of i_{10} and i_{20} by differentiating Eq. [22] and [23]. We thus obtain

$$1/i_0 = \left(\frac{1}{4}\right)\left(1/i_{10} + 1/i_{20}\right) \quad [26]$$

$$\rho/i_0 = \left(\frac{1}{4}\right)\left(1/i_{10} - 1/i_{20}\right) \quad [27]$$

The parameter ρ ranges in value between -1 and $+1$, depending on the relative magnitudes of i_{10} and i_{20}. If $i_{10} >> i_{20}$, slow electrochemical desorption, $\rho = -1$; if $i_{10} << i_{20}$, slow primary discharge, $\rho = +1$. If the exchange current for the two elementary steps have the same value, $\rho = 0$.

Inversion of Eq. [26] and [27] yields

$$i_{10} = i_0/2(1+\rho) \quad [28]$$

$$i_{20} = i_0/2(1-\rho) \quad [29]$$

Using Eq. [28] and [29] in Eq. [23] and solving for θ, we obtain

$$\frac{\theta}{\theta_0} = \frac{(1-\rho)\,e^{\alpha_1\eta} + (1+\rho)\,e^{\alpha_2\eta} - [(1-\rho)\,e^{\alpha_1\eta} - (1+\rho)\,e^{\alpha_2\eta}]\tanh\frac{1}{2}\eta}{(1-\rho)\,e^{\alpha_1\eta} + (1+\rho)\,e^{\alpha_2\eta} - (2\theta_0-1)\,[(1-\rho)\,e^{\alpha_1\eta} - (1+\rho)\,e^{\alpha_2\eta}]\tanh\frac{1}{2}\eta} \quad [30]$$

Substitution of Eq. [30] in Eq. [22] yields for the current density i

$$i^{-1} = \frac{e^{\frac{1}{2}\eta}}{4\,i_0}\left\{\frac{(1+\rho)\,e^{-\alpha_1\eta} + (1-\rho)\,e^{-\alpha_2\eta}}{\sinh\frac{1}{2}\eta} + \frac{(2\theta_0-1)\,[(1+\rho)\,e^{-\alpha_1\eta} - (1-\rho)\,e^{-\alpha_2\eta}]}{\cosh\frac{1}{2}\eta}\right\} \quad [31]$$

If we set $\theta_0 = 0$ in Eq. [31], the equation is equivalent to that of Vetter (6); Vetter's derivation does not consider explicitly the effect of saturation of the surface on the activity of the adsorbed hydrogen atoms. In a later publication (7), Vetter considers the effect of saturation of the surface for the case, $i_{10} >> i_{20}$, and includes the effect of slow adsorption and desorption of molecular hydrogen.

The graphical determination of the various parameters in Eq. [31] is difficult, if not impossible, without some simplifying assumption. We shall assume that $\alpha_1 = \alpha_2 = \alpha$. This reduces Eq. [30] and [31] to

$$\frac{\theta}{\theta_0} = \frac{1 + \rho\tanh\frac{1}{2}\eta}{1 + (2\theta_0-1)\,\rho\tanh\frac{1}{2}\eta} \quad [32]$$

$$i^{-1} = (2i_0)^{-1}\,e^{-(\alpha-1/2)\eta}\left[1/\sinh\frac{1}{2}\eta + (2\theta_0-1)\,\rho/\cosh\frac{1}{2}\eta\right] \quad [33]$$

A characteristic function g_1 is defined:

$$g_1 = \left[e^{(\alpha-1/2)\eta}\sinh\frac{1}{2}\eta\right] \Big/ i \quad [34]$$

Using Eq. [34] in Eq. [33] we obtain

$$g_1 = (2i_0)^{-1}\left[1 + (2\theta_0 - 1)\,\rho \tanh\frac{1}{2}\eta\right] \quad [35]$$

Equation [35] is a convenient form of the current-potential relation which is advantageous in that it is correct over the anodic and cathodic ranges of potential values. Provided only that the value of α be known, the characteristic function can be plotted against $\tanh\frac{1}{2}\eta$ to determine the exchange current and the parameter $(2\theta_0 - 1)\,\rho$. An additional advantage of the characteristic function is that it is always positive since negative currents correspond to negative overpotentials and thus negative values of $\sinh\frac{1}{2}\eta$. The fact that $\tanh\frac{1}{2}\eta$ is limited to values between -1 and $+1$ as η varies between $-\infty$ and $+\infty$ enables the line to be extrapolated to the limiting values for infinite overpotential, g_∞ and $g_{-\infty}$. These limiting values will be of interest later. It is interesting to notice that the function g_1 is antisymmetric in the overpotential about the value $1/2i_0$. A definite disadvantage in using g_1 is that it is a deviation function: the principal variation of i is represented by $\sinh\frac{1}{2}\eta$; consequently, as techniques develop to yield more precise data, the utility of equations such as [35] should increase.

Determination of the Parameters

α: The parameter α may be determined in either of two ways. Inspection of Eq. [6], [11], and [26] shows that i_0 is proportional to $a_{e^-}^{\alpha}$. Consequently if i_0 is determined at various values of pH through a plot of i *vs.* η at low overpotentials, then α may be gotten by the relation

$$(\partial \log i_0/\partial\ \mathrm{pH})_{p_0} = -\alpha \quad [36]$$

Another method for determining α depends on the fact that ρ is independent of pH; *cf.* Eq. [6], [11], and [27]. Consequently, at constant η, i depends on pH only through i_0; hence the relation

$$(\partial \log |\,i\,|/\partial\ \mathrm{pH})_{\eta,p_0} = -\alpha \quad [37]$$

The slope of a plot of $\log |\,i\,|$ at a given overpotential *vs.* pH is equal to $-\alpha$. An equivalent method for determining α has been used frequently by Gerischer (4, 8).

Having determined α by one of these methods it is now possible to plot the characteristic function g_1 against $\tanh\frac{1}{2}\eta$ to determine the intercept, $1/2i_0$, and the slope, $(2\theta_0 - 1)\,\rho/2i_0$. These serve to determine a value of $\rho(2\theta_0 - 1)$. The surface coverage at equilibrium θ_0 can be gotten only if i_0 and $\rho(2\theta_0 - 1)$ are measured at several different hydrogen pressures.

The equilibrium Galvani potential difference between electrode and solution is given by Eq. [5] or [10]. Since both reactions 1 and 2 are taking place on the surface, setting the ϵ_0's equal in these two equations the adsorption isotherm is obtained:

$$\theta_0/(1-\theta_0) = (K_2/K_1)^{1/2}\,p_0^{1/2} \quad [38]$$

Comparison of Eq. [38] with Eq. [15] shows that $K_3 = K_2/K_1$. To simplify, we define

$$K = K_3^{1/2} = (K_2/K_1)^{1/2} \quad [39]$$

By the use of Eq. [26], [27], [38], [6], and [11], the measured quantities can be written explicitly as functions of p_0

$$(2i_0)^{-1}\,[1 + (2\theta_0 - 1)\,\rho]\,p_0^{-\alpha/2} = I + S/p_0 \quad [40]$$

$$(2i_0)^{-1}\,[1 - (2\theta_0 - 1)\,\rho] = (I/K + KS)\,p_0^{(\alpha-1)/2} \quad [40a]$$

in which

$$I = (1/4k_1)\,(K_1K/a_0)^{\alpha} \quad [41]$$

$$S = k_1 I/k_2 \quad [42]$$

A plot of the function on the left of Eq. [40] *vs.* $1/p_0$ yields values of I and S. A plot of the function on the left of Eq. [40a] *vs.* $p_0^{(\alpha-1)/2}$ yields a value of $I/K + KS$. From this information K may be calculated then θ_0 may be calculated at any pressure through Eq. [38]. Once θ_0 is determined, ρ may be calculated from the slope of the plot of Eq. [35]. Knowing ρ and i_0, the individual values i_{1_0} and i_{2_0} can be gotten from Eq. [28] and [29]. If desired, the rate constants k_1 and k_2 can then be calculated from Eq. [6] and [11].

The preceding treatment allows the evaluation of all of the parameters of the electrochemical mechanism in a systematic way and is subject to the one restriction that $\alpha_1 = \alpha_2$. For a complete treatment, the current density-overpotential measurements must be made over a range of pH and of pressure.

One additional feature is important in the electrochemical mechanism. Consider the surface coverage as a function of overpotential as expressed by Eq. [32]. If electrochemical discharge (reaction 2) is slow, $\rho = -1$. Then as $\eta \to +\infty$, $\theta \to 0$; and as $\eta \to -\infty$, $\theta \to 1$. That is to say that anodic polarization depletes the surface and cathodic polarization covers the surface with adsorbed hydrogen. On the other hand, if the electrochemical discharge is extremely rapid compared to the rate of primary discharge, $\rho = +1$. Then Eq. [32] predicts that as $\eta \to +\infty$, $\theta \to 1$; and as $\eta \to -\infty$, $\theta \to 0$. In this situation cathodic polarization denudes the surface of adsorbed hydrogen atoms while anodic polarization covers the surface. Consideration of the two elementary reactions shows that this makes good physical sense.

The Combination Mechanism

Reaction 1 together with reaction 3 constitutes the combination mechanism. The steady-state conditions are

$$i = i_1, \qquad i_1 = i_3 \quad [43\text{-}44]$$

The parameters i_0 and ρ, defined by Eq. [24] and [25], can be evaluated for this mechanism by differentiating Eq. [43] and [44] with the help of Eq. [19] and [21]. By this procedure

$$1/i_0 = 1/i_{1_0} + 1/2i_{2_0} \quad [45]$$

$$\rho/i_0 = -1/2i_{2_0} \quad [46]$$

Inversion of Eq. [45] and [46] yields

$$i_{10} = i_0/(1+\rho) \qquad [47]$$

$$i_{20} = -i_0/2\rho \qquad [48]$$

For this mechanism, ρ is restricted to the range, -1 to 0. When $\rho = 0$, $i_{20} >> 1 >> i_{10}$; this corresponds to slow primary discharge. When $\rho = -1$, $i_{10} >> 2i_{20}$; this corresponds to slow atom combination.

From Eq. [47] and [48], Eq. [43] and [44] can be written explicitly

$$(1+\rho)(i/i_0)\, e^{-\eta} = \theta/\theta_0 - [(1-\theta)/(1-\theta_0)]\, e^{-\eta} \qquad [49]$$

$$-i/i_0 = (1/2\rho)\,\{[(1-\theta)/(1-\theta_0)]^2 - (\theta/\theta_0)^2\} \qquad [50]$$

Elimination of i between Eq. [49] and [50] yields an implicit relation between θ and η; since θ occurs quadratically it is simpler to proceed in an alternate way. Equation [49] is solved for θ

$$\theta/\theta_0 = 1 - \frac{(1-\theta_0)\left\{2\sinh\frac{1}{2}\eta - (1+\rho)(i/i_0)\, e^{-(\alpha-1/2)\eta}\right\}}{\cosh\frac{1}{2}\eta + (1-2\theta_0)\sinh\frac{1}{2}\eta} \qquad [51]$$

Using Eq. [50] and [51] we obtain

$$\left[(2\theta_0-1)(1+\rho)(i/i_0)\, e^{-(\alpha-1/2)\eta} - 2\cosh\frac{1}{2}\eta\right] \cdot \left[(1+\rho)(i/i_0)\, e^{-(\alpha-1/2)\eta} - 2\sinh\frac{1}{2}\eta\right] = -2\rho\,(i/i_0)\left[\cosh\frac{1}{2}\eta + (1-2\theta_0)\sinh\frac{1}{2}\eta\right]^2 \qquad [52]$$

Equation [52] is convenient in that it allows the equations for the special cases to be derived easily. Case I. $\rho = 0$; slow primary discharge; $i_0 \simeq i_{10}$

Setting $\rho = 0$ in Eq. [52] requires that the second factor on the left side be zero. (It is clear that the first factor is zero only in very exceptional circumstances.) We obtain for this case then

$$g_1 = 1/2i_0 \qquad [53]$$

The characteristic function g_1 appears again. For this case, g_1 is a constant; the parameters α and i_0 may be evaluated by the same methods as in the electrochemical case. The $i - \eta$ relation is independent of θ_0 except insofar as i_0 depends on θ_0. For the pressure dependence of i_0, Eq. [6] and [15] yield

$$p_0^{(1-\alpha)/2}/i_0 = (1/k_1)K_1^{\alpha}K^{\alpha-1}a_0^{-\alpha}(1 + Kp_0^{1/2}) \qquad [54]$$

From the plot of the left side of Eq. [54] against $p_0^{1/2}$, the value of K is obtained and so the value of θ_0.

Case II. $\rho = -1$; slow atom combination; $i_0 \simeq 2i_{20}$

Setting $\rho = -1$ in Eq. [52] permits it to be arranged in the form

$$g_2 = (2i_0)^{-1/2}\left[1 + (1-2\theta_0)\tanh\frac{1}{2}\eta\right] \qquad [55]$$

where g_2 is a second characteristic function defined by

$$g_2 = \left[\left(\tanh\frac{1}{2}\eta\right)\Big/\, i\right]^{1/2} \qquad [56]$$

a plot of g_2 *vs.* $\tanh\frac{1}{2}\eta$ should be linear; from the slope and intercept θ_0 can be gotten immediately.

The pressure dependence of i_0 in this case is deduced from Eq. [14] and [15]

$$(2i_0)^{-1/2} = (2k_{-2})^{-1/2}(1 + K/p_0^{1/2}) \qquad [57]$$

Equation [57] permits the evaluation of k_{-2} and a confirming value of θ_0 through the value of K.

Case III. $\theta_0 = \frac{1}{2}$; an accidental case.

If it should happen that $\theta_0 = \frac{1}{2}$, then Eq. [52] takes the form

$$g_1 = (2i_0)^{-1}(1 + \rho - \rho e^{(\alpha-1/2)\eta}\cosh\frac{1}{2}\eta \qquad [58]$$

When $\rho = 0$, Eq. [58] reduces to Eq. [53] as it must. When $\rho = -1$, Eq. [58] becomes

$$g_2 = (2i_0)^{-1/2} \qquad [59]$$

Equation [59] is equivalent to Eq. [55] when $\theta_0 = \frac{1}{2}$.

General Evaluation of Parameters for the Combination Mechanism

Equation [52] does not lend itself readily to the evaluation of the parameters if i_{10} and i_{20} have comparable values. The combination mechanism predicts limiting cathodic and anodic currents i_c and i_a given from Eq. [13] and [14] by

$$i_c = -i_{20}/\theta_0^2 = -k_{-2} \qquad [60]$$

$$i_a = i_{20}/(1-\theta_0)^2 = k_2 p_0 \qquad [61]$$

A measurement of i_a as a function of pressure yields a value of k_2; measurement of i_c yields k_{-2}. The equilibrium coverage θ_0 may then be calculated using Eq. [15]. The parameter ρ may be gotten from the equation

$$\rho = i_0/2i_L\,(2\theta_0 - 1) \qquad [62]$$

which follows from Eq. [14], [45], [46], [60], and [61] and in which

$$1/i_L = 1/i_a + 1/i_c \qquad [63]$$

Then i_{20} can be gotten from Eq. [45] since i_0 is known from the slope of the i *vs.* η curve at low current densities. Finally, α is gotten as the slope of a plot of log i_{10} *vs.* pH; see Eq. [6]. All of this presupposes that diffusion currents of H^+ or H_2 are not limiting; this is a severe restriction

Effect of Limiting Diffusion Currents in Special Cases

It frequently happens that the diffusion current densities are small enough to be rate determining. The inclusion of such effects complicates the treatment somewhat; however, in special cases the final expressions in terms of the characteristic functions are simple.

The diffusion processes can be written as Reactions 4 and 5.

Reaction 4: $H^+(\text{surface}) \rightarrow H^+(\text{bulk})$

Reaction 5: $H_2(\text{bulk}) \rightarrow H_2(\text{surface})$

The rates of these reactions are

$$i_4 = i_{40}\,(a/a_0 - 1) \qquad [64]$$

$$i_5 = i_{50}\,(1 - p/p_0) \qquad [65]$$

In Eq. [65] the ratio of concentrations of H_2 at the surface and in the bulk of the solution has been replaced by a pressure ratio. The parameters i_{40} and i_{50} are given by

$$i_{40} = \mathbf{F} D_{H^+}\, a_0/\delta_{H^+} \qquad [66]$$

$$i_{50} = 2\mathbf{F} D_{H_2}\, C_{0H_2}/\delta_{H_2} \qquad [67]$$

in which D's are diffusion coefficients and δ's appropriate thicknesses of the Nernst diffusion layers; C_{0H_2} is the concentration of H_2 (moles/cc) in the bulk of the solution which is in equilibrium with H_2 gas at pressure p_0.

Case I. Slow discharge with a limiting ionic diffusion current.

In this case we assume that atom combination and diffusion of H_2 from the surface is very fast. Then $\theta/\theta_0 = 1$ and $p/p_0 = 1$. The steady-state conditions are $i = i_3$ and $i_3 = i_4$ or

$$i = i_{30}\, e^{\alpha\eta}\,[1 - (a/a_0)\, e^{-\eta}] \qquad [68]$$

$$i = i_{40}\,(a/a_0 - 1) \qquad [69]$$

Eliminating a/a_0 from Eq. [68] and [69] we obtain for g_1

$$g_1 = 1/2i_{30} + (1/2i_{40})\, e^{(\alpha-1)\eta} \qquad [70]$$

If α is known, a plot of g_1 *vs.* $e^{(\alpha-1)\eta}$ yields values of i_{30} and i_{40}. α can be determined by using Eq. [37] at low values of η before the diffusion limit exerts its effect.

Case II. Slow atom combination with a limiting molecular diffusion current.

In this case, if primary discharge and ionic diffusion are very fast we have $a/a_0 = 1$ and $\theta/(1-\theta) = \theta_0\, e^{-\eta}/(1-\theta_0)$. Then in the steady state

$$i = i_{30}\,\{[(1-\theta)^2/(1-\theta_0)^2]\,(p/p_0) - (\theta/\theta_0)^2\} \qquad [71]$$

and

$$i = i_{50}\,(1 - p/p_0) \qquad [72]$$

Elimination of θ and p/p_0 from these equations yields ultimately

$$g_2 = \left(\frac{1}{2}\right)\left\{\left[1 + (1-2\theta_0)\tanh\frac{1}{2}\eta\right]^2 \Big/ i_{30} + \left[1 + \tanh\frac{1}{2}\eta\right]^2 i_{50}\Big/\right\}^{1/2} \qquad [73]$$

If $i_{30} >> i_{50}$, Eq. [73] reduces to Eq.[55] as it must. However if $i_{30} << i_{50}$, Eq. [73] becomes

$$g_2 = (2i_{50})^{-1/2}\,(1 + \tanh\frac{1}{2}\eta) \qquad [74]$$

In this situation also, g_2 is a linear function of $\tanh\frac{1}{2}\eta$. The limiting cathodic and anodic currents predicted by Eq. [73] are gotten by setting $\tanh\frac{1}{2}\eta$ equal to -1 and $+1$, respectively. Thus

$$1/i_c = -\theta_0^2/i_{30} \qquad [75]$$

$$1/i_a = (1-\theta_0)^2/i_{30} + 1/i_{50} \qquad [76]$$

The effect of the slow diffusion is entirely on the anodic current. If the limiting diffusion current is very small then $i_{50} << i_{30}$ and by Eq. [76], $i_a = i_{50}$. In this situation, no conclusion about surface coverage can be drawn from a measurement of the limiting anodic current.

Coupling of Reactions 3 and 2

Another two-step mechanism is possible. Suppose that the reverse of reaction 3 occurs, followed by reaction 2. The current density is then $i = i_2$ and the steady-state condition is $i_2 = -i_3$. Following the same procedure as for the combination mechanism we find $1/i_c = 1/i_{30} + 2i_{50}$, $\rho/i_c = 1/2i_{50}$. The values of ρ lie between zero and unity. When reaction 2 is slow, $\rho = 0$; when reaction 3 is slow, $\rho = 1$. The final $i - \eta$ relation is

$$\left[(2\theta_0 - 1)(1-\rho)(i/i_c)\, e^{-(\alpha-1/2)\eta} + 2\cosh\frac{1}{2}\eta\right] \times \left[(1-\rho)(i/i_c)\, e^{-(\alpha-1/2)\eta} - 2\sinh\frac{1}{2}\eta\right] = -2\rho\,(i/i_c)\left[\cosh\frac{1}{2}\eta + (2\theta_0 - 1)\sinh\frac{1}{2}\eta\right]^2 \qquad [77]$$

Case I: $\rho = 0$

Equation [77] becomes

$$g_1 = 1/2i_c \qquad [78]$$

Equation [78] differs from Eq. [53] only in the pressure dependence of i_c.

Case II: $\rho = 1$

Equation [78] becomes

$$g_2 = (2i_c)^{-1/2}\left[1 + (2\theta_0 - 1)\tanh\frac{1}{2}\eta\right] \qquad [79]$$

This case is similar to that involving rapid primary discharge and slow combination; however, the sign of the second term on the right is different.

Logarithmic Isotherm

The foregoing discussion has been based on the Langmuir isotherm. However, it may be shown that if the isotherm is of the logarithmic type, *e.g.* $[\theta/(1-\theta)]\,\exp\,[w(1-2\theta)/RT] = (Kp)^{1/2}$, the characteristic functions are still "natural" functions for the representation of the data. The characteristic functions are not linear functions of $\tanh\frac{1}{2}\eta$ but have the form $g_1 = (2i_c)^{-1}\left[1 + A_1\tanh\frac{1}{2}\eta + A_2\tanh^2\frac{1}{2}\eta + \ldots.\right]$ or $g_2 = (2i_c)^{-1/2}\left[1 + B_1\tanh\frac{1}{2}\eta + B_2\tanh^2\frac{1}{2}\eta + \ldots.\right]$ Even in this logarithmic case the coefficients A_1 and B_1 are the same as for the Langmuir isotherm. The difference lies in the coefficients of the higher terms. Details of this situation will be discussed in the next paper (9).

Table I

Mechanism	i-η Relationship	Restrictions
Electrochemical:		
Case I: General	$g_1 = (2i_o)^{-1}\left[1 + (2\theta_o - 1)\rho \tanh \frac{1}{2}\eta\right]$	$\alpha_1 = \alpha_2$
Case II: $\rho = 1$	$g_1 = (2i_o)^{-1}\left[1 + (2\theta_o - 1) \tanh \frac{1}{2}\eta\right]$	Slow primary discharge
Case III: $\rho = -1$	$g_1 = (2i_o)^{-1}\left[1 - (2\theta_o - 1) \tanh \frac{1}{2}\eta\right]$	Slow electrochemical desorption
Combination:		
Case I: $\rho = 0$	$g_1 = \frac{1}{2}i_o$	Slow primary discharge
Case II: $\rho = -1$	$g_2 = (2i_o)^{-1/2}\left[1 + (1 - 2\theta_o) \tanh \frac{1}{2}\eta\right]$	Slow combination
Electrochemical Discharge and Combination:		
Case I: $\rho = 0$	$g_1 = \frac{1}{2}i_o$	Slow electrochemical discharge
Case II: $\rho = 1$	$g_2 = (2i_o)^{-1/2}\left[1 + (2\theta_o - 1) \tanh \frac{1}{2}\eta\right]$	Slow combination

Summary

The equations for the various mechanisms are summarized in Table I.

Acknowledgment

The author wishes to express his thanks to Dr. J. C. White for his advice and encouragement and to Sigmund Schuldiner for many stimulating discussions.

Manuscript received Jan. 4, 1960; revised manuscript received Aug. 23, 1960.

Any discussion of this paper will appear in a Discussion Section to be published in the December 1961 JOURNAL.

REFERENCES

1. J. O'M. Bockris and E. C. Potter, *This Journal*, **99**, 169 (1952); R. Parson, *Trans. Faraday Soc.*, **47**, 1332 (1951); P. van Rysselberghe, *J. Chem. Phys.*, **17**, 1226 (1949); **20**, 1522, (1952); K. J. Vetter, *Z. Elektrochem.*, **59**, 435 (1955).
2. Parsons, *loc. cit.*
3. Vetter, *loc. cit.*
4. H. Gerischer, *Z. Elektrochem.*, **55**, 98 (1951); H. Gerischer, *Z. physik. Chem.*, **202**, 292 (1953).
5. S. Glasstone, K. J. Laidler, and H. Eyring, "The Theory of Rate Processes," pp. 356ff, McGraw-Hill Book Co., Inc., New York (1941).
6. K. J. Vetter, *Z. Elektrochem.*, **59**, 435 (1955).
7. K. J. Vetter, *ibid.*, **60**, 1072 (1956).
8. H. Gerischer, *Z. physik. Chem.*, **202**, 302 (1953); *Z Elecktrochem.*, **57**, 604 (1953).
9. G. W. Castellan, *This Journal*, **108**, 282 (1961).

Characteristic Functions and Parameters in the Theory of Hydrogen Overpotential

II. Interpretation of Some Measurements of Hydrogen Overpotential on Palladium

Gilbert W. Castellan[1]

U. S. Naval Research Laboratory, Washington, D. C.

ABSTRACT

The hydrogen overpotential measurements of Hoare and Schuldiner on β-palladium in acid solutions can be interpreted quantitatively in terms of slow primary discharge of H_3O^+ and very rapid atom combination. In solutions in the pH range 1.5-1.8 the mechanism is influenced by a limiting diffusion current of H_3O^+.

An extensive series of measurements of the hydrogen overpotential on palladium has been made by Hoare and Schuldiner (1). These investigators have interpreted the mechanism from the slopes of the Tafel plots and conclude that in solutions of low pH, electrochemical discharge $H_{ad} + H^+ + e^- \rightarrow H_2$ is rate-determining, while at a somewhat higher pH (≈ 1.8), atom recombination $2H_{ad} \rightarrow H_2$ is rate-determining. These investigations exhibit several puzzling features. The first is the observation of a linear region in the Tafel plot at overpotentials of 15-25 mv; these values are well below the values where one would expect linearity in the Tafel plot on the basis of theory. Second, these investigators

[1] Regularly at The Catholic University of America, Washington, D. C.

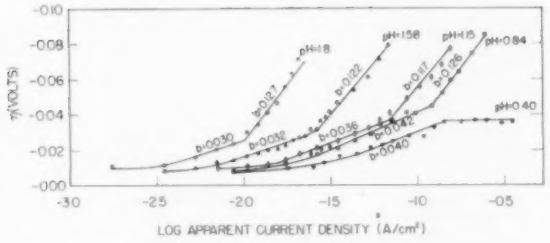

Fig. 1. η vs. log (—i) for hydrogen evolution on palladium. [after Hoare and Schuldiner (1)]

find a linear relation between i_o, the exchange current density, and pH, while electrochemical theory requires a linear relation between log i_o and pH. Third, they observed a potential plateau in the Tafel plot at pH = 0.40, with overpotential independent of current density. In view of these unusual observations, it seems appropriate to look at these measurements from a more careful theoretical point of view.

Selection of the Rate Equation

Figure 1 shows the Tafel plot for the hydrogen-evolution reaction on palladium given by Hoare and Schuldiner (1). The marked dependence of the curves on pH eliminates the possibility of the combination reaction being the principal rate-determining reaction. This leaves two major possibilities: Mechanism 1

$$H^+ + e^- \rightarrow H, \qquad H + H^+ + e^- \rightarrow H_2$$

Mechanism 2

$$H^+ + e^- \xrightarrow{\text{slow}} H, \qquad H + H \xrightarrow{\text{fast}} H_2$$

It has been shown that the rate laws for these two mechanisms can be written (2) for mechanism 1

$$g_1 = (2i_o)^{-1}\left[1 + (2\theta_o - 1)\rho \tanh \frac{1}{2}\eta\right] \qquad [1]$$

and, for mechanism 2

$$g_1 = 1/2i_o \qquad [2]$$

In these equations, η is a dimensionless overpotential in units of RT/F; i_o the exchange current density $= (di/d\eta)_{\eta=0}$; ρ is a characteristic parameter $\rho = \{d \ln [\theta/(1-\theta)]/d\eta\}_{\eta=0}$; θ_o is the fraction of the surface covered by H atoms at equilibrium and g_1 is defined

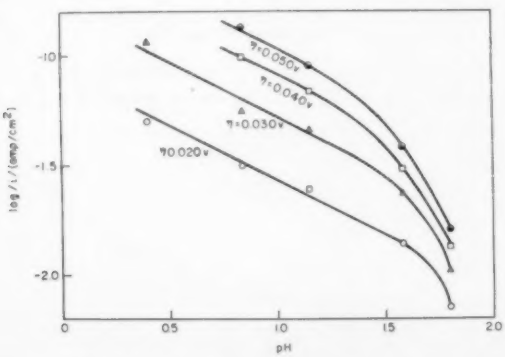

Fig. 2. log |i| vs. pH at constant overvoltage

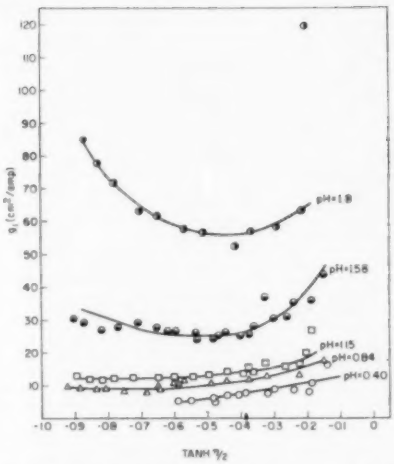

Fig. 3. g_1 vs. tanh(η/2) at various values of pH

as equal to $i^{-1} \sinh\left(\frac{1}{2}\eta\right) \exp\left[\left(\alpha - \frac{1}{2}\right)\eta\right]$. In either case, α is determined by the equation

$$-\alpha = (\partial \log i/\partial \mathrm{pH})_\eta \qquad [3]$$

Figure 2 shows a plot of log |i| *vs.* pH at η = 0.020, 0.030, 0.040 and 0.050 v. The best line of slope equal to −0.5 has been fitted to the points at low pH. It is clear that this choice of α does no damage to the data except at the two highest values of pH. Thus in a preliminary way we choose $\alpha = 0.5$ and write Eq. [1] and [2] as

$$g_1 = i^{-1} \sinh\left(\frac{1}{2}\eta\right) = (2i_o)^{-1}\left[1 + (2\theta_o - 1)\rho \tanh \frac{1}{2}\eta\right] \qquad [3]$$

and

$$g_1 = i^{-1} \sinh \frac{1}{2}\eta = 1/2i_o \qquad [4]$$

First Fit of the Data

Figure 3 shows a plot of the characteristic function g_1 *vs.* $\tanh \frac{1}{2}\eta$ for several values of pH. At the three lowest pH values, the points at overpotentials more negative than −20 mv seem to lie on a horizontal line. (The arrow on the horizontal axis marks the 20 mv value.) At overpotentials more positive than −20 mv the curve has an upward tilt, which is more pronounced the higher the pH. A number of attempts were made to fit the points in the overpotential range from 0 to −20 mv into a consistent theoretical scheme. These attempts failed and so, in what follows, these points are ignored. Further justification for this decision lies in the fact that the i *vs.* η plots of the points in this range, where the $i - \eta$ relation should be linear, do not go through the origin as they should (1).

In Fig. 3 the curves at pH = 1.58 and 1.8 show an upward inclination at large negative values of overpotential. This behavior suggests the influence of a limiting diffusion current of H_3O^+ ions.

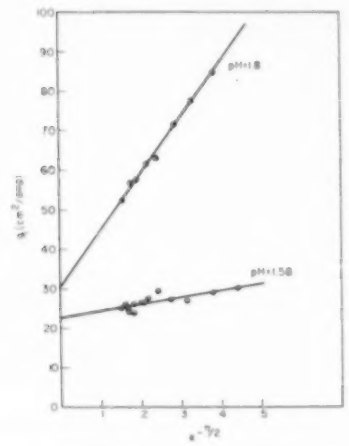

Fig. 4. g_1 vs. $\exp(-\eta/2)$ at pH = 1.58 and 1.8

Having discarded the points above −20 mv, the characteristic function appears to be reasonably constant, hence Eq. [4] is appropriate. Equation [4] is the rate law for slow primary discharge coupled with rapid combination of H atoms. For the higher pH values, a limiting current of H^+ ions together with slow primary discharge yields the rate law (2)

$$g_1 = i^{-1} \sinh \frac{1}{2}\eta = (2i_o)^{-1} + (2i_L)^{-1} \exp\left(-\frac{1}{2}\eta\right) \qquad [5]$$

where i_L is the limiting diffusion current

$$i_L = \mathbf{F}\, D_{H^+}\, a_o/\delta \qquad [6]$$

and D_{H^+} is the diffusion coefficient of H^+ ion, a_o the activity of H^+ ions in the bulk of the solution, and δ the thickness of the Nernst diffusion layer.

Figure 4 is a plot of g_1 against $e^{-\eta/2}$ for the data at pH = 1.58 and 1.8. The linearity is reasonably good. A least-squares fit of the points yields values of $1/2i_o$ and $1/2i_L$ corresponding to the values of i_o and i_L given in Table I.

The values of i_L in the last column are calculated from Eq. [6] using $D_{H^+} = 9.6 \times 10^{-5}$ cm²/sec and assuming that $\delta = 0.005$ cm. The values of i_L obtained from the plots agree reasonably well with these calculated values.

Table I. Constants of the g_1 Eq. [5] from Fig. 4

pH	i_o (amp-cm^{-2})	i_L (amp-cm^{-2})	i_L (amp-cm^{-2}) From Eq. [6]
1.58	2.210×10^{-2}	0.286	0.525
1.80	1.638×10^{-2}	0.0350	0.0316

Table II. Exchange current densities from Eq. [4] or [5]

pH	$i_o \times 10^2$ (amp/cm²)
0.40	8.515
0.84	5.375
1.15	4.005
1.58	2.210
1.80	1.638

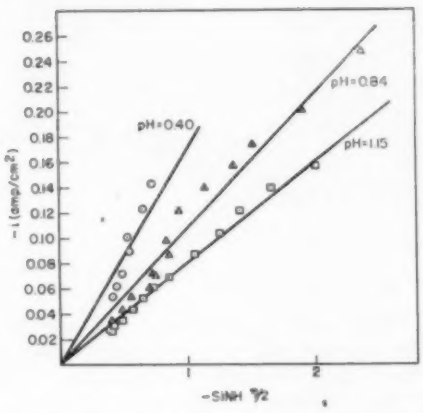

Fig. 5. —i vs. —sinh(η/2) at pH = 0.40, 0.84, 1.15

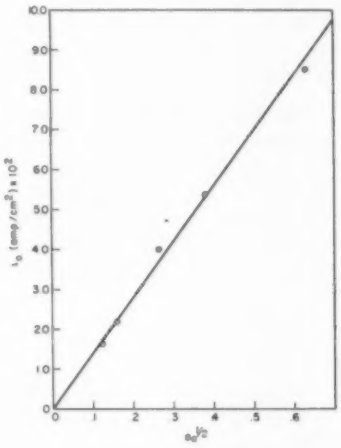

Fig. 6. i_o vs. $a_o^{1/2}$

The data at the lawer pH are now fitted to Eq. [4] (data between 0 and −20 mv being again excluded from the least-squares treatment). The values of i_o obtained by this method are shown in Table II, together with the values at the higher pH's from Table I. The curves of Eq. [4] are shown in Fig. 5.

Final Fit of Data

A plot of the values of i_o *vs.* $a_o^{1/2}$ should be linear since $\alpha = \frac{1}{2}$. This plot is shown in Fig. 6. The linearity is very good, the slope being 0.1390 with a probable error of 0.0041. The exchange current is then written

$$i_o = 0.139\, a_o^{1/2} \text{ amp/cm}^2 \qquad [7]$$

The Tafel plots are now constructed using the value of i_o from Eq. [7] and using either Eq. [5] or

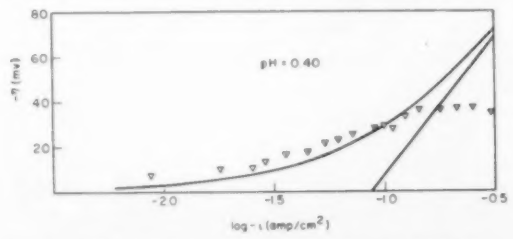

Fig. 7 a-d. Tafel plots at the various values of pH

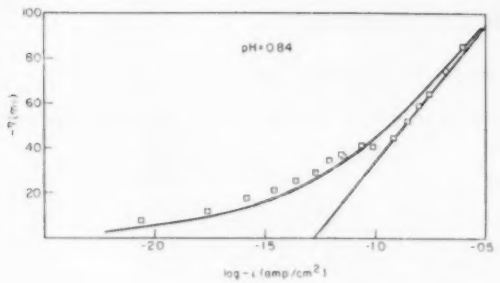

Fig. 7b

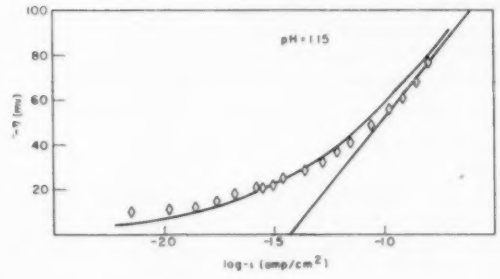

Fig. 7c

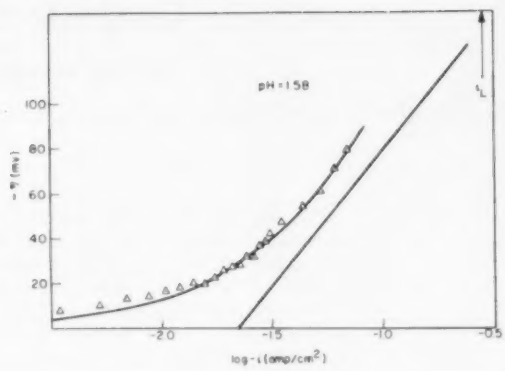

Fig. 7d

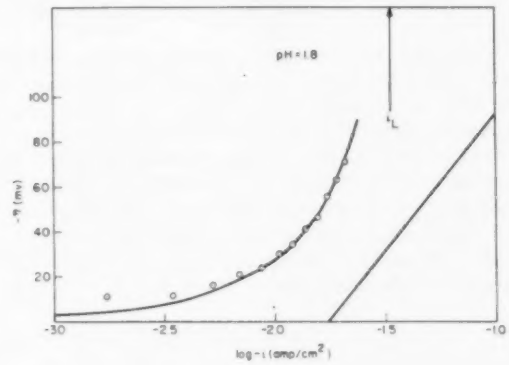

Fig. 7e

[4] to calculate i from η. These plots are shown in Fig. 7a, b, c, d, e. In all these figures, the curve is the calculated curve, the straight line is the corresponding Tafel line. The value of the limiting current is indicated by the arrow in Fig. 7d and 7e.

The final fit of the curves is generally good except for pH = 0.40 where the curious plateau appears. No explanation is offered here for this plateau. The points in the range 0 to −20 mv do not fit particularly well. It may be that the electrode was not truly in a steady-state at these low c. d.'s. The curves were traversed several times with increasing and decreasing c. d.'s. It may be that the electrode surface stored extra hydrogen at the high c. d. and gave it up slowly as the current density was lowered. This would account for the overpotential being more negative than would be expected at the low current densities.

Conclusion

The overpotential data obtained by Schuldiner and Hoare on β-palladium-hydrogen in acid solution can be interpreted satisfactorily in terms of slow primary discharge of hydronium ion. The exchange current is given by Eq. [7]. At pH's of 1.58 and 1.80 the kinetics are influenced by the diffusion of hydronium ion to the surface of the electrode. There appears to be no justification for assuming that water is discharged under the conditions of these experiments, nor that the electrochemical reaction is slow.

Acknowledgment

The author wishes to express his thanks to Mr. Sigmund Schuldiner of the U. S. Naval Research Laboratory for his kindness in lending his original data and figures for the present theoretical study.

Manuscript received Jan. 4, 1960; revised manuscript received Aug. 23, 1960.

Any discussion of this paper will appear in a Discussion Section to be published in the December 1961 JOURNAL.

REFERENCES

1. J. P. Hoare and S. Schuldiner, *This Journal*, **102**, 485 (1955).
2. G. W. Castellan, *ibid.*, **108**, 277 (1961).

Conductivities in Emulsions

Robert E. Meredith[1] **and Charles W. Tobias**

Lawrence Radiation Laboratory and Department of Chemical Engineering, University of California, Berkeley, California

ABSTRACT

The dependence of the conductivity of water-propylenecarbonate emulsions on volume fraction f of the dispersed phase, on the conductivities of the continuous phase k_c, and of the discontinuous phase k_d, has been measured in the ranges of $0 < f < 0.5$ and $0.172 < k_d/k_c < 101$. The results indicate that when $f > 0.2$ neither Maxwell's equation nor Bruggemann's approximation represents the behavior of data satisfactorily. In an attempt to take into account the interaction of fields around particles of the dispersed phase, a simple approximation is proposed, based on Maxwell's equation. In the range of conductivities investigated in the present study the new equation represents the conductivity of emulsions with reasonable accuracy.

Numerous experimental and theoretical studies have been conducted in the past concerning the problem of evaluating the effective conductivities of dispersions. The classical solution for the dependence of the effective conductivity k_m of a dispersion which consists of a continuous phase of conductivity k_c, a dispersed phase of conductivity k_d, and a dispersed phase volume fraction f, has been derived by Lorentz (1), Lorenz (2), and Maxwell (3). This solution,

$$K_m = \frac{K_d + 2 - 2f(1 - K_d)}{K_d + 2 + f(1 - K_d)} \qquad [1]$$

where $K_m = k_m/k_c$ and $K_d = k_d/k_c$ is valid only for the case where the dispersed phase exists in the form of spherical particles. Equation [1] is further restricted to the requirement that the distance between spheres must be large compared to their diameter.

A more general solution has been developed by Fricke (4), who obtained

$$K_m = 1 - \frac{f(K_m - K_d)}{3(1-f)} \sum_i \frac{1}{1-(1-K_d)L_i} \qquad [2]$$

$$i = 1, 2, 3$$

for the effective conductance of dilute dispersions containing ellipsoidal particles. The three values of L_i involve elliptic integrals of the second kind, and are functions of the lengths of the semiprincipal axes (a, b, c) of the ellipsoids. Solutions are obtained in closed form only when the particles are spheroids, *i.e.*, $b = c$. For the case of spheres, $a = b = c$, all three L terms assume the value of 1/3, and Eq. [2] becomes identical to Maxwell's equation [1].

Representation of effective conductivities in concentrated suspensions ($f > 0.2$) requires consideration of the interactions of fields in the vicinity of neighboring particles. Although Lord Rayleigh (5) considered such interactions for the case of uniform size spheres in cubic lattices almost seventy years ago,[2] mathematical techniques still have not been developed for treatment of suspensions of random particles.

Since Maxwell's work was published numerous attempts have been made at representing the conductivities of dispersions of random particles in the concentrated range of volume fraction by approximations based on Eq. [1]. One such relation, which has been reviewed repeatedly in recent years, is that due to Bruggeman (6) where

$$1 - f = \frac{K_m - K_d}{K_m^{1/3}(1 - K_d)} \qquad [3]$$

The physical model corresponding to this latter expression requires an infinite range of particle sizes within the dispersion, and the use of this equation on suspensions which contain uniform size spheres is subject to question. De La Rue and Tobias (7) recently reported good agreement of data with Eq. [3] on suspensions which consisted of nonconducting spheres that varied in size by three orders of magnitude. These same authors found however, that when narrow size ranges were used, the data fell between the curves representing Eq. [1] and [3].

The present investigation was undertaken to allow for a more accurate comparison of data behavior relative to the limits represented by Eq. [1] and [3]. Conductivities of dispersions in which the dispersed phase does not conduct are far less sensitive to changes in volume fraction than in the case where $k_d >> k_c$. Unfortunately, with the exception of isolated measurements on narrowly restricted ranges of variables (9-14), no work has been reported on dispersions where both phases are conducting. The reason for this lies in the fact that until recent years no suitable stable system had been found that allowed for ionic conduction in both phases to any appreciable extent.

Experimental

In selecting components for preparing emulsions, water was chosen as one of the solvents for the obvious advantages that it offers. For a second solvent, propylene carbonate was found to be very attractive since it is partially miscible with water and allowed emulsions to be formed with excellent physical and chemical stability (15). A wide range of ionic solutes proved to be soluble in both phases.

[1] Present address: Oregon State College, Corvallis, Oregon.

[2] By introducing certain techniques in Rayleigh's derivation, Meredith and Tobias (8) obtained an improved relation which received good confirmation in the critical range of volume fraction near close packing.

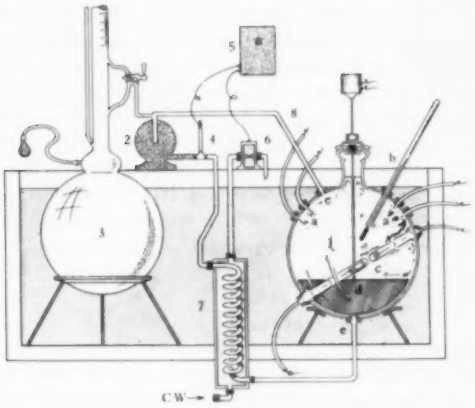

Fig. 1. Schematic drawing of the equipment used in the emulsion study.

In cases where it was desirable to impart a higher conductivity to the aqueous phase, KCl was used as the solute. Addition of quaternary ammonium iodide salts allowed for the reverse condition. Conductivities in the individual phases ranged approximately from 10^{-4} to 10^{-2} ohm^{-1} cm^{-1}.

The conductivity cell and emulsifying equipment are shown in Fig. 1. The apparatus depicted consisted of the following parts:

1. A 5-liter round-bottom flask which was modified and designed to act as a cell and mixing chamber. The components included in this flask were: (*a*) two pairs of bright platinum electrodes made from 20-mil Pt sheet. One pair of these electrodes had surfaces which were circular in shape with a diameter of 2 cm. The separation between these electrodes was approximately 3 cm. The other pair of electrodes was located on the opposite side of the flask and had surfaces in the shape of small squares with a dimension of 0.5 cm on a side. The separation between conducting surfaces for this pair was about 8 cm; (*b*) a differential thermometer which read in units of 1/100°C and which was fitted with a tapered joint; (*c*) a photocell and light source which were placed in the cell opposite the large electrodes described above. The gap that could be occupied by liquid between the light source and the photocell was approximately 1 cm; (*d*) a stirring unit that consisted of a sector of a Teflon disk which sat in the bottom of the flask. The disk was driven by a glass rod that was attached to a magnetic coupling unit at the top of the flask. This unit, in turn, was driven by a small universal motor; (*e*) outlets near the top and bottom of the flask for circulating the fluid.
2. A small pump with a Teflon rotary seal and a universal motor. This pump was used both to circulate the liquid under study and to keep the phases emulsified.
3. A 100-cc automatic buret.
4. A fixed-contact mercury thermostat set at 25°C.
5. A mercury plunger electronic relay.
6. A 115-v solenoid valve.
7. A small, metal heat exchanger controlled by the thermostat, relay, and solenoid valve mentioned above. The purpose of this heat exchanger was to remove the heat that the liquid picked up in passing through the circulating pump.
8. Tygon tubing and glass tees, stopcocks, and ground joints used to connect various parts of the system.

Table I. Typical size of the particles in the emulsion studies

Volume fraction of dispersed phase	Surface area per unit vol. of dispersed phase, cm^{-1}	Diameter of the dispersed droplet, μ
Emulsion type: oil in water		
0.00397	869	69.0
0.00794	851	70.5
0.01191	733	81.9
0.01588	630	95.3
0.0238	492	122
0.0316	397	151
0.0394	337	178
0.0471	291	206
Emulsion type: water in oil		
0.0048	5309	11.3
0.00797	3896	15.4
0.0159	2083	28.8
0.02315	1438	41.7
0.0315	1107	54.2
0.0392	902	66.5

In addition to this equipment, several small conductivity cells of various geometries and cell constants were used in determining K_4 values.

All measurements were made at 25°C unless otherwise noted. This isothermal condition was obtained by using a 50-gal water bath that was kept at 25° ± 0.02°C.

For low volume fractions of the dispersed phase estimates of the sizes of spherical droplets were obtained by evaluating the turbidity of the emulsions and then applying the correlation proposed by Langlois, Gullberg, and Vermeulen (16) (Table I). Even in the most concentrated emulsions, droplet diameters did not exceed approximately 500 μ. Visual observations indicated that in any given emulsion the size range of droplets was within less than an order of magnitude.

The bridge employed to obtain electrical conductivity data was of conventional design (17). The oscillator, null detector, and decade resistance box were selected so that the bridge frequency could be varied up to 50 kcs.

The experimental procedure was as follows. Approximately 6 l each of propylene carbonate and distilled water were equilibrated in a 12-l flask at 25°C with the proper amounts of solutes to give the desired conductivity ratio. The phase that was to constitute the continuous medium was then separated from the mixture, and a known amount, about 5400 cc, was added to the system depicted in Fig. 1. Initial readings on both the photocell and the conductivity bridge were taken and the circulation

pump was started. In finite steps, small amounts of the second phase were buretted into the system. After about 5 min, or when the system had come to equilibrium, conductivity and photocell readings were recorded. An amount of mixture, equal in volume to the amount of the second phase that was added, was then drawn off and the above steps repeated. The amount of the dispersed phase that was present in the liquid that was drawn off was taken into account in calculating the volume fractions. Data were taken in this manner until the volume fraction of the dispersed phase approached 0.5. Above this value there was a possibility that phase inversion would take place in localized regions of the system. When the roles of two phases A and B are *partially* inverted the value of the effective conductance of such a dispersion lies somewhere between the two extreme values of k_m obtained when A or B is the continuous phase throughout.

The character of the emulsion was observed through a section of glass tubing as it passed to the suction side of the centrifugal pump. If the phases seemed to have had any tendency to separate at this point, the pump, which acted as the primary mixer, was increased in speed. In most cases, the addition of the electrolyte gave added stability to the emulsion, and because the propylene carbonate-water emulsion always seemed to have had some stability of its own, phase separation in the mixing flask never became a problem.

Volumetric measurements were carried out with great care to reduce cumulative errors. Measurements of conductances on a given emulsion were reproducible to within 0.2%. Taking all sources of error into consideration, it is estimated, for a given volume fraction, that the value of the conductance obtained was within 1% of the true value (18).

When emulsions were studied where the conductivity of the dispersed phase was greater than that of the continuous medium, it was found that for small volume fractions, a bridge frequency of 1000 cps gave lower K_m values than those predicted by Maxwell's equation. Such behavior was also noted in the work of Fradkina (13) on measurements of the dielectric constants of water-in-oil dispersions [Fig. 2]. To balance the conductivity bridge under these conditions required a greater shunt capacity across the decade box than was required in the case of either phase alone. The probable cause of this phenomenon is that when the interfacial area per unit volume is large (Table I), then the capacitive reactance at the interface is large enough to influence appreciably the impedance of the equivalent circuit, and the system is no longer approximated by a parallel resistor and capacitor. Increasing the bridge frequency to 10,000 cps or above eliminated this phenomenon.[a] At this frequency, measurements on emulsions where K_d was carefully adjusted to unity (*e.g.*, $k_d = k_c$) yielded $K_m = 1$ for all volume fractions.

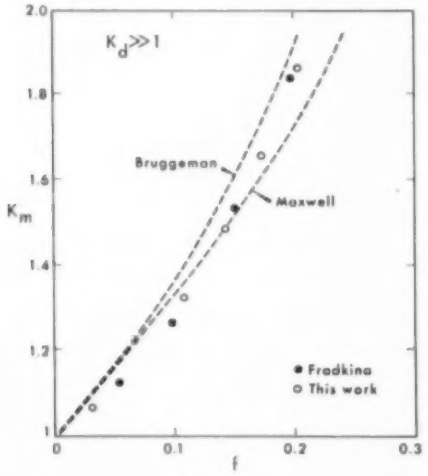

Fig. 2. An illustration of surface reactance effects: electrical conductivity data on emulsions as open circles at a bridge frequency of 1000 cps. Comparable data by Fradkina (13) on the dielectric constants of emulsions as closed circles.

Discussion

It is evident from graphical representations (Fig. 3a-d) of the data, that the effective conductivity of emulsions can be represented satisfactorily by Maxwell's equation when the volume fraction of the dispersed phase is less than 0.2. Above this value however, deviations from Eq. [1] become progressively larger as the volume fraction increases. This is particularly true when $K_d >> 1$. The relation proposed by Bruggeman, Eq. [3], appears to be equally inadequate, although all of the data obtained appear to lie between Eq. [1] and [3].

Maxwell's equation, on the basis of assumptions made in its derivation, should be applicable only when the dispersed particles are so distant from each other that the field around each particle is essentially the same as if each particle were present alone. On the other hand, the Bruggeman approximation attempts to account for the interaction of fields by assuming that the change in conductivity obtained upon the addition of each particle to a suspension is equivalent to the change incurred when a particle is placed in a continuum. Since Bruggeman used the first two terms of the Taylor expansion of Eq. [1] to evaluate in successive steps the effective conductances obtained after the addition of each particle, it is obvious, from the point of view of each newly added particle, that the existing suspension must be regarded as very dilute or else the use of Eq. [1] would not be justified.

Bruggeman's expression requires an unrealistic model which consists of a large number of particle size fractions. Thus, as much larger particles are added to a medium that contains all of the fractions of smaller particles, it is possible to treat the latter as a continuum. Most of the real dispersions do not correspond to this model; they consist of particles of a single size or they are made up of particles which differ in size at the most by one order of magnitude.

Representing suspensions in which particle sizes are within narrow ranges, we may attempt to treat

[a] An explanation of this effect was drawn to the attention of the authors after work on this paper was terminated. T. Hanai [*Kolloid-Zeitschrift*, 171, 23 (1960)] has considered the dielectric dispersion of emulsions and points out that the observed frequency effect would be significant when $K_d > 1$ and less noticeable when $K_d < 1$.

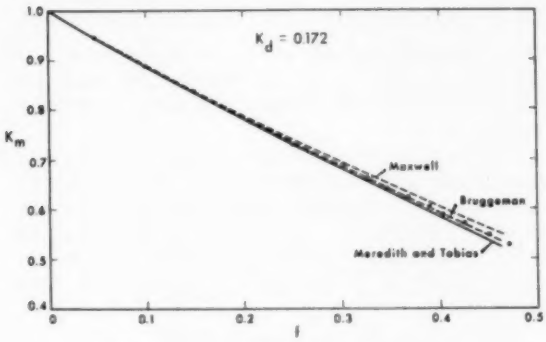

Fig. 3a. $K_d = 0.172$ data on emulsions

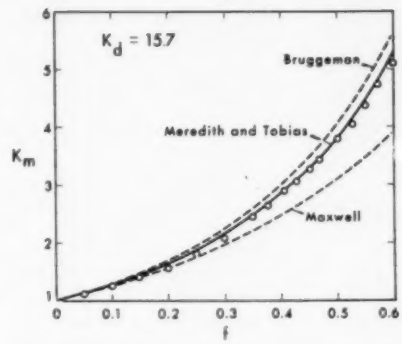

Fig. 3b. $K_d = 15.7$ data on emulsions

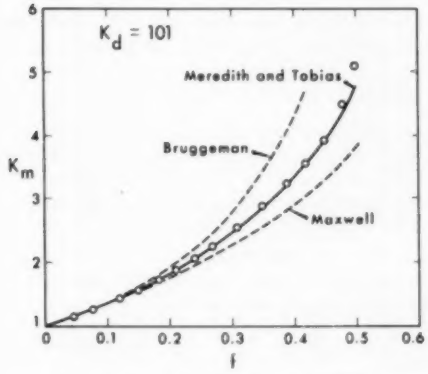

Fig. 3c. $K_d = 101$ data on emulsions

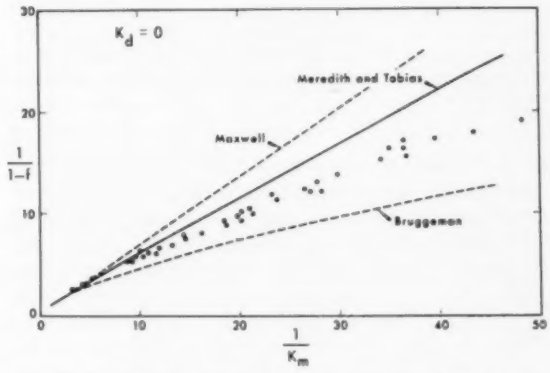

Fig. 3d. $K_d = 0$ data on foams for high volume fractions (19)

Fig. 3a-d. Comparison of equations by Maxwell (Eq. [1]), Bruggeman (Eq. [3]) and present authors (Eq. [7]) with experimental data.

our system as if it contained particles of only two different sizes, each being present in equal volume fractions, f_1 and f_2. According to our definition:

$$f_1 = f_2 \text{ and } f = f_1 + f_2 \qquad [4]$$

Now if the larger particles are removed, and if the remaining suspension is not too concentrated the effective conductance of the remaining suspension, k_e', may be approximated by Eq. [1] for the case of spheres, or by Eq. [2] for ellipsoids, *i.e.*,

$$k_e' = \frac{1 + (WK_d - 1)f_1'}{1 + (W-1)f_1'} k_e \qquad [5]$$

where

$$W = \frac{1}{3} \sum_i \frac{1}{1 - (1 - K_d)L_i}$$

and

$$f_1' = f_1/(1 - f_1)$$

Upon addition of the larger particles we may write

$$k_m = \frac{1 + (WK_d - 1)f_2}{1 + (W-1)f_2} k_e' \qquad [6]$$

treating the suspension that contains only the smaller particles as a continuum. Combining and rearranging Eq. [4], [5], and [6] we obtain

$$K_m = \left(\frac{2 + (WK_d - 1)f}{2 + (W-1)f}\right)\left(\frac{2(1-f) + WK_d f}{2(1-f) + Wf}\right) \qquad [7]$$

For the case of suspensions of spherical particles, all three of the L's are equal to 1/3 and W takes on the value of $3/(K_d + 2)$. Equation [7] thus becomes

$$K_m = \left(\frac{2 + 2Xf}{2 - Xf}\right)\left(\frac{2 + (2X-1)f}{2 - (X+1)f}\right) \qquad [8]$$

where

$$X = (K_d - 1)/(K_d + 2)$$

If the spheres are also nonconducting, the above reduces to

$$K_m = \frac{8(2-f)(1-f)}{(4+f)(4-f)} \qquad [9]$$

and if the spheres are very much better conductors than the continuous phase, i.e., $K_d >> 1$

$$K_m = \frac{(1+f)(2+f)}{(1-f)(2-f)} \qquad [10]$$

Equation [8] is compared with data in Fig. 3a-3d. The relatively large deviation between Clark's (19) data on foams (Fig. 3d) and Eq. [9] is not surprising in view of the fact that in the concentrated region very large size ranges may have been present, and serious deviations from spherical shape

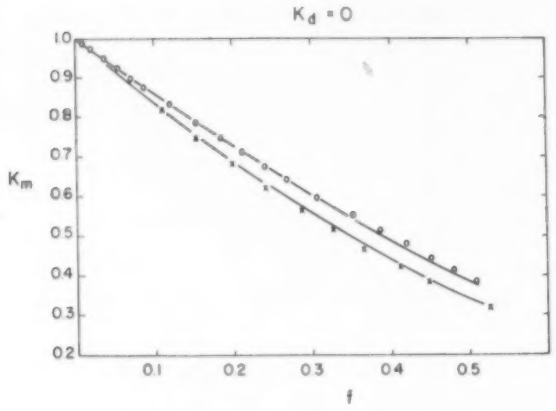

Fig. 4. Data by the present authors on emulsions (spherical particles) as — — O — — compared with the curve for Eq. [9] and data by Stewart (21) on dog's red blood cells (oblate spheroids) as — — X — — compared with the curve for Eq. [14].

in the dispersed phase may have occurred. On the other hand, the excellent agreement with data on emulsions as shown in Fig. 3a, 3b, and 3c may be attributed to the closer correspondence between the theoretical model and the experimental conditions.

In order to use Eq. [7] in its more general form where the dispersed particle has the shape of an ellipsoid, it is necessary to evaluate L_1, L_2, and L_3. Closed form is obtained only in the case of spheroids (20), where:

$$L_1 + L_2 + L_3 = 1 \text{ and } L_2 = L_3 \qquad [11]$$

If a, b, and c denote the lengths of the semi-principal axes of the spheroid, and if we set $A = (b/a)^2$, we have for prolate spheroids ($a > b$):

$$L_1 = \frac{A}{(A-1)}\left[1 - \frac{1}{2(1-A)^{1/2}} \ln \frac{1+(1-A)^{1/2}}{1-(1-A)^{1/2}}\right] \qquad [12]$$

and for oblate spheroids ($a < b$):

$$L_1 = \frac{A}{(A-1)}\left[1 - \frac{1}{(A-1)^{1/2}} \arctan (A-1)^{1/2}\right] \qquad [13]$$

A test of the usefulness of Eq. [7] on nonspherical particles may be made by using Stewart's data on the conductivity of dog's blood (21). In a dispersion of this type the continuous phase is the blood serum and the dispersed phase is made up of nonconducting red blood cells which resemble oblate spheroids where $b/a = 3$. For this dispersion we find that L_1 has a value of 0.636 and W is equal to 1.73. Equation [7] thus reduces to

$$K_m = (2-f)(1-f)/(1+0.365f)(2-0.27f) \qquad [14]$$

The results of this test are given in Fig. 4. In this same figure data are also plotted for the case of a dispersion of spheres in order to illustrate the effect of shape.

Although Eq. [7] apparently represents data over a wide range of variables rather well, this agreement should be regarded as a result of errors balancing each other The application of Eq. [2] at the volume fractions f_1' and f_2 would tend to make the correction on K_m at the total volume fraction f too small, while treating the suspension containing f_1' as a continuum has the opposite effect.

As a practical conclusion it is suggested that Eq. [1] or [2] may be used to represent conductivities of suspensions as long as the volume fraction of the dispersed phase is less than 0.2. For more concentrated dispersions the newly proposed approximation, Eq. [7], appears to yield much better agreement with data.

Manuscript received June 13, 1960; revised manuscript received Oct. 17, 1960. This paper was prepared for delivery before the Chicago Meeting, May 1-5, 1960.

Any discussion of this paper will appear in a Discussion Section to be published in the December 1961 JOURNAL.

REFERENCES

1. H. A. Lorentz, *Wied. Ann.*, **11**, 70 (1880).
2. L. Lorenz, *ibid.*, **9**, 641 (1880).
3. J. C. Maxwell, "A Treatise on Electricity and Magnetism," 2nd ed., Vol. 1, p. 435, Clarendon Press (1881).
4. H. Fricke, *Phys. Rev.*, **24**, 575 (1924).
5. Lord Rayleigh, *Phil. Mag.*, **34**, 481 (1892).
6. D. A. G. Bruggeman, *Ann. Physik*, **24**, 636 (1935).
7. R. E. De La Rue and C. W. Tobias, *This Journal*, **106**, 827 (1959).
8. R. E. Meredith and C. W. Tobias, *J. Appl. Phys.*, **31**, 1270 (1960).
9. A. Slawinski, *J. Chim. Phys.*, **23**, 710 (1926).
10. G. S. Frey, *Z. Elektrochem.*, **38**, 260 (1932).
11. C. A. R. Pearce, *Brit. J. Appl. Phys.*, **6**, 113 (1955).
12. A. Eucken, *V. D. I. Forschungheft*, No. 353 (1948).
13. E. M. Fradkina, *Zhur. Eksptl. i. Teoret. Fiz.*, **11**, 1011 (1950).
14. R. H. Wang and J. G. Knudsen, *Ind. Eng. Chem.*, **50**, 1667 (1958).
15. W. S. Harris, Electrochemical Studies in Cyclic Esters, University of California Radiation Laboratory Report 8381 (1958).
16. G. E. Langlois, J. E. Gullberg, and T. Vermeulen, *Rev. Sci. Instr.*, **25**, 360 (1954).
17. S. Glasstone, "An Introduction to Electrochemistry," p. 33, D. Van Nostrand Co., New York (1942).
18. R. E. Meredith, Studies on the Conductivities of Dispersions, University of California Radiation Laboratory Report 8667 (1959).
19. N. O. Clark, *Trans. Faraday Soc.*, **44**, 13 (1948).
20. H. C. van de Hulst, "Light Scattering by Small Particles," John Wiley & Sons, Inc., New York (1957).
21. G. N. Stewart, *J. Physiol.*, **24**, 356 (1899).

Exchange between Single-Crystal Cadmium and Its Ions

Cecil V. King, David S. Newman, and Ernest Suriani

Department of Chemistry, New York University, New York, New York

ABSTRACT

The rate of cadmium-cadmium ion exchange has been studied, using electropolished specimens of single-crystal cadmium immersed in deaerated solutions of $Cd(ClO_4)_2$ containing Cd^{115} as tracer. The exchange rate is shown to be controlled by self-diffusion within the metal. In solutions 0.1M or higher in concentration, exchange at the interface is complete and rapid compared to internal diffusion, and corrosion, film formation, or local cell action do not interfere. Consequently the surface concentration to be used in calculations is approximately equal to the metal concentration in the solid phase.

In a previous study of exchange between cadmium and its ions in aqueous solution (1), it was shown that the continuing exchange is due to diffusion within the metal at a rate which is appreciable even at room temperature. That study was made with polycrystalline metal so that both grain-boundary and lattice diffusion were involved in interpreting the results. Since the measured rate then depends on grain size and grain-boundary area, it was only possible to calculate the ratio of grain-boundary and lattice diffusion coefficients.

The objective of the present studies is of course not to determine the self-diffusion coefficients, but to examine, so far as possible, the nature of the interfacial process in the exchange reaction. For this purpose it is evident that experiments with single-crystal specimens can give more useful results. The problem is then one of homogeneous diffusion with fixed boundary conditions, provided that corrosion or other effects do not change the nature of the metal surface while in contact with the solution.

Experimental

A rod of single-crystal cadmium, 1.9 cm in diameter, was cut on a slow-turning lathe into disks 1.5 mm thick. A 1-mm hole was drilled near the edge of each disk. After smoothing and polishing the surfaces, the disks were annealed at 110°C for 24 hr. Immediately before use each disk was electropolished in a cyanide bath as described previously (1). After immersion in the tracer solution and counting, the radioactive layer was removed by electropolishing again. All washing was done with methanol.

The orientation of the crystal was determined by examining the distortion patterns appearing around small punch-marks (2) and was verified by a transmission x-ray pattern. The disk surfaces were inclined at about 27° to the basal or hexagonal planes of the crystal.

A stock solution of $Cd(ClO_4)_2$ was prepared and standardized as before (1); its pH was adjusted to 4.7. Cd^{115m}, obtained as the nitrate in HNO_3, was converted to the perchlorate. The immersion solutions were deaerated with nitrogen which was passed over hot copper, then through water; with careful attention to deaeration the coupons remained shiny for 5 days or longer and the surface showed little change under low magnification. A small amount of cadmium dissolved, as discussed later. Measurement of radioactivity and conversion to gram-atoms of exchange per square centimeter were carried out as usual. All experiments were at 25°C.

Exchange as function of time.—If the exchange is controlled by homogeneous diffusion into the metal from a surface layer of fixed concentration c_o, the total exchange a_t (in gram-atoms/cm^2) can be expressed by the equation

$$a_t = 2\, c_o\, (Dt/\pi)^{1/2} \qquad (1)$$

where D is the diffusion coefficient and t is the time of immersion. Experiments of this type are given in Table I, where the second column in each case gives gram-atoms of exchange divided by square root of time to test the above equation. Each value is the average of four readings, obtained from the two sides of two disks which were immersed simultaneously. The maximum divergence in any set of four counts was about 17%, the average much less than this. In the most dilute solutions there is a tendency for the value to increase with time, but in general the square-root relation is obeyed reasonably well.

Exchange as function of depth.—According to the theory of homogeneous diffusion with the present boundary conditions, after a fixed time of immersion t the concentration of exchanged material c_x at the depth x is given by Eq. [2]

$$c_x/c_o = \text{erfc}\,[x/2\,(Dt)^{1/2}] \qquad [2]$$

where erfc refers to the compliment of the error function, and it is again assumed that c_o is constant during the experiment.

Disks were immersed in the tracer solution long enough to be sure of sufficiently deep penetration of radioactivity. Thin layers were then removed in the electropolishing solution, the disks being counted and weighed on the microbalance after each treatment. Some disks were spoiled by removing too much metal in the first etch, others by erratic behavior of the polishing process. The most consistent results are given in Tables II and III, where weight losses have been converted to thickness of the layer removed. The second column in each case gives the amount of exchange remaining below the etch depth, as measured by the residual activity after etching. Each value is the average for the two sides.

Analysis and Results

The experiments summarized in Tables II and III will be discussed first for reasons which will be evi-

Table I. Total exchange as function of time

$min^{1/2}$	gram-atoms cm^{-2} $min^{-1/2}$ × 10^8	$min^{1/2}$	gram-atoms cm^{-2} $min^{-1/2}$ × 10^8	$min^{1/2}$	gram-atoms cm^{-2} $min^{-1/2}$ × 10^8
1.4×10^{-4}M Cd^{++}		0.01M Cd^{++}		0.05M Cd^{++}	
2	0.67	2	1.44	3	2.8
3	0.45	2.6	2.00	4	2.6
4	0.69	3	2.75	5	3.2
7	0.92	5	2.92	6	3.5
29	1.19	32	3.06	7	3.0
		73	4.80	8	3.0
	avg 0.78			9	3.4
			avg 2.8	10	2.9
				11	3.2
				36	3.2
					avg 3.1
2.8×10^{-4}M Cd^{++}		0.01M Cd^{++}		0.10M Cd^{++}	
4.1	0.47	2	4.1	1.41	6.8
5	0.57	3	3.9	2.24	7.1
6	0.64	4	4.8	2.65	6.8
7	0.61	5	4.1	3.16	5.8
		6	4.1	4.47	4.7
	avg 0.57	7	4.0	7.75	4.1
		8	4.0	10.95	3.9
		9	4.0	19.1	5.8
		10	3.9	29.5	4.4
				31.6	5.7
			avg 4.1		
					avg 5.5
1.4×10^{-3}M Cd^{++}		0.05M Cd^{++}		0.20M Cd^{++}	
2	1.76	1	3.4	8	4.8
3	1.43	2	4.1	9	5.5
4	2.63	3	5.1	10	5.4
6	2.12	5	4.4	11	5.9
7	2.56	10	4.5	12	5.9
15.5	2.11	12	3.9	36	5.7
38.7	2.67	15	3.7		
54.2	3.23	28.4	3.6		avg 5.6
	avg 2.22		avg 4.1		
				0.28M Cd^{++}	
				7.74	5.3
				31.0	5.0
				38.7	4.6
				54.2	5.4
					avg 5.1

dent later. Equation [2] should be applicable, but both D and c_o are unknowns and c_x is the slope, at depth x, of the curve obtained by plotting residual exchange *vs.* depth. The same problem was encountered by Rohan, Pickering, and Kennedy (4) in studying the diffusion of Sb^+ into Si. Their method of solution was to use the equation for residual activity obtained by differentiating Eq. [2] followed by integration between the limits x and ∞. By using pairs of points on the experimental curve c_o could be temporarily eliminated and D found by successive approximation.

In the present case the experimental values are not sufficiently accurate to use directly in this way, and the following procedure was adopted. The residual exchange was plotted *vs.* depth, smooth curves were drawn, and the slopes were determined graphically. Disks 1 and 2 were treated together, and the initial part of the curve is in some doubt. The slopes (c_x) were then plotted *vs.* depth and these curves were extrapolated to zero depth to obtain c_o. On replotting on another scale the slopes and values of c_o obtained may differ by a few per cent, but this

Table II. Residual exchange as function of etch depth. Each disk immersed in 0.05M $Cd(ClO_4)_2$ for 5.93×10^5 sec, at 25°C

Disk 1		Disk 2	
Depth cm × 10^6	gram-atoms/ cm^{-2} × 10^8	Depth cm × 10^6	gram-atoms/ cm^{-2} × 10^8
0	5.21	0	5.13
0.67	4.89	1.32	4.85
2.28	4.11	1.98	3.60
3.33	3.11	4.02	2.76
6.21	2.46	7.4	2.10
8.4	1.72	10.8	1.72
15.5	1.37	17.2	1.62

Table III. Disk 3 immersed in 0.28M $Cd(ClO_4)_2$ at 25°C for 4.31×10^5 sec; Disk 4 in same solution for 6.02×10^5 sec

Disk 3		Disk 4	
Depth cm × 10^6	gram-atoms/ cm^{-2} × 10^8	Depth cm × 10^6	gram-atoms/ cm^{-2} × 10^8
0	4.14	0	5.40
2.29	3.09	1.66	3.65
3.86	2.08	4.01	2.72
5.57	0.94	6.70	1.61
8.24	0.61	12.5	0.68
10.6	0.35	15.1	0.57
16.9	0.15	19.2	0.27

does not change the calculated diffusion coefficient drastically.

The values of c_x and c_o obtained in this way were inserted in Eq. [2] to calculate D, the error function or its compliment being taken from suitable tables. Representative values are given in Table IV.[1]

It will be noted in Table IV that values of c_o obtained by the extrapolation are near the concentration of cadmium metal, namely 0.077 gram-atoms/cm^3. That the values are somewhat too high may be due to a roughness factor greater than unity, since the measured area was used in all calculations. If the ratio c_x/c_o is too small at any point, the calculated D is also too small.

Exchange as function of time.—It is convenient to reverse the calculation here, assuming a value for D and calculating c_o. Using $D = 3.6 \times 10^{-15}$ cm^2/sec (average of last two columns, Table IV) and the average values of the slopes $a_t/t^{1/2}$ from Table I to insert in Eq. [1], the c_o values given in Table V are obtained (the time is of course used in seconds).

Discussion

Because of the uncertain nature of the experimental procedures and of the cadmium surface, closer examination of the data seems unwarranted. For example, D should be a constant, independent of depth or of tracer concentration since the isotope effect must be small. Several factors may account for the trend in Table IV. Disks 1 and 2 lost 0.234 and 0.286 mg in weight, respectively, during immersion, corresponding to a layer about 5×10^{-4} cm in thickness if dissolution is uniformly distributed over the entire surface. This should decrease the apparent values of D somewhat. Several hours were

[1] As a sample calculation take the depth 4×10^{-6} cm for disks 1 and 2: $c_x/c_o = 0.037/0.090 = 0.411 = \text{erfc}\,[x/2(Dt)^{1/2}]$. From the tables, $x/2(Dt)^{1/2} = 0.58$, and on inserting x and t (Table II). $D = 2.01 \times 10^{-15}$ cm^2/sec.

Table IV. Slopes of the curves from Tables II and III, and calculated values of the diffusion coefficient D

Depth, cm × 10^4	c_x and c_o, gram-atoms cm^{-3} Disks 1, 2	Disk 3	Disk 4	D, cm^2 sec^{-1} × 10^{15} Disks 1, 2	Disk 3	Disk 4
0	(0.090)	(0.088)	(0.091)	—	—	—
1	0.071	0.073	0.079	1.2	2.6	3.0
2	0.055	0.062	0.068	1.3	3.2	3.1
4	0.037	0.043	0.048	2.0	3.8	3.3
6	0.022	0.025	0.032	2.3	3.8	3.4
8	0.018	0.014	0.022	3.3	3.7	3.9
10	0.014	0.009	0.015	4.2	4.3	4.3

Table V. Calculation of c_o from Eq. [1]

$C_{Cd^{++}}$, M	c_o, gram-atoms per cm^3	$C_{Cd^{++}}$, M	c_o, gram-atoms per cm^3
1.4×10^{-4}	0.015	0.05	0.059
2.8×10^{-4}	0.011	0.05	0.078
1.4×10^{-3}	0.042	0.10	0.105
0.01	0.078	0.20	0.107
0.01	0.053	0.28	0.097

required to dissolve thin layers, count activity, and weigh the specimens; during this time diffusion continued, but no correction could be made for this. Microroughness of the metal surface could account for the apparently high surface concentration and large values of D below the depth of the original pores. There is no assurance that etching is quite uniform since electropolishing is an uncertain method for removing such thin layers. In addition, the error function curve is of such a shape that a simple curve through the experimental points is not quite correct.

The outstanding feature of the investigation is that, in spite of such uncertainties, the entire course of the exchange can be explained very simply in terms of rapid attainment of surface equilibrium in the more concentrated solutions, lack of serious interference by corrosion, film formation or metal dissolution, and a diffusion coefficient which is correct to less than an order of magnitude.

Self-diffusion coefficients in single-crystal cadmium have been measured by the dry method, in the temperature range 110°-315°C, by Wajda, Shirn, and Huntington (2). Extrapolation to 25°C by means of their temperature-coefficient equations gives $D = 1.0, 2.2 \times 10^{-15}$ cm^2/sec for the two major directions in the crystal. The present results are in satisfactory agreement with this uncertain extrapolation. A larger value may be correct; if D were taken as 5×10^{-15} cm^2/sec the last three values of c_o in Table V would fall in the range 0.08-0.09 gram-atoms/cm^3 as in Table IV.

In the more dilute solutions it appears that the exchange current falls off sharply and is too small to maintain surface equilibrium, i.e., the ratio of active to inactive Cd is smaller in the surface layer than it is in the solution. An alternative explanation may be that exchange must be preceded by adsorption and that a full monolayer is adsorbed only at 0.1M and above. The smallest amount of pickup recorded in Table I is equivalent to full exchange in about 4 apparent monolayers, but this does not insure that full exchange has taken place in the first layer.

In the most dilute solutions there was some indication of "concentration polarization" wth respect to the tracer ion, in the shortest runs. Extra stirring in addition to the deaerating nitrogen bubbles resulted in somewhat greater activity pickup, but the effect did not last more than 5 min.

Exchange studies with a tracer, such as the present, can show whether the exchange current is large or not, but do not enable quantitative calculation. The exchange current with pure cadmium does not seem to have been reported. It has been measured with cadmium amalgam by a nontracer method (5). Exchange studies by the tracer method with cadmium amalgam have shown that the exchange current is large (6). Exchange with polarized amalgam, using the tracer method, has been studied (7), but the authors did not explain how the amalgam could be polarized without causing electrolysis.

Acknowledgment

This work was supported by the U.S. Army Office of Ordnance Research under a contract with New York University.

Manuscript received June 17, 1960; revised manuscript received Oct. 17, 1960.

Any discussion of this paper will appear in a Discussion Section to be published in the December 1961 JOURNAL.

REFERENCES

1. C. V. King and R. Skomoroski, *J. Phys. Chem.*, **63**, 1819 (1959).
2. E. S. Wajda, G. A. Shirn, and H. B. Huntington, *Acta Met.*, **3**, 39 (1955).
3. H. S. Carslaw and J. C. Jaeger, "Conduction of Heat in Solids," 2nd ed., p. 60, Oxford, Clarendon Press (1959); L. S. Darken and R. W. Gurry, "Physical Chemistry of Metals," Chap. 18, McGraw-Hill Book Co., New York (1953).
4. J. J. Rohan, N. E. Pickering, and J. Kennedy, *This Journal*, **106**, 705 (1959).
5. J. E. B. Randles and K. W. Somerton, *Trans. Faraday Soc.*, **48**, 951 (1952).
6. S. Fronaeus, *Acta Chem. Scand.*, **7**, 764 (1953); **8**, 412 (1954).
7. A. M. Baticle and Y. Thouvenin, *Compt. rend.*, **248**, 1330 (1959).

Technical Notes

Effect of Dissolved Gases on Oxide Film Formation

J. J. Polling

United Kingdom Atomic Energy Authority, Atomic Energy Research Establishment, Harwell, Didcot, Berkshire, England

When many metals are oxidized, interference colors are seen which are an excellent guide to the thickness of the oxide film. If the oxidation is carried out electrolytically, these colors are usually very uniform because the ionic current which causes the oxidation is extremely sensitive to changes in the strength of the field which enables the ions to surmount a potential barrier at the oxide/metal interface. The field strength is proportional to the voltage applied and inversely proportional to the thickness of the film. Thus, should the film be thinner in one place than elsewhere the ionic current density will be greater in that place, causing a rapid local growth until an even thickness over the whole surface is achieved.

In the course of experiments on the possible effect of the hardness of the metal on the potential barrier at the metal/oxide interface, some zirconium specimens were annealed *in vacuo*. Zirconium was chosen because, unlike aluminum, it shows interference color on oxidation, and because its melting point is not as high as that of tantalum, making it more amenable to heat treatment. After being annealed, some of the specimens were severely work-hardened and all of them were anodized in parallel. Had the potential barrier been altered by the hardening, the thickness of the oxide formed on the specimens would have been different for the same voltage of formation, and this would have shown itself by a difference of color. It was found that work hardening had no appreciable effect, but a curious phenomenon was observed which it is the object of this note to describe. The work has been alluded to elsewhere, but not reported in detail (1).

Experimental

Ten specimens of zirconium sheet 0.125 mm thick, in the shape of rectangles 7.5 x 2 cm, were placed together like a pack of cards in an alumina crucible and heated at 800°C for 4 hr in a vacuum of 10^{-5} mm Hg. They were allowed to cool overnight, and on removal from the furnace it was noticed that the outer faces of the two outermost specimens had become slightly brown in color; this was attributed to a slight oxidation. The brown markings had also penetrated between the specimens for a short distance, causing a light brown margin to appear. The color was characteristic of an anodic potential of about 5 v. The central areas remained silvery in appearance.

When the specimens were anodized in parallel, a concentric spectrum of colors appeared on each one, both annealed and work-hardened alike. The color at the center of every specimen was the same and was characteristic of the voltage applied. Toward the edge, however, where the faint brown marks had been, the color became nonuniform, passing through a whole order of the spectrum. The sequence indicated an increase of optical thickness, the oxide layer at the edge being about twice as thick optically as that at the center.

The only surfaces which did not exhibit this nonuniformity of color were the two outer faces of the outermost specimens of the pack, but the optical thickness on these faces was twice as great as usual. This was assumed to be due to an increase of physical thickness since no conceivable change in the structure of the oxide could double the refractive index.

It was desirable to determine whether the variation in thickness was a simple difference or a ratio, and this was done by anodizing a specimen in stages and noting the thickness at various points on the surface. The specimen was anodized in steps of 10 v from zero to 150 v. This was repeated with other specimens and with the outermost faces, and in this way it was established that the variation was indeed a ratio, the maximum variation observed with certainty being about 2. The step gauge used to compare the colors did not extend high enough to determine the ratio beyond a formation voltage of 150 v, but anodization up to 300 v continued to show a variation of color.

The outermost faces which produced a uniform color were especially useful in so far as they could be used for capacity measurements, by coating the inner faces with paint. Surprisingly, when the capacities of the annealed and normal specimens were compared they were found to be much the same within experimental error. In this respect the phenomenon resembles that of the growth of oxide films under irradiation by ultraviolet light which has been reported by Young (2) and Vermilyea (3). During irradiation oxide films held at a constant voltage of formation can attain thicknesses up to twenty times greater than would normally be expected for the ap-

plied voltage. This is confirmed by color and weight changes, but the capacity measurements show little or no change. Vermilyea attributes this to porous oxide growth under ultraviolet light, but this view is doubted by Young and Bray who have used Van Geel's method of filling the supposed pores by subsequent "dark" anodization and noting the rate of change of thickness. This should be artificially high when the pores are being filled owing to the effective reduction of surface area by the pores. When the pores are completely filled the rate of growth should revert abruptly to normal. Young and Bray found that the rate of growth was normal and constant throughout the experiment. Whatever the mechanism of the abnormal film growth, the present experiments show a marked similarity.

Microscopic examination of a specimen exhibiting a spectrum of colors was carried out, and it was observed that no difference of surface structure existed in the various colored regions which might account for the variation.

A final fact was obtained from this set of specimens. One of them had been anodized to 20 v, a bright blue color, prior to annealing. On examination afterward it was found that the blue color had almost completely disappeared leaving the specimen silvery and to all appearances nonanodized. Subsequent anodization showed that it behaved like a nonanodized specimen, the voltage across it being initially zero and rising steadily with the passage of constant current. At 20 v the blue color was obtained again, and there was no discontinuity in the voltage/time curve at this point.

Discussion

A tentative theory was developed to account for these facts. It was proposed that in the course of the heat treatment the zirconium had absorbed gases from the vacuum system, and these had formed a solid solution with the metal. The temperature was too low for rapid diffusion, and the solution areas were confined to the places where the gas atoms had actually struck the metal. This could alter the optical reflectivity and account for the faint brown markings round the edges of the inner specimens. The presence of gases in solution in the metal could conceivably lower the potential barrier at the metal/oxide interface, and a given formation voltage would then produce a thicker film over those particular regions.

To test this theory an attempt was made to produce a number of specimens containing known concentrations of oxygen in solution. Four weighed zirconium specimens were placed in alumina boats and sealed in similar silica vessels under ⅛, ¼, ⅜, and ½ atm pressures of oxygen, respectively. The pressure in each vessel was made up to ¾ atm with argon in order to prevent the evaporation of the zirconium after all the oxygen had been absorbed. The tubes were heated in a furnace for two days at 1020°C. Three of the specimens were of a golden appearance as though a nitride film had been formed, while the fourth, the specimen sealed under the lowest oxygen press, was of normal color, but the alumina boat was dirty as though thorough evaporation had taken place in spite of the argon. All the specimens showed an increase of weight but the increment for the evaporated specimen was smaller than expected. On attempting to anodize these specimens it was found that the partially evaporated one behaved in the usual way, but it was impossible to form an oxide film on the three which had a golden color. Under a powerful lens the surfaces of all the specimens were mottled, resembling a mosaic of tiny areas, each colored differently.

It was assumed that the golden film was in fact due to nitrogen contamination, and an attempt was made to remove it by abrasion. It proved to be exceedingly hard and resisted all except the coarsest emery paper. The operation was further complicated by the brittleness of the specimens. Eventually one of the specimens was ground in convex form with a ridge of golden film still present down the center. This area was painted out, leaving only the silvery internal areas showing, and the specimen was anodized. Its voltage/current characteristics were now normal, but a variation of color appeared. When, for example, the voltage of formation was 80 v, the color close to the yellow ridge was characteristic of 97 v, while at the edge of the specimen, where most of the metal had been removed by abrasion, the color represented a formation voltage of only 72 v. At an intermediate position the color corresponded to the correct figure of 80 v. The other specimens behaved in a similar manner and also showed a tendency to periodic passivation, i.e., the voltage tends to fall and the current tends to rise for a period, then the reverse holds true.

The fact that there was a variation of color with depth of material abraded away shows that the specimens had absorbed oxygen, but the solution so formed was not homogeneous, being more concentrated near the surface than at the center. Nevertheless, the brittleness of the specimens showed that some oxygen had penetrated deeply into the structure. The temperature needed to produce an appreciable diffusion rate which would enable a homogeneous solution to be obtained within reasonable time is of the order of 1500°C. At this temperature silica and quartz containers become porous so special apparatus would be needed capable of retaining high vacua at this temperature.

The theory that the dissolution of oxygen in the zirconium lattice could alter the dimensions of the potential barrier is supported by the work of de Boer and Fast (4) and Treco (5) who have found that oxygen atoms in zirconium occupy interstitial positions and cause an increase in lattice parameters of the metal. This could quite conceivably alter the work function required to withdraw an ion from the metal.

Such a mechanism does not explain the apparent lack of concordance between optical and capacitance measurements, unless it is assumed that the oxide film formed under these circumstances is to some extent conducting.

Manuscript received Sept. 26, 1960.

Any discussion of this paper will appear in a Discussion Section to be published in the December 1961 JOURNAL.

REFERENCES
1. J. J. Polling, Compte Rendu du XXVII e Congres International de Chimie Industrielle, 1954.
2. L. Young, *Trans. Faraday Soc.*, **50**, 153 (1954).
3. D. A. Vermilyea, *J. Appl. Phys.*, **26**, 489 (1955).
4. J. H. de Boer and J. D. Fast, *Rec. Trav. Chim.*, **59**, 161 (1940).
5. R. M. Treco, *Trans. Am. Soc. Metals*, **45**, 872 (1953).

Recombination Radiation from an N-Type Germanium Cathode in Heavy Water

P. F. Schmidt and C. H. Church

Research Laboratories, Westinghouse Electric Corporation, Pittsburgh, Pennsylvania

Reduction of an ion at an n-Ge electrode can occur by transfer of an electron either from the conduction or the valence band of the n-Ge. By electrochemical methods it has been shown (1, 2) that the reduction of the $[Fe(CN)_6]^{-3}$ ion occurs by transfer of an electron from the valence band.

Dewald and Turner (3) repeated the experiments of Brattain and Garrett (4) on the hydrogen evolution reaction on n-Ge (which were carried out at current densities ≤ 10 ma/cm^2), and showed that at least part of the 10% hole injection postulated by Brattain and Garrett is due to the presence of dissolved O_2 in the solution.

It is postulated here that the extraction of electrons from the valence band of n-Ge must lead to the emission of recombination radiation corresponding to the gap width in the same manner as it has been observed for a p-n junction in Ge under forward bias (5). The effect should be easily observable because hole injection occurs at the very surface of the n-Ge.

Radiation with $\lambda > 1.4\,\mu$ is strongly absorbed by H_2O. In order to observe recombination radiation from Ge [which according to the experimental results of Newman (5) appears to be approximately gaussian and is centered at 0.67 ev], an 0.1N solution of Na_2SO_4 in D_2O was used as the electrolyte, a Pt anode completing the circuit. D_2O is quite transparent up to wave length of about 1.9 μ, and actually has a transmission peak at 1.75 μ; it is thus very well suited to observe the radiation centered at 0.67 ev.

A Ge wafer, total exposed area about 3 cm^2, was immersed in the above solution contained in a Pyrex vessel. The spacing between Ge electrode and wall of the vessel was about 1 cm. The system was enclosed in a black box to exclude external radiation.

At current densities of the order $\geq$100 ma/cm^2 a strong signal was detected by means of an Eastman Kodak Ektron lead sulfide photoconductive cell after being chopped at 90 cps.

The output of the cell was amplified, passed through a filter tuned to 90 cps, and displayed on an oscilloscope.

No signal was detected when a solution of Na_2SO_4 in H_2O was used instead of in D_2O.

The fact that there is only a small contribution from hole injection at low current densities ($<10\%$), but strong hole injection at large current densities is in agreement with the fact that cathodic etching of Ge (formation of GeH_4) is possible only at large current densities (6).

Because of the unfavorable geometry no attempt was made to measure the intensity of the signal quantitatively.

Manuscript received Oct. 18, 1960.

Any discussion of this paper will appear in a Discussion Section to be published in the December 1961 JOURNAL.

REFERENCES
1. F. Beck and H. Gerischer, *Z. Elektrochem.*, **63**, 943 (1959).
2. Iu. V. Pleskov, *Dokl. Akad. Nauk S.S.S.R.*, **126**, 111 (1959).
3. D. R. Turner, Private communication; also "Semiconductors," N. B. Hannay, Editor, ACS Monograph No. 140, Reinhold Publishing Corp. New York (1959), paper on semiconductor electrodes by J. F. Dewald.
4. W. H. Brattain and C. G. B. Garrett, *Bell Syst. Tech. J.*, **34**, 129 (1955).
5. R. Newman, *Phys. Rev.*, **91**, 1313 (1953).
6. J. Bardeleben, *Z. Phys. Chem. N. F.*, **17**, 39 (1958).

Dissolution Rate of Germanium in Aqueous Hydrogen Peroxide and Saturated Ozone Solutions

K. J. Miller

Bell Telephone Laboratories, Incorporated, Murray Hill, New Jersey

Etching solutions which remove fractional parts of a micron depth of germanium are of particular interest for cleaning Ge with thin diffused layers. Dissolution rates for Ge were determined at various temperatures in 3.4% by volume H_2O_2 solutions and in saturated aqueous ozone solutions. From these data, activation energies for the over-all dissolution process were determined.

Dissolution rates were determined by weight-loss measurements. All solutions were stirred and ther-

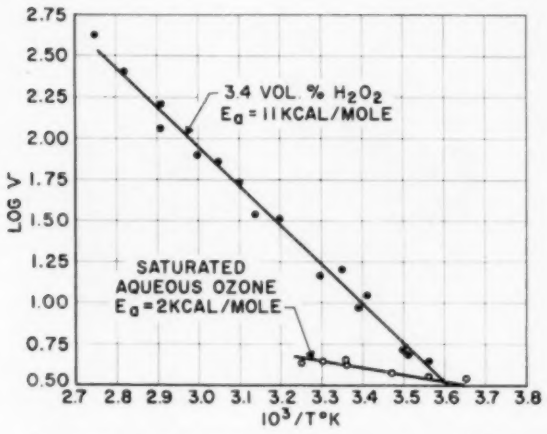

Fig. 1. Logarithm of Ge dissolution rate in $\mu g/cm^2/min$ vs. $1/T\ °K^{-1}$.

mostated to ±1°C. Solutions were of pH 5. Hydrogen peroxide solutions were made up using Merck C.P. Superoxol solution (about 30%) and concentrations were determined by titration with permanganate. Ozone solutions were prepared by bubbling oxygen-ozone, generated by a Welsbach Model T-23 laboratory ozonizer, into water. The ozone solutions were analyzed by iodometric titration. When 1.7×10^{-4} mole/l of ozone gas was bubbled into the solutions, they were analyzed to contain 0.77×10^{-5} mole/l O_3 (aq) at 15°C and 0.52×10^{-5} mole/l O_3 (aq) at 25°C. Samples were thin slabs of 2 ohm-cm p-type Ge, (111) oriented. The surface was polished with Linde B compound and CP-4 etched. The areas of samples were determined by an optical planimeter and were approximately 1.3 cm^2.

Figure 1 shows the logarithm of the dissolution rate, v ($\mu g/cm^2$ min), as a function of $1/T\ °K^{-1}$ for Ge. The relatively low value of 2 kcal/mole for the activation energy in ozone solutions is indicative that diffusion of ozone to the Ge surface is rate determining. For hydrogen peroxide solutions the activation energy for the rate-determining step was found to be 11 kcal/mole, close to the magnitude found by Camp (1) for H_2O_2-HF solutions.

Manuscript received Aug. 8, 1960; revised manuscript received Oct. 9, 1960.

Any discussion of this paper will appear in a Discussion Section to be published in the December 1961 JOURNAL.

REFERENCE

1. P. R. Camp, *This Journal*, **102**, 589 (1955).

Technical Feature

Is the Lead-Acid Storage Battery Obsolete?

Paul Rüetschi

The Carl F. Norberg Research Center,
The Electric Storage Battery Company, Yardley, Pennsylvania

The history of the lead-acid storage battery may be said to have started one hundred years ago with the famous investigations of Gaston Planté. In 1860 Planté found "that the secondary electromotive force obtained with lead plates in water, acidulated with sulfuric acid, was greater, and persisted longer than that of other combinations". Some years before Planté, Joseph Sinsteden had experimented with lead electrodes in sulfuric acid. However, it was Planté who first made a practical storage battery. Planté had no direct-reading voltmeter. He compared the voltages of his cells with that of a Bunsen element and found that "the potential varied between 1.17 and 1.45 Bunsen values." This is, in today's unit, 2.1 and 2.6 v, corresponding to the open-circuit voltage and charging voltage, respectively. Planté's cells consisted of two sheets of lead, separated by sheets of heavy linen, felt, or rubber strips. The sheets were sometimes rolled into spirals. Figure 1 shows one of these early cells. Planté called his secondary cells accumulators. He found that the capacity was increased by repeated charging and discharging. From time to time he reversed the polarity and repeated the process of charge and discharge, which treatment he called formation. For the formation process he used an acid concentration of 10%. Planté claimed that his electrodes gave 7.25 amp hr/lb of lead. Forty years after Planté, Treadwell wrote: "This result has not been exceeded in any cell of the same type on the market today."

During Planté's time the only available direct current for the formation of accumulators was from primary battery elements. This current was of course limited and expensive. However, soon after Werner von Siemens' invention of the dynamo-electric generator in 1867, steam engine driven

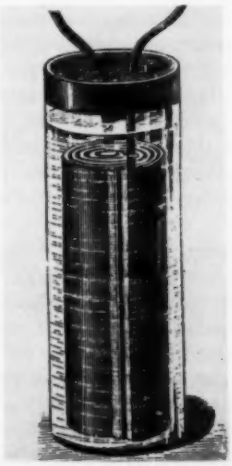

Fig. 1. Lead acid battery constructed by Plante in 1860

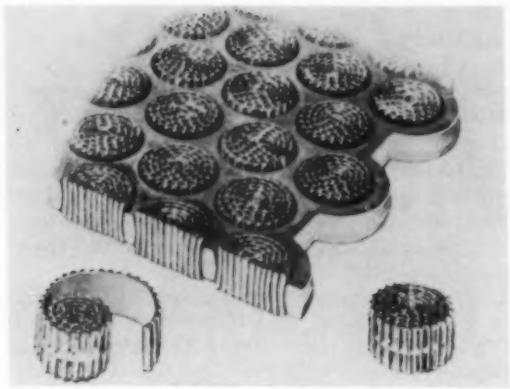

Fig. 2. "Manchester" type positive Plante-plate

Fig. 3. Electric automobile built in 1895

electric plants began to produce cheaper electric energy.

Planté published his work, which he began in 1859, in the famous article "Recherches sur l'électricité," Paris 1883. In this article, he also described flat-plate-type batteries, with groups of sheet-lead, supported in vertical position, connected to make up positive and negative groups, substantially as it is done in today's batteries. Planté's original formation procedure, namely, cycling in dilute H_2SO_4, took a considerable time, 30-40 days. Later, additives were found which accelerated the anodic attack of the forming acid and allowed faster conversion of lead to lead dioxide. The most common additives were nitric acid and nitrates, patented in 1886 by Dujardin. The action of these additives is the formation of soluble lead salts.

Planté's name has been perpetuated in connection with storage batteries by the so-called Planté-plate. This type of plate consists of an element of lead on which the active material, PbO_2, is formed electrochemically from the lead of the plate itself.

Even today, Planté-plates are still used. One of these plates, called the Manchester type, has a peculiar construction, illustrated on Fig. 2. It was introduced in 1891 (U.S. Patent 453,950—Walter). The plate comprises a grid of lead with circular holes and buttons made of spirals of corrugated pure lead ribbons. The buttons are pressed in the circular holes and the expansion due to peroxidation locks them firmly in place, producing an extended surface area. Batteries of this type have an extremely long useful service life, sometimes exceeding 30 years. Many other methods of producing large surface area plates have been proposed, for instance, by casting, but most of them have been abandoned.

Continuing through the history of the lead-acid storage battery, the most important invention next to Planté's came in 1881 when Camille Faure and Charles Brush patented the application of pasted, finely divided lead compounds to a carrier, or framework of lead, as a means of forming a large surface area active material more rapidly. The lead compounds are mixed with liquids to form a stiff paste and then spread over suitably shaped plates or grids. Formation then converts the paste readily into lead dioxide in the positives and spongy metallic lead in the negatives. Most plates made today are of this type.

A further important contribution to the battery art came in 1882 when Sellon recommended the use of a lead-antimony alloy for the grids or carriers of the active materials.

It is interesting to note that one of the first applications of the lead-acid storage battery was the electric automobile. In the 1890's gasoline operated automobiles developed by Daimler showed many weaknesses; the highest speed reached during car races was about 15 mph. At this time, electric motors were well developed and electrically operated cars could compete favorably with gasoline driven cars. France, in particular the "Compagnie Générale de Voitures," was leading in the development of electric cars. In 1895 Jeantaud ran an electric automobile from Paris to Bordeaux, a distance of 600 km, during which the batteries were frequently exchanged. The replacement of "horse and buggy" with electric cars seemed to be a complete success. Around 1895 some electric cars were built in Chicago. One of these cars is shown in Fig. 3. Another car, built about 1904 in Berlin by Bergmann Elektrizitätswerke, is shown in Fig. 4.

Why did the electric automobile lose the battle against the gasoline driven vehicle? The answer is

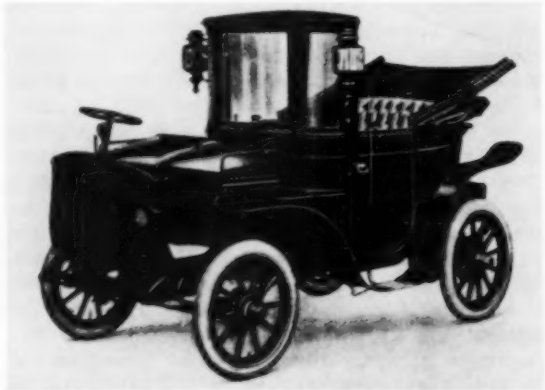

Fig. 4. "Convertible" electric automobile made in Germany 1904.

simple. The batteries were too bulky and too heavy. The batteries for an electric car should be extremely compact, light, inexpensive. A long cycle life must be paired with high power output per unit weight and volume. The problems today are exactly the same.

It seems, at first sight, that nothing essential has been added to the lead-acid storage battery since 1900. However, a closer look shows that many improvements have been made. Although the basic system remains, the developments of the past 60 years are impressive. They comprise improved lead alloys and casting techniques for the grids, better and finer oxides for the pastes, higher utilization of lead in the active materials, negative paste formulations containing expanders, stronger, lighter and more durable containers, improved microporous separators, higher power output per unit weight and volume, and above all, an understanding of the thermodynamics and kinetics of the electrochemistry of the $PbO_2/PbSO_4$ and $Pb/PbSO_4$ electrode systems. Since 1900 a large variety of lead-acid storage batteries have been manufactured for many different applications. They range from small telephone cells to very large submarine cells. The size of the latter is demonstrated in Fig. 5.

With regard to construction, most storage batteries have pasted, flat plates, as illustrated in Fig. 6. The negative plates and the positive plates are made by applying a paste of lead oxide and sulfuric acid to a grid of antimonial lead. A separator of a microporous material isolates positives and negatives from each other.

Another plate-type is the so-called "Ironclad"[1] construction. As shown in Fig. 7, the positive plate consists of vertical tubes, which are slotted, perforated or otherwise porous and made of rubber, glass, PVC, or polyethylene. The active material is contained in the tubes. In the center of each tube there is a thin lead-antimony rod, forming the core for the pencil of active material in the tube. Ironclad batteries have exceptionally good cycle life.

To give an idea of the magnitude of today's storage battery industry, estimated retail battery sales in the United States for the year 1959 are given in Table I. The yearly production of about 30,000,000 automobile batteries has been steady over the past 10 years. Out of these, about 24,000,000 are replacement batteries and about 6,000,000 are for original equipment.

It is quite appropriate on this centennial of the first practical lead-acid storage battery to review the field of packaged power and to evaluate the potential threat posed by more prominent competitive battery systems. Is the lead-acid battery obsolete? Why is it still widely used today, 100 years after its introduction by Planté? Why is it not replaced by other more "modern" systems?

If we are to consider any of the rival systems as possible replacements for all, or even a significant part of the lead-acid production, because of any superior electrochemical performance, then let us have a look at the availability of materials. Shown in Table II are the figures on national and world

[1] T.M. Reg., The Electric Storage Battery Co.

Fig. 5. Early submarine lead-acid cell

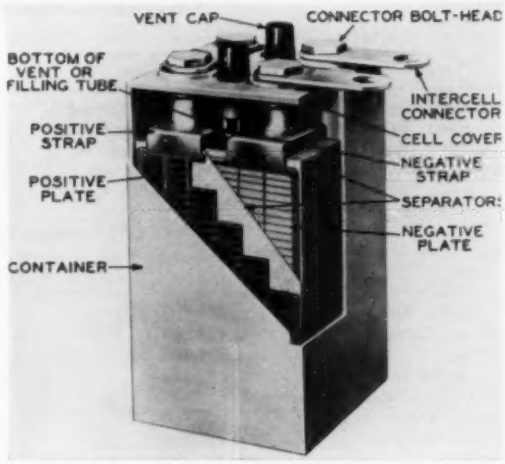

Fig. 6. Construction of lead-acid battery with flat, pasted plates.

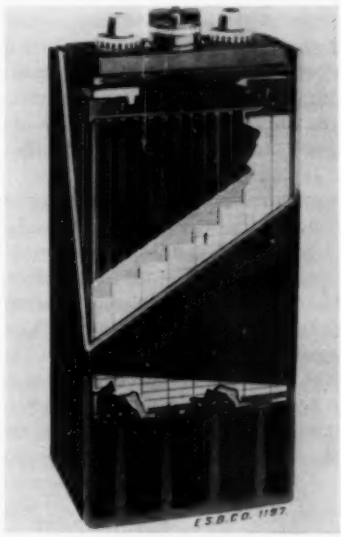

Fig. 7. "Ironclad" lead-acid battery construction

Table I. Estimated battery sales in the United States—1959

Lead acid	Nickel cadmium nickel iron	Silver zinc	Primary cells
$625,000,000 including more than 30,000,000 automotive batteries valued at $400,000,000	$20,000,000 including a large number of hermetically sealed cells of the button type	$18,000,000 mostly for military purposes	$150,000,000 comprising about 1.5 billion units of the LeClanché type and 30,000,000 HgO/Zn batteries valued at $30,000,000

Table II. 1959 Production figures for battery metals (in 2000 lb)

	Lead	Nickel	Cadmium	Silver	Zinc
USA production	239,400	11,600	4,300	800	417,000
World production	2,420,200	309,000	10,000	7,900	3,071,000
USA use	1,091,100	112,700	7,000	4,900	933,800
USA use for batteries	380,700	600	100	120	25,000
Percentage of use	34.9	0.5	1.4	2.5	2.7
Average price ($ per lb)	0.122	0.74	1.40	13.30	0.115

production of metals used in batteries in 1959. These figures are quite revealing.

If it is assumed that but 30% of the lead used in lead-acid batteries enters into the electrochemical reactions in the cells, the remainder being used for grids, post, connectors, and "inactive" active materials, the amount of lead used annually in the United States for the electrochemically active component of lead-acid batteries would be 30% of 380,700 or 114,200 tons.

We can now calculate how much cadmium would be required annually to replace the lead-acid battery market by nickel-cadmium batteries by making the not necessarily accurate assumption of equal substitution on a watthour basis. Taking into account the difference in molecular weights, the different voltage levels, and the fact that cadmium is used only in the negatives, one calculates that about 45,000 tons of cadmium would be required. This requirement represents about four times the world's annual production, or about ten times the annual output in the United States. Similar considerations apply to silver. Battery usage is so widespread today that any system to be widely used is restricted to materials which are plentiful. Of course this does not mean that the Ni-Cd and the Ag-Zn systems do not have a place in several large specialized markets, which are extremely attractive. In consideration of the choice of a battery system best to fulfill requirements of an application many factors other than capacity must be weighed. Usually it is a compromise of many characteristics among which are weight, volume, availability, rechargability, cycle life, stand life, cost, and maintenance. In Table III are listed values for 12 v 100 Ah batteries at the 10-hr rate.

Table III. Energy data of battery systems 12 v-100 ah

System	wh/lb	wh/in.^{3}
Lead acid		
Aviation	13.1	1.0
Ironclad	13.1	1.35
Automotive	15.0	1.30
Nickel cadmium		
Pocket	11.0	0.6
Sintered	11.5	0.88
Nickel iron		
Tubular	10.6	0.92
Silver zinc	40-72	3-5
Silver cadmium	30-45	2-3

Other factors which affect the choice of a battery system are shown in Table IV. These factors include cycle life and economic considerations.

The figures in Tables III and IV show that the lead-acid battery is a most economical source of portable power. This is the reason why it is still the workhorse of the battery industry. There may, of course, be particular instances where price considerations must be abandoned. The nickel-cadmium battery lends itself to fabrication in hermetically sealed containers, which offers advantages for application in outer space, where open cells cannot be used. The nickel-iron battery needs less maintenance than the lead-acid battery and has a longer useful life which would make it more practical where servicing or replacement is difficult. On the other hand, there are cases where the weight of

Table IV. Comparison of battery systems 12 v-100 Ah. Complete cycles at controlled potential recharge

Battery type	Estimated life	Estimated initial cost, $	Cost per year, $	Cost per cycle, ¢
Lead acid				
Automotive	3 years 300 cycles	40.00	13.00	13
Industrial	5-10 years 1600 cycles	70.00	9.00	4.3
Nickel cadmium				
Pocket	10-20 years 2000 cycles	150.00	6.00	7.5
Sintered	10-20 years 3000 cycles	300.00	20.00	10
Nickel iron				
Tubular	15-20 years 2000 cycles	130.00	7.50	6.5
Silver zinc	1 year 200 cycles	800.00	800.00	400
Silver cadmium	2-3 years 1000 cycles	1000.00	400.00	100

the battery, or rather the watt hours per pound figure, becomes all-important as for applications in outer space. Here, the silver-zinc storage battery will be preferred. So far we have considered the challenge to the lead-acid battery posed by electrochemical systems which are generally considered as storage batteries. What now is the chance of the newer, more exotic packaged power devices, like nuclear batteries, solar cells, thermoelectric and thermoionic generators, and fuel cells, to replace lead-acid storage batteries?

Using a Sr-90 nuclear heat source and a lead-telluride thermoelectric generator, one could build a packaged power unit delivering 100 w for 10 years. The unit would only weigh 380 lb which amounts to 22,000 wh/lb, but the cost would be high, $219,000, or $25.40 per kwh output. A thermoelectric generator, heated with 3000 curies of polonium 210, has already been demonstrated publicly. This unit realized 1600 wh/lb over the first half-life (138 days).

Because of the high price of the radioactive fuel, the application of such devices will be seriously limited to very special cases of long term operation without additional energy supply. Thermoelectric cells will suffer generally from efficiency limitations imposed by the thermal cycle. Solar converters can convert up to 13% of the energy of sunlight into electricity. Operated in conjunction with rechargable storage batteries, they make economic power sources for long term application. However, relatively large collector areas are required, because of the low energy density of sunlight, and the cost for efficient collector materials, such as silicon, is prohibitive for large power output, namely, in the order of $40,000 per kw.

There has been a great amount of publicity relative to the fuel cell, creating widespread interest and excitement, which has resulted in many extravagant claims. In fact, many problems must still be solved in making fuel-cells commercially feasible. In particular, for large-scale use, the capital investment per kwh must become competitive with the one for storage batteries. Moreover, inexpensive fuels must be utilized in a practical cell since the

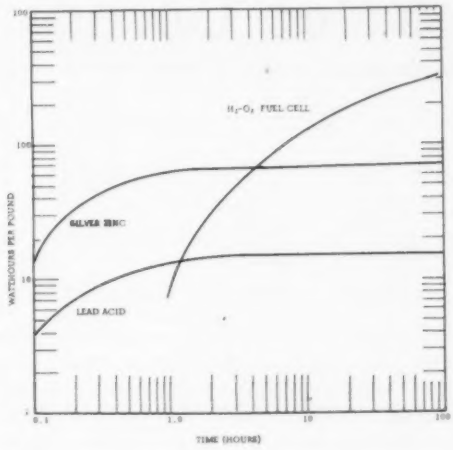

Fig. 8. Comparison of energy output of battery systems and hydrogen-oxygen fuel cells.

electric energy derived from fuels like H_2 and O_2, will be more expensive than the energy from power-lines, which can be used efficiently to recharge light-weight storage batteries. In discussing the application of fuel cells it must also be considered that regardless of the watt-hour capacity of the unit, there is a definite fixed weight and volume attributable to the reactor only, apart from the fuels, which is determined by the peak power output. The fuel cell is therefore at a decided disadvantage weight- and volume-wise for applications of short duration. This is illustrated in Fig. 8. Therefore, there is reason to believe that the fuel cell will create its own markets as an extension of battery application, rather than as a replacement. We must conclude that Planté's invention will continue to maintain its position in the storage battery field, and will be used for years to come as a source of cheap dependable packaged power.

Manuscript received Oct. 10, 1960. This paper was prepared for delivery before the Houston Meeting, Oct. 9-13, 1960.

Any discussion of this paper will appear in a Discussion Section to be published in the December 1961 JOURNAL.

Brief Communications

The JOURNAL accepts short technical reports having unusual importance or timely interest, where speed of publication is a consideration. The communication may summarize results of important research justifying announcement before such time as a more detailed manuscript can be published. Consideration also will be given to reports of significant unfinished research which the author cannot pursue further, but the results of which are of potential use to others. Comments on papers already published in the JOURNAL should be reserved for the Discussion Section published biannually.

Submit communications in triplicate, typewritten double-spaced, to the Editor, Journal of The Electrochemical Society, 1860 Broadway, New York 23, N. Y.

Brief Communication

Brookite Film on Titanium

S. Yamaguchi

Institute of Physical and Chemical Research, Tokyo, Japan

It was found to be impossible to identify the oxide formed anodically on the surface of titanium by the aid of reflection electron diffraction. As a matter of fact, we observed here only an "amorphous" pattern. In the present study, the author has separated the oxide film from the titanium substrate for electron transmission experiments and has used hard electrons (wave length: 0.0272Å) in order to obtain an analyzable diffraction pattern.

The surface of a plate of pure Ti (thickness: 0.2 mm) was oxidized by an anodic process. Electrolyte: H_2SO_4 (50% by weight); current density: 30 $\mu a/cm^2$; duration of electrolysis: 5 hr. The surface of the specimen thus treated showed a blue interference color. The oxide layer was separated from the substrate by means of the Mahla-Nielsen procedure, *i.e.*, by immersing the specimen in a methanol-bromine solution (1). The methanol used was rigorously freed of water. The thickness of the isolated film was about 3000Å. A diffraction pattern obtained from this oxide film consisted of diffuse rings, but it was analyzable enough to identify the oxide in question. In Table I, the interplanar spacings measured are compared with those of the brookite crystal determined by Hickman and Gulbransen (2). In this table we see good agreement between the specimen and brookite. According to the width of the diffraction rings from the specimen, the particle size of the brookite crystallites was about 50Å. Since the dielectric constant of brookite is lower than that of rutile or anatase, the surface of titanium treated by the anodic process is somewhat inferior as an electric condenser.

Table I

d, Å*	d of brookite (2) †
3.46 (4)	3.46 (6)
3.20 (10)	3.22 (10)
2.87 (4)	2.87 (6)
2.46 (6)	2.45 (8)
	2.17 (2)
1.88 (4)	1.881 (3)
	1.842 (1)
1.68 (10)	1.681 (10)
	1.654 (1)
1.62 (8)	1.619 (6)

* d, the interplanar spacings of the oxide film formed anodically on Ti.

† No. in parentheses is intensity of the diffraction rings in arbitrary scale; several weak rings omitted.

Manuscript received Oct. 7, 1960.

Any discussion of this paper will appear in a Discussion Section to be published in the December 1961 JOURNAL.

REFERENCES

1. E. M. Mahla and N. E. Nielsen, *J. Appl. Phys.*, **19**, 379 (1948).
2. J. W. Hickman and E. A. Gulbransen, *Anal. Chem.*, **20**, 158 (1948).

Manuscripts and Abstracts for Fall 1961 Meeting

Papers are now being solicited for the Fall Meeting of the Society, to be held at the Statler Hotel in Detroit, Mich., October 1, 2, 3, 4, and 5, 1961. Technical sessions probably will be scheduled on Batteries, Corrosion (including a Symposium on Surface Structure vs. Corrosion Behavior), Electrodeposition (including symposia on Addition Agents and on Electrodeposited Magnetic Films), Electronics (Semiconductors), Electro-Organics, and Electrothermics and Metallurgy.

To be considered for this meeting, triplicate copies of abstracts (*not exceeding 75 words in length*) must be received at Society Headquarters, 1860 Broadway, New York 23, N. Y., *not later than May 15, 1961. Please indicate on abstract for which Division's symposium the paper is to be scheduled and underline the name of the author who will present the paper.* No paper will be placed on the program unless one of the authors, or a qualified person designated by the authors, has agreed to present it in person. An author who wishes his paper considered for publication in the JOURNAL should send triplicate copies of the manuscript to the Managing Editor of the JOURNAL, 1860 Broadway, New York 23, N. Y.

Presentation of a paper at a technical meeting of the Society does not guarantee publication in the JOURNAL. However, all papers so presented become the property of The Electrochemical Society, and may not be published elsewhere, either in whole or in part, unless permission for release is requested of and granted by the Editor. Papers already published elsewhere, or submitted for publication elsewhere, are not acceptable for oral presentation except on invitation by a Divisional program Chairman.

Guide for the Preparation and Publication of Synopses

Provided by United Nations Educational, Scientific, and Cultural Organization (UNESCO)

1. "Synopsis" is a term adopted by the Royal Society of London (in fulfillment of a recommendation of the Scientific Information Conference sponsored by the Society in 1948) and by the Unesco International Conference on Science Abstracting, 1949, to describe an author's summary of a scientific paper which is published simultaneously with the paper itself after editorial scrutiny by the editor of the journal in which it is published.

2. The purpose of a synopsis is not only to convenience the readers of the journal in which it is published, but also to reduce the cost and to expedite the work of the abstracting journals, and thus to contribute to the general improvement of informational services in the scientific field.

3. The synopsis should comprise a brief and factual summary of the contents and conclusions of the paper, a pointer to any new information which it may contain, and an indication of its relevance. It should enable the busy reader to decide more surely than he can from the mere title of the paper whether it merits his reading it.

4. The author of every paper is consequently requested to provide also a synopsis of it, in accordance with the following suggestions.

Style of Writing

5. Use complete sentences rather than a mere list of headings. Any reference to the author of the article should be in the third person. Standard rather than proprietary terms should be used. Unnecessary contractions should be avoided. It should be presumed that the reader has some knowledge of the subject but has not read the paper. The synopsis should therefore be intelligible in itself without reference to the paper. (For example, it should not cite sections or illustrations by their numerical references in the text.)

Content

6. As the title of the paper is usually read as part of the synopsis, the opening sentence should be framed accordingly so as to avoid repetition of the title. If, however, the title is not sufficiently indicative, the opening sentence should indicate the subjects covered. Usually, the beginning of a synopsis should state the objects of the investigation.

7. It is sometimes valuable to indicate the treatment of the subject by words such as: brief, exhaustive, theoretical, etc.

8. The synopsis should indicate newly observed facts, conclusions of an experiment or argument, and, if possible, the essential parts of any new theory, treatment, apparatus, technique, etc.

9. It should contain the names of any new compound, mineral species, etc., and any new numerical data such as physical constants; if this is not possible, it should draw attention to them. It is important to refer to new items and observations, even though some may be incidental to the main purpose of the paper; such information may otherwise be hidden although in fact it might be very useful.

10. When giving experimental results the synopsis should indicate the methods used; for new methods the basic principle, range of operation, and degree of accuracy should be given.

References, Citations

11. If it is necessary to refer in the synopsis to earlier work, the reference should always be given in the same form as in the paper; otherwise, references should be omitted.

12. Citations to scientific journals should be made in conformity with the standard practice of the journal for which the paper is written. (The International Conference on Science Abstracting has recommended the standard proposed by the International Organization for Standardization, Technical Committee 46, names of journals being abbreviated as in the *World List of Scientific Periodicals.*)

Length

13. The synopsis should be as concise as possible. It should only in exceptional cases exceed 200 words, so as—among other things—to permit it, when printed, to be cut out and mounted on a 3 × 5 inch card.

Publication—Language and Format

14. The International Conference on Science Abstracting has recommended that synopses be published in one of the more widely used languages, no matter what the original language of the paper, in order to facilitate its international usefulness.

15. The International Conference on Science Abstracting also commended the practice of certain journals in which all the synopses appearing in a single issue are printed together either inside the cover or with advertisements on the back in such a way that they can be cut out and mounted on index cards for reference without mutilating pages of the journal itself. For this purpose the synopses should be not more than about 4 inches wide so as to be mounted on 3 × 5 inch cards.

The Electrochemical Society

INSTRUCTIONS TO AUTHORS OF PAPERS

(Revised as of 1/1/61)

Address all correspondence to the **Editor**, JOURNAL OF THE ELECTROCHEMICAL SOCIETY, 1860 BROADWAY, NEW YORK 23, N. Y.

GENERAL

Manuscripts must be submitted in triplicate to expedite review. They should be typewritten, double-spaced, with 2½-4 cm margins.

Title should be brief, followed by the author's name and business or university connection. Authors should be as brief as is consistent with clarity and should omit introductory or explanatory material which may be regarded as familiar to specialists in the particular field. Proprietary and trade names should be avoided if possible; if used, they should be capitalized to protect the owners' rights.

Authors may suggest qualified reviewers for their papers, but the JOURNAL reserves the right of final choice.

TYPES OF ARTICLES

Technical Articles must describe original research of basic nature and must have adequate scientific depth. Articles of wide diversity of interest are appropriate, but subjects primarily covered in other specialized journals (*e.g.*, analytical or nuclear chemistry) are not considered appropriate. An ***Abstract*** of about 100 words should state the scope of the paper and summarize its results. Suitable headings and subheadings should be included, but sections should not be numbered. Articles in recent issues of the JOURNAL should be consulted for current style.

Technical Notes are used for reporting briefer research, developmental work, process technology; new or improved devices, materials, techniques, or processes which do not involve more basic scientific study. No abstract is required.

Brief Communications are used only to report new information of scientific or technological importance which warrants rapid dissemination.

ILLUSTRATIONS

Drawings and ***Graphs*** ordinarily will be reduced to column width, 8.3 cm, and after such reduction should have lettering no less than 0.15 cm high. Lettering must be of letter-guide quality. India ink on tracing cloth or paper is preferred, but India ink on coordinate paper with blue ruling is acceptable. The sample graph shown on the reverse page conforms to suggestions of the American Standards Association (ASA Report Y15.1-1959).

Photographs should be used sparingly, must be glossy prints, and should be mailed with protection against folding. ***Micrographs*** should have a labeled length unit drawn or pasted on the picture.

Captions for figures (including photographs) must be included on a separate sheet. Captions and figure numbers must *not* appear in the body of the figure; they will be removed if they do.

Numerical Data should not be duplicated in tables and figures.

EQUATIONS

Mathematical Equations should be written on a single line if possible, and parentheses, brackets, the solidus (/), negative exponents, etc., may be used freely for this purpose. Authors are urged to consult Chapter VI of the "Style Manual" of the American Institute of Physics (available for $1.00 at American Institute of Physics, 57 East 55 St., New York 22, N. Y.) and to follow the patterns described there.

SYMBOLS

If more than a few ***Symbols*** are used, they should be defined in a list at the end of the paper, with units given. For example:

$a, b \ldots =$ empirical constants of Brown equation

$f_i^\circ =$ fugacity of pure ith component, atm

$D_v =$ volume diffusion coefficient, cm^2/sec

ABBREVIATIONS

The AIP "Style Manual" referred to here gives a suitable list of common ***Abbreviations***. Units usually will be abbreviated without periods throughout the text, as sec, min, hr, cm, mm, etc.

UNITS

Metric Units should be used throughout, unless English units are clearly more appropriate in the area of discussion.

POTENTIAL SIGNS

Electrode Potentials: Authors are urged to state and make use of the polarity of test electrodes with respect to the reference electrode used, *i.e.*, Zn is normally negative, Cu normally positive with respect to the standard hydrogen electrode. The sign for the emf of a cell should conform to the free energy change of the chemical reaction as written or implied, in accordance with the definition $\Delta G = -nFE$. These suggestions agree with the IUPAC conventions adopted in 1953. If any other convention is used, it should be stated clearly and used consistently throughout the manuscript.

REFERENCES

Literature References should be listed on a separate sheet at the end of the paper in the order in which they are cited in the text. Authors' initials must be given, and the style and abbreviations adopted by *Chemical Abstracts* should be used. Any recent issue of the JOURNAL may be consulted.

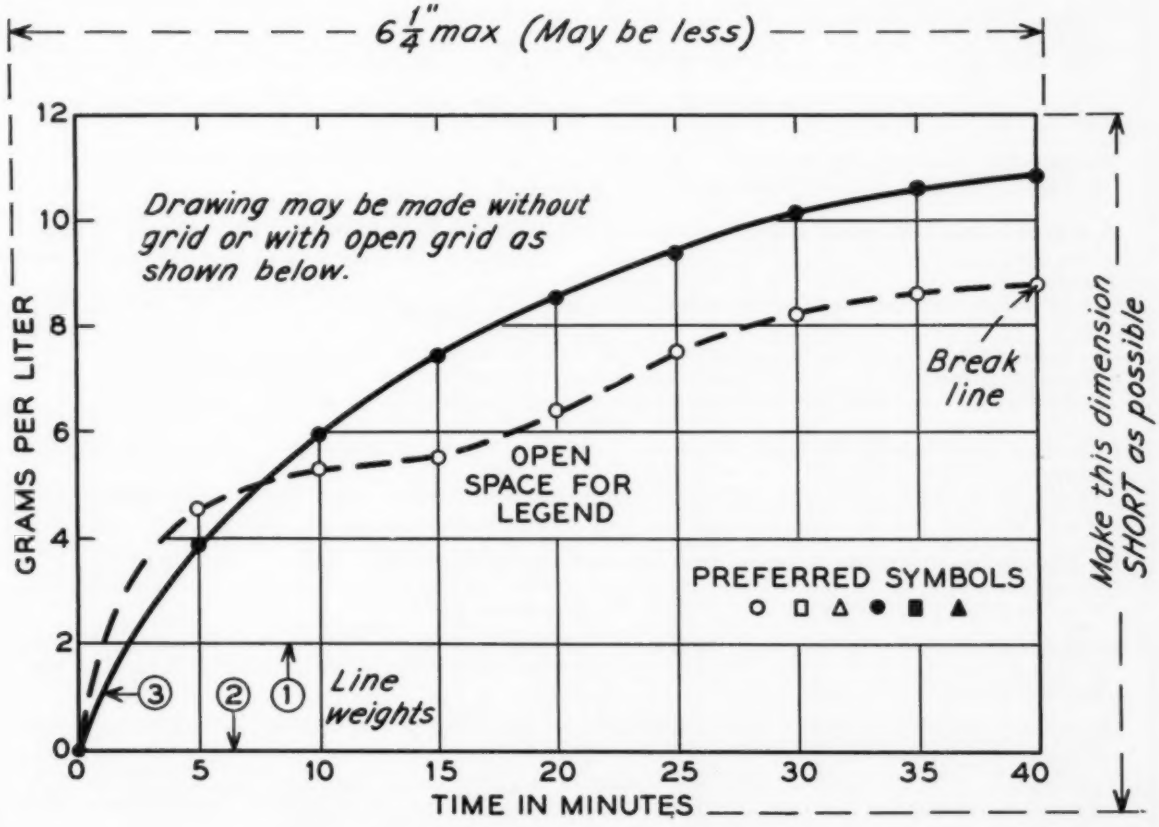

Remarks: Line weight 2 is used for borders and zero lines. When several curves are shown, each may be numbered and described in the caption. Lettering shown is approximately ⅛ in. In plotting current or potential as ordinate, increasing negative values should go down.

SAMPLE CURVE DRAWING FOR REDUCTION TO $\frac{1}{2}$ SIZE

Monographs of The Electrochemical Society

ECS Series

The following are books developed and sponsored by The Electrochemical Society and published by John Wiley & Sons, Inc., 440 Fourth Ave., New York 16, N. Y. Members of The Electrochemical Society can receive a 33 1/3% discount by ordering volumes from Society Headquarters, 1860 Broadway, New York 23, N. Y. Book and invoice will be mailed by John Wiley & Sons. Nonmembers (including subscribers) should order direct from Wiley.

Corrosion Handbook. Edited by Herbert H. Uhlig. Published 1948, 1188 pages, **$16.00**

Modern Electroplating. Edited by Allen G. Gray. Published 1953, 563 pages, **$8.50**

Abstracts of the Literature on Semiconducting and Luminescent Materials and Their Applications. Compiled by Battelle Memorial Institute.

Vol. I, 1953 Issue—published 1955, 169 pages, **$5.00** (soft cover)

Vol. II, 1954 Issue—published 1955, 200 pages, **$5.00** (soft cover)

Vol. III, 1955 Issue—Edited by E. Paskell; published 1957, 322 pages, **$10.00** (hard cover)

Vol. IV, 1956 Issue—Edited by E. Paskell; published 1959, 456 pages, **$12.00** (hard cover)

Vol. V, 1957 Issue—Edited by C. S. Peet; published 1960, 449 pages, **$12.00** (hard cover)

Vol. VI, 1958 Issue—Edited by J. J. Bulloff and C. S. Peet; published 1961, 528 pages, **$14.00** (hard cover)

Electrochemistry in Biology and Medicine. Edited by Theodore Shedlovsky. Published 1955, 369 pages, **$11.50**

Vapor Plating (The Formation of Metallic and Refractory Coatings by Vapor Deposition), by C. F. Powell, I. E. Campbell, and B. W. Gonser. Published 1955, 158 pages, **$5.50**

High-Temperature Technology (Materials, Methods, and Measurements). Edited by I. E. Campbell. Published 1956, 526 pages, **$15.00**

Stress Corrosion Cracking and Embrittlement. Edited by W. D. Robertson. Published 1956, 202 pages, **$7.50**

Arcs in Inert Atmospheres and Vacuum. Edited by W. E. Kuhn. Published 1956, 188 pages, **$7.50**
(Papers Presented at the Symposium on Arcs in Inert Atmospheres and Vacuum of the Electrothermics and Metallurgy Division of The Electrochemical Society, April 30 and May 1, 1956, San Francisco, Calif.)

Technology of Columbium (Niobium). Edited by B. W. Gonser and E. M. Sherwood. Published 1958, 120 pages, **$7.00**
(Papers Presented at the Symposium on Columbium—Niobium of the Electrothermics and Metallurgy Division of The Electrochemical Society, May 15 and 16, 1958, Washington, D. C.)

The Structure of Electrolytic Solutions. Edited by Walter J. Hamer. Published 1959, 441 pages, **$18.50**
(Based on a Symposium held in Washington, D. C., in May 1957, sponsored by The Electrochemical Society, New York, and The National Science Foundation, Washington, D. C.)

Mechanical Properties of Intermetallic Compounds. Edited by J. H. Westbrook. Published 1959, 435 pages, **$9.50**
(A Symposium, Sponsored by the Electrothermics and Metallurgy Division of The Electrochemical Society, May 4, 5, and 6, 1959, Philadelphia, Pa.)

The Surface Chemistry of Metals and Semicoductors. Edited by Harry C. Gatos, with the assistance of J. W. Faust, Jr., and W. J. La Fleur Published 1960, 526 pages, **$12.50**

[Proceedings of an International Symposium Sponsored Jointly by the Office of Naval Research and The Electrochemical Society, Inc. (Corrosion and Electronics Divisions), October 19, 20, and 21, 1959, Columbus, Ohio]

Vacuum Metallurgy

Vacuum Metallurgy, third printing, 1958. Edited by J. M. Blocher, Jr.; 216 pages; **$5.00, less a 20% discount** to ECS members only. Available from Electrochemical Society Headquarters, 1860 Broadway, New York 23, N. Y.
(Papers Presented at the Vacuum Metallurgy Symposium of the Electrothermics and Metallurgy Division of The Electrochemical Society held in Boston, Mass., October 6 and 7, 1954)

Indianapolis Meeting

THE ELECTROCHEMICAL SOCIETY

One Hundred and Nineteenth Meeting

April 30, May 1, 2, and 3, 1961

Sunday through Wednesday

CONDENSED TECHNICAL PROGRAM

Monday, May 1, 1961

Battery—Industrial Electrolytic—Theoretical Electrochemistry (Abstracts 99-103) 9:00 A.M.-11:30 A.M. (Assembly Hall, 8th floor)
Battery—Industrial Electrolytic (Abstracts 104-108) 2:30-4:45 P.M. (Assembly Hall, 8th floor)
Electric Insulation (Abstracts 1-7) 9:00-11:30 A.M.; 2:00-5:00 P.M. (Tower Room, 9th floor)
Electronics-Luminescence (Abstracts 22-35) 9:00 A.M.-12:00 M.; 2:00-4:55 P.M. (Sky Room, 9th floor)
Electronics-Semiconductors (Abstracts 41-52) 9:30 A.M.-12:00 M. (Riley Room, Mezzanine)
Electrothermics and Metallurgy (Abstracts 76-79) 2:00-4:00 P.M. (Florentine Room, Mezzanine)
Industrial Electrolytic—Theoretical Electrochemistry—Battery (Abstracts 99-103) 9:00 A.M.-11:30 A.M. (Assembly Hall, 8th floor)
Industrial Electrolytic—Battery (Abstracts 104-108) 2:30-4:45 P.M. (Assembly Hall, 8th floor)
Theoretical Electrochemistry—Industrial Electrolytic—Battery (Abstracts 99-103) 9:00 A.M.-11:30 A.M. (Assembly Hall, 8th floor)
Theoretical Electrochemistry (Abstracts 127-132) 2:00-5:00 P.M. (Lincoln Room, 14th floor, Sheraton-Lincoln Hotel)

Tuesday, May 2, 1961

Battery—Industrial Electrolytic (Abstracts 109-116) 9:00-11:45 A.M.; 2:00-4:30 P.M. (Assembly Hall, 8th floor)
Electric Insulation (Abstracts 8-15) 9:30-11:30 A.M.; 2:00-4:00 P.M. (Tower Room, 9th floor)
Electronics-Luminescence (Abstracts 36-38) 9:00-11:30 A.M. (Sky Room, 9th floor)
Electronics-Semiconductors (Abstracts 53-65) 9:00 A.M.-12:00 M.; 2:00-5:00 P.M. (Riley Room, Mezzanine)
Electrothermics and Metallurgy (Abstracts 80-88) 9:30-11:30 A.M.; 2:00-4:30 P.M. (Florentine Room, Mezzanine)
Industrial Electrolytic—Battery (Abstracts 109-116) 9:00-11:45 A.M.; 2:00-4:30 P.M. (Assembly Hall, 8th floor)
Theoretical Electrochemistry (Abstracts 133-144) 9:00 A.M.-12:00 M.; 2:00-5:00 P.M. (Lincoln Room, Sheraton-Lincoln Hotel)

Wednesday, May 3, 1961

Electric Insulation (Abstracts 16-21) 9:00 A.M.-12:00 M.; 2:00-5:00 P.M. (Tower Room, 9th floor)
Electronics-Semiconductors (Abstracts 66-75) 9:00 A.M.-11:05 A.M.; 2:00-5:00 P.M. (Riley Room, Mezzanine)
Electrothermics and Metallurgy (Abstracts 89-98) 9:00-11:30 A.M.; 2:00-4:30 P.M. (Florentine Room, Mezzanine)
Industrial Electrolytic (Abstracts 118-126) 9:30-11:45 A.M.; 2:00-4:30 P.M. (Assembly Hall, 8th floor)
Theoretical Electrochemistry (Abstracts 145-160) 9:00 A.M.-12:05 P.M.; 2:00-5:20 P.M. (Chateau Room, Lobby floor, Claypool Hotel)

GENERAL INFORMATION

Convention Headquarters is the Claypool Hotel, 14 North Illinois St., Indianapolis, Ind.

Rates per day for rooms, with bath, are: single rooms, $7.00, 8.00, 9.00; double-bed rooms, $10.50, 11.00; twin-bed rooms, $12.00, 14.00, 16.00, 18.00, 20.00; studio suite, 1 or 2 persons, $13.50; parlor suite, 1 or 2 persons, $20, 25, 30, 75.

Requests for room reservations should be mailed to the Claypool Hotel, 14 North Illinois St., Indianapolis, Ind. If accommodations are not available at the Claypool, that hotel will make suitable reservations for you at a nearby hotel at a comparable price.

BE SURE to state that you will be attending The Electrochemical Society Meeting. If your wife will be attending, be sure to so indicate on your request for reservations.

The Office of the Secretary is Parlor S, Mezzanine.

The Indianapolis Local Section Office is Parlor E, Mezzanine.

The Ladies' Headquarters is the Louis XIV Room, Mezzanine.

REGISTRATION

The Registration Desk will be on the Mezzanine Sunday through Wednesday, April 30 through May 3, 1961.

The registration schedule is:

Sunday, April 30—3:00 to 9:00 P.M.
Monday, May 1—7:30 A.M. to 5:00 P.M.
Tuesday, May 2—8:00 A.M. to 4:00 P.M.
Wednesday, May 3—8:00 A.M. to 12:00 M.

Registration fees are:

Technical Session Registration (Men and Women)	
Member	$ 7.00
Nonmember Speakers and Coauthors	7.00
Nonmembers	20.00*
Student Members	Complimentary
Student Nonmembers	2.00
Wednesday Only	5.00
Ladies' Registration Fee for Social Events	5.00

* If a nonmember fills out an application form and subsequently is elected to membership in the Society, the difference between the nonmember and member registration fee will be applied to his first year's dues. If his membership begins on January 1 he is entitled to the entire differential; if his membership begins on July 1, he is entitled to half the differential.

INFORMATION ABOUT INDIANAPOLIS

Indianapolis, state capital of Indiana, is the most centrally located large city in the United States from the standpoint of population distribution. According to the Federal Bureau of Census, the exact center of population of the entire country is only a few miles south and west of Indianapolis. Visitors should find many places of interest in and around the city.

Information about places of interest will be available at the Registration Desk and Local Section Headquarters, Parlor E, Mezzanine.

SYMPOSIA

The Electric Insulation Division has scheduled symposia on: Thin Dielectric Films on Monday, May 1; and on Epoxy Resins on Tuesday and Wednesday, May 2 and 3; all sessions in the Tower Room, 9th floor.

The Electronics Division-Luminescence Group has scheduled 3 sessions, two on Monday, one on Tuesday morning; all in the Sky Room, 9th floor.

The Electronics Division-Semiconductor Group has scheduled symposia on: Crystal Growth and Structure, Monday morning; Semiconductor Surfaces, Monday afternoon; Compound Semiconductors, Tuesday morning; Device Processing and Characterization, Tuesday afternoon; Diffusion—Oxidation, Wednesday morning; and Etching, Wednesday afternoon; all sessions in the Riley Room, Mezzanine.

The Electrothermics and Metallurgy Division has scheduled a session on High-Temperature Materials; Extractive Metallurgy on Monday afternoon; and a symposium on Ultrafine Particles, Production on Tuesday; Properties on Wednesday morning; and Particle Size Measurement and Surface Effects on Wednesday afternoon; all sessions in the Florentine Room, Mezzanine.

The Industrial Electrolytic—Theoretical Electrochemistry—Battery Divisions have scheduled a Joint Symposium on Fuel Cells on Monday morning, Assembly Hall, 8th floor.

The Industrial Electrolytic—Battery Divisions have scheduled a Joint Symposium on Fuel Cells Monday afternoon and Tuesday, Assembly Hall, 8th floor.

The Industrial Electrolytic Division has scheduled two general sessions on Wednesday, both in the Assembly Hall, 8th floor.

The Theoretical Electrochemistry Division has scheduled a Symposium on Modern Instrumentation and Techniques of Electrochemical Measurements sponsored by the National Science Foundation—ECS on Monday afternoon, Tuesday, and Wednesday morning; Monday and Tuesday sessions in the Lincoln Room, 14th floor, Sheraton-Lincoln Hotel, Wednesday morning session in the Chateau Room, Lobby floor, Claypool Hotel. The Division has also scheduled a general session Wednesday afternoon in the Chateau Room, Lobby floor, Claypool Hotel.

GENERAL FUNCTIONS

Symposia Chairmen Breakfasts

Special breakfasts will be held for Symposia Chairmen on Monday, Tuesday, and Wednesday, May 1, 2, and 3. On the day on which he presides at a technical session, each Symposium Chairman should be in the Main Dining Room, Lobby floor, **at 7:45 A.M.**

Monday Evening Mixer

There will be a Monday evening social get-acquainted gathering in the Riley Room, Mezzanine, from 8:00 to 10:00 P.M. All those registered for The Electrochemical Society Meeting are invited to attend. Beer, soft drinks, and snacks will be served on a complimentary basis. Admission is by registration badge.

Tuesday Society Luncheon and Business Meeting

The Electrochemical Society Luncheon and Business Meeting will be held at 12:15 P.M. on Tuesday, May 2, in the Travertine Room, 14th floor, Sheraton-Lincoln Hotel, 117 W. Washington St.

Tuesday Evening Reception and Banquet

A reception honoring Dr. and Mrs. Ralph Schaefer will be held at 6:30 P.M. on Tuesday, May 2, in the Riley Room, Mezzanine. Cocktails will be served from 6:30 to 7:30 P.M., followed by dinner. Dr. Schaefer will deliver the Presidential Address.

LADIES PROGRAM

All the ladies are invited to make the Louis XIV Room, Mezzanine, their headquarters during their stay in Indianapolis. Members of the Ladies' Committee will be there to give information and assist in any way they can to make the visit to Indianapolis a pleasant one.

Monday, May 1—Coffee get-acquainted hour from 9:00 to 10:00 A.M. in the Louis XIV Room. At 10:30 A.M. a trip to scenic Brown County has been arranged, with luncheon at Indiana University followed by a tour of the new Lilly Library and points of interest on the campus. Monday evening the ladies are invited to attend the Society Mixer from 8:00 to 10:00 P.M. in the Riley Room, Mezzanine.

Tuesday, May 2—Coffee hour from 9:00 to 10:00 A.M. The rest of the day has been left free. The ladies are invited to attend the Reception and Banquet at 6:30 P.M. in the Riley Room, Mezzanine.

Wednesday, May 3—Coffee hour from 9:00 to 10:00 A.M. At 10:15 A.M. there will be a sight-seeing tour of Indianapolis, luncheon at the Columbia Club, more sightseeing in the afternoon, and at 2:30 a talk at the John Herron Institute.

LUNCHEONS AND BUSINESS MEETINGS

Electric Insulation Division Business Meeting, Monday, May 1, at 9:00 in the Tower Room, 9th floor.

Electronics Division Luncheon and Business Meeting, Monday, May 1, at 12:30 P.M. in the Riley Room, Mezzanine.

Electrothermics and Metallurgy Division Luncheon and Business Meeting, Wednesday, May 3, at 12:30 P.M. in the Empire Room, Mezzanine.

Industrial Electrolytic Division Luncheon and Business Meeting, Wednesday, May 3, at 12:30 P.M. in the Assembly Hall, 8th floor.

Theoretical Electrochemistry Division Luncheon and Business Meeting, Wednesday, May 3, at 12:30 P.M. in the Lincoln Room, 14th floor, Sheraton-Lincoln Hotel.

BOARD AND COMMITTEE MEETINGS

Sunday, April 30, 2:00 P.M.—**Board of Directors,** Empire Room, Mezzanine.

Monday, May 1, 2:00 P.M.—**National Convention Committee,** Parlor T, Mezzanine.

Monday, May 1, 4:30 P.M.—**Council of Local Sections,** Empire Room, Mezzanine.

Monday, May 1, 5:00 P.M.—**Editorial Staff of the Journal,** Parlor D, Mezzanine.

Tuesday, May 2, 5:00 P.M.—**Membership Committee,** Empire Room, Mezzanine.

Wednesday, May 3, 12:15 P.M.—Luncheon Meeting of the **General Chairman of Future Meetings,** Parlor T, Mezzanine.

COST OF VARIOUS FUNCTIONS

(other than registration)

Please buy tickets as early as possible.

Symposia Chairmen Breakfasts	Standard menu prices
Monday Evening Mixer	Complimentary
Division Luncheons	$3.00
Tuesday Society Luncheon	3.00
Tuesday Reception and Banquet	7.00
Ladies functions: Monday trip and luncheon	1.50
Wednesday trip and luncheon	1.00

JOURNALS

Copies of the January, February, March, and April issues of the "Journal of The Electrochemical Society" will be available at the Registration Desk. The price of a single copy of the "Journal" is $1.70 to members and $2.25 to nonmembers.

EXTENDED ABSTRACTS

The Electronics Division is making available an extended abstract booklet containing 1000-word abstracts of most of the papers presented before the Electronics Division at the Indianapolis Meeting. Copies will be available at the Registration Desk or may be obtained about two weeks before the meeting by request to A. E. Hardy, Radio Corp. of America, New Holland Pike, Lancaster, Pa. Price $3.50 with a discount of $00.50 per copy for orders accompanied by payment and requiring no invoice.

1961 FALL MEETING

at the

Statler Hotel
DETROIT, MICHIGAN
October 1, 2, 3, 4, and 5, 1961

Sessions probably will be scheduled on:

Batteries
Corrosion
Electrodeposition (including symposia on Addition Agents and on Electrodeposited Magnetic Films)
Electronics-Semiconductors
Electro-Organic
Electrothermics and Metallurgy

Abstracts for the Detroit Meeting (*not exceeding 75 words in length*) must reach Society Headquarters, 1860 Broadway, New York 23, N. Y., *not later than May 15, 1961* to be included in the Detroit program. Please indicate on abstract for which Division's symposium the paper is to be scheduled and underline the name of the author who will present the paper. No paper will be placed on the program unless one of the authors, or a qualified person designated by the authors, has agreed to present it in person. An author who wishes his paper considered for publication in the JOURNAL should send triplicate copies of the manuscript to the Managing Editor of the "JOURNAL," 1860 Broadway, New York 23, N. Y.

Presentation of a paper at a technical meeting of the Society does not guarantee publication in the "JOURNAL." However, all papers so presented become the property of The Electrochemical Society and may not be published elsewhere, either in whole or in part, unless permission for release is requested of and granted by the Editor. Papers already published elsewhere, or submitted for publication elsewhere, are not acceptable for oral presentation except on invitation by a Divisional program Chairman.

DISCUSSION

No recordings will be made of oral discussion. Those contributing to the discussion of a paper and desiring their remarks to be published will be supplied by the symposium chairman with a printed form on which any discussion may be written. These forms should be given to the symposium chairman or to the Managing Editor of the Journal after the session; or they can be mailed to the Managing Editor of the Journal, 1860 Broadway, New York 23, N. Y. The discussion will then be referred to the author for reply. Publication of the discussion and the comments of the author depends on publication of the article in the "Journal".

Written discussion of a published paper should be submitted within two months following publication of the article in the "Journal." A Discussion Section is published semiannually in the "Journal."

EMPLOYMENT POSTERS

Companies which desire to recruit employees at the Indianapolis Meeting will have posters to this effect on a Bulletin Board adjacent to the Registration Desks (see Registration for location). Companies are requested to confine their announcements to this Bulletin Board.

NOTE

Photographing of lantern slides, charts, etc., will be permitted unless specifically prohibited by the speaker. Photo flash and photo floods are prohibited.

Technical Program

Indianapolis Meeting

Monday A.M., May 1, 1961

BATTERY — INDUSTRIAL ELECTROLYTIC — THEORETICAL ELECTROCHEMISTRY

Joint Symposium on Fuel Cells, with C. W. Tobias presiding

(ASSEMBLY HALL, 8th floor)

SEE Industrial Electrolytic—Theoretical Electrochemistry—Battery Program.

ELECTRIC INSULATION

9:00 A.M.—Business Meeting of the Electric Insulation Division with A. J. Sherburne presiding

(TOWER ROOM, 9th floor)

Thin Dielectric Films, with C. C. Houtz presiding

(TOWER ROOM, 9th floor)

9:30 A.M.—"Electrolytic Oxide Films" by C. C. Houtz (Abstract No. 1)

10:00 A.M.—"Electrical Properties of Evaporated Aluminum Oxide Films" by E. M. DaSilva and P. White (Abstract No. 2)

10:30 A.M—"Charge Storage Effects in Tantalum Oxide Films" by Rudolf Dreiner (Abstract No. 3)

11:00 A.M.—"Polarity of Tantalum Oxide Printed Capacitors" by N. Schwartz and M. Gresh (Abstract No. 4)

ELECTRONICS—LUMINESCENCE

with E. F. Apple presiding

(SKY ROOM, 9th floor)

9:00 A.M.—"Visible Fluorescence of Rare Earth Activated Phosphors" by S. P. Keller, Invited Speaker (Abstract No. 22)

9:40 A.M.—"Studies of Color Centers Produced in Apatite Halophosphates by Shortwave Ultraviolet Radiation" by Lawrence Suchow (Abstract No. 23)

10:05 A.M.—"Luminescence of Copper-Activated Orthophosphates of the Type $ABPO_4$ (A = Ca, Sr, or Ba and B = Li, Na, or K)" by W. L. Wanmaker and H. L. Spier (Abstract No. 24)

10:25 A.M.—"Crystal Growth and Structural Study of the Barium Titanium Phosphate Phosphor" by D. E. Harrison and G. Shirane (Abstract No. 25)

10:50 A.M.—"Magnesium Lithium Antimonate Phosphors" by R. W. Mooney (Abstract No. 26)

11:15 A.M.—"Particle Size Measurement of Phosphors. A Correlation of Methods" by R. F. Quirk, E. W. Brewster, and R. C. Ropp (Abstract No. 27)

11:40 A.M.—"Measurement of Phosphor Brightness" by J. E. Eby (Abstract No. 28)

12:30 P.M.—Electronics Division Luncheon and Business Meeting, Riley Room, Mezzanine.

ELECTRONICS—SEMICONDUCTORS

Crystal Growth and Structure, with J. E. McNamara presiding

(RILEY ROOM, Mezzanine)

9:30 A.M.—"Epitaxial Growth of Germanium onto Germanium Substrates by Thermal Evaporation" by O. Weinreich, G. Dermit, and C. Tufts (Abstract No. 41)

9:50 A.M.—"Dendritic Growth in Heavily Doped Melts" by R. L. Longini (Abstract No. 42)

10:00 A.M.—"Periodic Growth in Germanium Dendrites" by R. G. Seidensticker and D. R. Hamilton (Abstract No. 43)

10:20 A.M.—Ten-minute intermission

10:30 A.M.—"Distribution Coefficient of Antimony in Silicon from Solvent Evaporation Experiments" by F. A. Trumbore, P. E. Freeland, and R. A. Logan (Abstract No. 44)

10:45 A.M.—"Structure Analysis of Semiconductor Single Crystals by Anomalous Transmission of X-Rays" by G. H. Schwuttke (Abstract No. 45)

11:10 A.M.—Recent News Papers. Titles and short abstracts will be available at the Registration Desk.

12:30 P.M.—Electronics Division Luncheon and Business Meeting in the Riley Room, Mezzanine.

INDUSTRIAL ELECTROLYTIC—THEORETICAL ELECTROCHEMISTRY—BATTERY

Joint Symposium on Fuel Cells, with C. W. Tobias presiding

(ASSEMBLY HALL, 8th floor)

9:00 A.M.—Opening Remarks by J. E. Currey

9:05 A.M.—"Mechanisms of Oxygen Producing Reactions in Molten Carbonate Electrolysis" by G. J. Janz and Fumihiko Saegusa (Abstract No. 99)

MEETING ROOM SCHEDULE

Meeting	Monday		Tuesday		Wednesday	
	AM	PM	AM	PM	AM	PM
Electric Insulation	A	A	A	A	A	A
Electronics—Luminescence	B	B	B			
—Semiconductor	C	C	C	C	C	C
Electrothermics and Metallurgy—General		D				
—Ultrafine Particles			D	D	D	D
Industrial Electrolytic					E	E
Joint Industrial Electrolytic—Theoretical Electrochemistry—Battery	E					
Joint Industrial Electrolytic—Battery		E	E	E		
Theoretical Electrochemistry		G	G	G	F	F

Claypool Hotel
A—Tower Room, 9th floor
B—Sky Room, 9th floor
C—Riley Room, Mezzanine
D—Florentine Room, Mezzanine
E—Assembly Hall, 8th floor
F—Chateau Room, Lobby floor

Sheraton-Park Hotel
G—Lincoln Room, 14th floor

9:30 A.M.—"Fuel Cell Thermodynamics" by A. J. deBethune (Abstract No. 100)
10:00 A.M.—"Temperature Coefficients of Electrode Potentials, II. The Second Isothermal Temperature Coefficient" by G. R. Salvi and A. J. deBethune (Abstract No. 101)
10:30 A.M.—"Molten Carbonate as Electrolytes" by G. J. Janz and M. R. Lorenz (Abstract No. 102)
11:00 A.M.—"The DSK System of Fuel Cell Electrodes" by E. Justi and A. Winsel (Abstract No. 103)

MONDAY P. M., MAY 1, 1961

BATTERY—INDUSTRIAL ELECTROLYTIC (cont'd)

Joint Symposium on Fuel Cells (cont'd), with J. E. Currey presiding

(ASSEMBLY HALL, 8th floor)

SEE Industrial Electrolytic—Battery Program.

ELECTRIC INSULATION (cont'd)

Thin Film Dielectrics (cont'd), with R. A. Ruscetta presiding

(TOWER ROOM, 9th floor)

2:00 P.M.—"Dielectric Properties of Evaporated Film Capacitors" by F. S. Maddocks and R. E. Thun (Abstract No. 5)
2:30 P.M.—"Physical and Dielectric Properties of Thin Film SiO_2 Capacitors" by J. A. Minahan, J. L. Sprague, and O. J. Wied (Abstract No. 6)
3:00 P.M.—"Electrical Properties of Evaporated Thin Film SiO Capacitors" by D. B. York (Abstract No. 7)
3:30 P.M.—Round Table Discussion of Thin Film Dielectrics with C. C. Houtz, E. M. DaSilva, R. Dreiner, M. Gresh, F. S. Maddocks, J. A. Minahan, N. Schwartz, J. L. Sprague, R. E. Thun, P. White, O. J. Wied, and D. B. York

ELECTRONICS—LUMINESCENCE (cont'd)

with R. E. Shrader presiding

(SKY ROOM, 9th floor)

2:00 P.M.—"Boron Nitride Phosphors" by W. Lehmann (Abstrdct No. 29)
2:25 P.M.—"Activator Solubility and Structural Transformations in ZnS:Cu,Cl" by J. W. Nickerson, P. Goldberg, and D. H. Baird (Abstract No. 30)
2:50 P.M.—"ZnS:Cu,Si Phosphors" by A. Wachtel (Abstract No. 31)
3:15 P.M.—"Luminescence of Self-Activated ZnS, ZnSCdS, and ZnSe Phosphors" by R. A. W. Gill and S. Rothschild (Abstract No. 32)
3:40 P.M.—"Decay of Cathodoluminescence and Nonradiative Processes in Manganese-Activated Phosphors" by G. F. J. Garlick and M. Sayer (Abstract No. 33)
4:05 P.M.—"Cathodoluminescent Characteristics of Manganese-Activated Potassium-Magnesium Fluoride" by R. J. Kurtz (Abstract No. 34)
4:30 P.M.—"Transparent Luminescent Films by Solution Spraying" by R. D. Kirk and J. H. Schulman (Abstract No. 35)

ELECTRONICS—SEMICONDUCTORS (cont'd)

Semiconductor Surfaces, with D. Turner presiding

(RILEY ROOM, Mezzanine)

2:10 P.M.—"Electropolishing of N-Type Germanium and P- and N-Type Silicon" by D. L. Klein, G. A. Kolb, L. A. Pompliano, and M. V. Sullivan (Abstract No. 46)
2:30 P.M.—"A Chemical Polishing Technique for Gallium Arsenide" by M. V. Sullivan and L. A. Pompliano (Abstract No. 47)
2:50 P.M.—"Electrolytic Slicing of Germanium" by Sumner Sheff (Abstract No. 48)
3:10 P.M.—"Electron Diffraction Study of Some Crystalline Films on Germanium Surfaces" by J. J. Oberly (Abstract No. 49)
3:30 P.M.—Ten-minute intermission
3:40 P.M.—"Stabilization of Semiconductor Surfaces, I. Chemical Treatment" by G. W. Cullen, J. A. Amick, and D. Gerlich (Abstract No. 50)
3:55 P.M.—"Stabilization of Semiconductor Surfaces, II. Electrical Measurements" by D. Gerlich, G. W. Cullen, and J. A. Amick (Abstract No. 51)
4:10 P.M.—"Stabilization of Germanium Surfaces, III. Chemical Analysis" by J. A. Amick, G. W. Cullen, and D. Gerlich (Abstract No. 52)
4:30 P.M.—Recent News Papers. Titles and short abstracts will be available at the Registration Desk.

ELECTROTHERMICS AND METALLURGY

High-Temperature Materials; Extractive Metallurgy, with E. M. Sherwood presiding

(FLORENTINE ROOM, Mezzanine)

2:00 P.M.—"Coatings for Columbium" by S. T. Wlodek (Astract No. 76)
2:30 P.M.—"High-Temperature Phase Studies in the Tantalum-Boron System between Ta and TaB" by J. M. Leitnaker, M. G. Bowman, and P. W. Gilles (Abstract No. 77)
3:00 P.M.—"Arc-Melting of Intermetallic, Interstitial, and Inorganic Compounds" by R. J. Van Thyne (Abstract No. 78)
3:30 P.M.—"Electrolytic Recovery of Manganese from Sulfurous Leach Liquors" by H. J. Read and J. W. Andrews (Abstract No. 79)

INDUSTRIAL ELECTROLYTIC—BATTERY (cont'd)

Joint Symposium on Fuel Cells (cont'd), with J. E. Currey presiding

(ASSEMBLY HALL, 8th floor)

2:00 P.M.—"Fuel Cells—State of the Art, 1961" by W. Mitchell (Abstract No. 104)
2:30 P.M.—"Thermodynamic Aspects of Electrochemical Fuel Cells" by M. Eisenberg (Abstract No. 105)
3:00 P.M.—Fifteen-minute intermission
3:15 P.M.—"The Fuelox Cell—Solution Variables Affecting Its Performance" by Walter Juda and C. E. Tirrell (Abstract No. 106)
3:45 P.M.—"High-Temperature Methane Fuel Cells" by E. B. Shultz, Jr., L. G. Marianowski, and K. S. Vorres (Abstract No. 107)
4:15 P.M.—"Electrolyte for Low-Temperature Fuel Cells" by K. R. Williams and D. P. Gregory (Abstract No. 108)

THEORETICAL ELECTROCHEMISTRY

Modern Instrumentation and Techniques of Electrochemical Measurements, sponsored by the National Science Foundation—ECS, with P. Ruetschi presiding

(LINCOLN ROOM, 14th floor, SHERATON-LINCOLN HOTEL, 117 W. Washington St.)

2:00 P.M.—Introductory Remarks by P. Ruetschi
2:05 P.M.—"Electrical Units and Electrochemical Constants" by W. J. Hamer (Abstract No. 127)
2:30 P.M.—"The Design and Use of Potentiostats" by M. Fleischmann (Abstract No. 128)
3:00 P.M.—"Precision Direct Current Regulators" by Karl Eklund (Abstract No. 129)
3:30 P.M.—"Interrupter Techniques" by Ernest Yeager and John Yeager (Abstract No. 130)
4:00 P.M.—"The Use of Operational Amplifiers for Measurement and Control" by C. G. Enke (Abstract No. 131)
4:30 P.M.—"Experimental Difficulties in the Measurement of Low Level Transients of Single Electrodes" by B. D. Cahan (Abstract No. 132)

TUESDAY A.M., May 2, 1961

BATTERY—INDUSTRIAL ELECTROLYTIC (cont'd)

Joint Symposium on Fuel Cells (cont'd), with R. F. Bechtold presiding

(ASSEMBLY HALL, 8th floor)

SEE Industrial Electrolytic—Battery Program.

ELECTRIC INSULATION (cont'd)

Epoxy Resins, with L. J. Frisco presiding

(TOWER ROOM, 9th floor)

9:30 A.M.—"Epoxy Resins from Fats. Monomer Structure and Resin Properties" by W. S. Port (Abstract No. 8)
10:00 A.M.—"A Flame Retardant Epoxy Resin" by R. A. Cass (Abstract No. 9)

10:30 A.M.—"Preparation of Silicone-Epoxy Resins and Their Properties in Glass Cloth Laminates" by S. A. Brady (Abstract No. 10)
11:00 A.M.—"Strength Retentivity of Cured Epoxy Systems in Mineral Acids" by John Delmonte (Abstract No. 11)
12:15 P.M.—Electrochemical Society Luncheon and Business Meeting, Travertine Room, 14th floor, SHERATON-LINCOLN HOTEL, 117 W. Washington St.

ELECTRONICS—LUMINESCENCE (cont'd)

with Henry Ivey presiding

(SKY ROOM, 9th floor)

9:00 A.M.—"Preparation and Properties of ZnO Phosphors" by A. Pfahnl (Abstract No. 36)
9:25 A.M.—"Electroluminescence in Zinc Sulfide as Due to Minority Carrier Injection" by W. A. Thornton (Abstract No. 37)
9:50 A.M.—"The Dember Effect in ZnS-Type Phosphors" by F. Morehead and A. Fowler (Abstract No. 38)
10:15 A.M.—General Discussion
12:15 P.M.—Electrochemical Society Luncheon and Business Meeting, Travertine Room, 14th floor, SHERATON-LINCOLN HOTEL, 117 W. Washington St.

ELECTRONICS—SEMICONDUCTORS (cont'd)

Compound Semiconductors, with A. C. Beer presiding

(RILEY ROOM, Mezzanine)

9:00 A.M.—"Precipitation in Gallium Phosphide" by M. Gershenzon, C. J. Frosch, and R. M. Mikulyak (Abstract No. 53)
9:20 A.M.—"Growth Steps on the Surfaces of GaAs Dendrites" by G. R. Booker (Abstract No. 54)
9:40 A.M.—"Dendritic Growth of Indium Antimonide" by N. Albon and A. E. Owen (Abstract No. 55)
10:00 A.M.—"Phase Diagram for the Binary System Indium-Tellurium" by E. G. Grochowski and D. R. Mason (Abstract No. 56)
10:20 A.M.—Ten-minute intermission
10:30 A.M.—"Growth from the Vapor of Large Single Crystals of Lead Selenide of Controlled Composition" by A. C. Prior (Abstract No. 57)
10:50 A.M.—"Single Crystal P-N Junction and Photoconductive Detectors in Lead Selenide" by D. G. Coates, M. Kimmitt, W. D. Lawson, and A. C. Prior (Abstract No. 58)
11:15 A.M.—"Semiconducting Properties of α-Nb_2O_5" by E. H. Greener, D. H. Whitmore, and M. E. Fine (Abstract No. 59)
11:40 A.M.—Recent News Papers. Titles and short abstracts will be available at the Registration Desk.
12:15 P.M.—Electrochemical Society Luncheon and Business Meeting, Travertine Room, 14th floor, SHERATON-LINCOLN HOTEL, 117 W. Washington St.

ELECTROTHERMICS AND METALLURGY (cont'd)

Ultrafine Particles—Production of Ultrafine Particles, with W. E. Kuhn presiding

(FLORENTINE ROOM, Mezzanine)

9:30 A.M.—Introductory Remarks by W. E. Kuhn
9:45 A.M.—Keynote Address by John Turkevich (Abstract No. 80)
10:00 A.M.—"Ultrafine Metal Oxides by Decomposition of Salts in a Flame" by M. L. Nielsen, P. M. Hamilton, and R. J. Walsh (Abstract No. 81)
10:30 A.M.—"Preparation and Properties of Ultrafine Tungsten Powder" by R. L. Ripley and H. Lamprey (Abstract No. 82)
11:00 A.M.—"Fine Particles Obtained by Evaporation of Metals in an Inert Gas" by Paul Till and John Turkevich (Abstract No. 83)
12:15 P.M.—Electrochemical Society Luncheon and Business Meeting, Travertine Room, 14th floor, SHERATON-LINCOLN HOTEL, 117 W. Washington St.

INDUSTRIAL ELECTROLYTIC—BATTERY (cont'd)

Joint Symposium on Fuel Cells (cont'd), with R. F. Bechtold presiding

(ASSEMBLY HALL, 8th floor)

9:00 A.M.—"Oxidation of Methyl and Isopropyl Alcohol in a Low-Temperature Fuel Cell" by J. F. Yeager (Abstract No. 109)
9:30 A.M.—"Development of a Portable Air-Breathing Fuel Cell Power-Pack for Field Application" by E. A. Oster and L. E. Chapman (Abstract No. 110)
10:00 A.M.—Fifteen-minute intermission
10:15 A.M.—"Automatic Determination of Fuel Cell Polarization Curves" by W. N. Carson, Jr. (Abstract No. 111)
10:45 A.M.—"Evaluation Criteria for Fuel Cell Systems" by A. M. Moos (Abstract No. 112)
11:15 A.M.—"On CHO Fuel Problems" by W. Vielstich (Abstract No. 113)
12:15 P.M.—Electrochemical Society Luncheon and Business Meeting, Travertine Room, 14th floor, SHERATON-LINCOLN HOTEL, 117 W. Washington St.

THEORETICAL ELECTROCHEMISTRY (cont'd)

Modern Instrumentation and Techniques of Electrochemical Measurements (cont'd), sponsored by the National Science Foundation—ECS, with Norman Hackerman presiding

(LINCOLN ROOM, 14th floor, SHERATON-LINCOLN HOTEL, 117 W. Washington St.)

9:00 A.M.—"True Surface Areas of Solid Electrodes" by Norman Hackerman (Abstract No. 133)
9:30 A.M.—"The Single Crystal as a Tool in Electrochemical Research" by A. T. Gwathmey (Abstract No. 134)
10:00 A.M.—"Electrochemical and Adsorption Measurements on Single Crystals" by H. C. Gatos, W. J. LaFleur, and W. W. Harvey (Abstract No. 135)
10:30 A.M.—"Electron Diffraction, Light Microscopy, and X-Ray Analysis of Electrode Surfaces" by Ernest Raub (Abstract No. 136)
11:00 A.M.—"Microscope Techniques for the Study of Electrochemical Processes" by A. C. Simon and E. L. Jones (Abstract No. 137)
11:30 A.M.—"Radioactive Methods and Techniques in Electrochemistry" by M. Haissinsky (Abstract No. 138)
12:15 P.M.—Electrochemical Society Luncheon and Business Meeting, Travertine Room, 14th floor, SHERATON-LINCOLN HOTEL, 117 W. Washington St.

TUESDAY P.M., May 2, 1961

BATTERY—INDUSTRIAL ELECTROLYTIC (cont'd)

Joint Symposium on Fuel Cells (cont'd), with J. C. Cole presiding

(ASSEMBLY HALL, 8th floor)

SEE Industrial Electrolytic—Battery Program

ELECTRIC INSULATION (cont'd)

Epoxy Resins (cont'd), with A. J. Sherburne presiding

(TOWER ROOM, 9th floor)

2:00 P.M.—"Electrical Properties of Epoxide Polymers" by R. W. Warfield and M. C. Petree (Abstract No. 12)
2:30 P.M.—"Mechanical and Electrical Properties of Oxiron Resins" by C. W. Johnston and M. H. Reich (Abstract No. 13)
3:00 P.M.—"Effect of Curing Agent Types and Concentrations on the Mechanical and Electrical Properties of Epoxy Resins" by P. A. Teliha (Abstract No. 14)
3:30 P.M.—"Mechanical and Electrical Properties of New U.C.P.C Epoxy Systems" by F. L. Williamson (Abstract No. 15)

ELECTRONICS—SEMICONDUCTORS (cont'd)

Device Processing and Characterization, with D. R. Mason presiding

(RILEY ROOM, Mezzanine)

2:00 P.M.—"Transistor Potting Material Characteristics" by M. Kowal and E. S. Lukacs (Abstract No. 60)
2:25 P.M.—"Effect of Low Moisture Partial Pressures on Transistor Parameters" by R. J. Gnaedinger, Jr., S. S. Flaschen, M. A. Hall, and E. J. Richez (Abstract No. 61)
2:50 P.M.—"Electrodeposition of Molten Metals and Alloys from Glycerine Solutions" by G. L. Schnable (Abstract No. 62)
3:10 P.M.—Ten-minute intermission
3:20 P.M.—"Anomalous Breakdown Characteristics in Silicon Diffused Junctions" by M. L. McNamara (Abstract No. 63)
3:45 P.M.—"Ambient Studies on the Switching Characteristics of the Avalanche Transistor" by W. T. Eriksen, P. H. Robinson, and H. Vartanian (Abstract No. 64)

4:05 P.M.—"A Very Low Current Controlled Rectifier" by C. W. Heath and W. M. Robinson (Abstract No. 65)
4:30 P.M.—Recent News Papers. Titles and short abstracts will be available at the Registration Desk.

ELECTROTHERMICS AND METALLURGY (cont'd)

Ultrafine Particles—Production of Ultrafine Particles (cont'd), with E. M. Sherwood presiding

(FLORENTINE ROOM, Mezzanine)

2:00 P.M.—"Formation of Elongated Iron Particles by Electrodeposition into Mercury" by F. E. Luborsky (Abstract No. 84)
2:30 P.M.—"Ultrafine Ferrite Particles" by Wm. J. Schuele and V. D. Deetscreek (Abstract No. 85)
3:00 P.M.—"Ultrafine Particles Produced by an Electric Arc" by James Amick and John Turkevich (Abstract No. 86)
3:30 P.M.—"Fine Particle Sizes by Jet Pulverization" by Hugh Boyd (Abstract No. 87)
4:00 P.M.—"Properties and Potentialities of Metal Microcrystals Made by the Freeman Process" by M. W. Freeman, J. H. L. Watson, and Anthony Arrott (Abstract No. 88)

INDUSTRIAL ELECTROLYTIC—BATTERY (cont'd)

Joint Symposium on Fuel Cells (cont'd), with J. C. Cole presiding

(ASSEMBLY HALL, 8th floor)

2:00 P.M.—"The Alkali Metal Amalgam Oxygen Continuous Feed Cell" by E. Yeager (Abstract No. 114)
2:30 P.M.—"Optimization Calculations for Fuel Cell Systems" by J. Van Winkle and W. N. Carson, Jr. (Abstract No. 115)
3:00 P.M.—Fifteen-minute intermission
3:15 P.M.—"The Alcohol Cells. Study of the Successive Oxidation Reactions of the Fuel" by O. Bloch, M. Prigent, and J. C. Balaceanu (Abstract No. 116)
3:45 P.M.—Panel Discussion on Fuel Cells.

THEORETICAL ELECTROCHEMISTRY (cont'd)

Modern Instrumentation and Techniques of Electrochemical Measurements (cont'd), with W. J. Hamer presiding

(LINCOLN ROOM, 14th floor, SHERATON-LINCOLN HOTEL, 117 W. Washington St.)

2:00 P.M.—"Techniques of Electrochemical Measurements at High Temperatures" by H. A. Laitinen (Abstract No. 139)
2:30 P.M.—"Electrochemical Measurements at High Pressures" by A. Disteche (Abstract No. 140)
3:00 P.M.—"Electron Spin Resonance Measurements in the Study of Electrode Processes" by D. H. Geske (Abstract No. 141)
3:30 P.M.—"A New Method for the Measurement of Fast Ionic Reactions" by H. Strehlow (Abstract No. 142)
4:00 P.M.—"Instrumentation for Electrochemical Calorimetry" by J. M. Sherfey (Abstract No. 143)
4:30 P.M.—"Modern Techniques for Determining Transport Numbers" by F. R. Duke (Abstract No. 144)

WEDNESDAY A.M., May 3, 1961

ELECTRIC INSULATION (cont'd)

Epoxy Resins (cont'd), with A. Gunzenhauser presiding

(TOWER ROOM, 9th floor)

9:00 A.M.—"Effects of Radiation on the Electrical Properties of Epoxy Resins" by J. W. Kallander (Abstract No. 16)
9:30 A.M.—"Physical and Electrical Properties of Epoxy Resins as a Function of Chemical Composition" by C. L. Segal (Abstract No. 17)
10:00 A.M.—"Comparative Rheological and Fracture Properties of Epoxy Resins in the Glass Transition Range" by D. H. Kaelble (Abstract No. 18)
10:30 A.M.—"Effect of Elevated Temperature on the Physical and Electrical Properties of Epoxy Resin Bonded Glass Fabric Base Laminates" by A. H. Haroldson (Abstract No. 19)
11:00 A.M.—"Properties of Paper-Based and Glass-Based Copper Clad Epoxy Laminates" by H. R. Levine (Abstract No. 20)
11:30 A.M.—"Wire Insulation Life Determined as a Chemical Reaction Rate Function" by E. L. Brancato (Abstract No. 21)

ELECTRONICS—SEMICONDUCTORS (cont'd)

Diffusion—Oxidation, with E. Paskell presiding

(RILEY ROOM, Mezzanine)

9:00 A.M.—"Thermal Oxidation of Germanium" by S. S. Flaschen, D. A. Kallander, and C. M. Lufty (Abstract No. 66)
9:15 A.M.—"Accelerated Thermal Oxidation of Silicon" by D. A. Kallander, S. S. Flaschen, R. J. Gnaedinger, Jr., and C. M. Lufty (Abstract No. 67)
9:40 A.M.—"Studies of the Diffusion of Antimony into Germanium" by J. E. McNamara and H. M. Robertson (Abstract No. 68)
10:05 A.M.—Ten-minute intermission
10:15 A.M.—"Diffusion of Boron in Silicon" by T. H. Yeh and W. Armstrong (Abstract No. 69)
10:40 A.M—"New Techniques for the Measurement of the Impurity-Density Distribution in Diffused-Base Structures" by D. P. Sanders and E. S. Schlegel (Abstract No. 70)

ELECTROTHERMICS AND METALLURGY (cont'd)

Ultrafine Particles (cont'd)—Properties of Ultrafine Particles, with R. L. Reddy presiding

(FLORENTINE ROOM, Mezzanine)

9:00 A.M.—"A Novel Fine Alumina Powder: Fibrillar Boehmite" by John Bugosh, R. L. Brown, J. R. McWhorter, G. W. Sears, and R. J. Sippel (Abstract No. 89)
9:30 A.M.—"Aerosols and Electrical Phenomena" by Bernard Vonnegut and A. W. Doyle (Abstract No. 90)
10:00 A.M.—"Some Characteristics of Arc Vaporized Submicron Particulates" by C. Sheer, J. O. Gibson, and J. D. Holmgren (Abstract No. 91)
10:30 A.M.—"Physical Characteristics and Surface Properties of Pyrogenic Oxides of Silicon and Aluminum" by K. A. Loftman (Abstract No. 92)
11:00 A.M.—"Properties of Submicron Silicon Carbide Produced by Vaporization of Silica and Carbon in the Electric Arc" by W. E. Kuhn (Abstract No. 93)
12:30 P.M.—Electrothermics and Metallurgy Division Luncheon and Business Meeting, Louis XIV Room, Mezzanine.

INDUSTRIAL ELECTROLYTIC

General Session, with W. D. Sherrow presiding

(ASSEMBLY HALL, 8th floor)

9:30 A.M.—"Influence of Some Factors on Cathodic Formation of Hydrogen in the Mercury Cell" by J. H. Entwisle and W. E. Cowley (Abstract No. 118)
10:00 A.M.—"Liquidus Curves for Aluminum Cell Electrolyte, III. Systems Cryolite and Cryolite-Alumina with Aluminum Fluoride and Calcium Fluoride" by Anne Fenerty and E. H. Hollingshead (Abstract No. 119)
10:30 A.M.—Fifteen-minute intermission
10:45 A.M.—"Important Properties of Zirconium and Titanium Boride as Electrode Materials" by R. W. Love and R. A. Alliegro (Abstract No. 120)
11:15 A.M.—"The Uhde Cell and Factors Affecting Large Cell Development and Trends" by F. B. Grosselfinger and J. Schuecker (Abstract No. 121)
12:30 P.M.—Industrial Electrolytic Division Luncheon and Business Meeting, Assembly Hall, 8th floor.

THEORETICAL ELECTROCHEMISTRY (cont'd)

Modern Instrumentation and Techniques of Electrochemical Measurements (cont'd), sponsored by the National Science Foundation—ECS, with E. Yeager presiding

(CHATEAU ROOM, Lobby floor, Claypool Hotel)

9:00 A.M.—"New Developments in the Measurement of Mass Transfer Polarization and Limiting Currents" by C. W. Tobias (Abstract No. 145)
9:30 A.M.—"Rates of Electrode Processes by the Rotating Disk Method" by D. Jahn and W. Vielstich (Abstract No. 146)
10:00 A.M.—"Faradaic Rectification and Electrode Processes, I. Theory" by Mitsugi Senda and Paul Delahay (Abstract No. 147)

10:30 A.M.—"Faradaic Rectification and Electrode Processes, II. Experimental Studies" by Hideo Imai, Mitsugi Senda, and Paul Delahay (Abstract No. 148)
11:00 A.M.—"A-C Methods in Interfacial Electrical Phenomena" by Akira Watanabe (Abstract No. 149)
11:30 A.M.—"Electrokinetic Studies with an X-Y Pulsed Measuring System" by C. H. Presbrey, Jr., and Sigmund Schuldiner (Abstract No. 150)
12:00 M.—Concluding Remarks by P. Ruetschi
12:30 P.M.—Theoretical Electrochemistry Division Luncheon and Business Meeting, Lincoln Room, 14th floor, SHERATON-LINCOLN HOTEL, 117 W. Washington St.

WEDNESDAY P.M., MAY 3, 1961

ELECTRIC INSULATION (cont'd)

Epoxy Resins (cont'd) with L. L. Deer presiding

(TOWER ROOM, 9th floor)

2:00-5:00 P.M.—Round-Table Discussion of Epoxy Resins with S. A. Brady, E. L. Brancato, R. A. Cass, J. Delmonte, A. H. Haroldson, C. W. Johnston, D. H. Kaelble, J. W. Kallander, H. R. Levine, M. C. Petree, W. S. Port, M. H. Reich, C. L. Segal, R. B. Feuchtbaum, P. A. Teliha, R. W. Warfield, and F. L. Williamson

ELECTRONICS—SEMICONDUCTORS (cont'd)

Etching, with H. F. John presiding

(RILEY ROOM, Mezzanine)

2:00 P.M.—"Effect of Different Mechanisms of Minority Carrier Generation on Capacity and Polarization Characteristics of the Silicon/Electrolyte Interface" by P. T. Wrotenbery and R. M. Hurd (Abstract No. 71)
2:20 P.M.—"Chemical Etching Rates of Germanium in the HF-HNO_3-H_2O System" by T. E. Burgess (Abstract No. 72)
2:35 P.M.—"Etching Rate of Indium Alloy Junctions on N-Type Germanium" by William Richardson (Abstract No. 73)
2:55 P.M.—"Preferential Plating and Etching; New Techniques for Microminiature and Other Devices" by W. Rindner and J. M. Lavine (Abstract No. 74)
3:20 P.M.—"Etched Semiconductor Integrated Microcircuit" by W. B. Glendinning (Abstract No. 75)
3:45 P.M.—Ten-minute intermission
3:55 P.M.—Recent News Papers. Titles and short abstracts will be available at the Registration Desk.

ELECTROTHERMICS AND METALLURGY (cont'd)

Ultrafine Particles (cont'd)—Particle Size Measurement and Surface Effects, with C. Sheer presiding

(FLORENTINE ROOM, Mezzanine)

2:00 P.M.—"The Array Method for Sizing Monodisperse Particles" by H. E. Kubitschek (Abstract No. 94)
2:30 P.M.—"Submicron Sizing by X-Ray Technique" by J. J. Martin, J. H. Brown, and P. L. de Bruyn (Abstract No. 95)
3:00 P.M.—"Adsorption Methods of Measuring Surface Areas of Very Fine Particles" by G. F. Agar and P. L. de Bruyn (Abstract No. 96)
3:30 P.M.—"A Kinetic Model for Diffusion Controlled Tarnishing Reactions" by Ralph Carter (Abstract No. 97)
4:00 P.M.—"Use of Submicron Metal and Nonmetal Powders for Dispersion-Strengthened Alloys" by W. S. Cremens (Abstract No. 98)

INDUSTRIAL ELECTROLYTIC (cont'd)

General Session (cont'd) with J. Wood presiding

(ASSEMBLY HALL, 8th floor)

2:00 P.M.—"Platinum Titanium Anodes" by H. B. Berman (Abstract No. 122)
2:30 P.M.—"Studies of the Electrolysis of Sodium Sulfate Solution" by Shinzo Okada, Shiro Yoshizawa, Fumio Hine, Hiromichi Hara, Satoshi Ando, and Isao Kimura (Abstract No. 123)
3:00 P.M.—"On the Estimation of Graphite Packing of Amalgam Decomposer" by Shinzo Okada, Shiro Yoshizawa, and Fumio Hine (Abstract No. 124)
3:30 P.M.—"Theory of Electrolytic Chlorate Formation" by T. R. Beck (Abstract No. 125)
4:00 P.M.—"Graphite Anodes in Brine Electrolysis. Potential Measurements on Horizontal Anodes" by R. C. Coats and Luther Vaaler (Abstract No. 126)

THEORETICAL ELECTROCHEMISTRY (cont'd)

General Session, with Paul Delahay presiding

(CHATEAU ROOM, Lobby floor, Claypool Hotel)

2:00 P.M.—"Effect of Organic Molecules on the Adsorptive Properties of Platinum Electrodes" by Manfred Breiter (Abstract No. 151)
2:20 P.M.—"Characteristic Functions and Parameters in the Theory of Hydrogen Overpotential" by G. W. Castellan (Abstract No. 152)
2:40 P.M.—"Kinetics of Hydrogen Evolution at Zero Hydrogen Partial Pressure" by Sigmund Schuldiner (Abstract No. 153)
3:00 P.M.—"Effects of Electrostatic Fields on the Surface Tension of Salt Solutions" by G. M. Schmid, R. M. Hurd, and E. S. Snavely, Jr. (Abstract No. 154)
3:20 P.M.—"Contact-Potential Olfactometry; Specificity and Sensitivity in Adsorption of Organic Vapors on Solids" by Andrew Dravnieks (Abstract No. 155)
3:40 P.M.—"Measurement of Small Surface Areas by Krypton Adsorption" by Tennyson Smith (Abstract No. 156)
4:00 P.M.—"Continuous Coulometric Analysis of Chlorine Bleach Solutions" by E. L. Eckfeldt and E. R. Kuczynski (Abstract No. 157)
4:20 P.M.—"The Electrokinetic Streaming Potential as a Source of Energy" by R. E. Meredith (Abstract No. 158)
4:40 P.M.—"Polarization Curves of Redox Systems Involving Consecutive Electron Transfers: Some Theoretical Aspects" by R. M. Hurd (Abstract No. 159)
5:00 P.M—"A Model for Electrochemical Reaction Kinetics of Solid-State Phase Transformations in Reversible Electrodes" by G. T. Croft and Donald Tuomi (Abstract No. 160)

Abstracts

ELECTRIC INSULATION

Abstract No. 1

Electrolytic Oxide Films

C. C. Houtz, Bell Telephone Labs., Inc., Murray Hill, N. J.

The nature of the dielectric film in electrolytic capacitors has been a subject of continuing interest over the past fifty years, and it is surprising that not more is known about the nature of these films, their chemical and physical properties, or their mechanism of formation. The increasing economic importance of other metals in the electrolytic capacitor field has renewed interest in the fundamental properties of anodic oxides, and a considerable amount of recent work covers the determination of thickness, dielectric constant, and electrical resistivity. The advent of the diode-capacitor with voltage sensitive properties and the solid electrolytic capacitor developed by Bell Labs. has increased interest in the interface which is the seat of the dielectric, and it appears that we are dealing in both cases with a p-n junction whose properties are not yet well understood. Recent work in the above areas is discussed.

Abstract No. 2

Electrical Properties of Evaporated Aluminum Oxide Films

E. M. DaSilva and **P. White,** International Business Machines Corp., Research Center, Yorktown Heights, N. Y.

This report describes the preparation of aluminum oxide capacitors as thin films of oxide between aluminum electrodes by evaporation techniques. The metal electrodes were prepared by high vacuum evaporation of aluminum, and the oxide dielectric by evaporation from a second aluminum source in an oxygen atmosphere. Values of dielectric constant and dissipation factor of these films have been measured under a variety of conditions and are compared with the electrical properties of aluminum oxide films formed by anodization.

Abstract No. 3

Charge Storage Effects in Tantalum Oxide Films

Rudolf Dreiner, Sprague Electric Co., North Adams, Mass.

Polarization effects are described which have been observed on anodic oxide films of tantalum in an electrolyte when the previously anodically charged film is discharged. The discharge current decreases with time according to an inverse time law, and illumination temporarily decreases and then increases its magnitude. Illumination also affects the residual voltage which arises when the discharge is interrupted by imposing open-circuit conditions.

Abstract No. 4

Polarity of Tantalum Oxide Printed Capacitors

N. Schwartz and **M. Gresh,** Bell Telephone Labs., Inc., Murray Hill, N. J.

The printed capacitor structure [R. W. Berry and D. Sloan, *Proc IRE*, **47**, 1070 (1959)] allows an investigation of the influence of water on the rectification properties of anodic oxide films. These capacitors are partially asymmetric in that their cathodic breakdown voltage is only 10-50% of the anodic value. This asymmetry is probably due to trace amounts of water, since vacuum baking at 100°C results in almost symmetric breakdown voltages equal to the original cathodic value. The cathodic breakdown voltage is strongly dependent on the area of the cathode. For areas of 5×10^{-3} cm² or less, the breakdown voltage approaches the full formation voltage, indicating a dependence on local inhomogeneities in the oxide film. These preliminary results are discussed in reference to current theories on rectification for anodic oxide films.

Abstract No. 5

Dielectric Properties of Evaporated Film Capacitors

F. S. Maddocks and **R. E. Thun,** International Business Machines Corp., Federal Systems Div., Command Control Center, Kingston, N. Y.

The preparation of film capacitors by evaporation is described utilizing the following dielectric materials: silicon monoxide, silicon dioxide, magnesium fluoride, lanthanum fluoride, cerium fluoride, cerium dioxide, and zinc sulfide. The dielectric constants and loss tangents of these materials are presented as functions of the deposition parameters, and the contribution of the lead and condenser plate losses to the apparent loss tangents is shown. The necessary evaporation conditions are discussed for optimizing the dielectric properties of the chosen insulator material. For cerium fluoride, a deposition method consisting essentially in a controlled partial decomposition is described yielding dielectric constants up to $E/Es = 300$ without an undue increase of the capacitor losses.

Abstract No. 6

Physical and Dielectric Properties of Thin Film SiO_2 Capacitors

J. A. Minahan, J. L. Sprague, and **O. J. Wied,** Sprague Electric Co., North Adams, Mass.

Thin film capacitors using SiO_2 as the dielectric material have been prepared by the thermal oxidation of silicon. Physical and optical characteristics of the oxide dielectric are given, and the permittivity and loss tangent of the capacitors are shown as functions of a-c frequency and d-c bias. The dielectric properties are seen to be functions of the conductivity type and resistivity of the substrate silicon.

Abstract No. 7

Electrical Properties of Evaporated Thin Film SiO Capacitors

D. B. York, International Business Machines Corp., Federal Systems Div., Command Control Center, Kingston, N. Y.

The absorption coefficient and transmission of vacuum deposited films of SiO were used as a measure of the reproducibility of the composition of the resulting films. The composition of the films can be reproduced by controlling the evaporation rate and partial pressure of oxygen. Reproducibility of composition does not insure reproducible electrical properties since the surface condition of the electrode material greatly affects the electrical properties.

Abstract No. 8

Epoxy Resins from Fats. Monomer Structure and Resin Properties

W. S. Port, Eastern Regional Research Lab., Philadelphia 18, Pa.

The relationship between the structure of fatty epoxy monomers and the physical properties of the resin produced therefrom with phthalic anhydride was investigated. The principal physical criterion used was the heat distortion temperature (HDT); a secondary basis was the tensile strength. For a series of epoxidized fatty acid esters of comparable structure, HDT was a function of the number of epoxide groups in the monomer or, alternately considered, the number of acyl chains. HDT varied inversely with the distance between epoxy groups and, consequently, it was shown that a pronounced increase in HDT could be achieved by the proper architecture of the epoxy monomers. A comparison was made between HDT of resins derived from epoxidized esters and structurally analogous amides. A significant increase in HDT was produced by the substitution of the amide for the ester structure, but the simple relationship found for the esters did not carry over to the amides. For resins from a series of epoxy diamides, HDT was greater in the old aliphatic, cycloaliphatic, aromatic diamines used in the preparation of the diamide.

Abstract No. 9

A Flame Retardant Epoxy Resin

R. A. Cass, Monsanto Chemical Co., St. Louis, Mo.

The paper discusses a flame retardant epoxy resin produced from tetrachloro bisphenol A and a chemically resistant polyester produced from hydrogenated bisphenol A.

Abstract No. 10

Preparation of Silicone-Epoxy Resins and Their Properties in Glass Cloth Laminates

S. A. Brady, Dow Chemical Corp., Midland, Mich.

Procedures have been developed for copolymerizing silicone and epoxy resins to give new and different laminating resins. The procedure calls for reaction of the silicone and epoxy resins at elevated temperatures in the presence of a solvent and a third reactant. The resulting silicone-epoxy resin gives relatively high structural strengths measured by flexural strength in low-pressure glass cloth laminates. This strength is maintained and in many cases increased after long-term heat aging at 500°F. The nature of the silicone-epoxy resin is dependent on the type and amount of silicone present. At high silicone content, additional strength has been coupled with the good moisture and electrical properties of the silicone. At high epoxy content, better heat age properties have been added to the high strength of the epoxy.

Abstract No. 11

Strength Retentivity of Cured Epoxy Systems in Mineral Acids

John Delmonte, Furane Plastics, Inc., Los Angeles 39, Calif.

Various epoxy resins are cured with both amine and anhydride curing agents, alone and in conjunction with various reactive diluents. The bisphenol A-epichlorohydrin and Novolac type resins and some of the next diepoxides are included in the study. Comparisons are made as to the strength retentivity after long periods of immersion in more important acids and as influenced by cure conditions.

Abstract No. 12

Electrical Properties of Epoxide Polymers

R. W. Warfield and **M. C. Petree,** U.S. Naval Ordnance Lab., Silver Spring, Md.

The electrical volume resistivity, ρ, of several typical epoxide polymers has been determined during iso-

thermal polymerization. After polymerization is complete, ρ has also been determined as a function of temperature. Data so obtained are employed to select the optimum manner in which to conduct a polymerization. Resistivity *vs.* temperature data are also used to determine the glass transition temperature, *Tg*, of a polymer. The relation between *Tg* and the mechanical and electrical properties of a polymer is indicated. Dielectric constants and loss tangents have also been determined over broad temperature and frequency ranges and the results correlated with resistivity measurements. Various results are discussed further in terms of the over-all polymeric structures.

Abstract No. 13

Mechanical and Electrical Properties of Oxiron Resins

C. W. Johnston and **M. H. Reich,** Food Machinery and Chemical Corp., P. O. Box 8, Princeton, N. J.

Oxiron resins are epoxidized polydiolefins made by the Food Machinery and Chemical Corp. These resins contain epoxy and hydroxyl groups as well as ethylenic unsaturation, which imparts to Oxiron resins greater versatility than is possessed by the commercial polyglycidyl polyether resins. Several different types of cure systems may be employed to harden Oxiron resins, namely, aliphatic and aromatic amines with a phenolic catalyst, anhydride-polyols, and maleic anhydride-polyolperoxide. These recipes are covered in the paper, and the mechanical and electrical properties of the resultant castings are reviewed.

Abstract No. 14

Effect of Curing Agent Types and Concentrations on the Mechanical and Electrical Properties of Epoxy Resins

P. A. Teliha, Technical Service Lab., Shell Chemical Co., Union, N. J.

Variations in the electrical and mechanical properties of select epoxy resins arising from changes in the concentration and type of curing agent have been studied.

Abstract No. 15

Mechanical and Electrical Properties of New U.C.P.C. Epoxy Systems

F. L. Williamson, Union Carbide Plastics Co., Bound Brook, N. J.

The volume of epoxy resin systems used in electrical applications for potting, encapsulation, coating, and as structural components is increasing constantly. New resins are being developed with improved flexibility, heat resistance, electrical properties, and handling characteristics. Selection of the best epoxy system for a typical electrical application may be made from comparative properties of new and established resins. Cured epoxy resins ranging from rubber-like materials to rigid compounds may be achieved through proper selection of resin and hardeners.

Abstract No. 16

Effects of Radiation on the Electrical Properties of Epoxy Resins

J. W. Kallander, U.S. Naval Research Lab., Washington 25, D. C.

Considerations of the usage of epoxy resins to cement solar cells to satellite skins has resulted in the need for knowledge concerning the effects of high-energy radiation on the electrical properties of epoxy resins. Therefore, measurements of the effects of high-energy radiation on the electrical properties of an epoxy adhesive have been made. These measurements included volume resistivity, capacitance, and dissipation factor as function of dosage. They lead to various results including the conclusion that the volume resistivity, the most critical property from the standpoint of the space application, undergoes a very rapid degradation followed by a stable plateau.

Abstract No. 17

Physical and Electrical Properties of Epoxy Resins as a Function of Chemical Composition

C. L. Segal and **R. B. Feuchtbaum,** Hughes Research Labs., Culver City, Calif.

The coefficient of thermal expansion, compressive strength, tensile strength, and infrared spectra of two different epoxy resins were determined as a function of the stoichiometric ratio of the hardener (either an aromatic amine or an aromatic anhydride) to the base resin. The resin/hardener system which yielded the best physical data was then further subjected to moisture conditioning at 96% relative humidity and also to heat aging. Changes in dielectric constant and loss factors were recorded along with any changes in structure as shown by infrared spectra. This investigation should do much toward determining the relative merit of anhydride-epoxy and amine-epoxy resins as environmentally resistant electrical insulations.

Abstract No. 18

Comparative Rheological and Fracture Properties of Epoxy Resins in the Glass Transition Range

D. H. Kaelble, Minnesota Mining and Manufacturing Co., St. Paul, Minn.

This discussion extends previous description of the dynamic mechanical tensile deformation and tensile fracture properties of epoxies by direct comparison with equivalent properties for elastomers and thermoplastic resins. The essential similarities and differences between epoxies and these comparative polymers are discussed in terms of molecular chemistry and physics.

Abstract No. 19

Effect of Elevated Temperature on the Physical and Electrical Properties of Epoxy Resin Bonded Glass Fabric Base Laminates

A. H. Haroldson, Continental-Diamond Fibre Corp., Newark, Del.

The physical and electrical properties of epoxy resin bonded glass fabric laminates change significantly when subjected to elevated temperatures.

Abstract No. 20

Properties of Paper-Based and Glass-Based Copper Clad Epoxy Laminates

H. R. Levine, Laminated Products Dept., General Electric Co., Coshocton, Ohio

The properties of paper-based and glass-based copper clad epoxy laminates are reported, and the variables involved in the formulation and manufacture of epoxy laminates discussed.

Abstract No. 21

Wire Insulation Life Determined as a Chemical Reaction Rate Function

E. L. Brancato, U.S. Naval Research Lab., Washington 25, D. C.

Life *vs.* temperature relationships of wire and cable insulations are needed to provide aircraft and missile engineers with information to design electrical circuits utilizing the minimum wire sizes required to maintain maximum reliability and yet reduce weight and bulk to a minimum. A procedure for obtaining this relationship has been developed, employing the philosophy of functional evaluation and the principles of statistical analysis. Experimental results show that wire insulation deterioration follows a chemical reaction rate relationship as expressed by a variation of the classical Arrhenius equation. In addition, cycling temperature studies verify the application of a relative aging factor formula to convert cyclic aging to the equivalent aging of a single temperature exposure. Advancing studies will probe the mechanisms of deterioration and failures of insulating materials to provide nondestructive test methods which will greatly accelerate the evaluation process.

ELECTRONICS—LUMINESCENCE

Abstract No. 22

Visible Fluorescence of Rare Earth Activated Phosphors

S. P. Keller, Research Center, International Business Machines Corp., Yorktown Heights, N. Y.

Different rare earth ions have been incorporated into various materials such as SrS, $BaTiO_3$, and yttrium gallium garnets. Some optical properties have been determined. Data in terms of the interactions of the rare earth centers and the crystalline lattice are discussed. Such interactions include crystal field and phonon effects. New information that can be obtained using rare earth doping as an experimental tool is discussed also.

Abstract No. 23

Studies of Color Centers Produced in Apatite Halophosphates by Shortwave Ultraviolet Radiation

Lawrence Suchow, (present address: Research Center, International Business Machines Corp., P.O. Box 218, Yorktown Heights, N. Y.), Research Dept., Westinghouse Electric Corp., Bloomfield, N. J.

Because many fluorescent lamp phosphors consist of suitably activated alkaline earth halophosphates, and because phosphors receive 1849Å radiation along with 2537Å radiation in lamps, an investigation has been made of the effects of such shortwave ultraviolet radiation on nonluminescent base materials in which it is possible to isolate other electronic effects from those of luminescence. A variety of color centers have been found to be formed. All colors may be bleached thermally and some optically as well. In some cases, bleaching is accompanied by luminescence.

Abstract No. 24

Luminescence of Copper-Activated Orthophosphates of the Type $ABPO_4$ (A = Ca, Sr, or Ba and B = Li, Na, or K)

W. L. Wanmaker and **H. L. Spier,** Light Div., N. V. Philips' Gloeilampenfabrieken, Eindhoven, Netherlands

Activation of orthophosphates of the type $ABPO_4$ with copper gives some efficient phosphors. Especially good results were obtained with $SrLiPO_4{\cdot}Cu$ (λ max. = 4150Å) and $BaLiPO_4{\cdot}Cu$ (λ max. = 4600Å). Addition of manganese causes sensitization, giving rise to a red emission peak. The x-ray diagrams of the compounds investigated are given. The properties of compounds with two kinds of alkaline-earth or alkaline ions, respectively, were also studied.

Abstract No. 25

Crystal Growth and Structural Study of the Barium Titanium Phosphate Phosphor

D. E. Harrison and **G. Shirane,** Research Labs., Westinghouse Electric Corp., Pittsburgh 35, Pa.

Examination of single crystals and powder samples of the compound $2BaO{:}TiO_2{:}P_2O_5$ revealed a reversible crystallographic inversion at about 1050°C. The two modifications have monoclinic symmetry and can be indexed with very similar lattice constants, but they have quite different line intensities. Powder patterns of both phases have been indexed to 40° 2θ. The high-temperature form has parameters a_o = 16.578, b_o = 5.437, c_o = 4.756, β = 94°O′, and the low-temperature phase has parameters a_o = 16.591, b_o = 5.435, c_o = 4.758, β = 94°O′. Single crystal Weissenberg photographs reveal weak spots which cannot be indexed on the primitive unit cell. This substructure can be indexed by doubling the a_o and c_o lattice parameters. Crystals grown from the melt were always twinned, with two types of twinning being distinguished. In one case the b-c plane and in the other case the a-b plane is the twin or composition plane. Fluorescent emission spectra of the high- and low-temperature phases are identical in shape, and they are characterized by a double peak. The spectrum of the high-temperature form lies about 0.02 ev toward longer wavelengths than does the low-temperature form.

Abstract No. 26

Magnesium Lithium Antimonate Phosphors

R. W. Mooney, Chemical and Metallurgical Div., Sylvania Electric Products Inc., Towanda, Pa.

The preparation and properties of phosphors of composition $Mg_3Li_2Sb_2O_{12}$ activated by Mn, U, Ti, Nb, and W are described. It is suggested that the transitions responsible for fluorescence in the Mn- and U-activated phosphors are associated with inner shell electrons while those in the Ti-, Nb-, and W-activated phosphors arise from transitions between the filled 2p band of the oxygen lattice and a d band formed by the overlap of nonbonding d orbitals of neighboring transition metal atoms.

Abstract No. 27

Particle Size Measurement of Phosphors. A Correlation of Methods

R. F. Quirk, Sylvania Electric Products Inc., 75 Sylvan St., Danvers, Mass., **E. W. Brewster,** Sylvania Electric Products Inc., 60 Boston St., Salem, Mass., and **R. C. Ropp,** Sylvania Electric Products Inc., Towanda, Pa.

Particle size distribution is an important property of phosphors during synthesis and subsequently during bulb coating. The particle size of most commercial lamp phosphors falls within the range of 0.5-50μ. Of the number of methods currently available for making particle size measurements, four are discussed. These are: turbidimetric, centrifugal sedimentation, micromesh sieving, and electronic counting. Measurements on the same materials by the four methods are compared, and the advantages and limitations of each discussed.

Abstract No. 28

Measurement of Phosphor Brightness

J. E. Eby, Sylvania Lighting Products, Inc., 60 Boston St., Salem, Mass.

A new instrument for the measurement of plaque brightness of fluorescent lamp phosphors is described. This instrument is of double-beam design, comparing the brightness of a sample to that of standard phosphor. The reading is obtained from a mechanical beam attenuator, at a point when a null-type signal is obtained from the end-on-type photomultiplier detector. The instrument is capable of making relative brightness measurements with an accuracy of 0.2%. Broad band filters are used to compare brightness of the blue, green, and red emission.

Abstract No. 29

Boron Nitride Phosphors

W. Lehmann, Research Dept., Westinghouse Electric Corp., Bloomfield, N. J.

Experimental work on the preparation of boron nitride phosphors and some of their properties are described. A wide variety of complex emission spectra could be observed. Impurity activation seems unlikely. The idea is advanced that the luminescence of boron nitride phosphors may be due to contamination of nonluminescent BN with aromatic hydro-boron-nitrides, similar in structure to aromatic hydrocarbons, but every two carbon atoms replaced by one boron and one nitrogen atom.

Abstract No. 30

Activator Solubility and Structural Transformations in ZnS:Cu, Cl

J. W. Nickerson, P. Goldberg, and **D. H. Baird,** General Telephone and Electronics Labs. Inc., Bayside, N. Y.

Chemical analyses and x-ray powder photographs have shown that thermal treatment of hexagonal ZnS:Cu, Cl phosphors in H_2S and He:$ZnCl_2$ atmospheres results in structural transformations and solubility changes of activator and coactivator. The temperature at which these changes occur depends on the

copper concentration. One or more of the following factors may be of importance in initiating the transformation of hexagonal to cubic zinc sulfide: (*a*) removal of copper and chloride from the lattice, (*b*) removal of oxygen from the phosphor, and (*c*) exceeding the solubility of copper in the hexagonal modification.

Abstract No. 31

ZnS:Cu, Si Phosphors

A. Wachtel, Research Dept., Westinghouse Electric Corp., Bloomfield, N. J.

Firing of ZnS + Cu + SiS_2 causes incorporation of Cu and promotes orange fluorescence. Some other tetravalent elements, especially Th, have a similar effect. Possibly, $1Si^{4+} + 2Cu^{1+}$, all at cation sites, may replace $3Zn^{2+}$ in the ZnS lattice. With high concentrations of Cu and Si, a ternary (Zn,Cu,Si)S forms which may show deep-red fluorescence peaked at 840μ.

Abstract No. 32

Luminescence of Self-Activated ZnS, ZnSCdS, and ZnSe Phosphors

R. A. W. Gill and **S. Rothschild,** Mullard Research Labs., Salfords nr. Redhill, Surrey, England

The spectral distribution of the luminescence of self-activated phosphors at low temperatures was found to vary with the concentration of the donor impurity. At low concentrations a band on the short wavelength side of the SA- band with or without some other bands prevailed. It is assumed that the short wavelength band is due to nonassociated coactivator centers. The effects of varying the ratio of ZnS:CdS and of the presence of oxygen on the luminescence at low temperatures were also investigated.

Abstract No. 33

Decay of Cathodoluminescence and Nonradiative Processes in Manganese-Activated Phosphors

G. F. J. Garlick and **M. Sayer,** (present address: University of British Columbia, Vancouver, B. C., Canada) Dept. of Physics, University of Hull, U. K.

Decay constants and emission spectra for single crystals, evaporated layers, and microcrystalline layers of manganese-activated zinc sulfide and silicate and calcium fluoride have been measured for different primary electron energies, etc. Clear evidence of nonradiative processes associated with the single crystal surfaces is found. It is shown that such processes which predominate at low beam penetration are not due to thermal effects or directly to high electron densities. In striking contrast powder layers with large surface areas do not show changes in decay constant with primary electron energy.

Abstract No. 34

Cathodoluminescent Characteristics of Manganese-Activated Potassium-Magnesium Fluoride

R. J. Kurtz, Research Dept., Westinghouse Electric Corp., Bloomfield, N. J.

The brightness, persistence, and maintenance of light output during life of cathode-ray excited MgF_2:Mn phosphors were studied as a function of (*a*) Mn concentration, (*b*) K:Mg ratio, (*c*) ZnF_2 addition, and (*d*) firing conditions. The emission spectra and brightness-voltage and brightness-current characteristics of these samples also are discussed. (Work supported by Government Contract NObsr-77582.)

Abstract No. 35

Transparent Luminescent Films by Solution Spraying

R. D. Kirk and **J. H. Schulman,** U.S. Naval Research Lab., Washington 25, D. C.

Spraying solutions of zinc chloride or cadmium iodide with activator onto preheated Pyrex or silica glass yields cathodoluminescent films by direct reaction with the glass. The activated silicate films have excellent adherence, good transparency, and, on silica, a brightness comparable to that of evaporated films on Vycor. Films on silica require refiring in air.

Abstract No. 36

Preparation and Properties of ZnO Phosphors

A. Pfahnl, Bell Telephone Labs., Inc., Murray Hill, N. J.

The relative cathodoluminescent intensity I and the absolute value of the decay time τ were determined for the green emission band of several ZnO phosphors. It was found that higher intensities are in general related to longer decay times. The preparation conditions for ZnO phosphors presenting the shortest decay time for a given intensity were then investigated. The form of the decay, temperature dependence of I and τ, aging characteristics, and dependence of the decay time on the exciting current density are also discussed.

Abstract No. 37

Electroluminescence in Zinc Sulfide as Due to Minority Carrier Injection

W. A. Thornton, Research Dept., Westinghouse Electric Corp., Bloomfield, N. J.

Under the proper experimental conditions, which can be fulfilled in conventional electroluminescent ZnS phosphor powder dispersions in dielectric material or in films, the a-c currents follow the diode equation (for forward bias) $I = I' [\exp (V/V') - 1]$, where V is the applied rms voltage. It is found that $I' \propto \exp(-T'/T)$ where T' is a parameter independent of temperature, and $V' \propto T$. DC electroluminescence at 2.0 v, again with an exponential current increase, also indicates carrier injection. Arguments for collision ionization are discounted.

Abstract No. 38

The Dember Effect in ZnS-Type Phosphors

F. Morehead and **A. Fowler,** Research Center, International Business Machines Corp., Yorktown Heights, N. Y.

The sign of the more mobile carrier in powder phosphors can be determined conveniently from the direction of a diffusion current pulse produced by a pulse of band gap radiation (Dember effect) onto a conventional electroluminescent cell. Reversals observed in many cases at longer wavelengths are attributed to fast surface states. Along with observations of photoluminescence, electroluminescence, and electrophotoluminescence, this effect gives useful information on phosphor excitation and recombination mechanisms.

ELECTRONICS—SEMICONDUCTORS

Abstract No. 39

(There is no Abstract No. 39.)

Abstract No. 40

(There is no Abstract No. 40.)

Abstract No. 41

Epitaxial Growth of Germanium onto Germanium Substrates by Thermal Evaporation

O. Weinreich, G. Dermit, and **C. Tufts,** Bayside Labs., General Telephone & Electronics Labs. Inc., Bayside 60, N. Y.

An investigation of the crystal structure and electrical properties of germanium films obtained by thermal evaporation of germanium onto germanium single crystals in a vacuum of 10^{-6} mm Hg has been made. The substrate temperatures during deposition were varied between 450° and 900°C. The (110), (111), and (100) planes were exposed to the vapor. Reflection electron diffraction patterns indicate a high perfection of orientation of the deposit when the substrates were heated to 600° and 870°C during evaporation. At substrate temperatures between 450° and 600°C oriented growth was revealed by preferential etching of the films for all planes used in the experiments. When substrates and source materials were appropriately

doped, junction formation between substrate and film was observed.

Abstract No. 42

Dendritic Growth in Heavily Doped Melts

R. L. Longini, Research Labs., Westinghouse Electric Corp., Pittsburgh, Pa.

Dendritic growth has been explained in its normally observed form as being the result of nucleation at re-entrant corners. When the melt is heavily doped, however, these re-entrant corners trap segregated impurity thus lowering the melting point locally and removing the supercooling there. Corners sticking out in the melt are thus the most supercooled positions, and growth results from nucleation in the region of these points. (The research reported in this paper was sponsored in part by the Air Force Office of Scientific Research.)

Abstract No. 43

Periodic Growth in Germanium Dendrites

R. G. Seidensticker and **D. R. Hamilton,** Research Labs., Westinghouse Electric Corp., Pittsburgh 35, Pa.

The growth interface of a germanium dendrite is considered to be composed of three regions: the tip where the twin plane mechanism is operative; an intermediate region, described in this paper; and the "H" arm region, where lateral growth takes place. A growth mechanism operative in the intermediate region is discussed, and it is shown that this mechanism provides steady-state oscillation in growth which leads to periodic facet formation on the interface. (This work was supported by the U. S. Air Force through the Electronic Technology Lab. of the Wright Air Development Div.)

Abstract No. 44

Distribution Coefficient of Antimony in Silicon from Solvent Evaporation Experiments

F. A. Trumbore, P. E. Freeland, and **R. A. Logan,** Bell Telephone Labs., Inc., Murray Hill, N. J.

Distribution coefficients have been calculated from Hall effect measurements on heavily doped silicon crystals grown by a solvent evaporation technique from melts containing between 2 and 8.4 at. % antimony. Nearly a twofold decrease in the distribution coefficient (from 0.02 to 0.01) was observed in this concentration range. From the results of this work it appears that near-equilibrium solid solubilities were obtained and that any "facet effect," if present, was small.

Abstract No. 45

Structure Analysis of Semiconductor Single Crystals by Anomalous Transmission of X-Rays

G. H. Schwuttke, Bayside Labs., General Telephone & Electronics Labs., Inc., Bayside 60, N. Y.

Anomalous transmission of x-rays in nearly perfect crystals is strongly decreased in the immediate vicinity of imperfections. This effect has been used by Borrmann (divergent beam technique) and Barth and Hosemann (parallel beam technique) and others to photograph imperfections in single crystals. However, results obtained by these methods are inferior to those results obtained by the x-ray extinction contrast method in which the crystal is scanned. We have improved the parallel beam technique by using a collimator, and as a result we were enabled to obtain high-quality photographs of dislocations and other imperfections in Si, Ge, and GaAs which reveal many details. This technique is simpler and experimentally easier to handle than extinction contrast methods and makes possible the investigation of crystal areas several square centimeters in size without moving the crystal. [The research reported in this paper was sponsored by The Electronics Research Directorate of the Air Force Cambridge Research Center, Air Research and Develompent Command, under contract No. AF 19-(604)-3482.]

Abstract No. 46

Electropolishing of N-Type Germanium and P- and N-Type Silicon

D. L. Klein, G. A. Kolb, L. A. Pompliano, and **M. V. Sullivan,** Bell Telephone Labs., Inc., Murray Hill, N. J.

A specially designed electropolishing apparatus has produced flat, mirror-like surfaces on both germanium and silicon. The technique makes use of an intensive stirring action between the surface being polished and an inert cathode. For n-type material the holes necessary for the dissolution of the semiconductor can be furnished by strong illumination. The effects of etch composition, current density, resistivity, and the electrical contact to the semiconductor are discussed.

Abstract No. 47

A Chemical Polishing Technique for Gallium Arsenide

M. V. Sullivan and **L. A. Pompliano,** Bell Telephone Labs., Inc., Murray Hill, N. J.

The rate at which gallium arsenide is etched by H_2SO_4-H_2O_2-H_2O mixtures can be accelerated by more than a factor of ten if intensive stirring is employed. By using a flat stirring plate which is moved very close to the gallium arsenide any high points are etched preferentially, and a very smooth flat surface is produced. Etching techniques and etching compositions are described.

Abstract No. 48

Electrolytic Slicing of Germanium

Sumner Sheff, Semiconductor Div., Raytheon Co., 55 Chapel St., Newton 58, Mass.

Thin germanium slices of controlled thickness and orientation have been cut anodically from large n- and p-type germanium single crystals. The cathode was a small diameter tungsten wire surrounded by a stream of NaOH (aq.) electrolyte. Slicing was accomplished by applying a constant voltage between the cathode wire and the germanium anode, while the latter was moved mechanically through the electrolyte stream. The nature of the germanium surfaces was investigated as a function of the parameters of the experiments.

Abstract No. 49

Electron Diffraction Study of Some Crystalline Films on Germanium Surfaces

J. J. Oberly, Research Div., Raytheon Co., Waltham 54, Mass.

Some crystalline films which appear on single-crystal germanium surfaces have been studied by reflection diffraction of 50 kv electrons. The surface treatments used include electrochemical in NaOH and acetic acid and chemical in CP-4 and NaOH. The possible identification of some of the film constituents as oxides and germanates is discussed. Examples of the partial orientation of some films on the germanium substrate are presented.

Abstract No. 50

Stabilization of Semiconductor Surfaces, I. Chemical Treatment

G. W. Cullen, J. A. Amick, and **D. Gerlich,** RCA Labs., Radio Corp. of America, Princeton, N. J.

In an effort to obtain reproducible and stable semiconductor surfaces a treatment has been developed which is designed to terminate each surface atom with a saturated carbon chain. The rationale for the approach is presented, and the preparative procedure is outlined. The electrical and chemical characteristics of alkylated germanium surfaces are presented in the two following papers.

Abstract No. 51

Stabilization of Semiconductor Surfaces, II. Electrical Measurements

D. Gerlich, G. W. Cullen, and **J. A. Amick,** RCA Labs., Radio Corp. of America, Princeton, N. J.

Measurements of both the trapped charge density in the fast states and the recombination velocity are reported for alkylated germanium surfaces. In the region of surface potential examined, the charge distribution can be described by two discrete surface states. Results show that the surface structure is reproducible, stable, and insensitive to ambients. Measurements of large signal photovoltage and slow states conductivity relaxation are also reported for these surfaces.

Abstract No. 52

Stabilization of Germanium Surfaces, III. Chemical Analysis

J. A. Amick, G. W. Cullen, and **D. Gerlich,** RCA Labs., Radio Corp. of America, Princeton, N. J.

Mass spectrometric and radiotracer techniques have been used to obtain information about the chemical nature of alkylated germanium surfaces. The presence of alkyl groups on the surfaces has been demonstrated. Within experimental accuracy, there is one alkyl group for each germanium atom on a (111) surface. The strength of the bond between the ethyl group and the surface is confirmed by an examination of the chemical stability of the treated surface in different environments.

Abstract No. 53

Precipitation in Gallium Phosphide

M. Gershenzon, C. J. Frosch, and **R. M. Mikulyak,** Bell Telephone Labs., Inc., Murray Hill, N. J.

Microscopic examination of gallium phosphide ingots prepared in graphite boats has revealed the presence of a second phase which is absent after floating zone recrystallization. The precipitated phase is correlated with the carbon that is removed during floating zone purification. Precipitation from crystals saturated with zinc occurs on dislocations and other crystal imperfections, in regions of high strain and near grain boundaries and gives rise to Rayleigh scattering in the visible region of the spectrum.

Abstract No. 54

Growth Steps on the Surfaces of GaAs Dendrites

G. R. Booker, Research Labs., Westinghouse Electric Corp., Pittsburgh 35, Pa.

The methods of optical interference and electron microscopy have been used to study the growth steps occurring on the two main faces of GaAs dendrites. The steps on the Ga face consist of precisely oriented {111} planes, while the steps on the As face do not. Reasons for the difference are given. (This work was supported by the U. S. Air Force through the Electronic Technology Lab. of the Wright Air Development Div.)

Abstract No. 55

Dendritic Growth of Indium Antimonide

N. Albon and **A. E. Owen,** Research Labs., Westinghouse Electric Corp., Pittsburgh 35, Pa.

Recent experiments on the growth of InSb dendrites have revealed growth in the 110 and 321 directions. It has been found that the supercooling of the melt and the twin structure of the seed are both critical for these modes of propagation. The experimental conditions for such growth are described. Photographs of InSb dendrites exhibiting growth in these directions will be shown and some of their characteristic features discussed. (This work was supported by the U. S. Air Force through the Electronic Technology Lab. of the Wright Air Development Div.)

Abstract No. 56

Phase Diagram for the Binary System Indium-Tellurium

E. G. Grochowski and **D. R. Mason,** Dept. of Chemical and Metallurgical Engineering, University of Michigan, Ann Arbor, Mich.

The phase diagram for the binary system indium-tellurium has been clarified and corrected, particularly in the region near the composition In_2Te_3, because of the potential importance of this material as a semiconductor. Results of this study were obtained by correlating differential thermal analysis (DTA), chemical analyses of zone refined ingots, microscopic analysis, and x-ray determinations. A new phase, In_4Te_7 (ϵ), which transforms peritectic alloy at 625°C, was identified from DTA and chemical analysis of peritectically zone refined ingot. The congruently melting disordered In_2Te_3 (δ) phase (59.8 ± 0.3 at. % Te) undergoes a eutectoid reaction at 59.5 ± 0.5 at. % Te and 600° ± 5°C. Chemical analysis of a zone refined ingot of InTe gave the composition of pure γ-phase as 50.8 at. % Te.

Abstract No. 57

Growth from the Vapor of Large Single Crystals of Lead Selenide of Controlled Composition

A. C. Prior, Royal Radar Establishment, Malvern, England

PbSe crystals have been grown by sublimation using a technique in which almost the whole charge of a few grams is frequently converted into only one single crystal. A substantial measure of control of the Pb:Se ratio of the resulting crystals is achieved by independent control of the partial vapor pressure of selenium during growth, giving carrier concentrations more than an order lower than has been achieved in crystals grown from the melt.

Abstract No. 58

Single Crystal P-N Junction and Photoconductive Detectors in Lead Selenide

D. G. Coates, M. Kimmitt, W. D. Lawson, and **A. C. Prior,** Royal Radar Establishment, Malvern, England

A crystal with a thin surface p-n junction has been grown from the vapor and its photovoltaic properties measured at various temperatures. This detector has high quantum efficiency, but low electrical resistance, which is discussed. A chemical etch for lead selenide has been developed and used for the preparation, from crystals grown from the vapor, of thin photoconducting specimens with high sensitivity at room temperature.

Abstract No. 59

Semiconducting Properties of α-Nb_2O_5

E. H. Greener (present address: Marquette University, Milwaukee, Wis.), **D. H. Whitmore,** and **M. E. Fine,** Dept. of Materials Science, Northwestern University, Evanston, Ill.

α-Nb_2O_5 has been found to be a metal-excess, n-type semiconductor with near-stoichiometric activation energy of 1.65 ev under constant oxygen partial pressure. The conductivity is related to the ambient oxygen partial pressure by the expression δ = constant $P_{O_2}^{-0.24\pm0.01}$. For dilute concentration of defects, the temperature dependence of the conductivity yielded activation energies of approximately 0.5 ev in the temperature range 100° to —77°C. Equal additions of Mg^{2+} to pure α-Nb_2O_5 were about ten times more effective in lowering the conductivity than Ti^{4+}. The conductivity may be ascribed to a mechanism whereby oxygen ion defect levels are created and electrons are thermally excited from these levels into the conduction band.

Abstract No. 60

Transistor Potting Material Characteristics

M. Kowal and **E. S. Lukacs,** Semiconductor & Materials Div., Radio Corp. of America, Somerville, N. J.

This paper discusses the physical characteristics of some transistor potting materials. Data and testing

techniques are given for characteristics such as volume resistivity, moisture content, dielectric strength, and thermal conductivity. The relationship between some of these characteristics and device performance and manufacture is evaluated, and the development of a new method for determining the moisture content of potting materials is described. Results of tests evaluating the effects of sealing ambient conditions and potting-material moisture content on device characteristics are also presented. The development and investigation of a transistor potting material using the methods presented are also discussed.

Abstract No. 61

Effect of Low Moisture Partial Pressures on Transistor Parameters

R. J. Gnaedinger, Jr., S. S. Flaschen, M. A. Hall, and **E. J. Richez,** Semiconductor Products Div., Motorola, Inc., Phoenix, Ariz.

It has been found that moisture at levels below 0.3% relative humidity has a strong influence on the surface recombination velocity of germanium transistors. By controlling the moisture partial pressure at any given level within hermetically sealed devices, it is possible to preselect different ranges of final, stabilized device parameters, such as h_{fe} and I_{co}, without changing device fabrication procedure. The discussion includes the manner in which moisture pressure is controlled at levels below 0.1 mm H_2O and a theoretical interpretation of device behavior.

Abstract No. 62

Electrodeposition of Molten Metals and Alloys from Glycerine Solutions

G. L. Schnable, Lansdale Div., Philco Corp., Lansdale, Pa.

Various metals and alloys, including indium, tin, and cadmium alloys used in the fabrication of Surface Barrier and micro-alloyed transistors (SBT, MAT, MADT), have been electrodeposited in molten form on small wires using solutions of metal halides in glycerine. Since high current densities can be employed in molten plating, electrodeposition can be very rapid and binary alloys of metals separated by over 0.6 v in the electromotive series can be codeposited readily.

Abstract No. 63

Anomalous Breakdown Characteristics in Silicon Diffused Junctions

M. L. McNamara, Bell Telephone Labs., Inc., Lauraldale, Pa.

Certain anomalies in the reverse voltage-current characteristics of large area Si diffusion junctions are attributed to circular inclusions apparently formed during diffusion of acceptors into n-type Si. Evidence is presented to show that the boundaries of these inclusions, which form minute p-n junctions, consist of a closed ring of microplasmas. Special distribution of such inclusions are discussed with reference to device fabrication and performance. The roles of surface damage, impurity segregation, and heat treatment in the formation of these inclusions are discussed.

Abstract No. 64

Ambient Studies on the Switching Characteristics of the Avalanche Transistor

W. T. Eriksen, P. H. Robinson, and **H. Vartanian,** Semiconductor Div., Raytheon Co., 55 Chapel St., Newton 58, Mass.

Electrical parameters of the Avalanche Transistor, a silicon npn structure (2N1468), were measured under various ambient conditions, namely, anhydrous NH_3 an electropositive gas, and BF_3 an electronegative gas. The switching characteristics, i.e., rise and delay time, were measured as a function of gas pressure, and preliminary results indicate they were noticeably affected by the amount of gas present. The delay time decreased as the ammonia pressure increased. The grounded emitter amplification factor (β) varied along with changes in delay time. Reverse currents and breakdown voltages of emitter and collector junctions were also measured as a function of ambient pressure. A mechanism for these changes in switching characteristics also is presented.

Abstract No. 65

A Very Low Current Controlled Rectifier

C. W. Heath and **W. M. Robinson,** Electronics Components Div., General Electric Co., Auburn, N. Y.

The ZJ203 Very Low Current Silicon Controlled Rectifier is housed in the standard JEDEC TO-5 package. This device employs a welded case, glass-to-metal seals, complete absence of soft solders, and a painted external surface for maximum heat dissipation. Design objectives are discussed which have resulted in the development of a PNPN device with very high gate sensitivity, blocking voltages up to 400 v, and extremely uniform characteristics. Processes for producing this all-diffused device are presented in detail. A unique method of silicon pellet bonding is discussed together with the relatively new ultrasonic technique of ohmic contact bonding to silicon. Pellet diffusion and fabrication processes are presented, with slides depicting device construction and characteristics and specialized manufacturing equipment. These and other production processes and tests, also to be discussed, have the prime goal of producing a highly reliable product.

Abstract No. 66

Thermal Oxidation of Germanium

S. S. Flaschen, D. A. Kallander, and **C. M. Lufty,** Semiconductor Products Div., Motorola, Inc., Phoenix, Ariz.

The kinetics of the thermal oxidation of a germanium surface are compared to that of silicon. In the Ge-O_2 system, monoxide volatilization predominates the oxidation reaction above 550°C. At and below 500°C the nonvolatile dioxide forms. If the transport phenomenon is accelerated at this temperature, protective oxide can be formed to thicknesses of 4000Å.

Abstract No. 67

Accelerated Thermal Oxidation of Silicon

D. A. Kallander, S. S. Flaschen, R. J. Gnaedinger, Jr., and **C. M. Lufty,** Semiconductor Products Div., Motorola, Inc., Phoenix, Ariz.

Rate mechanism studies of the thermal oxidation of silicon have led to a low-temperature "accelerated oxidation" process for formation of the protective surface oxide. Typically 5000Å films can be grown at atmospheric pressure in 1 hr at 600°C. Under these conditions surface channelling or redistribution of p-n doping impurities are absent. 2000-hour aging data under high humidity, power conditions are reported for oxide surface protected, uncanned devices.

Abstract No. 68

Studies of the Diffusion of Antimony into Germanium

J. E. McNamara and **H. M. Robertson,** Materials Research Dept., Semiconductor Products Div., Motorola, Inc., Phoenix, Ariz.

Using a radioactive tracer method, a monolayer of antimony was observed to form on germanium surfaces during certain diffusion processes. The formation and properties of this monolayer are discussed. The rate of out-diffusion of antimony from germanium was measured for a number of external "sink" phases over the temperature range of 600°-700°C. The use of shallow diffused gradients to measure resistivity profiles in thin epitaxial germanium and silicon films is discussed.

Abstract No. 69

Diffusion of Boron in Silicon

T. H. Yeh and **W. Armstrong,** Product Development Labs., International Business Machines Corp., Poughkeepsie, N. Y.

Diffusion of boron into silicon has been investigated over a temperature range of 1150°-1310°C by using an oxidizing carrier gas, 1~50 volume percentage of oxygen with nitrogen, in the two-zone diffusion process. The optical polished silicon surface can be retained after this diffusion process. Wide range of surface concentration, from 10^{17} to 10^{20} atoms/cm^3, can be obtained by varying the impurity (B_2O_3) source temperature. Low diffusion coefficient and a higher activation energy ($\Delta H = 99$ kcal) were obtained than those reported previously.

Abstract No. 70

New Techniques for the Measurement of the Impurity-Density Distribution in Diffused-Base Structures

D. P. Sanders and **E. S. Schlegel,** Philco Corp., C and Tioga St., Philadelphia, Pa.

Inter-relationships between depletion layer thicknesses, electrostatic potentials, and their gradients have been utilized to determine quantitatively the impurity-density distribution of seimconductor material. The technique developed provides a rapid and reproducible means for locating the edge of a diffused layer. The distribution of impurities along a direction perpendicular to the plane of the sample can be calculated from empirical data. The theory is described and data are presented showing the practicality of the methods.

Abstract No. 71

Effect of Different Mechanisms of Minority Carrier Generation on Capacity and Polarization Characteristics of the Silicon/Electrolyte Interface

P. T. Wrotenbery and **R. M. Hurd,** Texas Research Associates, 1701 Guadalupe St., Austin 1, Texas

The effects of light and of an oxidizing redox system on space charge capacities and polarization characteristics of n-type silicon surfaces in various electrolytic environments have been studied. Illumination of the surface, which creates hole-electron pairs throughout the space charge region, gives rise, in the region of inversion, to an increase in both current saturation level and space charge capacity. The presence of the oxidizing couple, which creates holes only at the silicon-electrolyte interface, gives rise to an increased current saturation level, but leaves the capacity unaffected. The effect of the oxidizing couple is not observed in those electrolytic environments in which an oxide film is present, although the effect of light on the space charge capacity is still measurable.

Abstract No. 72

Chemical Etching Rates of Germanium in the HF-HNO_3-H_2O System

T. E. Burgess, Sprague Electric Co., North Adams, Mass.

A study of the kinetics of the etching reactions of germanium in HF-HNO_3-H_2O solutions has been made under isothermal conditions. Temperature control of the reactions was maintained by employing rapid mechanical stirring of the etching solutions in a controlled temperature bath and was monitored by cementing a thermocouple to the germanium surface before etching. The effect of crystal orientation, resistivity, and solution composition has been investigated. Slower etch rates than previously reported in literature have been measured.

Abstract No. 73

Etching Rate of Indium Alloy Junctions on N-Type Germanium

William Richardson, Sprague Electric Co., North Adams, Mass.

The etching of indium alloy junctions to germanium in etchants of the nitric-hydrofluoric acid system is described. With certain etchants the etching rate of germanium at close vicinity to the alloyed indium is enhanced creating a pronounced moat surrounding the indium dot, while the etching rate of indium alloyed to germanium is retarded compared to that of indium unattached to germanium. These results are discussed considering local temperature changes during etching and electrochemical potentials arising between indium and germanium.

Abstract No. 74

Preferential Plating and Etching; New Techniques for Microminiature and Other Devices

W. Rindner and **J. M. Lavine,** Research Div., Raytheon Co., Waltham, Mass.

Qualitative aspects of a preferential plating technique are described which permits the fabrication of miniature and microminiature ohmic and doped contacts in complex configurations on a variety of semiconductor materials. These techniques involve the preferential nucleation of chemiplated and electroplated metals on microscopically fine lines scribed on semiconductor surfaces. A supplementary technique involving the preferential chemical etching of similarly scribed lines also is described. Lines of the order of 10^{-4} cm have been plated with a variety of metals including doping elements, and alloyed into germanium and silicon surfaces. These techniques have yielded p-n junctions and offer promise of the fabrication of p-n junction devices at least two orders of magnitude smaller than those currently available. These techniques are also potentially useful in the fabrication of conventionally sized devices such as power transistors. Resistance elements ranging from 10 ohms to 100 kilohms have also been fabricated using preferential plating techniques. Microphotographs of several deposits and various aspects of the film growth will be shown.

Abstract No. 75

Etched Semiconductor Integrated Microcircuit

W. B. Glendinning, U.S. Army Research and Development Lab., Fort Monmouth, N. J.

A fabrication approach to microelectronics systems is described which utilizes semiconductor vapor deposited layers. Simple masking, etchings, and surface finishing techniques are employed upon a multilayer semiconductor slab in such a way as to readily yield an operating microcircuit. An 8-layer silicon sandwich was treated so as to become a 3-terminal circuit capable of yielding an oscillatory output.

ELECTROTHERMICS AND METALLURGY

Abstract No. 76

Coatings for Columbium

S. T. Wlodek, Technology Dept., Union Carbide Metals Co., Niagara Falls, N. Y.

Ten different types of protective coatings for columbium were evaluated for protection against high-temperature oxidation. Although chromium, stainless steel, and Nichrome protected columbium from gross oxidation in the temperature range 950°-1150°C for hundreds of hours, chromium coatings allowed oxygen contamination of the columbium to occur as low as 950°C. A coating of LM-5 (Mo-Si-Cr-B-Al) prevented all reaction for about 1000 hr at 1150° and 100 hr at 1500°C. This coating behaved well under stress and exhibited some self-healing properties and thermal-shock resistance. A duplex coating of LM-5 and a Cb-Ti-Cr-Al-Ni alloy layer retained the static exposure resistance and strain-rate insensitivity of the LM-5 and withstood 30 water-quenches from 1150°C before failure.

Abstract No. 77

High-Temperature Phase Studies in the Tantalum-Boron System between Ta and TaB

J. M. Leitnaker and **M. G. Bowman,** University of California, Los Alamos Scientific Lab., Los Alamos,

N. M., and **P. W. Gilles,** Dept. of Chemistry, University of Kansas, Lawrence, Kan.

Phase relationships in the tantalum-boron system between Ta and TaB have been studied. A phase diagram of the solid portion of the system has been determined and is shown. Two three-phase equilibria exist within the system; [1] Ta-Ta_2B-Ta_3B_2 at 2040° ± 30°C, and [2] Ta_2B-Ta_3B_2-TaB at 2180° ± 20°C. The chemical composition of the Ta_2B phase is $Ta_{2.4\pm0.2}B$. The composition of the Ta_3B_2 phase is $Ta_{1.60\pm0.05}B$. The melting point of TaB lies above 2800°C. The extreme slowness of reactions within the system has been investigated qualitatively, and the necessity for seeding at temperatures in the neighborhood of 2000°C has been noted. The results disagree markedly with data previously reported in the literature.

Abstract No. 78

Arc-Melting of Intermetallic, Interstitial, and Inorganic Compounds

R. J. Van Thyne, Metals Research, Armour Research Foundation of Illinois Institute of Technology, 10 W. 35th St., Chicago 16, Ill.

Nonconsumable-electrode arc-melting procedures have been developed to produce high-purity homogeneous compounds. Stoichiometric carbides have been melted. Intermetallic compounds with a volatile constituent may be prepared if close control of charged composition and melting procedures is maintained. Techniques are described that allow metallic oxides with high electrical resistance to be melted.

Abstract No. 79

Electrolytic Recovery of Manganese from Sulfurous Leach Liquors

H. J. Read and J. W. Andrews, Dept. of Metallurgy, Pennsylvania State University, University Park, Pa.

Leaching of ferriferous, low-grade manganese ores from central Pennsylvania with sulfur dioxide yields a manganous sulfate solution low in iron and other readily depositable ions. Electrolytic extraction of manganese was successful only after discovery that the sulfide-ion concentration of the solution is critical. Data on the effects of operating variables on current efficiency are presented.

Abstract No. 80

Keynote Address

John Turkevich, Chemistry Dept., Princeton University, Princeton, N. J.

(No abstract received)

Abstract No. 81

Ultrafine Metal Oxides by Decomposition of Salts in a Flame

M. L. Nielsen, P. M. Hamilton (present address: Monsanto Chemical Co., 800 N. Lindbergh Blvd., St. Louis 66, Mo.), and **R. J. Walsh,** Monsanto Chemical Co., Research and Engineering Div., Dayton 7, Ohio

Decomposition of metal salts atomized in solution within a flame has been investigated as a means of preparing ultrafine metal oxides. Products which have been prepared and characterized include single oxides such as delta-alumina, alpha-ferric oxide, gamma-ferric oxide, titania, zirconia, and others; mixed oxides such as Cr_2O_3-Al_2O_3, NiO-Al_2O_3, CuO-Al_2O_3, and others; and compounds such as $CoAl_2O_4$, $MgFe_2O_4$, and others. Particles are generally spheroidal, with diameters ranging from 0.01 to 5μ, although platelets and hollow spheres are formed under certain conditions.

Abstract No. 82

Preparation and Properties of Ultrafine Tungsten Powder

R. L. Ripley and **H. Lamprey,** Union Carbide Metals Co., P.O. Box 580, Niagara Falls, N. Y.

A process is described for producing tungsten and certain other heavy metal powders in the form of powders of 0.01-0.1μ average particle diameter. Some of the common physical and chemical properties of these materials are discussed, together with data pointing to catalytic and metallurgical uses of the products. Some of the hazards of working with these fine powders are also described.

Abstract No. 83

Fine Particles Obtained by Evaporation of Metals in an Inert Gas

Paul Till and **John Turkevich,** Chemistry Dept., Princeton University, Princeton, N. J.

Ten elements were evaporated in helium of varying pressure and collected at various distances from the source of evaporation. Particle size determinations were made of the particles collected as a function of the above parameters. These distribution curves were interpreted in terms of nucleation, growth, and aggregation of the fine particles. A mechanism was proposed for both nucleation and growth. The nucleation ability of the atoms was correlated to the physical properties of the element.

Abstract No. 84

Formation of Elongated Iron Particles by Electrodeposition into Mercury

F. E. Luborsky, Research Lab., General Electric Co., Schenectady, N. Y.

The preparation of 100-300Å diameter highly elongated fibers of iron by electrodeposition into mercury is described. The mechanism of formation of these fibers is deduced from direct electron microscopic examination of the structures formed during electrolysis. The relations between the structure of these initial fibers, parameters of formation, and ultimate magnetic properties are discussed.

Abstract No. 85

Ultrafine Ferrite Particles

Wm. J. Schuele and **V. D. Deetscreek,** Labs. for Research and Development, Franklin Institute, Philadelphia 3, Pa.

Ultrafine particles of ferrites (less than 100Å) were prepared by chemical precipitation and grown hydrothermally. Increase in crystallite size as a function of growing time was confirmed by x-ray line broadening and electron diffraction patterns. Magnetic measurements at 25° and −196°C also confirm the increase in particle size as the result of hydrothermal treatment. Data on crystal structure were obtained from x-ray and electron diffraction patterns, and chemical composition by analysis. (This research was supported by the U.S. Air Force under Contract No. AF33(616)-6922 monitored by Wright Air Development Div.)

Abstract No. 86

Ultrafine Particles Produced by an Electric Arc

James Amick and **John Turkevich,** Chemistry Dept., Princeton University, Princeton, N. J.

An electron microscope examination and electron diffraction measurements have been made of 26 elements volatilized in a direct current electric arc. It was found that the oxides so formed showed a definite morphology characteristic of the chemical species. The electron diffraction was used to determine the chemical structure of the fine particles. The particle size distribution obtained in the case of silver was used as a basis for the proposed mechanism of particle formation.

Abstract No. 87

Fine Particle Sizes by Jet Pulverization

Hugh Boyd, Majac Inc., 23 St., Sharpsburg, Pittsburgh 15, Pa.

Jet pulverization is used to produce finer, more precisely controlled particle size distributions by dry methods than are produced by other milling tech-

niques. In this paper, some particle size distribution curves in the range of 80% or more —2μ are discussed and illustrate the production of low and submicron particles. In addition, the principles of jet pulverization to achieve these ends are discussed.

Abstract No. 88

Properties and Potentialities of Metal Microcrystals Made by the Freeman Process

M. W. Freeman, M. W. Freeman Co., 401 David Whitney Bldg., Detroit 26, Mich., **J. H. L. Watson,** Edsel B. Ford Institute for Medical Research, Detroit 2, Mich., and **Anthony Arrott,** Scientific Lab., Ford Motor Co., Dearborn, Mich.

Metal microcrystals made by the Freeman process are different from other crystals of similar size. The properties which contribute to this differentiation and the potential applications which result from unique characteristics of the microcrystals are described as they relate to the wide spectrum of their emphases in medicine, magnetics, polymerization, and strengths of materials. Desirable physical and chemical properties imparted to materials by the microcrystals can be predicted, *e.g.*, when the crystals are used in polymeric complexes, the moduli of elasticity may be increased by 200%. Anticipated tensile strengths for bulk metals are extrapolated from present data as high as 10^6 psi.

Abstract No. 89

A Novel Fine Alumina Powder: Fibrillar Boehmite

John Bugosh, R. L. Brown, J. R. McWhorter, G. W. Sears, and **R. J. Sippel,** Industrial and Biochemicals Dept., E. I. duPont de Nemours & Co., Inc., Wilmington, Del.

An unusual alumina powder has been developed, consisting of porous aggregates of fibrillar particles of boehmite about 50Å wide yet over 1000Å long. A monolayer of acetate groups on the fibrils permits spontaneous dispersion in water to a sol which can be dried to a clear alumina film. Different properties of the powder, characterized by electron micrographs and physical data, are related to possible types of practical uses.

Abstract No. 90

Aerosols and Electrical Phenomena

Bernard Vonnegut and **A. W. Doyle,** Arthur D. Little, Inc., 30 Memorial Drive, Cambridge 42, Mass.

Some fundamental facts of aerosol behavior under the influence of various electrical phenomena are discussed. The electrical generation of aerosols is described and illustrated. In addition, factors such as methods of charging aerosols, methods of discharging aerosols, maximum charge on aerosols, aerosol mobilities, and methods of measurements are discussed.

Abstract No. 91

Some Characteristics of Arc Vaporized Submicron Particulates

C. Sheer, J. O. Gibson, and **J. D. Holmgren,** Vitro Labs., West Orange Lab., 200 Pleasant Valley Way, West Orange, N. J.

The technique of producing ultrafine powders by vaporization in the high-intensity arc has been applied to a number of refractory materials, including oxides, carbides, and metals. Particle size ranges of the products obtained lie generally between 100 and 1000Å. Following a brief description of the processing technique, a report on the particulate characteristics thus far investigated is presented. Such properties as average size, shape, size distribution, solid state, and surface reactivity have been examined, chiefly by electron microscopy, x-ray diffraction, and sintering tests.

Abstract No. 92

Physical Characteristics and Surface Properties of Pyrogenic Oxides of Silicon and Aluminum

K. A. Loftman, Cabot Corp., Boston, Mass.

Pyrogenic silica and alumina offer the unusual combination of fine particle size, high external surface area, and low apparent density. Determination of particle size, shape, and distribution by electron microscopy is discussed. Evidence of the presence of active surface groups is given and their behavior on heat treatment up to and beyond the sintering temperature. The advantages of using these submicron powders in combination with powdered pigments, chemicals, and plastics are discussed briefly.

Abstract No. 93

Properties of Submicron Silicon Carbide Produced by Vaporization of Silica and Carbon in the Electric Arc

W. E. Kuhn, The Carborundum Co., Research and Development Div., Niagara Falls, N. Y.

Some properties and characteristics of submicron silicon carbide generated by arc vaporization of silica and carbon are described and discussed. The silicon carbide powder consists of a mixture of submicron alpha and beta silicon carbide particles in the shape of plates, fibers, ribbons, and whiskers. The morphology and composition of the arc produced product are interpreted in terms of the mechanism and chemistry of formation. Problems of x-ray, chemical, and particle size measurement are discussed. Its physical, chemical, abrasive, and electrical properties are described and related to possible applications.

Abstract No. 94

The Array Method for Sizing Monodisperse Particles

H. E. Kubitschek, Div. of Biological and Medical Research, Argonne National Lab., Argonne, Ill.

For monodisperse particles the mean diameter may be determined simply, quickly, and with great precision when these particles can be arranged in arrays. The method, which is applicable to particles with diameters below the limit of resolution, has been used for the recalibration of several standard monodisperse polystyrene latexes using an optical microscope. For 1μ particles an accuracy of 10Å is readily attainable. The method also provides an estimate of the variability in particle diameters. (This work was done under the auspices of the U.S.A.E.C.)

Abstract No. 95

Submicron Sizing by X-Ray Technique

J. J. Martin, J. H. Brown (Present address: U.S. Steel Corp., Monroeville, Pa.), and **P. L. de Bruyn,** Dept. of Metallurgy, Massachusetts Institute of Technology, 77 Cambridge Ave., Cambridge 37, Mass.

An apparatus consisting of a bowl-like centrifuge fitted with an x-ray source and detector for absorption measurements was developed and used to examine the size distribution of a brittle material. This technique circumvents the inconsistencies introduced by such factors as Brownian movement, light scattering, and sampling, common to microscopic and other techniques. Experimental data reproducible within about ±5% and in good agreement with theory were obtained for particles as fine as 0.2μ with indications that sizes as fine as 0.05μ or less could have been analyzed. Details of the apparatus, method, and interpretation of data are given.

Abstract No. 96

Adsorption Methods of Measuring Surface Areas of Very Fine Particles

G. F. Agar and **P. L. de Bruyn,** Dept. of Metallurgy, Massachusetts Institute of Technology, 77 Cambridge Ave., Cambridge 37, Mass.

(No abstract received)

Abstract No. 97

A Kinetic Model for Diffusion Controlled Tarnishing Reactions

Ralph Carter, Research Lab., General Electric Co., Schenectady, N. Y.

A model for tarnishing reactions on spherical particles has been developed The oxidation of uniformly

sized nickel spheres has been shown to fit this model to 100% reaction. Previously reported models are inadequate because they do not meet the boundary conditions. The inadequacy of earlier experimental work results because of failure to meet experimentally the conditions imposed by the model.

Abstract No. 98

Use of Submicron Metal and Nonmetal Powders for Dispersion-Strengthened Alloys

W. S. Cremens, Lewis Research Center, Cleveland, Ohio

A mechanical mixing technique for forming dispersion-strengthened alloys of the S.A.P. type is reviewed. Significant parameters for the powders are described and related to the densified alloy microstructure. Various definitions of particle size of powders and of particle spacing in the alloy microstructure are reviewed and evaluated. A summary is given of the current research program on these matters at the NASA Lewis Research Center.

INDUSTRIAL ELECTROLYTIC THEORETICAL ELECTROCHEMISTRY—BATTERY

Abstract No. 99

Mechanisms of Oxygen Producing Reactions in Molten Carbonate Electrolysis

G. J. Janz and **Fumihiko Saegusa,** Dept. of Chemistry, Rensselaer Polytechnic Institute, Troy, N. Y.

A study of oxygen evolution in molten carbonate electrolysis with platinum, gold, and silver anodes is reported. A kinetic analysis of various possible processes contributing to anodic oxygen evolution is presented by extension of the general theory of consecutive reaction rates to molten salt system. In the range of 600°C the process is

$$MO + O^{=} \rightarrow M + O_2 + 2e^{-}$$

is found to be rate determining. At 800°C and higher, processes such as dissolution of metal and reduction of oxides are greatly enhanced.

Abstract No. 100

Fuel Cell Thermodynamics

A. J. deBethune, Chemistry Dept., Yale University, New Haven, Conn.

The work output of a simple fuel cell is $-\Delta G$ of the fuel-oxygen reaction. The "fuel-cell gain" is the ratio of this quantity to the Carnot output of the same amount of fuel and is expressible in terms of fundamental entropy and heat-capacity data. The output of a regenerative fuel cell cycle obeys Carnot's theorem in integral or differential form. The output of an idealized practical irreversible cycle is also given.

Abstract No. 101

Temperature Coefficients of Electrode Potentials, II. The Second Isothermal Temperature Coefficient

G. R. Salvi and A. J. deBethune, (present address: Dept. of Chemistry, Yale University, New Haven, Conn.) Chemistry Dept., Boston College, Chestnut Hill, Mass.

The second isothermal temperature coefficient of electrode potentials is $\Delta C_p/n\mathbf{F}T$ where ΔC_p is the heat capacity change of the "SHE/Electrode" cell reaction. The mass-action dependence of the second coefficient is given, and values tabulated for 54 standard electrodes, together with the first coefficients [*JES*, **106**, 616 (1959)]. First and second coefficients are related to fundamental entropy and heat capacity data necessary to screening of possible fuel cell reactions.

Abstract No. 102

Molten Carbonate as Electrolytes

G. J. Janz and **M. R. Lorenz,** Dept. of Chemistry, Rensselaer Polytechnic Institute, Troy, N. Y.

The results of an investigation of the properties of surface tension, density, and electrical conductance for molten Li_2CO_3, Na_2CO_3, and K_2CO_3 and some mixtures in the temperature range of 750°-1000°C are reported. The ionic nature of the molten carbonates is examined from the physicochemical criteria based on these properties; the mechanism of electrical transport is considered in the light of current theoretical concepts. Relative to Na_2CO_3-K_2CO_3 mixtures, the surface tensions and partial molal volumes indicate but little deviation from thermodynamic ideality.

Abstract No. 103

The DSK System of Fuel Cell Electrodes

E. Justi and **A. Winsel,** Technische Hochschule, Pockelstrasse 4, Braunschweig, Germany

Elevated operation temperatures of high drain fuel cells can be avoided by increasing the catalytic activity of electrodes. Unfortunately, the most active catalysts, *e.g.*, Raney-metals, do exist inevitably as powders only because of their lattice defects. The authors have developed the "Double Skeleton Katalyst-System" (DSK) to combine the high catalytic activity of powders with mechanical strength and electronic conductivity of bulk metals. DSK-electrodes consist of a microscopic supporting skeleton (sintered carbonyle nickel), containing the submicroscopic skeletons of disordered Raney metal. The authors disclose the preparation of such electrodes for both H_2 and O_2, reaching limiting current densities of 700 ma/cm² at 40 mv polarization at 80°C on H_2-side, and 500 ma/cm² at 500 mv on O_2-side.

INDUSTRIAL ELECTROLYTIC—BATTERY

Abstract No. 104

Fuel Cells—State of the Art, 1961

W. Mitchell, Research Lab., Allis-Chalmers Mfg. Co., Milwaukee, Wis.

(No abstract received)

Abstract No. 105

Thermodynamic Aspects of Electrochemical Fuel Cells

M. Eisenberg, Lockheed Missiles and Space Div., Lockheed Aircraft Corp., Bldg. 102B, Dept. 58-17, P. O. Box 504, Sunnyvale, Calif.

The thermodynamics of galvanic cells is discussed from the point of view of general considerations of free energy and enthalpy changes. Following presentation of the generalized Nernst equation the effects of temperature, pressure, and concentration changes on the reversible open-circuit potential are obtained. Characteristics of fundamental types of electrodes, including gas diffusion electrodes, are described.

The major causes of electrode process irreversibility are considered, and their relation to the efficiency aspects of a fuel cell operation are given. The effect of reaction mechanism of the oxygen electrode in aqueous electrolyte is shown to have a direct effect on the half-cell potential of that electrode. Finally, some specific fuel cells are discussed, and the thermodynamics of a thermally regenerative fuel cell system is presented.

Abstract No. 106

The Fuelox Cell—Solution Variables Affecting Its Performance

Walter Juda and **C. E. Tirrell,** Ionics Inc., 152 Sixth St., Cambridge 42, Mass.

The Fuelox Cell is a regenerative ion-membrane type of fuel cell powered by a bromine solution in the

cathode and gaseous hydrogen at the anode. Typical cells have operated at power densities of 2.3 kw/ft². Cell performance has been investigated as a function of the following variables: membrane composition, bromine concentration, hydrogen concentration, Br_2 and Br^- diffusion (diffusion from the cathode to the anode), membrane selectivity, Br_2 tolerance of hydrogen electrode.

Abstract No. 107

High-Temperature Methane Fuel Cells

E. B. Shultz, Jr., and **L. G. Marianowski**, Institute of Gas Technology, 17 W. 34th St., Chicago 16, Ill., and **K. S. Vorres**, University of Miami, Coral Gables, Fla.

High-temperature methane fuel cells were constructed with molten carbonate electrolytes held in ceramic matrices. With methane/steam feed mixtures, porous nickel anodes were used to react methane via primary catalytic reforming and shift reactions on the anode surface. Effects of the major operating variables on performance characteristics of leak-tight cells are presented. Preliminary studies on the use of solid oxide electrolytes to replace carbonates are described.

Abstract No. 108

Electrolyte for Low-Temperature Fuel Cells

K. R. Williams and **D. P. Gregory**, Shell International Petroleum Co. Ltd., St. Helen's Court, Great St. Helen's, London, EC 3, England

From consideration of the function and behavior of the electrodes it is suggested that only strong acids or strong bases can be considered as electrolytes for commercially acceptable low-temperature fuel cells. Since an alkaline electrolyte will not continue to function in the presence of carbon dioxide, only acid electrolytes can be used if carbonaceous fuels are employed. It is therefore suggested that the development of a practical low-temperature hydrocarbon-burning fuel cell is unlikely.

Abstract No. 109

Oxidation of Methyl and Isopropyl Alcohol in a Low-Temperature Fuel Cell

J. F. Yeager, Research Lab., Union Carbide Consumer Products Co., Division of Union Carbide Corp., Parma 30, Ohio

Methyl and isopropyl alcohols may be used as fuels for low-temperature fuel cells having carbon electrodes. Some of the oxidation products of these fuels have been identified. In the case of methyl alcohol the product identification accounts for more than 95% of the final product as potassium formate; in the case of the isopropyl alcohol the product identification accounts for more than 70% of the product as acetone. Polarization data are presented for the methyl alcohol anode.

Abstract No. 110

Development of a Portable Air-Breathing Fuel Cell Power-Pack for Field Application

E. A. Oster and **L. E. Chapman**, Aircraft Accessory Turbine Dept., General Electric Co., Lynn, Mass.

A complete fuel cell power-pack has been developed for transportation as a back pack by a single foot soldier. The 200-w output is obtained at 24 VDC with a power density of approximately 9 w/ft² using ambient air as the oxidant. The electrochemical reaction takes place across a cation-exchange polymer-electrolyte which is covered with catalytic electrodes. The hydrogen fuel is produced in an attached generator using a light-weight sodium berohydride and sulfuric acid system.

Abstract No. 111

Automatic Determination of Fuel Cell Polarization Curves

W. N. Carson, Jr., General Engineering Lab., General Electric Co., Schenectady, N. Y.

The design and general operation of a data-logging instrument that is used to determine the polarization curves (power output *vs.* voltage) of from 1 to 10 test cells is described. In the cycle, each cell is tested in turn by being connected to a programmed load sequence; the output current-time, output voltage-time, and output power-output voltage curves are plotted. The relay programmer permits flexible cell loading and use of special polarizing circuits.

Abstract No. 112

Evaluation Criteria for Fuel Cell Systems

A. M. Moos, Patterson Moos Research, Div. of Leesona Corp., 90-28 Van Wyck Expressway, Jamaica 18, N. Y.

A set of criteria permitting evaluation of the fuel cell in terms of a competitive market are described. These criteria can be used to: (*a*) define the research and development guidelines; (*b*) establish the basis for engineering and management decisions for product development and testing; (*c*) compare the utility of the fuel cell system *vs.* conventional power equipment; and (*d*) specify maintenance, fuel costs, and endurance requirements.

Abstract No. 113

On CHO Fuel Problems

W. Vielstich, Institut fur Physikalische Chemie, Universitat Bonn, Wegelerstrasse 12, Bonn Germany

Unlike gaseous and liquid hydrocarbons, CHO fuels can be used in galvanic fuel cells at ambient temperature. Open-circuit potentials are near the hydrogen electrode potential. At higher current densities oscillation phenomena often occur. For the study of reaction mechanism different methods are discussed.

Abstract No. 114

The Alkali Metal Amalgam Oxygen Continuous Feed Cell

Ernest Yeager, Dept. of Chemistry, Western Reserve University, Cleveland 6, Ohio

The anode of the sodium amalgam-oxygen continuous feed cell consists of a vertical steel electrode with liquid amalgam flowing continuously down its surface. Porous carbon electrodes of the semi-lyophobic type have been used as the cathode. The amalgam is produced external to the cell by introducing sodium directly into mercury. The over-all cell reaction is $4Na + O_2 + 2H_2O \rightarrow 4NaOH$. Performance characteristics are reported for a small single-cell laboratory unit as well as a 5-cell unit of several hundred watt capacity. (Research supported by Office of Naval Research.)

Abstract No. 115

Optimization Calculations for Fuel Cell Systems

J. Van Winkle and **W. N. Carson, Jr.**, General Engineering Lab., General Electric Co., Schenectady, N. Y.

In the design of fuel cell systems, a number of parameters must be assigned before the system can be specified. Usually one of these parameters, the cell operating voltage, can assume a range of values and thus can be used to optimize the system. This paper presents methods for such calculations, using the engineering parameters of the cell and fuel supply and the imposed operational restraints upon the system. The equations for size, weight, or cost are described.

Abstract No. 116

The Alcohol Cells. Study of the Successive Oxidation Reactions of the Fuel

O. Bloch, M. Prigent, and **J. C. Balaceanu**, Institut Francais du Petrole, Rueil-Malmaison, (S-&-O), France

Fuel oxidation in a fuel cell necessarily implies successive chemical reactions, whose nature determines the recoverable potential and intensity. Our studies consist in the identification of the products formed during the oxidation of various alcohols with preparation of the balances: electricity recovered products

obtained. Influence of the reaction products on the electric characteristics of the fuel cell is studied, and results are compared with those of simple catalytic dehydrogenation reactions.

INDUSTRIAL ELECTROLYTIC

Abstract No. 117

(There is no Abstract No. 117)

Abstract No. 118

Influence of Some Factors on Cathodic Formation of Hydrogen in the Mercury Cell

J. H. Entwisle and **W. E. Cowley,** Associated Ethyl Co., Ltd., Ellesmere Port, Cheshire, England

The influence of variations in brine pH and concentration, cathodic current density, sodium concentration in amalgam, and movement of the cathode on cathodic hydrogen formation in the mercury cell have been studied in a laboratory cell and by polarographic methods. Results indicate that the extent of hydrogen ion discharge is controlled by (*a*) transfer of hydrogen ions to the cathode surface, and (*b*) transfer of dissolved sodium from the cathode surface into its bulk.

Abstract No. 119

Liquids Curves for Aluminum Cell Electrolyte, III. Systems Cryolite and Cryolite-Alumina with Aluminum Fluoride and Calcium Fluoride

Anne Fenerty (present address: Flint, Mich.) and **E. A. Hollingshead,** Aluminium Labs. Ltd., Arvida, Quebec, Canada

Liquidus curves have been determined by means of cooling curves and visual examination of the cooling melt. The binary systems of cryolite with aluminum fluoride and calcium fluoride gave, respectively: peritectic point at 30% aluminum fluoride and 739°C, eutectic point at 40% aluminum fluoride and 694°C, eutectic point at 26% calcium fluoride and 945°C. In the system cryolite-alumina-calcium fluoride the ternary eutectic point was at 2.9% alumina, 21% calcium fluoride and 933°C. (Compositions are in weight %.) Diagrams are given for the cryolite-rich part of the systems cryolite-calcium fluoride, cryolite-alumina-aluminum fluoride, cryolite-alumina-calcium fluoride, and cryolite-alumina-aluminum fluoride-calcium fluoride.

Abstract No. 120

Important Properties of Zirconium and Titanium Boride as Electrode Materials

R. W. Love and **R. A. Alliegro,** Refractories Div., Norton Co., Worcester 6, Mass.

The chemical and physical properties of titanium and zirconium diborides are discussed along with effects imposed by varying the method of manufacture. The possible impact of diborides on the aluminum industry and the historical progress to date are reviewed. The data obtained from an operating laboratory aluminum cell are presented together with photomicrographs of the borides before and after immersion in the cell. Other areas of application in the electrochemical industry are reviewed.

Abstract No. 121

The Uhde Cell and Factors Affecting Large Cell Development and Trends

F. B. Grosselfinger, Hoechst-Uhde Corp., 350 5th Ave., New York 1, N. Y., and **J. Schuecker,** Friedrich Uhde GmbH, Dortmund, Germany

Uhde and other mercury cell designers have been developing cells with higher unit production capacities. This has been attained by increasing both the cathode surface and the current density. These factors, and an anode adjustment device developed for decreasing cell voltage, directly affect the economics of chlorine production and also have an indirect influence on such economics in connection with plant capacity, rectifier characteristics, cell room size, power and labor costs, and others. This paper briefly discusses these points.

Abstract No. 122

Platinum Titanium Anodes

H. B. Berman, Chemical Div., Englehard Industries, Inc., 113 Astor St., Newark 2, N. J.

(No abstract received)

Abstract No. 123

Studies of the Electrolysis of Sodium Sulfate Solution

Shinzo Okada, Shiro Yoshizawa, and **Fumio Hine,** (present address: Dept. of Chemistry, Western Reserve University, Cleveland 6, Ohio), Dept. of Industrial Chemistry, Kyoto University, Yosida, Kyoto, Japan, and **Hiromichi Hara, Satoshi Ando,** and **Isao Kimura,** Kanegafuchi Spinning Co., Ltd., Tokyo, Japan

The electrolysis of sodium sulfate solution by 1500 amp vertical mercury cell has been investigated. Lead alloy containing 2% Ag and 1% Te was selected as the anode, and fine porous rubber sheets or blue asbestos cloths were used as the diaphram. The concentrations of sulfuric acid and caustic soda obtained were 200-250 g/l H_2SO_4 and 30-45% NaOH, respectively, under the condition of 30 amp/cm^2 of current density by continuous operation. The terminal voltage was less than 5.0 v and the current efficiency and the consumption of the anode were 90-95% and 2-3 mg/amp-hr, respectively.

Abstract No. 124

On the Estimation of Graphite Packing of Amalgam Decomposer

Shinzo Okada, Shiro Yoshizawa, and **Fumio Hine** (present address: Dept. of Chemistry, Western Reserve University, Cleveland 6, Ohio), Dept. of Industrial Chemistry, Kyoto University, Yosida, Kyoto, Japan

The amalgam decomposition tower is a kind of packing column. The height is given by the product of H.T.U. and N.T.U., that is, both H.T.U. and N.T.U. are as follows:

$$\text{H.T.U.} = 1/K \quad M/S \qquad [1]$$

$$\text{N.T.U.} = -\int_{y_0}^{y_1} \frac{dy}{E - \pi_h^\circ} \qquad [2]$$

where

$$\frac{1}{K} = \frac{1}{k_A Y} + \frac{1}{k_H} + \frac{1}{k_{FK}} \div \frac{1}{k_H} + \frac{1}{k_{FK}} \qquad [3]$$

H.T.U. is, therefore, controlled by the geometry which occurs between the graphite packing and the amalgam drops. N.T.U. also is determined by the hydrogen overpotential of the graphite. Hence, the performance of the graphite packing may be estimated by those physical and electrochemical characteristics, if they are established empirically.

Abstract No. 125

Theory of Electrolytic Chlorate Formation

T. R. Beck, Electrochemical Section, American Potash & Chemical Corp., P. O. Box 55, Henderson, Nev.

Literature on the electrolytic formation of chlorates was reviewed. Equations were derived for quantitatively expressing current efficiency as a function of cell variables. Current efficiency was correlated in terms of certain dimensionless groups.

Abstract No. 126

Graphite Anodes in Brine Electrolysis. Potential Measurements on Horizontal Anodes

R. C. Coats and **L. E. Vaaler,** Niagara Falls Development Lab., Union Carbon Co., Niagara Falls, N. Y.

A laboratory mercury cell is described in which single electrode potential measurements can be made, denuder materials evaluated, and the effect of anode and brine impurities studied. Potential measurements

with a Luggin probe are reported for a variety of anode materials and shapes. The effect of the formation and dispersion of gas bubbles on potential fluctuations is discussed.

THEORETICAL ELECTROCHEMISTRY

Abstract No. 127

Electrical Units and Electrochemical Constants

W. J. Hamer, National Bureau of Standards, Washington, D. C.

Experimental methods used at present to establish the electrical units of current, resistance, and emf are outlined. Considerations are given to the concrete representations (standards) used in maintaining the units, including an evaluation of the over-all accuracy inherent in "absolute" determinations of the units. The role electric units play in modern instrumentation in electrochemistry is discussed from two angles: their direct relation and their indirect role through the medium of electrochemical constants.

Abstract No. 128

The Design and Use of Potentiostats

M. Fleischmann, Chemistry Dept., King's College, University of Durham, Newcastle upon Tyne 1, England

The factors influencing the design of potentiostats are considered. Particular attention is paid to the following points: accuracy to which a desired potential can be maintained; frequency range over which measurements can be made; stabilization of the regulators and the time dependence of the error signal. The way in which these factors are influenced by the cell design and in turn affect the design of the instruments are discussed, and practical circuits are described. Examples of the use of potentiostats in electrochemical measurements are given.

Abstract No. 129

Precision Direct Current Regulators

Karl Eklund, 66 Cliff Ave., Hempstead, N. Y.

A wide range of direct current and voltage regulators may be designed and constructed easily using a simple configuration of an unregulated power supply, a current passing tube, and an operational amplifier. Applications made to low and high current supplies are described. The use of the configuration in a kiloampere regulator operating at 0.2 megawatt and the use of solid-state elements also are discussed.

Abstract No. 130

Interrupter Techniques

Ernest Yeager, Western Reserve University, Cleveland 6, Ohio, and **John Yeager,** Union Carbide Research Center, Parma, Ohio

The interrupter technique for the measurement of polarization is considered in terms of (*a*) general advantages and limitations of the method; (*b*) design and performance characteristics of various circuits using vacuum tubes, thyratrons, transistors, and relays for the switching function; (*c*) apparatus for time-received potential measurements; and (*d*) optimized design of electrochemical cells for use with interrupter techniques.

Abstract No. 131

The Use of Operational Amplifiers for Measurement and Control

C. G. Enke, Princeton University, Princeton, N. J.

The operational amplifier is a high gain, stable, inverting, d-c amplifier. The amplifier controls the current in a feedback path in response to an input current. In conjunction with a few resistors and capacitors, the operational amplifier can be made into a controlled current source, a potentiostat, an isolation amplifier, an electrometer, an oscillator, a sweep generator, and many other devices, all having very high accuracy, stability, and response speed.

Abstract No. 132

Experimental Difficulties in the Measurement of Low Level Transients of Single Electrodes

B. D. Cahan, Research Div., Philco Corp., Philadelphia 34, Pa.

Theoretical and practical treatments of experimental measurements of single electrodes using pulses with rise times less than 1.0 μsec are given. The effects of ground loops, capillary size and placement, and input amplifier loading on the behavior of square-wave, step-function, interrupter, and pulse techniques are discussed. Circuitry for extremely high input impedance ($<$0.1 $\mu\mu$f), 10 mμsec rise time pre-amps, and 10 mμsec interrupters is presented in the light of the above.

Abstract No. 133

True Surface Areas of Solid Electrodes

Norman Hackerman, Dept. of Chemistry, University of Texas, Austin 12, Texas

This paper considers some of the more effective methods for determining the actual areas of solid surfaces. It is presumed that the surface to be seen does not exist in deep, narrow pores. It is also noted that electrode area is not wholly a function of the solid, *i.e*, it depends to a large extent on the size of the particle of interest in the solution phase. This follows from the fact that it is really the accessible area which is important. Microscopic measurements, electron and optical; differential capacity measurements; adsorption from solution, both by equilibrium and by rate studies; and adsorption of gases are considered. It is concluded that within the limitation of proper assignment of areas occupied per molecule of adsorbate the last of these methods provides the best information.

Abstract No. 134

The Single Crystal as a Tool in Electrochemical Research

A. T. Gwathmey, Dept. of Chemistry, University of Virginia, Charlottesville, Va.

Since the single crystal is the unit of which crystalline solids are composed, it offers a special opportunity for the study of many variables which control the electrochemistry of solid surfaces. The influence of surface structure, including crystal face, atomic steps, and imperfections, may be investigated, and little information has hitherto been available on the effects of these structural factors. Techniques for making such studies and the significance of the results obtained are discussed.

Abstract No. 135

Electrochemical and Adsorption Measurements on Single Crystals

H. C. Gatos, W. J. LaFleur, and **W. W. Harvey,** Lincoln Lab., Massachusetts Institute of Technology, Lexington 73, Mass.

An apparatus is described for electrochemical studies on single crystals under controlled environmental conditions. By employing radioactive tracers adsorption, desorption, and exchange reaction kinetics can be studied concurrently with the electrochemical measurements. The amount adsorbed is measured *in situ* with a scintillation counter. The surface of the single-crystal electrode can be cleaned and characterized after mounting in position, and the composition of the electrolyte can be altered without disturbing the sample under study. In addition, the effects of illumination on the surface behavior of single crystals of semiconductors can be investigated conveniently. Preliminary measurements on germanium single crystals are presented indicating the salient points and limitations of the apparatus.

Abstract No. 136

Electron Diffraction, Light Microscopy, and X-Ray Analysis of Electrode Surfaces

Ernest Raub, Forschungsinstitut fur Edelmetalle und Metallchemie, Schwabisch Gmund, Fernruf 3913, Stuttgart, Germany

X-ray analysis, electron diffraction, electron and light microscopy are used to investigate the surface of electrodes at anodical treatment (formation of anodic oxide layers, changes of the surface structure by electrolytic polishing) and at cathodic deposition. Of special interest are the crystal growth without and under the influence of cathodic adsorption films and the structure of electrodeposited metals and alloys. Modern techniques and the possibilities of their application are discussed for some practical instances.

Abstract No. 137

Microscope Techniques for the Study of Electrochemical Processes

A. C. Simon and **E. L. Jones,** U.S. Naval Research Lab., Washington 25, D. C.

The use of the microscope for the study of electrode processes is discussed. Various special techniques and apparatus are discussed that have been used successfully by the authors in the study of corrosion, cell reactions, and the analysis of electrode products. Methods are given for preparing samples for examination, for constructing various types of microcells, and for obtaining analytical samples from very small areas.

Abstract No. 138

Radioactive Methods and Techniques in Electrochemistry

M. Haissinsky, Laboratoire Curie, 11, Rue Pierre-Curie, Paris 5, France

This review describes the methods and techniques which are used in the study of electrode reactions (with or without net passage of current) by means of radioactive tracers and also in the study of the electrolytic behavior of ions in extremely dilute solutions. The use of radiochemical methods in the investigation of the static and dynamic properties of electrolytes and the effects of nuclear radiation on the behavior of electrodes are also briefly considered.

Abstract No. 139

Techniques of Electrochemical Measurements at High Temperatures

H. A. Laitinen, Dept. of Chemistry and Chemical Engineering, University of Illinois, Urbana, Ill.

Experimental techniques suitable for electrochemical measurements in LiCl-KCl at 400°—500° are emphasized, with a discussion of the problems involved in extending the techniques to higher temperatures and to other solvents. Solvent purification, introduction of reactants, preparation of micro-electrodes, reference electrodes, liquid and membrane junctions, materials of construction, etc., are included. Some inter-relationships between the type of measurement being made (*e.g.*, equilibrium potential, steady-state current, potential or current transient, impedance) and the experimental technique are brought out.

Abstract No. 140

Electrochemical Measurements at High Pressures

A. Distèche, Lab. of General Biology, University of Liège, Liège, Belgium

Most experimental data concerning high-pressure electrochemistry are obtained from conductance measurements covering a very wide pressure range (127,000 atm). Glass electrodes can be made to withstand 1500 atm and give reliable information on pH changes resulting from ionization shifts in buffers, acids, and weak bases. The electrode is used for deep sea (2500 m) pH recordings from the French bathyscaphe. Multielectrode cells for simultaneous pH, rH, and conductance determinations might prove useful in various fields.

Abstract No. 141

Electron Spin Resonance Measurements in the Study of Electrode Processes

D. H. Geske, Dept. of Chemistry, Cornell University, Ithaca, N. Y.

Electron spin resonance spectroscopy is a uniquely sensitive technique for detection of free radicals. Thus it is a helpful tool in the characterization of electrode processes. Experimental techniques are reviewed with emphasis on the intracavity electrode. Factors affecting sensitivity of detection are presented. Various nitroaromatic anion radicals serve to illustrate the detection of relatively stable free radicals in polarographic reductions.

Abstract No. 142

A New Method for the Measurement of Fast Ionic Reactions

H. Strehlow, Max-Planck-Institut fur Physikalische Chemie, Gottingen, West Germany

The reestablishment of an ionic equilibrium $A^+ + X^- \rightleftharpoons AX$ after a pressure jump of 50 atm is followed by conductivity measurements. Thus relaxation times between about $5 \cdot 10^{-5}$ sec and 5 sec can be determined. The experimental technique and an example of an application are discussed. The mechanisms and kinetics for the interaction of Fe^{+++}-ions with different anions were elucidated.

Abstract No. 143

Instrumentation for Electrochemical Calorimetry

J. M. Sherfey, National Bureau of Standards, Washington 25, D. C.

The heat effects of electrolysis have been studied in an adiabatic calorimeter divided into two symmetrical compartments, each of which contains a half-cell. Essentially, the experiment entails the measurement of the reversible heat developed in each half-cell, and from this the half-cell entropy change is calculated. The associated electrical circuit is different from that ordinarily used in calorimetry and includes a reference probe which permits the measurement of irreversible electrolytic effects. Adiabatic control is made possible by sensitive thermopiles which can be immersed in the electrolyte.

Abstract No. 144

Modern Techniques for Determining Transport Numbers

F. R. Duke, Dept. of Chemistry and Institute for Atomic Research, Iowa State University, Ames, Iowa

During the past fifteen years there have been developed several new techniques for measuring transport numbers; in addition, there have been refinements of some older procedures. These methods depend on separation of anode and cathode compartments with a fine porous plug plus some other arrangement to prevent gravitational flow between compartments in most cases. Then a volume change, a weight change or radiotracer movement is measured as a function of charge passed, to assess the transport numbers.

Abstract No. 145

New Developments in the Measurement of Mass Transfer Polarization and Limiting Currents

C. W. Tobias, Dept. of Chemical Engineering, University of California, Berkeley, Calif.

Interpretation of mass transport measurements over extended electrode surfaces requires knowledge of distribution of transport rates. This may be obtained by simultaneous measurement of limiting currents or polarization on a suitable number of isolated electrode segments. Apparatus and technique for dynamic measurement of limiting currents and polarization are described for free and forced convection models, where the mass transfer boundary layer varies with position and time.

Abstract No. 146

Rates of Electrode Processes by the Rotating Disk Method

D. Jahn and **W. Vielstich,** Institut fur Physikalische Chemie der Universitat Bonn, Wegelerstrasse 12, Bonn, Germany

Diffusion coefficients and the kinetics of chemical reactions proceding an electron transfer can be measured by the rotating disk electrode, evaluating limiting currents. Moreover, it is possible to measure exchange currents by determining the current-speed relation near the equilibrium potential. Thus exchange current densities up to 10 amp/cm^2 can be obtained.

Abstract No. 147

Faradaic Rectification and Electrode Processes, I. Theory

Mitsugi Senda and **Paul Delahay,** Coates Chemical Lab., Louisiana State University, Baton Rouge, La.

Fundamentals of the faradaic rectification method for the measurement of electrode kinetics parameters are reviewed as follows: types of control of electrical variable; general treatment for control of the mean current equal to zero or the mean potential equal to the equilibrium potential; effect of the double layer charging and circuit resistance; third order effects and case of an alternating voltage exceeding a few millivolts; influence of a homogeneous or heterogenous chemical process preceding charge transfer; influence of specific adsorption without and with coupled charge transfer.

Abstract No. 148

Faradaic Rectification and Electrode Processes, II. Experimental Studies

Hideo Imai, Mitsugi Senda, and **Paul Delahay,** Coates Chemical Lab., Louisiana State University, Baton Rouge, La.

Experimental verification is presented for the essential points of the theory of faradaic rectification. An installation is described for measurements in the range 50 kc to 50 Mc/sec. Generation *in situ* of one reactant is also analyzed. The following measurements are discussed: direct measurement of rectification voltage; indirect determination of rectification voltage by comparison of current-time curves for rectification and for a voltage-step; influence of cell voltage, concentration of reactants, cell resistance, double layer capacity, preceding chemical reaction and specific adsorption. A comparison is made with other relaxation methods for fast electrode processes.

Abstract No. 149

A-C Methods in Interfacial Electrical Phenomena

Akira Watanabe, Institute for Chemical Research, Kyoto University, Takatsuki, Osaka-Fu, Japan

The mechanical vibration of the electrical double layer gives rise to generation of alternating voltage. In the case of glass-liquid interfaces this effect can be used to measure streaming potentials by a-c technique, and in the case of mercury-solution interfaces it is an effect of alternating capacity current generation, which provides a new method for double layer capacity measurements. Various other methods for these measurements are also discussed in detail.

Abstract No. 150

Electrokinetic Studies with an X-Y Pulsed Measuring System

C. H. Presbrey, Jr., and Sigmund Schuldiner, U.S. Naval Research Lab., Washington 25, D. C.

The X-Y Pulsed Measuring System developed at the Naval Research Lab. by Haas and Harris was modified for electrochemical studies. By the use of a versatile pulse generator and a modified double sweep oscilloscope, a highly flexible system giving accurate control of pulse rise time, repetiton rate, length, amplitude, and delay makes possible the quantitative determination of the electrokinetic parameters of fast reaction steps. An investigation of the hydrogen reaction on platinum in acid solution resulted in a quantitative separation and determination of solution resistance, charge on the double layer, and the discharge/ionization reaction step.

Abstract No. 151

Effect of Organic Molecules on the Adsorptive Properties of Platinum Electrodes

Manfred Breiter, Research Lab., General Electric Co., Schenectady, N. Y.

The effect of different amounts of organic molecules in 1*N* $HClO_4$ on hydrogen and oxygen adsorption of smooth platinum electrodes in the potential range between hydrogen and oxygen evolution, as found by impedance measurements and potentiostatic investigations, is discussed. In the double layer region the capacity decreases with growing molecule concentration on platinum as on mercury. However, no adsorption and desorption peaks of the capacity are found on platinum.

Abstract No. 152

Characteristic Functions and Parameters in the Theory of Hydrogen Overpotential

G. W. Castellan, Dept. of Chemistry, The Catholic University of America, Washington, D. C.

Three two-step mechanisms for the hydrogen evolution reaction are considered. In each case the current-potential relation can be arranged into a compact form which is useful for the graphical interpretation of the data. A characteristic function, calculated from the data, is plotted against tanh $F\eta/2RT$. The ratio of intercept to initial slope depends on the surface coverage and a parameter ρ. This ratio is independent of the adsorption isotherm.

Abstract No. 153

Kinetics of Hydrogen Evolution at Zero Hydrogen Partial Pressure

Sigmund Schuldiner, U.S. Naval Research Lab., Washington 25, D. C.

Polarization curves for the hydrogen evolution reaction on platinum and rhodium were determined in 1M H_2SO_4 solution stirred rapidly with helium. Here the partial pressure of hydrogen gas above the solution was virtually equal to zero. Experimental results indicated that for both metals the rate-determining step in the lowest current density range was primarily the electrochemical desorption of hydrogen atoms. As the current density increased the rate-determining step changed to one that was primarily controlled by atomic combination. Kinetic equations were derived and the calculated relationships compared favorably with the experimental results.

Abstract No. 154

Effects of Electrostatic Fields on the Surface Tension of Salt Solutions

G. M. Schmid, R. M. Hurd, and **E. S. Snavely, Jr.,** Texas Research Associates, 1701 Guadalupe St., Austin 1, Texas

A high sensitivity surface film balance has been adapted to permit measurement of surface tension changes induced by the application of electrostatic fields across the surface. Preliminary measurements on saline water solutions indicate that the surface tension is lowered by up to 0.2 dynes/cm at field strengths of 7000 v/cm. Using a modified Gibbs' equation, estimates of the surface concentration changes associated with the surface tension changes have been made.

Abstract No. 155

Contact-Potential Olfactometry; Specificity and Sensitivity in Adsorption of Organic Vapors on Solids

Andrew Dravnieks, Armour Research Foundation, 10 W. 35th St., Chicago 16, Ill.

Surface potentials of solids, measurable in terms of contact (Volta) potential differences, are notoriously

sensitive to presence of adsorbed films and could serve as a means of objective olfactometry. The necessary requirements would include sufficient specificity and sensitivity of the electrical effect. Theoretical considerations show that high sensitivities should be possible. Experimental data on several solid-organic vapor systems, such as potassium dichromatic-acetone and silver oxide-thiophene, give indications of the magnitudes of effects.

Abstract No. 156

Measurement of Small Surface Areas by Krypton Adsorption

Tennyson Smith, Atomics International, Division of North American Aviation, Inc., Canoga Park, Calif.

The surface area of glass sample holders (48-178 cm^2), sintered uranium dioxide pellets (69-2000 cm^2), granular zirconium and niobium beryllides (270-2200 cm^2), and small (50 mg) powder samples of UO_2, ZrO_2, CeO_2, and TiO_2 have been measured by the BET adsorption method with krypton as the adsorbate. Measurements were made rapidly (1-2 hr) with high precision (~1%) and reproducibility (~4%). All calculations were programmed for an IBM 709 computer. A good correlation was found between powder surface area and average particle diameter. A linear relation between BET surface area and rates of oxidation of sintered UO_2 pellets was found. The importance of surface area measurements for the interpretation of kinetic studies is discussed.

Abstract No. 157

Continuous Coulometric Analysis of Chlorine Bleach Solutions

E. L. Eckfeldt and **E. R. Kuczynski,** R&D Center, Leeds & Northrup Co., North Wales, Pa.

An experimental coulometric system was devised for continuously and automatically titrating chlorine bleach solutions which ranged in concentration from 20 ppm to 3%. The titrating reagent was produced cathodically, the cell current at equivalence being a measure of concentration. The special cell construction provided about ±1% measurement accuracy throughout the concentration range. Difficulties in holding the solution at equivalence with concentrated samples were met by means of a function-transforming circuit in the automatic control system.

Abstract No. 158

The Electrokinetic Streaming Potential as a Source of Energy

R. E. Meredith, Dept. of Chemical Engineering, Oregon State College, Corvallis, Oreg.

The electrokinetic streaming potential generated within a porous matrix may be employed as a modest source of electrical energy. Conditions and variables are discussed for maximizing the power that may be extracted from such an electrokinetic device. Although the streaming potential is theoretically independent of the area to length ratio of the porous bed, this variable is shown to be important in determining the potential when current is drawn from such a system.

Abstract No. 159

Polarization Curves of Redox Systems Involving Consecutive Electron Transfers: Some Theoretical Aspects

R. M. Hurd, Texas Research Associates, 1701 Guadalupe St., Austin 1, Texas

An equation, first worked out by Vetter, describing the complete polarization curves for redox systems involving two consecutive electron transfer steps, has been examined in detail by computer solutions. It is shown that quite wide variations in the values of the individual transfer coefficients have little effect on the shape of the theoretical curves. However, as the ratio of the individual exchange currents approached 100:1, two definite linear-logarithmic regions appear in one branch of the curve. It is further shown that in many cases the diffusion current masks the true Tafel portion, leaving the "pseudo-Tafel" part as the only observable linear-logarithmic region.

Abstract No. 160

A Model for Electrochemical Reaction Kinetics of Solid-State Phase Transformations in Reversible Electrodes

G. T. Croft (present address: Pitney-Bowes Inc., Stamford, Conn.) and **Donald Tuomi,** Thomas A. Edison Research Lab., West Orange, N. J.

An atomistic model is presented for the reversible oxidation-reduction of a compound, MX, which separates a metal, M, from an electrolyte containing anions X^-. The electrochemical film growth is assumed to depend on the presence of lattice imperfections. The detailed mass and charge transport mechanism is controlled by the particular set of exchange reactions at the M-MX and MX-electrolyte interfaces. If cation vacancies and holes are the relevant lattice and electronic imperfections, there are four possible sets of exchange reactions. Each set and the distribution of the overpotential across each interface determines a particular electrochemical mechanism.

INDEX TO AUTHORS

(The number in the right-hand column is the abstract number used in the Technical Program and in the Abstracts)

	Abstract No.
Agar, G. F.	96
Alliegro, R. A.	120
Albon, N.	55
Amick, J. A.	50, 51, 52
Amick, James	86
Ando, Satoshi	123
Andrews, J. W.	79
Armstrong, W.	69
Arrott, Anthony	88
Baird, D. H.	30
Balaceanu, J. C.	116
Beck, T. R.	125
Berman, H. B.	122
Bloch, O.	116
Booker, G. R.	54
Bowman, M. G.	77
Boyd, Hugh	87
Brady, S. A.	10
Brancato, E. L.	21
Breiter, Manfred	151
Brewster, E. W.	27
Brown, J. H.	95
Brown, R. L.	89
Bugosh, John	89
Burgess, T. E.	72
Cahan, B. D.	132
Carson, W. N., Jr.	111, 115
Carter, Ralph	97
Cass, R. A.	9
Castellan, G. W.	152
Chapman, L. E.	110
Coats, D. G.	58
Coates, R. C.	126
Cowley, W. E.	118
Cremens, W. S.	98
Croft, G. T.	160
Cullen, G. W.	50, 51, 52
DaSilva, E. M.	2
deBethune, A. J.	100, 101
de Bruyn, P. L.	95, 96
Deetscreek, V. D.	85
Delahay, Paul	147, 148
Delmonte, John	11
Dermit, G.	41
Distéche, A.	140
Doyle, A. W.	90
Dreiner, Rudolf	3
Dravnieks, Andrew	155
Duke, F. R.	144
Eby, J. E.	28
Eckfeldt, E. L.	157
Eisenberg, M.	105
Eklund, Karl	129
Enke, C. G.	131
Entwisle, J. H.	118
Eriksen, W. T.	64
Fenerty, Anne	119
Feuchtbaum, R. B.	17
Fine, M. E.	59
Flaschen, S. S.	61, 66, 67
Fleischmann, M.	128
Fowler, A.	38
Freeland, P. E.	44
Freeman, M. W.	88
Frosch, C. J.	53
Garlick, G. F. J.	33
Gatos, H. C.	135
Gerlich, D.	50, 51, 52
Gershenzon, M.	53
Geske, D. H.	141
Gibson, J. O.	91
Gill, R. A. W.	32
Gilles, P. W.	77
Glendinning, W. B.	75
Gnaedinger, R. J., Jr.	61, 67
Goldberg, P.	30
Greener, E. H.	59
Gregory, D. P.	108
Gresh, M.	4
Grochowski, E. G.	56
Grosselfinger, F. B.	121
Gwathmey, A. T.	134
Hackerman, Norman	133
Haissinsky, M.	138
Hall, M. A.	61
Hamer, W. J.	127
Hamilton, D. R.	43
Hamilton, P. M.	81
Hara, Hiromichi	123
Haroldson, A. H.	19
Harrison, D. E.	25
Harvey, W. W.	135
Heath, C. W.	65
Hine, Fumio,	123, 124
Hollingshead, E. H.	119
Holmgren, J. D.	91
Houtz, C. C.	1
Hurd, R. M.	71, 154, 159
Imai, Hideo	148
Jahn, D.	146
Janz, G. J.	99, 102
Johnston, C. W.	13
Jones, E. L.	137
Juda, Walter	106
Justi, E.	103
Kaelble, D. H.	18
Kallander, D. A.	66, 67
Kallander, J. W.	16
Keller, S. P.	22
Kimmitt, M.	58
Kimura, Isao	123
Kirk, R. D.	35
Klein, D. L.	46
Kolb, G. A.	46
Kowal, M.	60
Kubitschek, H. E.	94
Kuczynski, E. R.	157
Kuhn, W. E.	93
Kurtz, R. J.	34
LaFleur, W. J.	135
Laitinen, H. A.	139
Lamprey, H.	82
Lavine, J. M.	74
Lawson, W. D.	58
Lehmann, W.	29
Leitnaker, J. M.	77
Levine, H. R.	20
Loftman, K. A.	92
Logan, R. A.	44
Longini, R. L.	42
Lorenz, M. R.	102
Love, R. W.	120
Luborsky, F. E.	84
Lufty, C. M.	66, 67
Lukacs, E. S.	60
Maddocks, F. S.	5
Marianowski, L. G.	107
Mason, D. R.	56
McNamara, J. E.	68
McNamara, M. L.	63
McWhorter, J. R.	89
Meredith, R. E.	158
Mikulyak, R. M.	53
Minahan, J. A.	6
Mitchell, W.	104
Mooney, R. W.	26
Moos, A. M.	112
Morehead, F.	38
Nickerson, J. W.	30
Nielsen, M. L.	81

	Abstract No.
Oberly, J. J.	49
Okada, Shinzo	123, 124
Oster, E. A.	110
Owen, A. E.	55
Petree, M. C.	12
Pfahnl, A.	36
Pompliano, L. A.	46, 47
Port, W. S.	8
Pesbrey, C. H., Jr.	150
Prigent, M.	116
Prior, A. C.	57, 58
Quirk, R. F.	27
Raub, Ernest	136
Read, H. J.	79
Reich, M. H.	13
Richardson, William	73
Richez, E. J.	61
Rindner, W.	74
Ripley, R. L.	82
Robertson, H. M.	68
Robinson, P. H.	64
Robinson, W. M.	65
Ropp, R. C.	27
Rothschild, S.	32
Saegusa, Fumihiko	99
Salvi, G. R.	101
Sanders, D. P.	70
Sayer, M.	33
Schlegel, E. S.	70
Schmid, G. M.	154
Schnable, G. L.	62
Schuecker, J.	121
Schuele, Wm. J.	85
Schuldiner, Sigmund	150, 153
Schulman, J. H.	35
Schwartz, N.	4
Schwuttke, G. H.	45
Sears, G. W.	89
Segal, C. L.	17
Seidensticker, R. G.	43
Senda, Mitsugi	147, 148
Sheer, C.	91
Sheff, Sumner	48
Sherfey, J. M.	143
Shirane, G.	25
Shultz, E. B., Jr.	107
Simon, A. C.	137
Sippel, R. J.	89
Smith, Tennyson	156
Snavely, E. S., Jr.	154
Spier, H. L.	24
Sprague, J. L.	6
Strehlow, H.	142
Suchow, Lawrence	23
Sullivan, M. V.	46, 47
Teliha, P. A.	14
Thornton, W. A.	37
Thun, R. E.	5
Till, Paul	83
Tirrell, C. E.	106
Tobias, C. W.	145
Trumbore, F. A.	44
Tufts, C.	41
Tuomi, Donald	160
Turkevich, John	80, 83, 86
Vaaler, Luther	126
Van Thyne, R. J.	78
Van Winkle, J.	115
Vartanian, H.	64
Vielstich, W.	113, 146
Vonnegut, Bernard	90
Vorres, K. S.	107
Wachtel, A.	31
Walsh, R. J.	81
Wanmaker, W. L.	24
Warfield, R. W.	12
Watanabe, Akira	149
Watson, J. H. L.	88
Weinreich, O.	41
White, P.	2
Whitmore, D. H.	59
Wied, O. J.	6
Williams, K. R.	108
Williamson, F. L.	15
Winsel, A.	103
Wlodek, S. T.	76
Wrotenbery, P. T.	71
Yeager, E.	114, 130
Yeager, J. F.	109, 130
Yeh, T. H.	69
York, D. B.	7
Yoshizawa, Shiro	123, 124

Current Affairs

News Notes in the Electrochemical Field

1961 ECS Membership Directory

The 1961 Membership Directory of The Electrochemical Society will be off the press shortly. Any member of the Society who has not previously ordered a copy may secure one by sending his remittance in the amount of $1.00 to Society Headquarters, 1860 Broadway, New York 23, N. Y.

Latest Volume in ECS Series

The Electrochemical Society is pleased to announce the availability of the latest volume in The Electrochemical Series:

Vol. VI, 1958 Issue, of the **Abstracts of the Literature on Semiconducting and Luminescent Materials and Their Applications.** Compiled by Battelle Memorial Institute, under the auspices of The Electrochemical Society, Inc. Edited by J. J. Bulloff and C. S. Peet. Sponsored by the Air Force Office of Scientific Research and Battelle Memorial Institute. Price: $14.00; 528 pages (hard cover). (*See* advertisement on page 42*C* of this issue.)

The volume is available from the publisher, John Wiley & Sons, Inc., 440 Park Ave. South, New York 16, N. Y. *A 33 1/3% discount is offered to ECS members only and can be obtained by ordering through Society Headquarters, 1860 Broadway, New York 23, N. Y.*

Frontiers in Chemistry Lecture Series

The 20th annual Frontiers in Chemistry lectures, an activity of the Dept. of Chemistry of Western Reserve University, Cleveland, Ohio, began on February 10, and will continue through April 21. The 20th annual series covers two major topics: Part I. The Solid State, and Part II. The Chemistry of Large Molecules.

The lectures are scheduled on consecutive Fridays from February 10 through April 21, with the exception of March 31.

The complete program follows.

Part I

Feb. 10—"The Growth of Solids" by D. A. Vermilyea

Feb. 24—"Recent Studies of the Surface Chemistry of Metals with the Aid of Large Crystals" by A. T. Gwathmey

March 10—"The Effect of Pressure on Electronic Structures" by H. G. Drickamer

March 24—"Imperfections in Solids" by N. Cabrera

April 14—"Organic Semiconductors" by Jan Kommandeur

Part II

Feb. 17—"Preparation and Properties of Multi-Component Polymer Systems" by R. B. Mesrobian

March 3—"Phosphorous-Based Polymers. Structural Reorganization in Polymers" by J. R. Van Wazer

March 17—"Organometallic Polymers" by E. G. Rochow

April 7—"Some Aspects of Ionic Polymerization and Copolymerization" by C. G. Overberger

April 21—"Stereospecific Polymerization" by T. G. Fox.

Henri André Receives Gaston Planté Medal

Henri G. André, French scientist known as the "father" of the first practical rechargeable silver-zinc battery, received the Gaston Planté Medal and Prize of the Société Francaise des Electriciens, in Paris, France, in December 1960.

The Planté award is named for the 19th Century French inventor credited with the development of the first storage batteries. The Société is France's highest ranking professional association in the field of electrical engineering and related sciences.

Professor André also holds the Ampère Medal of the Société, awarded for his achievements in electrochemistry. His experience in the electrical field spans more than 40 years. Among his other honors is the Croix de Chevalier of the French Legion of Honor.

He is associated with Yardney International Corp., New York City, which holds world-wide rights to his inventions, and, for the past 12 years, has undertaken the further development of the silver-zinc battery. Professor André conducts his research in his private laboratory in Montmorency, France. The André-Yardney silver-zinc battery is manufactured in the United States by Yardney Electric Corp., New York City, under the trade name of Silvercel.

Professor André, frequent author and lecturer, has appeared before several American professional groups during his visits to the U. S. He has also become well known both in France and America as a proponent of the return of the battery-powered electric car; he has developed such experimental vehicles using silver-zinc batteries.

Professor André is a member of The Electrochemical Society.

Notice to Members

According to the Constitution of the Society, Article III, Section 9, "Any member delinquent in dues after April 1 of each year shall no longer receive the Society's publications. . . ." Such delinquents will not receive the May issue of the JOURNAL. A reminder notice was mailed to delinquents early in February; a final notice will be mailed about the first week in April.

G.E. Makes New, Large Diamonds

"For the first time in history, man has made large diamonds," according to Dr. Guy Suits, General Electric Co. vice-president and director of research. The large diamonds—over a carat in size—are dark in color and, because of structural imperfections, are not yet of sufficient mechanical strength for industrial applications.

This scientific feat was achieved at the General Electric Research Laboratory in Schenectady, N. Y., where the first man-made diamonds were announced in 1955. However, it was pointed out that work on the large diamonds is still in the early development stage and it is impossible to predict when G.E. will succeed in making large diamonds with me-

chanical properties comparable to its small industrial diamonds.

General Electric's diamond research program is directed by Dr. A. L. Marshall and A. J. Nerad. Drs. Francis P. Bundy, Herbert M. Strong, Peter Cannon, and Robert Wentorf of the Research Laboratory, and H. P. Bovenkerk, now with the Metallurgical Products Dept., are the leading scientists responsible for the progress of this program.

In response to industrial needs for larger diamonds, G. E. has succeeded in increasing its control over the size, mechanical quality, and shapes of its diamonds. Diamonds up to 1/10 of a carat in size, of excellent industrial quality, can now be made in the laboratory; however, they are not yet available commercially.

There is also a demand in industry for diamonds in full-carat ranges for drills, dressing tools, dies, and single point cutting tools. If G.E. can perfect the mechanical structure and improve the strength of its new, carat-size diamonds, the company will be able to compete with natural stones in the full industrial range.

Reynolds International to Build Plant in Venezuela

Reynolds International, Inc., Richmond, Va., has concluded an agreement with the Venezuelan government to form a corporation to build an aluminum reduction plant in the Caroni region of southeastern Venezuela.

The ultimate cost of the plant is expected to be more than $30,000,000. Initial production capacity will be about 25,000 tons per year. About 80% of this production is expected to be consumed in Venezuela and the remainder exported, until Venezuelan industry is able to absorb the entire output.

An agreement has been signed providing for 50% ownership by Reynolds International and 50% by a company owned by government interests. The contract provides for a 30-year power supply from the Caroni River hydroelectric project.

Reynolds International now has aluminum fabricating facilities in Venezuela, and the company plans to expand these.

Symposium on Titrimetric Methods of Analysis

A Symposium on Titrimetric Methods of Analysis sponsored by the Analytical Chemistry Division of The Chemical Institute of Canada will be held in Cornwell, Ont., on May 8 and 9, 1961.

Three aspects of titrimetric analysis will be emphasized: complexometric titrations, electrometric titrations, and titrations in nonaqueous solvents. In addition to the more usual contributed papers of 20 minutes' length, the symposium committee is accepting shorter papers illustrating specific applications.

Mr. J. R. McCallum, Courtaulds (Canada) Ltd., Cornwall, Ont., is in charge of the program.

Division News

Electronics Division

The Nominating Committee (C. T. Lattimer, Chairman; F. J. Biondi, L. Thorington) has selected the following nominees for officers of the Electronics Division during the two-year term 1961-1963:

Chairman—R. J. Ginther, U. S. Naval Research Lab., Washington 25, D. C.

Vice-Chairman (Luminescence)—H. F. Ivey, Westinghouse Electric Corp., Lamp Div., Research Dept., Bloomfield, N. J.

Vice-Chairman (General Electronics)—C. P. Marsden, National Bureau of Standards, Washington 25, D. C.

Vice-Chairman (Semiconductors)—F. H. Horn, General Electric Research Lab., Schenectady, N. Y.

Secretary-Treasurer—A. E. Hardy, Radio Corp. of America, Lancaster, Pa.

Each nominee has given assurance of his willingness to serve if elected.

The Bylaws of the Division provide that additional nominations may be made by petition signed by five members of the Division. Such petitions must be in the hands of the Chairman of the Nominating Committee before the election, and the nominees must have given assurance of their willingness to serve if elected.

The election will be held at the business meeting of the Electronics Division during the Spring Meeting of the Society in Indianapolis, April 30-May 3, 1961.

A. E. Hardy, *Sec.-Treas.*

Corrosion Division Special Symposium, 1961 Detroit Meeting

A special Symposium on Surface Structure versus Corrosion Behavior is being planned for the Detroit Meeting, October 1-5, 1961, by the Corrosion Division of The Electrochemical Society. Papers describing original research are invited for this session.

Of particular interest are studies which make use of a new or novel technique for identifying the point-to-point structure at the metal surface, and correlating this information with corrosion behavior. Examples that might be cited are the use of the electron probe, or the use of local-area electron diffraction, in developing information on the local character of the surface.

Other techniques that can find application in corrosion and oxidation experiments are the use of the field emission microscope, low-voltage electron diffraction, the ellipsometer, petrographic microscope, and the solid mass spectrometer.

If you can prepare a paper and wish it to be considered for this symposium, please send four copies of an abstract (*not exceeding 75 words*) of the proposed paper *before May 1, 1961* to Frederick W. Fink, Symposium Chairman, c/o Battelle Memorial Institute, 505 King Ave., Columbus 1, Ohio.

Please note the following policy of the Society: "The Chairman shall select a paper only if the author, one of the coauthors, or a qualified individual designated by the author, will present the paper."

Frederick W. Fink

Electrothermics and Metallurgy Division

The Nominating Committee (A. C. Haskell, Chairman) of the Electrothermics and Metallurgy Division presents the following slate of officers for the 1961-1963 term:

For Chairman—J. H. Westbrook, Ceramic Studies Section, Research Dept., General Electric Co., P. O. Box 1088, Schenectady, N. Y.

For Vice-Chairman—W. E. Kuhn, Carborundum Co., P. O. Box 337, Niagara Falls, N. Y.

Notice to Members and Subscribers
(Re Changes of Address)

To insure receipt of each issue of the JOURNAL, please be sure to give us your old address, as well as your new one, when you move. Our records are filed by states and cities, not by individual names. The Post Office does not forward magazines.

For Vice-Chairman—L. H. Juel, Great Lakes Carbon Corp., P. O. Box 637, Niagara Falls, N. Y.

For Secretary-Treasurer—L. M. Litz, Research Labs., National Carbon Co., P. O. Box 6116, Cleveland 1, Ohio

For Members-at-Large (four required)—T. D. McKinley, Pigment Dept., Experimental Station, E. I. du Pont de Nemours & Co., Wilmington 98, Del.; C. A. Hampel, 8501 Harding Ave., Skokie, Ill.; R. R. Rogers, Mines Branch, Dept. of Mines & Technical Surveys, 551 Booth St., Ottawa, Ont., Canada; M. C. Udy, Strategic-Udy Processes, Inc., 3986 Royal Ave., Niagara Falls, N. Y.

Each nominee has given assurance of his willingness to serve if elected.

The election will be held at the business meeting of the Division to be held during the Spring Meeting of the Society in Indianapolis, April 30-May 3, 1961.

L. H. Juel, *Sec.-Treas.*

Personals

Fred M. Berkey has been appointed assistant director in the engineering sales department of Monsanto Chemical Co.'s Inorganic Chemicals Division at St. Louis, Mo., after serving as manager of the electrolysis section in that department.

John J. Bohrer, director of research for International Resistance Co., Philadelphia, Pa., has been elected a Fellow of the New York Academy of Sciences. The election was in recognition of Dr. Bohrer's "outstanding work toward the advancement of science." He is the author of numerous technical studies on such subjects as copolymerization and organic semiconductors.

Dodd S. Carr has rejoined Bart Laboratories and Design, Inc., Newark, N. J., as vice-president of research. In addition to his duties in research on new and improved electroplating processes, Dr. Carr will serve as quality control director for the parent company, Bart Manufacturing Corp. Until recently, Dr. Carr was technical assistant to the vice-president of the Freeport Nickel Co., and from 1952 to 1959 he was director of research for the Bart Manufacturing Corp.

Herbert H. Kellogg, of the Henry Krumb School of Mines, Columbia University, New York City, and **Sujit K. Basu,** a graduate student at Purdue University, have been named to receive the 1961 Extractive Metallurgy Division Award of The Metallurgical Society of AIME for their paper on "Thermodynamic Properties of the System Pb-S-O to 1100°K," published in the society's "Transactions."

Rolf Lindenhayn, Jr., has been appointed western division manager of brush and railroad products for National Carbon Co., Division of Union Carbide Corp. Making his headquarters in San Francisco, Calif., Mr. Lindenhayn will be responsible for marketing activities in connection with industrial, railroad, fractional horsepower, and aircraft brushes; spectroscopic electrodes and powders; and railroad and navigational signaling batteries.

Samuel Eidensohn

Samuel Eidensohn, chief project engineer of Exide Industrial Division, Electric Storage Battery Co., Philadelphia, Pa., died on December 2, 1960 after an extended illness. He was 49 years old.

One of the country's outstanding authorities on submarine batteries, Mr. Eidensohn joined Exide in March 1958 after serving for 13 years as chief of the battery section of the U. S. Navy's Bureau of Ships. His post at Exide was created at the time of his appointment. He had authority over all engineering activities for submarine and alkaline battery development.

A native New Yorker, Mr. Eidensohn received a bachelor of science degree in electrical engineering from the College of the City of New York in 1936. After further study in electrochemistry, physical chemistry, and thermodynamics in the graduate school of the U. S. Dept. of Agriculture, Washington, D. C., he joined the battery section of the Bureau of Ships in 1939.

In 1956, Mr. Eidensohn received the Distinguished Civilian Service Award for developmental work in submarine batteries and improving submarine operation. This is the highest honor that the Navy confers on civilian employees.

His work on zinc-silver oxide storage batteries won him wide acclaim in the scientific world and in the battery industry.

Mr. Eidensohn was a member of The Electrochemical Society and one of the original members of its Battery Division.

He is survived by his wife, Esther, three sons, and two daughters, of Cinnaminson, Burlington County, N. J.

Book Reviews

Electropolishing, Anodizing and Electrolytic Pickling of Metals, by N. P. Fedot'ev and S. Ya. Grilikhes. Translated from the Russian by A. Behr. Published by Robert Draper, Ltd., 85 Udney Park Rd., Teddington, Middelsex, England, 1960. 285 pages; $8.40.

Professor Fedot'ev and Dr. Grilikhes describe the fundamentals of polishing, oxidation, pickling, and etching processes for metals carried out with the aid of an electric current. Information is given on the practical aspects of the processes, on bath compositions, methods of controlling and maintaining the solutions, and on the effect of various treatments on the properties of the metals.

The subject matter is quite complete and well organized. An extended theoretical treatment of the mechanism of electropolishing is given. Considerable attention is given to the sharpening of cutting tools by special electropolishing procedures. The chapter on anodizing of aluminum delves deeply into the theory and mechanism of the process. It presents the information in clearer fashion than do most American books on the subject. There was no mention, however, of anodic films of aluminum oxide of the type used in electrolytic capacitors.

This book would be equally useful to technical personnel engaged in metal finishing and to students at technical colleges.

Henry S. Myers

Electrochemical Engineering, 4th Edition, by C. L. Mantell. Published by McGraw-Hill Book Co., Inc., New York City, 1960. 680 pages; $16.50.

This book, under a new title, is the fourth edition of Dr. Mantell's "Industrial Electrochemistry" which was last revised in 1950. It remains the most comprehensive American treatise on industrial electrochemical practice.

The author states that the incentive for the new edition is to be found in the tremendous expansion of the industry in the last decade. However, the reader should not ex-

pect a completely new book. Some portions of the text have been rewritten, old material has been deleted, and newer products and processes added. At the same time, chapters have been rearranged in more logical fashion and their titles often have been changed. Large sections remain virtually unaltered.

In the earlier editions, the theoretical sector was weak. It remains so, despite the inclusion of the 1948 definitions of electrical units and a new treatment of electromotive force. The discussion of theory and principles is confusing and frequently in error. Although this area leaves much to be desired, the remainder of the book maintains the earlier standard of detailed and thorough coverage.

The discussion of electrorefining has been revised by modernizing the treatment of nickel and cobalt purification, but the chapter on electrowinning from aqueous electrolytes is substantially unchanged except for a small amount of material on newer metals. Electrolysis of alkali halides now includes a section on the electrolysis of HCl (thereby making the chapter title a misnomer) and an expansion of the previous description of fluorine production. The chapter on electrolytic hydrogen and oxygen has been fortified by the addition of deuterium separation. The section dealing with fused salts has undergone considerable revision and improvement both in the introductory portion and in the process descriptions. Under the new heading of "Chemelectrics," the author has combined the deleterious exergic process of corrosion with the beneficial one of energy production from primary and secondary cells. The material on corrosion has been expanded. Earlier chapters on rectifiers, materials of construction, and power generation have been combined into a new engineering section and have been amplified and modernized in the process.

Complete revision of a book of this size and detail is a task of no small magnitude, but it is to be hoped that Dr. Mantell will continue his efforts to keep it current. The changes that have been made in the new edition are welcome, and his work remains the best American source book of the entire electrochemical industry.

M. Kolodney

Transport Phenomena, by R. B. Bird, W. E. Stewart, and E. N. Lightfoot. Published by John Wiley & Sons, Inc., New York, 1960. xxi + 780 pages; $13.75.

It is generally recognized that there has long been a need for more efficient presentation of analogous or associated phenomena in the fields of engineering and the applied sciences. In this regard, it is a pleasure to welcome "Transport Phenomena" to the current list of textbooks, because this work certainly offers a start in that direction.

The volume brings together under one cover, and in three parts, a comprehensive coverage of momentum transport (flow of viscous fluids), energy transport (flow of heat), and mass transport (flow of chemical species in mixtures). Part I covers mechanisms of momentum transport; velocity distributions under a variety of conditions; and equations and balances for isothermal systems. Part II treats thermal conductivity and mechanisms of energy transport; temperature distribution problems for turbulent and laminar flow; energy transport by radiation; and energy equations and balances for nonisothermal conditions. Part III deals with variables which influence mass transport and rates of diffusion; concentration distributions in laminar and turbulent flow; and equations of change, macroscopic balances, and interphase transport in multicomponent systems. The book is appended with a section on mathematical relations; tables for predicting transport properties; and a summary of constants, conversion factors, and notation. A detailed index is given which makes this rather large book easy to use.

The authors follow a similar approach in developing each part of the book. First, the basic theory is introduced by means of illustrative problems that are designed to stress physical principles. Then more general methods are employed to solve a variety of problems of practical application. Finally, "macroscopic balances" (or the integrated form of the "conservation equations") are utilized to give an over-all view of the phenomenon. Each chapter is generously supplemented with numerical examples, discussion questions, and class problems.

The coverage of mass transport is an especially significant contribution to the textbook literature. This subject, which is inadequately described and ill defined in many texts, is presented in this book in a simple but precise manner with a remarkable absence of empiricism. It is unfortunate, however, that the authors have not only chosen to retain the exotic symbolism that seems to have

SEMICONDUCTOR DEVELOPMENT

Pacific Semiconductors, Inc., a pioneer in advanced semiconductor devices, needs senior

Physicists and Electrical Engineers

to augment its development programs. We seek men who have several years experience in semiconductor device development, with demonstrated capability of contributing to the state of the art in a significant way. Unusual opportunities in advancement and support of your work are offered by this leader in the industry.

Inquiries on this and other opportunities at Pacific Semiconductors, Inc. are invited. Please write in confidence to:

J. W. Peterson, *Vice President Research and Development*

PSI *Pacific Semiconductors, Inc.*

14520 South Aviation Boulevard
Lawndale (Los Angeles County), Calif.

become prevalent in this particular field, but also have chosen to add to it. Such notation always seems unduly to disturb the beginning student; and, even for those that have become hardened to it, this type of nomenclature makes it appear (regardless of the case) as if there were many more variables than equations.

This book will be slow reading for those who do not possess a strong mathematical background. Although the authors have attempted, in many places, to lead the reader by the hand through involved mathematical examples, one should be well familiar with vector and tensor notation, complex variables, and partial differential equations in order to follow some sections of this work. It is this factor that will restrict the use of this text to the graduate level in some engineering schools. The authors, nevertheless, are to be congratulated on essentially delivering the message, "This is the direction in which the field is moving, even though your students may not be able to keep up."

To some, the title may suggest that the book is primarily concerned with the task of forming analogies among momentum, energy, and mass transport processes. This, however, does not appear to be the intent of the authors. Each section is quite independent and may be read with only infrequent reference to preceding parts. The value of this combination is rather in the wise and conjunctive use that is obtained by carrying the applied mathematics from one subject to the next. The analogies are there, however, if one cares to use them.

The subject matter and its method of presentation are most likely to restrict the use of this book to chemical and mechanical engineering. The authors, nevertheless, are hoping also to gain readers in the fields of physical chemistry, soil physics, meteorology, and biology.

Robert E. Meredith

The Use of Organic Reagents in Inorganic Analysis, by A. I. Busev and N. G. Polianskii. Translated from the Russian by J. T. Greaves. Published by Pergamon Press, Inc., New York, 1960. 76 pages; $3.50.

This little photolithographed book reviews the work done on organic analytical reagents as reported in the literature, mainly Russian, between 1953 and 1955.

The general plan of the book is reminiscent of the sections on organic reagents which have appeared in the "Annual Analytical Reviews" of "Analytical Chemistry."

The methods outlined are *not* detailed enough to be used as laboratory procedures, but the text may prove useful as an index to the Russian literature on organic reagents for the years 1953-1955.

There are two chapters: I. Some General Problems in the Application of Organic Reagents; II. The Most Important Methods of Determining Elements Using Organic Reagents.

There is a table of contents, but no index. Also, there is a table of references listing 198 references for Chapter I, and 272 for Chapter II.

Barnet Naiman

Announcement from Publisher

Proceedings of 14th Annual Power Sources Conference

The PSC Publications Committee, P. O. Box 891, Red Bank, N. J., has a limited supply of the "Proceedings of the 14th Annual Power Sources Conference" available at $5.00 per copy. This volume contains 38 papers presented at the May 1960 Atlantic City meeting with sessions on thermal energy conversion, solar energy conversion, fuel cell batteries, secondary batteries, energy conversion systems, energy storage devices, high-rate batteries, and primary batteries.

Copies of the Proceedings of the earlier Conferences are now out of print and are available only from the Office of Technical Services, Dept. of Commerce, Washington 25, D. C., as photostatic copies at a cost varying from $20.00 to $30.00. The Proceedings of the 10th, 11th, 12th, and 13th Conferences (1956-1959) have been assigned numbers, PB 125427, PB 137392, PB 145520, and PB 145521, respectively.

New Products

99.999% Pure Silver. Engelhard Industries, Inc., Newark, N. J., has announced the availability, in large commercial quantities, of 99.999% pure silver at modest premiums over current prices for bulk silver of standard commercial 99.9% purity. Designated as Grade E-4 or "Spectropure" (trademark rights applied for) silver, the metal is being produced in the form of needles of approximately 1 to 3 mm maximum di-

RARELY
(IF EVER)

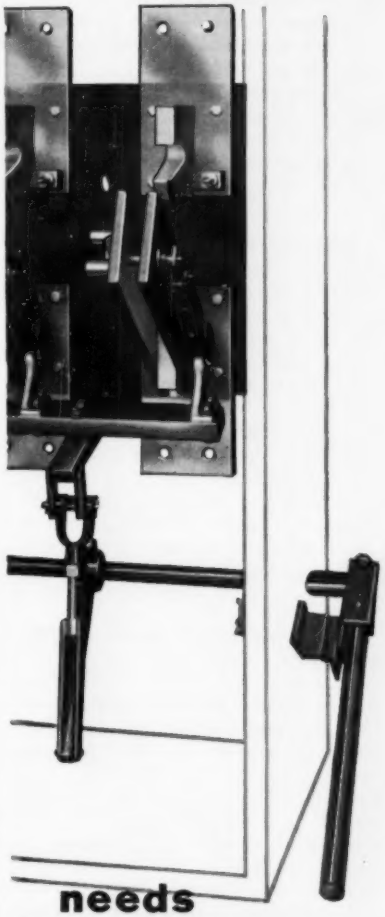

needs
MAINTENANCE

Pringle disconnect switches for high-current equipment carry as much as 50,000 amperes, continuously, with no more of a heat rise than you would get from copper bus bars bolted together. These switch blades actually are bolted together. Under a constant pressure of 600 lbs./sq. inch. Without springs. Yet, they open easily after months (or years) of closed operation. Heat, fatigue, lack of movement won't affect the operating mechanism. Constant, periodic maintenance is unnecessary.

Less complex than most high-capacity disconnect devices. Less expensive too. Available in single- or multi-pole models, front or rear connected, live front or steel enclosed. With or without high-capacity fuses. For use on crane conductor rails, transformer secondaries, or AC and DC switchboards. Wherever high-current equipment must be isolated for periodic servicing.

Write for Industrial Switch Catalog

PRINGLE
ELECTRICAL MANUFACTURING CO.
1910 NORTH SIXTH STREET
PHILADELPHIA 22, PENNA.

mension, and in the form of 2 x 4 x 15 in. ingots weighing approximately 700 troy oz, and 3 x 4 x 8 in. ingots weighing some 500 oz. Other size ingots, fabricated forms such as sheet or wire, and vacuum cast bars also can be supplied.

All batches of Engelhard Spectropure silver are subjected to a special high-precision spectrographic analysis; a certificate of analysis on each lot will be supplied if desired.

High-Purity Cadmium Plating Solution. Manufacturers of solid-state electronic components who plate semiconductors with cadmium are now offered high-purity cadmium fluoborate solution, direct from stock, by Fisher Scientific Co., 717 Forbes Ave., Pittsburgh 19, Pa. Reagent specialists at the Fisher Chemical Manufacturing Div. have brought the metal content of their new Certified Reagent-Grade Cadmium Fluoborate Solution to a new low (example: silver is kept below 0.00003%, copper below 0.00005%).

Doped-to-Specification Silicon. Single-crystal silicon doped to the specific requirements of device manufacturers is now available from Dow Corning. Rigid controls coupled with integrated production techniques result in material that permits easier processing and completed devices with smaller variations in characteristics. Produced in various diameters up to 26 mm (approx. 1 in.) and in lengths to 360 mm (approx. 14 in.), Dow Corning Doped Single-Crystal Silicon is now available in production quantities.

For further information, write Dept. CS-143, Dow Corning Corp., Midland, Mich.

Advertiser's Index

American Brass Company 44C

Bell Telephone Laboratories, Inc. 43C

Great Lakes Carbon Corp. Electrode Division ..... Cover 2

Hooker Chemical Corporation .. 80C

Lockheed Missiles & Space Division 80C

National Bureau of Standards .. 80C

Pacific Semiconductors, Inc. 78C

Pringle Electrical Mauufacturing Co. 79C

John Wiley & Sons, Inc. 42C

Employment Situations

Positions Available

Chemists and Chemical Engineers—We need physical, organic and inorganic chemists, and chemical engineers to carry out Engineering and development work in the rapidly growing power sources field. Research & Development center located in Minneapolis near University of Minnesota. Battery experience preferred but not required. Send resumés to: J. W. Baxter, Employee & Labor Relations, Gould-National Batteries, Inc., E. 1326 First National Bank Bldg., St. Paul 1, Minn.

Four challenging research positions for experienced surface chemists, in fully-equipped laboratory devoted to research and development on aluminum and copper alloys, involving: A. Electrochemical kinetics, adsorption, and oxide film structure investigations related to finishing processes. B. Studies of interfacial surface reactions between polymeric resins and metal oxide surfaces relating to strength and permanence of joints in the adhesive bonding of metals. C. Mechanisms relating to surface phenomena, associated with liquid metal-solid metal inter-action as applied to soldering and brazing. D. Surface and electrochemical reactions effecting the kinetics of general, localized, and stress corrosion processes. Pleasant living, with access to major university. Send reply to R. H. Endriss, Personnel Manager, Olin Mathieson Chemical Corp., 125 Munson St., New Haven, Conn.

Position Wanted

Chemical Engineer—B.S., registered professional engineer, 17 years of electrolytic background including development and production of tantalum capacitors, development in electrodeposition processes, corrosion. Desires responsible position in development or production work. *Reply to Box No. 371, c/o The Electrochemical Society, 1860 Broadway, New York 23, N. Y.*

PHYSICAL CHEMIST

or

ELECTROCHEMIST

Ph.D., strong background in fused salts for a basic and applied research program concerned with electrochemical energy conversion devices. This program is unclassified and publications are encouraged. Applicant must be capable of working independently and have a demonstrated experimental ability. Background in electrochemistry is desired but not essential.

Please address confidential inquiries to Mr. R. C. Birdsall, Employment Manager, Lockheed Missiles and Space Division, Dept. M-21B, 962 West El Camino Real, Sunnyvale, Calif. U.S. citizenship or existing Department of Defense industrial security clearance required.

Lockheed

MISSILES AND SPACE DIVISION

SUNNYVALE, PALO ALTO, VAN NUYS, SANTA CRUZ, SANTA MARIA, CALIFORNIA
CAPE CANAVERAL, FLORIDA • HAWAII

NATIONAL BUREAU OF STANDARDS
U. S. Department of Commerce

Opportunities for—
Electrochemists
Physical Chemists
Inorganic Chemists—
in electrochemical research
Original work on fundamental problems related to electrode reactions, non-aqueous electrolysis, electrocrystallization and polarization. Ph.D. in Chemistry required.

Career Civil Service. Salary $7560 to $10,635 depending on qualifications.

Apply to:
Dr. Abner Brenner
Chief, Electrodeposition Section
National Bureau of Standards
Washington 25, D. C.

OUTSTANDING OPPORTUNITY FOR ELECTROCHEMIST

Rapidly growing diversified chemical corporation requires an electrochemist with doctoral degree or equivalent experience. The field of work includes laboratory and plant studies on problems concerned in the development of industrial sales for the production of caustic-chlorine, chlorate and perchlorate.

Position involves supervision of a small laboratory with one or two technicians. Creative thinking is desired and opportunity for original work is afforded. The work concerns the basic products of a corporation which has a position of leadership in the field.

Send resume and salary requirement to Mr. A. V. Thorpe, Supervisor of Technical Placement,

HOOKER CHEMICAL CORP.
NIAGARA FALLS, N. Y.

The Electrochemical Society

Patron Members

Aluminum Co. of Canada, Ltd., Montreal, Que., Canada

International Nickel Co., Inc., New York, N. Y.

Olin Mathieson Chemical Corp., Chemicals Div., Industrial Chemicals Development Dept., Niagara Falls, N. Y.

Union Carbide Corp.
Divisions:
Union Carbide Metals Co., New York, N. Y.
National Carbon Co., New York, N. Y.

Westinghouse Electric Corp., Pittsburgh, Pa.

Sustaining Members

Air Reduction Co., Inc., New York, N. Y.

Ajax Electro Metallurgical Corp., Philadelphia, Pa.

Allen-Bradley Co., Milwaukee, Wis.

Allied Chemical Corp.
Solvay Process Div., Syracuse, N. Y.

Alloy Steel Products Co., Inc., Linden, N. J.

Aluminum Co. of America, New Kensington, Pa.

American Metal Climax, Inc., New York, N. Y.

American Potash & Chemical Corp., Los Angeles, Calif. (2 memberships)

American Smelting and Refining Co., South Plainfield, N. J.

American Zinc Co. of Illinois, East St. Louis, Ill.

American Zinc, Lead & Smelting Co., St. Louis, Mo.

American Zinc Oxide Co., Columbus, Ohio

M. Ames Chemical Works, Inc., Glens Falls, N. Y.

Armco Steel Corp., Middletown, Ohio

Basic Inc., Maple Grove, Ohio

Bell Telephone Laboratories, Inc., New York, N. Y. (2 memberships)

Bethlehem Steel Co., Bethlehem, Pa. (2 memberships)

Boeing Airplane Co., Seattle, Wash.

Burgess Battery Co., Freeport, Ill. (4 memberships)

Canadian Industries Ltd., Montreal, Que., Canada

Carborundum Co., Niagara Falls, N. Y.

Catalyst Research Corp., Baltimore, Md.

Columbian Carbon Co., New York, N. Y.

Columbia-Southern Chemical Corp., Pittsburgh, Pa.

Consolidated Mining & Smelting Co. of Canada, Ltd., Trail, B. C., Canada (2 memberships)

Continental Can Co., Inc., Chicago, Ill.

Cooper Metallurgical Associates, Cleveland, Ohio

Corning Glass Works, Corning, N. Y.

Diamond Alkali Co., Painesville, Ohio (2 memberships)

Dow Chemical Co., Midland, Mich.

Wilbur B. Driver Co., Newark, N. J. (2 memberships)

E. I. du Pont de Nemours & Co., Inc., Wilmington, Del.

Eagle-Picher Co., Chemical Div., Joplin, Mo.

Eastman Kodak Co., Rochester, N. Y.

Thomas A. Edison Research Laboratory, Div. of McGraw-Edison Co., West Orange, N. J.

Electric Auto-Lite Co., Toledo, Ohio
C & D Division, Conshohocken, Pa.

Electric Storage Battery Co., Yardley, Pa.

Englehard Industries, Inc., Newark, N. J. (2 memberships)

The Eppley Laboratory, Inc., Newport, R. I. (2 memberships)

Exmet Corp., Tuckahoe, N. Y.

Fairchild Semiconductor Corp., Palo Alto, Calif.

Food Machinery & Chemical Corp.
Becco Chemical Div., Buffalo, N. Y.
Westvaco Chlor-Alkali Div., South Charleston, W. Va.

Foote Mineral Co., Paoli, Pa.

Ford Motor Co., Dearborn, Mich.

General Electric Co., Schenectady, N. Y.
Chemistry & Chemical Engineering Component, General Engineering Laboratory
Chemistry Research Dept.
General Physics Research Dept.
Metallurgy & Ceramics Research Dept.
Aircraft Accessory Turbine Dept., West Lynn, Mass.

General Instrument Corp., Newark, N. J.

(Sustaining Members cont'd)

General Motors Corp.
Delco-Remy Div., Anderson, Ind.
Guide Lamp Div., Anderson, Ind.
Research Laboratories Div., Detroit, Mich.
General Telephone & Electronics Laboratories Inc., Bayside, N. Y. (2 memberships)
General Transistor Corp., Jamaica, N. Y.
Gillette Safety Razor Co., Boston, Mass.
Globe-Union, Inc., Milwaukee, Wis.
Gould-National Batteries, Inc., Minneapolis, Minn.
Grace Electronic Chemicals, Inc., Baltimore, Md.
Great Lakes Carbon Corp., New York, N. Y.
Hanson-Van Winkle-Munning Co., Matawan, N. J. (2 memberships)
Harshaw Chemical Co., Cleveland, Ohio (2 memberships)
Hercules Powder Co., Wilmington, Del.
Hill Cross Co., Inc., West New York, N. J.
Hoffman Electronics Corp., El Monte, Calif.
Hooker Chemical Corp., Niagara Falls, N. Y. (3 memberships)
Hughes Aircraft Co., Culver City, Calif.
International Business Machines Corp., Poughkeepsie, N. Y.
International Minerals & Chemical Corp., Skokie, Ill.
ITT Federal Laboratories, Div. of International Telephone & Telegraph Corp., Nutley, N. J.
Jones & Laughlin Steel Corp., Pittsburgh, Pa.
K. W. Battery Co., Skokie, Ill.
Kaiser Aluminum & Chemical Corp.
Div. of Chemical Research, Permanente, Calif.
Div. of Metallurgical Research, Spokane, Wash.
Kawecki Chemical Co., Boyertown, Pa.
Kennecott Copper Corp., New York, N. Y.
Keokuk Electro-Metals Co., Keokuk, Iowa
Libbey-Owens-Ford Glass Co., Toledo, Ohio
M. & C. Nuclear, Inc., Attleboro, Mass.
Mallinckrodt Chemical Works, St. Louis, Mo.
P. R. Mallory & Co., Indianapolis, Ind.
McGean Chemical Co., Cleveland, Ohio
Merck & Co., Inc., Rahway, N. J.
Metal & Thermit Corp., Detroit, Mich.
Minnesota Mining & Manufacturing Co., St. Paul, Minn.
Monsanto Chemical Co., St. Louis, Mo.
Motorola, Inc., Chicago, Ill.
National Cash Register Co., Dayton, Ohio
National Lead Co., New York, N. Y.
National Research Corp., Cambridge, Mass.
National Steel Corp., Weirton, W. Va.
New York Air Brake Co., Kinney Vacuum Div., Boston, Mass.
Northern Electric Co., Montreal, Que., Canada
Norton Co., Worcester, Mass.
Ovitron Corp., Long Island City, N. Y.
Peerless Roll Leaf Co., Inc., Union City, N. J.
Pennsalt Chemicals Corp., Philadelphia, Pa.
Phelps Dodge Refining Corp., Maspeth, N. Y.
Philco Corp., Philadelphia, Pa.
Philips Laboratories, Inc., Irvington-on-Hudson, N. Y.
Poor & Co., Promat Div., Waukegan, Ill.
Potash Co. of America, Carlsbad, N. Mex.
Radio Corp. of America
Tube Div., Harrison, N. J.
RCA Victor Record Div., Indianapolis, Ind.
Ray-O-Vac Co., Madison, Wis.
Raytheon Manufacturing Co., Waltham, Mass.
Reynolds Metals Co., Richmond, Va.
Rheem Semiconductor Corp., Mountain View, Calif.
Schering Corporation, Bloomfield, N. J.
Shawinigan Chemicals Ltd., Montreal, Que., Canada
Speer Carbon Co.
International Graphite & Electrode Div., St. Marys, Pa.
Sprague Electric Co., North Adams, Mass.
Stackpole Carbon Co., St. Marys, Pa.
Stauffer Chemical Co., New York, N. Y.
Sumner Chemical Co., Div. of Miles Laboratories, Inc., Elkhart, Ind.
Tennessee Products & Chemical Corp., Nashville, Tenn.
Texas Instruments, Inc., Dallas, Texas
Three Point Four Corp., Yonkers, N. Y.
Titanium Metals Corp. of America, Henderson, Nev.
Tung-Sol Electric Inc., Newark, N. J.
Udylite Corp., Detroit, Mich. (4 memberships)
Universal-Cyclops Steel Corp., Bridgeville, Pa.
Upjohn Co., Kalamazoo, Mich.
Victor Chemical Works, Chicago, Ill.
Western Electric Co., Inc., Chicago, Ill.
Wyandotte Chemicals Corp., Wyandotte, Mich.
Yardney Electric Corp., New York, N. Y.